University of Alberta

Measuring Pore-water Pressures in Partially Frozen Soils

by

Mohammadali Kia

A thesis submitted to the Faculty of Graduate Studies and Research
in partial fulfillment of the requirements for the degree of

Doctor of Philosophy
in
Geotechnical Engineering

Department of Civil and Environmental Engineering

Fall 2012
Edmonton, Alberta

Dedication

To my ever kind, loving parents

&

To all those who endeavor for the humanity of humans

Abstract

Knowledge of pore-water pressure is essential to predict the ‘effective stress’ that controls the ‘resistance and deformation’ of a soil and to assess the ‘flow’ of water through it. Flow of water towards the freezing fringe controls the amount of frost heave in freezing soils. Drainage of this excess water controls subsequent thaw settlements as the frozen soil thaws. Further, the rate of dissipation of pore-water pressures control the thaw-instability in warming permafrost slopes. Not all of the water in a soil is ice at subzero temperatures; therefore, these soils are ‘partially frozen’. Hence, the challenges associated with measuring pore-water pressure distribution in freezing, thawing, and frozen soils can all be considered as one category: measuring pore-water pressures within a ‘partially frozen soil’. Therefore, measurement of pore-water pressures in partially frozen soils and having methods for estimating the pore-water pressure response to the applied loads are desirable. In this research, first a new instrument was developed to accurately conduct these measurements. Then, the measured pore-water pressures were used to study stress transmission within a partially frozen soil under applied loads, as well as under warming conditions. It was shown that if a sufficient amount of unfrozen water exists in a soil at subfreezing temperatures, it provides a continuous liquid phase that transfers pressures independent from the solid phase. Therefore, effective stress material properties and analysis should be used to evaluate the resistance and deformation of these partially frozen soils. This is of practical significance in analyzing stability and in modeling constitutive behavior of soil masses in warm and warming permafrost, especially for assessing geohazards associated with climate change. It is also of practical significance in analyzing and designing foundations, retaining structures, underground facilities, and frozen-core dams in cold regions.

For the first time, measurements of Skempton’s B-bar coefficient in a partially frozen soil at various initial void ratios were presented and compared to that of the unfrozen soil. Thus, by assuming superposition, stress distribution between the soil matrix, pore-ice, and pore-water was evaluated. Further, decrease in load bearing of the ice matrix with increasing temperature was evaluated via measuring pore-water pressure distribution within a partially frozen soil during

undrained warming. It was also found that in both the partially frozen and unfrozen states, the pore-water pressure response of overconsolidated sand is bilinear with a well-defined inflection point. Further, it was shown that the change in effective stress under undrained loading is not zero in overconsolidated sand specimens; hence, frictional resistance is not zero under undrained loading due to the stiffer solid phase.

Keywords: Skempton's pore-pressure parameter, effective stress, permafrost, slope stability, cemented soils, rapid response piezometer, rigidity of a piezometer

Acknowledgement

I am most thankful to my Creator, The Merciful, The Beneficent, who gives purpose to the completion of another task.

I wish to extend my sincere gratitude to my supervisors, colleagues, and friends, who have always been supporting me in my conquest to make this research possible. Their friendship is an invaluable treasure for the rest of my life.

It has been a tremendous honorable privilege and a pleasant experience for me to work with my supervisors Dr. David C. Sego and Dr. Norbert R. Morgenstern. Intellectually stimulant discussions we had, led to great findings as well as to my personal growth. I also extend my special appreciation to Dr. Lukas Arenson for the initial technical discussions at the beginning of this research and to Mr. Stephen Gamble for his priceless technical assistance during the laboratory experiments. I will always remember Mr. Jerry Kowalyk and other staff at the University of Alberta's Cameron Library for their substantial help in accessing large amounts of multi-discipline literature pertaining to my research. Further, I acknowledge FISO Technologies Inc. for technical assistance with the fiber optic sensors, NSERC for financial support via the NSERC Discovery Grant, and the University of Alberta for financial support through the Provost Doctoral Entrance Award.

I am greatly thankful to my defense committee for meticulously examining this research and providing comments that improved the final text of the thesis.

Lastly, I wish to extend my most heartfelt thanks to my family, especially to my parents, for their prayers, unwavering support, encouragement, and patience, without whom this research would have never been accomplished.

Table of contents

List of tables

List of figures

List of figures

List of figures

List of figures

List of figures

List of symbols

$\boldsymbol{A}$: Skempton's $\boldsymbol{A}$ pore-water pressure parameter

$\boldsymbol{A_f}$: Skempton's $\boldsymbol{A}$ pore-water pressure parameter at failure

$\boldsymbol{B}$: Skempton's $\boldsymbol{B}$ pore-water pressure parameter

$\boldsymbol{B_t}$: Morgenstern's $\boldsymbol{B_t}$ pore-pressure parameter for undrained heating

$\overline{\boldsymbol{B}}_{\boldsymbol{f}}$: Skempton's $\boldsymbol{B}$ pore-water pressure parameter at failure

$\overline{\boldsymbol{B}}$: Skempton's $\overline{\boldsymbol{B}}$ pore-water pressure parameter

$\overline{\boldsymbol{B}}_{\boldsymbol{i}}$: Slope of the primary pore-water pressure response line

$\overline{\boldsymbol{B}}_{\boldsymbol{s}}$: Slope of the secondary pore-water pressure response line

$\widetilde{\overline{\boldsymbol{B}}} = \frac{(\overline{B}_s - \overline{B}_i)}{\overline{B}}$: Sress transmission parameter introduced in this reseach

$\overline{\boldsymbol{B}}_{\boldsymbol{ice}}$: Pore-ice pressure coefficient introduced in this reseach

$\overline{\boldsymbol{B}}_{\boldsymbol{Water,Unfrozen}}$: Pore-water pressure coefficient measured in unfrozen soil

$\overline{\boldsymbol{B}}_{\boldsymbol{Water,Partially\ frozen}}$: Pore-water pressure coefficient measured in soil at subfreezing temperatures

$\boldsymbol{C}$: Lambe and Whitman's $\boldsymbol{C}$ pore-water pressure coefficient

$\boldsymbol{C_l}$: Compressibility of the pore-water lines (1/kPa)

$\boldsymbol{C_d}$: Compressibility of the soil matrix (1/kPa)

$\boldsymbol{C_M}$: Compressibility of pore-pressure transducer (1/kPa)

$\boldsymbol{C_{sk}}$: Compressibility of the mineral skeleton (1/kPa)

$\boldsymbol{C_w}$: Compressibility of the pore fluid (1/kPa)

$\boldsymbol{C'_w}$: Compressibility of the fluid in the pore-water lines (1/kPa)

$\boldsymbol{D}$: Lambe and Whitman's $\boldsymbol{D}$ pore-water pressure coefficient

$\boldsymbol{e}$: Void ratio

$\boldsymbol{e_i}$: Initial void ratio

List of symbols

$\boldsymbol{h}$: Henry's volumetric coefficient of air solubility

H: Height of the specimen

$\boldsymbol{K}$: Lateral earth pressure coefficient

$\mathbf{K_0}$: At-rest lateral earth pressure coefficient

$\boldsymbol{K_c = \eta = \frac{q}{p}}$: Stress ratio in anisotropic preconsolidation

$\boldsymbol{K_i = (\frac{q}{p})_i}$: Initial stress state

$\boldsymbol{K}$: Dry or drained bulk modulus

$\boldsymbol{K_u}$: Undrained (or saturated) modulus

$\boldsymbol{M_i}$: Mass of ice (kg)

$\boldsymbol{M_s}$: Mass of soil particles (kg)

$\boldsymbol{n}$: Porosity of the soil

$\boldsymbol{n}$: Number of moles of gas

OCR: Overconsolidation ratio

$\boldsymbol{p = \frac{\sigma_1 - \sigma_3}{2}}$: Mean normal stress during triaxial tests

$\boldsymbol{P}$: Absolute pressure of gas (Pa)

$\boldsymbol{P}$: Environment pressure (absolute pressure, kPa)

$\boldsymbol{P_a}$: Absolute pressure in the pore fluid (kPa)

$\boldsymbol{P_0}$: Pre-shear isotropic consolidation pressure

$\boldsymbol{P_0'}$: Initial mean effective stress

$\boldsymbol{q = \frac{\sigma_1 - \sigma_3}{2}}$: Shear stress during triaxial tests

$\boldsymbol{r_u}$: Pore-pressure ratio

$\boldsymbol{R}$: Universal gas constant = 8.314472 $J \cdot K^{-1} \cdot mol^{-1}$

List of symbols

$\boldsymbol{R_s}$: radius of curvature of the oil contractile skin or the radius of the transfer tube

$\boldsymbol{S}$: Degree of saturation

$\boldsymbol{S_r}$: Degree of saturation

$\boldsymbol{t}$: Time (seconds)

$\boldsymbol{T}$: Temperature of gas (K)

$\boldsymbol{T}$: Temperature of soil (^{o}C)

$\boldsymbol{T_s}$: Surface tension of the oil in FRP

$\boldsymbol{u}$: Pore-water pressure (kPa)

$\boldsymbol{u_a}$: Air pressure

$\boldsymbol{u_\alpha}$: Barberis's u_α stress transmission parameter

$\boldsymbol{u_0}$: Initial pore-water pressure (kPa)

$\boldsymbol{u_{0i}}$: Intercept of the line fitted to the primary pore-water pressure response (kPa)

$\boldsymbol{u_{0s}}$: Intercept of the line fitted to the secondary pore-water pressure response (kPa)

$\boldsymbol{u_{equalization}}$: Pore-water pressure at which $\overline{\boldsymbol{B}}_{\boldsymbol{i}}$ approaches $\overline{\boldsymbol{B}}_{\boldsymbol{s}}$

$\boldsymbol{u_i}$: Initial backpressure

$\boldsymbol{u_{inflection}}$: Pore-water pressure at which the inflection point between primary and secondary responses occurs

$\boldsymbol{u_f}$: Pore-pressure at failure

$\boldsymbol{u_{mo}}$: Mineral oil pressure (pressure of oil in FRP)

$\boldsymbol{Uc} = (\boldsymbol{u_a} - \boldsymbol{u_{mo}})_{\text{FRP}}$: Air entry value of the FRP based on Kelvin's equation

$\boldsymbol{V}$: Volume of gas (m^3)

$\boldsymbol{V_0}$: Total volume of the test specimen (m^3)

$\boldsymbol{V_t}$: Volume of fluid in the pore-water measuring lines (m^3)

List of symbols

$\boldsymbol{\alpha}$: Barberis's α stress transmission parameter

$\boldsymbol{\alpha}$: Biot-Willis total volume effective-stress coefficient

$\boldsymbol{\alpha}$: Henkel's $\boldsymbol{\alpha}$ pore-pressure coefficient

$\boldsymbol{\beta}$: Barberis's $\boldsymbol{\beta}$ stress transmission parameter

$\boldsymbol{\beta}$: Compressibility of air-water mixture (1/kPa)

$\boldsymbol{\beta_w}$: Compressibility of water (1/kPa)

$\Delta\boldsymbol{\beta}$: Added tertiary compressibility (Pa^{-1})

$\boldsymbol{\Delta\sigma_1}$: Change in maximum principal stress

$\boldsymbol{\Delta\sigma_3}$: Change in minimum principal stress

$\boldsymbol{\Delta\sigma_t}$: Change in total pressure

$\Delta\boldsymbol{\sigma_B}$: Change in total stress at the bottom of the specimen

$\Delta\boldsymbol{\sigma_T}$: Change in total stress at the top of the specimen

$\Delta\boldsymbol{\sigma_x}$: Change in total stress at distance x downward from the top of the specimen

$\boldsymbol{\Delta T}$: Temperature increment (^oC)

$\boldsymbol{\Delta u}$: Excess pore-water pressure

$\Delta\boldsymbol{u_{eq}}$: Change in pore-water pressure within the specimen after equalization

$\boldsymbol{\Delta u_{ice}}$: Excess pressure in pore-ice due to changes in principal total stresses, $\Delta\sigma_1$ and $\Delta\sigma_3$ (kPa)

$\boldsymbol{\Delta\omega_i}$: Decrease in initial gravimetric ice content

$\boldsymbol{\eta_a}$: overconsolidation stress ratio

$\boldsymbol{\acute{\phi}}$: Effective friction angle

$\boldsymbol{\phi^b}$ = friction angle with respect to matric suction

$\boldsymbol{\sigma}$: Total pressure (kPa)

$\boldsymbol{\sigma_1}$: Maximum principal stress

List of symbols

$\boldsymbol{\sigma_2}$: Intermediate principal stress

$\boldsymbol{\sigma_3}$: Minimum principal stress

$\boldsymbol{\sigma_p}$: Effective preconsolidation pressure (kPa)

$\boldsymbol{\sigma'_{vo}}$: Initial effective vertical stress (kPa)

$\boldsymbol{\theta_u}$**:** Volumetric unfrozen water content

$\boldsymbol{\omega_i} = \frac{\boldsymbol{M_i}}{\boldsymbol{M_s}}$: Initial gravimetric ice content

1. Introduction

1.1 Definition of the problems

1.1.1 Background: what triggered this research?

McSaveney (2002) reported recent massive rock and ice falls (up to 11.8 million m^3), earthquakes (up to 3.9 Richter), floods (up to 7.8 million m^3 of water), and rapid rock-ice flow over long distances (up to 7.5 km at 60m/s) caused by 'catastrophic instability of slopes' triggered by climatic warming in high mountain permafrost.

The warming of ground ice in permafrost slopes can cause ice to melt or reduce its shear resistance. If the slope is ice rich, water-logged thawed soil at higher water contents than its liquid limit flows with negligible shear resistance. In other cases, partial thawing increases the pore-ice temperate and pore-water content and hence reduces the cohesion and shear resistance of the soil which can lead to instability of the soil mass.

Permafrost slopes that have previously undergone warming may have developed large negative pore-water pressures (due to rebounding or increased void space after ice melt) that keep them stable. These negative pore-water pressures may suddenly change to positive pore-water pressures and lead to instability of soil masses as:

- additional ice melts and water from melting ice or snow increases the degree of saturation in weak zones (especially in varved soils with non-homogenous ice distribution);
- positive pore-water pressures are generated during a sudden drop in air temperature after a thaw period when drainage is impeded during freezing of an unfrozen layer between two frozen layers; and
- soil deforms under undrained loading conditions.

The generated positive pore-water pressures reduce the in-situ effective stress, and hence the shear resistance of the soil. This situation may lead to slope instability.

To better understand and analyze the stability of soil masses in continuous and discontinuous permafrost, better understanding of the freezing and thawing processes, as well as mechanical behavior of soils at subfreezing temperatures close to 0^{o}C is required.

1.1.2 Outline

First, the practical demands for research on the mechanics of frozen, freezing, and thawing soils are outlined. To understand these mechanics, knowledge of 'pore-water pressure distribution' in these soils is essential to predict the 'effective stress' that controls the resistance and deformation of these soils, to assess hydraulic gradients that control 'flow' and 'drainage' of water through them, and to measure their hydraulic conductivity as they freezes or thaw. To date, no investigation supported by accurate measurements of 'pore-water pressure distribution' within soils at subzero temperatures and their relation to the effective stresses has been published.

Another application of measuring 'pore-water pressure distribution' is in better understanding the mechanisms that control frost heave, thaw settlement, and thaw instability. The flow of water towards the freezing fringe controls the amount of frost heave. Drainage of this excess water controls subsequent thaw settlements as the frozen soil thaws. Further, the rate of dissipation of pore-water pressure controls thaw-instability in warming permafrost slopes. Water-bearing soils at subfreezing temperatures close to 0^{o}C are 'partially frozen' as they contain unfrozen water. Therefore, the problem of measuring pore-water pressure within freezing, thawing, and frozen

soils close to 0°C can all be treated as one category: 'measuring pore-water pressure within partially frozen soils'. In this research, first a new instrument (Filter-less Rigid Piezometer) was developed to measure pore-water pressures in partially frozen soils. Then, this instrument and the experiment apparatus were tested in order to investigate factors affecting the interpretation of these measurements and validate the measurements. Finally, this new instrument was used to study stress transmission within a partially frozen soil under applied loads, as well as under warming conditions, via measuring pore-water pressure distribution within the soil.

Sand specimens at 30±1 ppt NaCl salinity were used for experiments at temperatures in the range of -5±0.01°C to +7±0.01°C and total stresses up to 430±1 kPa.

1.1.3 Practical demands for research on the mechanics of frozen, freezing, and thawing soils

The increased exploration of energy and mining resources in Northern Canada and the opening of a sea route between Asia and Europe through Canada's Northwest passage need reliable engineering theories and techniques to provide safe, economical designs for the land-based infrastructure required by these projects. The extraction of these resources and their transport require improved engineering to reduce the costs.

In addition, potential warming associated with climate change will contribute to deepening the active layer (seasonally freezing and thawing layer) in permafrost regions, which may reduce the resistance of the ground and increase the risks associated with geohazards: rock avalanches; earth slides, falls and flows; and deglaciations (Anisimov et al. 1997).

Since approximately 50% of the land in Canada is underlain with permafrost, global warming poses potential threats through the aforementioned geohazards that may affect the environment as well as engineering projects (highways, pipelines, railways, infrastructure, and forests). The resistance and deformation of frozen soils are of practical interest in cold regions for the analysis and design of:

- slopes (Huggel et al. 2010; Mason 1995; McRoberts 1973; McRoberts and Morgenstern 1974a; 1974b; McSaveney 2002; Stoker 1989; Tsui 1987);
- shallow and deep foundations (Johnston 1981; Ladanyi 1975; Neklyudov et al. 1992; Vangool 1996; Vyalov 1965; Wang et al. 2006; Weston and Williams 1986);
- dams (Cathro et al. 1992; Feringer 2008; Semenov 1967; Vasil'ev et al. 1988); and
- retaining structures (Laba 1975; Li et al. 2002; Novikov 1980; Vyalov et al. 1965).

Previous analysis and design methods in frozen soils either treat the soil as a Tresca (a material with only cohesion) or a frictional-cohesive material; in both cases, 'total stresses' and 'total stress material properties' have been used for their analysis and design. When a water phase with independent pore-pressure exists in the pore-space of a soil, the total stress material properties depend on the stress and stress path, and the 'total stresses' do not represent the 'actual stresses' carried by the solid phase. In these cases, conducting an effective stress analysis using effective stress material properties provides a more realistic representation of the field behavior of the ground. To evaluate effective stresses and effective stress material properties, measuring pore-water pressure distribution within these soils is required. The challenges in measuring pore-water pressure in frozen ground are more complicated than in thawed soil because phase changes (ice melting or formation) occur due to time-dependent heat and mass transfer. Further, melting of ice under increased pressures and formation of ice from supercooled water when its pressure declines, increase the complexity of the behavior of frozen soils. These processes occur near 0^{o}C and within the pressure range of interest for civil engineers. These processes result in viscous deformations, anisotropy, heterogeneity, and damage mechanisms that influence the resistance and deformation response of frozen ground (He et al. 2000; Ling and Zhang 2004; Newman and Wilson 1997).

The other 50% of Canada is underlain with seasonally freezing and thawing ground, which may be affected by frost heave, thaw weakening, and thaw settlement. Freezing- and thawing-induced deformations affect the serviceability and durability of highways and railroads, chilled gas pipelines, hot oil pipelines, municipality and communication infrastructure, and all other engineering structures in areas with cold climates. The cost of damage induced by freezing and

thawing is high. Hence, efforts need to focus on practical approaches to minimize the negative effects of freezing and thawing. Freezing and thawing mechanics are also of interest in artificial ground freezing for controlling groundwater seepage and contamination transport (Iskandar 1987; Iskandar and Jenkins 1985), structural support of deep and shallow excavation (Jessberger 1981), and liquid natural gas (LNG) storage (Goto and Minegishi 1988). The effects of freeze-thaw cycles are not only of great concern in geotechnical engineering, but also in food preservation (Chassagne-Berces et al. 2009; Haiying et al. 2007), cryosurgery (Chua and Chou 2009; Li et al. 2010), cryo-preservation of biological cells (Mazur 1970), preservation of human organs for implantation (Asselmeier et al. 1993; Briere et al. 1991; Halberstadt et al. 2003; Thirumala and Devireddy 2004), soil sciences for agricultural purposes (Sharratt 1993), birth and growth of pingos (mounds of earth-covered ice found in the Arctic and subarctic areas) (Mackay 1983b), and the masonry and mortar industry (Coussy and Monteiro 2008). Moreover, geomorphic development within the Arctic and Alpine areas including patterned ground formation, size sorting in soils, uplifting of stones by freezing, and frost weathering of rocks, are all related to frost heave, ice segregation and thaw deformations (Harris et al. 2009; Tharp 1987).

When subjected to freezing and thawing, fine-grained soils generally experience volume changes (Taber 1929), loss in shear strength (Broms and Yao 1964; Kok 1989), and sometimes alterations in their hydraulic conductivities during thawing (Wong and Haug 1991), which are significant in engineering design. Despite the previous research on freezing and thawing of fine-grained soils, quantitative correlations of the changes in the engineering properties of various soil types following freezing and thawing are not well established nor are the mechanics of these changes fully understood. These processes occur near 0^{o}C, within the pressure range of interest for civil engineers, and are controlled by pore-water migration and drainage within the freezing and thawing soils. Hence, measuring pore-water pressure distribution within these soils is required to measure hydraulic conductivity and hydraulic gradients that control these processes.

Addressing challenges associated with geohazards induced by climate change, seasonal and artificial freezing and thawing of soils, providing engineering solutions to minimize damages to

the existing infrastructure, and improving design procedures for future construction projects require measuring pore-water pressure distribution in these soils to establish reliable and realistic theories and techniques that accurately predict the resistance and deformation of frozen ground especially when it approaches 0^{o}C and during freezing and thawing of soils. The available research on the behavior of frozen, freezing, and thawing ground at temperatures close to 0^{o}C is minimal, even though the physical processes at these temperatures control the soil's resistance and deformation. The main reason for this lack of data is the difficulty in conducting experiments at temperatures close to 0^{o}C.

1.1.4 Need for measuring pore-water pressure in partially frozen soils

Establishing methods for measuring pore-water pressure in soils at subfreezing temperatures close to 0^{o}C increases the understanding of their mechanics under applied loads and the mechanism of freezing and thawing processes in these soils. These applications are discussed further in the following subsections.

1.1.4.1 Application in establishing the effective stress concept in partially frozen soils

Due to climate warming trends and backed by more than 100 years of extensive observation and analysis in glaciology (Ladanyi 2006), the accelerating creep of rock glaciers and frozen slopes has been of increasing interest, especially in recent years. Glaciologists identified the deformation behavior of glaciers as 'creep'. As a result, creep tests and creep modeling were used as tools to simulate the natural behavior of glaciers. The basic creep models are based on 'total stresses'; hence, the existing design approaches for frozen soils are also based on 'total stresses'. The first published research on frozen ground engineering from Russian resources (Razbegin et al. 1996; Sadovsky et al. 1988; Tsytovich 1940; 1959; Vyalov et al. 1969; 1965), followed by non-geotechnical engineers at CRREL (U.S. Army Cold Regions Research and Engineering Laboratory) who were familiar with von Mises failure criterion for metals, treated frozen soils as Tresca (or von Mises) materials (having only cohesion) and not porous media having both

frictional and cohesion strength components (especially with a continuous water phase). Only 'total stresses' are required for analysis when a Tresca material is considered. In these cases, generally the Glen creep constitutive model (Glen 1955; Sayles 1973) was used for geotechnical design of foundations and stability analysis of frozen soil masses based on a serviceability criterion.

Several authors studied the frictional behavior of frozen soils and ice (Alkire and Andersland 1973; Andersland and Alnouri 1970; Arenson and Springman 2005b; Bragg and Andersland 1981; Chamberlain et al. 1972; Fish and Zaretsky 1998; Goughnour and Andersland 1968; Ho et al. 1996; Neuber and Wolters 1977; Parameswaran and Jones 1981; Qi and Ma 2007; Repetto-Llamazares et al. 2011; Roggensack and Morgenstern 1978; Sadovskii et al. 1987; Sayles 1973; Sayles 1974; Song 1984; Tsytovich 1975; Vyalov and Shusherina 1964; Vyalov et al. 1965; Yang et al. 2010). In all of these studies, the frictional resistance of frozen soil is attributed to its dilatancy and the frictional nature of the soil matrix. Except for the works by Arenson and his colleagues (Arenson 2002; Arenson and Springman 2005a; Nater et al. 2008), all of the previous research on the frictional resistance of frozen soils was limited to the 'total stress friction angle'. Arenson (2002) attempted to measure 'effective friction angle' of natural permafrost samples that had high amount of air via measuring pore-water pressure at the top and bottom of (and not within) frozen soil samples in triaxial tests. The shortcomings of the method used by Arenson and his colleagues, in accurately measuring pore-water pressures, are discussed in Chapter 2.

The major obstacles in establishing the 'effective stress' principle in frozen soils have been:

- the difficulty of conducting reliable, accurate measurements of unfrozen pore-water pressures in frozen soils;
- the lack of data on the continuity of unfrozen pore-water within the soil; and
- periodic interest in or lack of funds available for research in cold regions engineering.

Therefore, 'creep deformation constitutive models' and 'creep failure criterion' have been traditionally used for analysis of the deformations of soil masses in frozen ground. However,

conducting creep tests to simulate field conditions is time-consuming and expensive. Further, the current creep tests on frozen soils do not consider pore-water pressure generation and dissipation in these soils. In reality, 'effective stresses' and 'effective stress material properties' control the resistance and deformation of the soil masses and therefore the existing creep methods are not an effective way for analysis of resistance and deformation of partially frozen soils that have a continuous water phase. Therefore, measuring pore-water pressure distribution in these soils is required.

The terms 'effective stress' and 'effective stress shear strength properties' have been used somewhat loosely in the literature with different meanings from those defined by geotechnical engineers. Effective stress shear strength properties are measured either in a true drained test or an undrained test together with measuring pore-water pressures. A true drained test does not allow any excess pore-water pressure to build up (its slow loading rate allows complete drainage). Alternatively, one can cancel the pore-water pressures from the total stresses to calculate the effective stresses by measuring pore-water pressures in an undrained test. To achieve this goal, this research developed a method to accurately measure pore-water pressure distribution within soils at subfreezing temperatures.

1.1.4.2 Applications in predicting frost heave, thaw settlement, and thaw weakening

Cryo-suction (negative pore-pressure) has been long identified to move water while causing excessive frost heave during freezing. There is also possibility of developing excessive positive pore-water pressure during the advance of the freezing front in freezing soils (McRoberts and Morgenstern 1975). On the other hand, generation of positive pore-water pressures during thawing due to delayed drainage can result in excessive loss of resistance and increased deformations in thawing soils.

Summaries of frost heave models (empirical, semi-empirical, hydrodynamic, rigid ice, thermo-mechanical, and segregation potential), their major assumptions, input and output parameters, and

their associated numerical methods are presented by several authors (Konrad and Shen 1996; Kujala 1994; 1997; Sheng 1994). While reviewing the literature on freezing and thawing soils, the author conceived that 'hydraulic conductivity' and 'tensile strength' of partially frozen soils near the freezing front are the soil properties that play major roles in micro and macro behavior of freezing soils. Furthermore, the transport of water during freezing is controlled by hydraulic gradients and hence pore-water pressure distribution within the soil. Estimating hydraulic conductivity of the frozen fringe is of paramount importance in predicting frost heave. So far, only estimations based on the thawed or frozen hydraulic conductivity (Horiguchi and Miller 1980; Williams and Burt 1974) are available for predicting frost heave. Several authors have measured tensile strength of frozen soils at temperatures close to 0^{o}C (Akagawa and Nishisato 2009; Azmatch et al. 2011; Bragg and Andersland 1981; Haynes 1978). Measuring pore-water pressure in partially frozen soils is presented in this thesis. Conducting experiments to measure 'hydraulic conductivity' and 'tensile strength' of partially frozen soils during freezing and thawing via direct measurement of pore-pressures remains for future research.

1.1.5 Need for conducting experiments at temperatures close to 0^{o}C and low applied pressures

While reviewing published experiments on freezing, thawing, and frozen soils, the author observed that -5 and -10^{o}C have been the most frequently used temperatures for the experiments. The author believes it is due to the perception that -10^{o}C is the representative temperature of permafrost at depths of 10 m or more (Baranov 1964; Chamberlain et al. 1972). Further, controlling temperature at colder temperatures is easier because as temperatures approach 0^{o}C phase change causes fluctuations. By the time the temperature is lowered to -5^{o}C, most of the 'free water' in the pores of most soils is ice, and the heat transfer associated with phase change induced by small temperature fluctuations is negligible. Ladanyi and Morel (1990) regard -5^{o}C as the melting point of frozen sand. By selecting a temperature used by other researchers, one can compare the experimental results with values found in the literature. These reasons may have led using -5 and -10^{o}C as experiment temperatures. In artificial ground freezing applications, colder

temperatures are generally the norm. However, in most common geotechnical engineering applications, the depth of influence of engineering activity or exploration is within the upper 10 m layer of the ground (most borehole logs are 9 m or less). Further, viscous flow of (partially) frozen slopes usually takes place at depths in the upper 1 to 2 m, where the ground is exposed to the influences of warm air temperatures. Parameswaran (1980) reports considerably lower values of strength and modulus of frozen sand at -2^{o}C, compared to those predicted by extrapolating the values measured at lower temperatures.

Extensive research in the former USSR on the mechanical behavior of frozen soils at temperatures warmer than -3^{o}C have been reported (Tsytovich 1975). However, the accuracy and the reporting of these experiments have been questioned during a personal communication with Dr. N.R. Morgenstern. Further, none of these studies investigated the effects of pore-water pressures. This study focuses on the measurement of pore-water pressure in soils at subfreezing temperatures close to 0^{o}C.

High stresses can be encountered when carrying out deep excavations using ground freezing techniques (e.g. shafts in mining projects and underground railways). For instance, Qi and Ma (2007) estimate a 20 MPa confining pressure in frozen soil at depths of 700 m in coal mines in Shandong Province, China, where ground freezing is applied to support the excavation walls. On the other hand, low stresses are of interest for ordinary geotechnical projects within shallow depths, where normal stresses are in the range of 50 to 200 kPa (e.g. slope stability, foundations, and shallow excavations for highways, railways, pipelines, and buildings). This study focuses on the measuring pore-water pressure in soils at effective stresses in the range of 50 to 300 kPa.

1.2 Description of the study

In Chapter 2, the theory and technical requirements for measuring pore-water pressures in partially frozen soils are discussed, and Filter-less Rigid Piezometer (FRP) is designed to measure 'pore-water pressure distribution' within these soils. It is necessary to measure the '*distribution*' of pore-water pressures within partially frozen soils to check the '*continuity*' of pore-water pressures

within these soils and to evaluate whether pore-water can have independent pressure from the total stress, hence validating the necessity of using effective stresses for analysis and design in these soils. Therefore, in Chapter 3, FRPs are used in the Modified Qiu and Sego (MQS) cell to investigate the continuity of the measured pore-water pressures in partially frozen soils, as well as factors affecting pore-water pressure measurements in the laboratory and their interpretation.

In Chapter 4, FRPs are used to study the pore-water pressure response to undrained loading and to undrained warming in a frozen soil at low confining pressures, under low applied backpressures, and at subfreezing temperatures close to 0^{o}C. These three conditions resemble near surface soil conditions of interest for geotechnical engineering in permafrost regions. Chapter 5 summarizes the findings of this research and their practical significance. It also provides recommendations for future research.

1.3 References

Akagawa, S., and Nishisato, K. 2009. Tensile strength of frozen soil in the temperature range of the frozen fringe. Cold Regions Science and Technology, **57**(1): 13-22.

Alkire, B.D., and Andersland, O.B. 1973. The effect of confining pressure on the mechanical properties of sand-ice materials. Journal of Glaciology, **12**(66): 469-481.

Andersland, B.D., and Alnouri, I. 1970. Time-dependent strength behavior of frozen soils. Journal of the Soil Mechanics and Foundations Division, ASCE, **96**(SM4): 1249-1265.

Anisimov, O.A., Shiklomanov, N.I., and Nelson, F.E. 1997. Global warming and active-layer thickness: results from transient general circulation models. Global and Planetary Change, **15**(3-4): 61-77.

Arenson, L.U. 2002. Unstable alpine permafrost: a potentially important natural hazard. Ph.D. dissertation, Institute for Geotechnical Engineering Technische Wissenschaften ETH, Zurich, Switzerland.

Arenson, L.U., and Springman, S.M. 2005a. Mathematical descriptions for the behaviour of ice-rich frozen soils at temperatures close to 0 °C. Canadian Geotechnical Journal, **42**(2): 431-442.

Arenson, L.U., and Springman, S.M. 2005b. Triaxial constant stress and constant strain rate tests on ice-rich permafrost samples. Canadian Geotechnical Journal, **42**(2): 412-430.

Asselmeier, M.A., Caspari, R.B., and Bottenfield, S. 1993. A review of allograft processing and sterilization techniques and their role in transmission of the human-immunodeficiency-virus. American Journal of Sports Medicine, **21**(2): 170-175.

Azmatch, T.F., Sego, D.C., Arenson, L.U., and Biggar, K.W. 2011. Tensile strength and stress-strain behaviour of Devon silt under frozen fringe conditions. Cold Regions Science and Technology, **68**(1-2): 85-90.

Baranov, I.J. 1964. Principles of geocryology. Technical Translation 1121. National Research Council of Canada.

Bragg, R.A., and Andersland, O.B. 1981. Strain rate, temperature, and sample size effects on compression and tensile properties of frozen sand. Engineering Geology, **18**(1-4): 35-46.

Briere, N., Cabana, C., and Magny, P. 1991. Freeze-fracture observations on human fetal kidney in serum-free organ-culture. Anatomical Record, **230**(2): 249-260.

Broms, B.B., and Yao, L.Y.C. 1964. Shear strength of soil after freezing and thawing. Journal of the Soil Mechanics and Foundations Division, ASCE, **90**(SM4, Part 1): 1-25.

Cathro, D.C., Keen, A.J., and Hayley, D.W. 1992. Design and construction of a permafrost core earth dam. *In* 2nd International Symposium on Mining in the Arctic. A.A. Balkema, Fairbanks, AK, USA, pp. 153-153.

Chamberlain, E.J., Groves, E., and Perham, R. 1972. The mechanical behavior of frozen earth materials under high pressure triaxial test conditions. Géotechnique, **22**(3): 469-483.

Chassagne-Berces, S., Poirier, C., Devaux, M.-F., Fonseca, F., Lahaye, M., Pigorini, G., Girault, C., Marin, M., and Guillon, F. 2009. Changes in texture, cellular structure and cell wall composition in apple tissue as a result of freezing. Food Research International, **42**(7): 788-797.

Chua, K.J., and Chou, S.K. 2009. On the study of the freeze-thaw thermal process of a biological system. Applied Thermal Engineering, **29**(17-18): 3696-3709.

Coussy, O., and Monteiro, P.J.M. 2008. Poroelastic model for concrete exposed to freezing temperatures. Cement and Concrete Research, **38**(1): 40-48.

Feringer, A. 2008. Design and construction of dams on permafrost. Power Technology and Engineering (formerly Hydrotechnical Construction), **42**(2): 78-82.

Fish, A.M., and Zaretsky, Y.K. 1998. Strength and creep of ice in terms of Mohr-Coulomb fracture theory. *In* 8th International Offshore and Polar Engineering Conference. ISOPE, Montreal, Canada, pp. 416-424.

Glen, J.W. 1955. The creep of polycrystalline ice. Proceedings of the Royal Society of London, **A228**: 519-538.

Goto , S., and Minegishi, K. 1988. Direct shear test at a frozen/unfrozen interface. *In* 5th International Symposium on Ground Freezing A.A.Balkema, Nottingham, England, pp. 559-560.

Goughnour, R.R., and Andersland, O.B. 1968. Mechanical properties of a sand-ice system. Journal of the Soil Mechanics and Foundation Division, ASCE, **94**(SM4): 923-950.

Haiying, W., Shaozhi, Z., and Guangming, C. 2007. Experimental study on the freezing characteristics of four kinds of vegetables. LWT - Food Science and Technology, **40**(6): 1112-1116.

Halberstadt, M., Bohnke, M., Athmann, S., and Hagenah, M. 2003. Cryopreservation of human donor corneas with dextran. Investigative Ophthalmology & Visual Science, **44**(12): 5110-5115.

Harris, C., Arenson, L.U., Christiansen, H.H., Etzemuller, B., Frauenfelder, R., Gruber, S., Haeberli, W., Hauck, C., Holzle, M., Humlum, O., Isaksen, K., Kaab, A., Kern-Lutschg, M.A., Lehning, M., Matsuoka, N., Murton, J.B., Nozli, J., Phillips, M., Ross, N., Seppala, M., Springman, S.M., and Muhll, D.V. 2009. Permafrost and climate in Europe: Monitoring and modelling thermal, geomorphological and geotechnical responses. Earth-Science Reviews, **92**(3-4): 117-171.

Haynes, F.D. 1978. Strength and deformation of frozen silt. *In* 3rd International Conference on Permafrost. National Research Council of Canada, Edmonton, Alberta, Can, pp. 655-661.

He, P., Zhu, Y., and Cheng, G. 2000. Constitutive models of frozen soil. Canadian Geotechnical Journal, **37**(4): 811-816.

Ho, C.L., Vela, J.C., Clark, P.U., and Jenson, J.W. Evaluation of long-term time-rate parameters of subglacial till. *In* the 1996 ASCE National Convention. Geotechnical Special Publication, n 61, Washington, DC, USA. 10-14 November 1996 1996. ASCE, pp. 122-136.

Horiguchi, K., and Miller, R.D. 1980. Experimental studies with frozen soil in an ice sandwich permeameter. Cold Regions Science and Technology, **3**(2-3): 177-183.

Huggel, C., Salzmann, N., Allen, S., Caplan-Auerbach, J., Fischer, L., Haeberli, W., Larsen, C., Schneider, D., and Wessels, R. Recent and future warm extreme events and high-mountain slope stability, 6 Carlton House Terrace, London, SW1Y 5AG, United Kingdom2010. Royal Society of London, pp. 2435-2459.

Iskandar, I.K. 1987. Ground freezing controls hazardous waste. Military Engineer, **79**(516): 456.

Iskandar, I.K., and Jenkins, T.F. 1985. Potential use of artificial ground freezing for contaminant immobilization. *In* Proceedings of the International Conference on New Frontiers for Hazardous Waste Management. EPA, Pittsburgh, PA, USA, pp. 128-137.

Jessberger, H.L. 1981. A state-of-the-art-report - ground freezing: mechanical properties, processes and design. Engineering Geology, **18**(1-4): 5-30.

Johnston, G.H. 1981. Permafrost Engineering Design and Construction. Wiley, Toronto.

Kok, H. 1989. Freeze-thaw-induced variability of soil shear strength. Ph.D. PhD Dissertation, University of Idaho, Idaho, United States.

Konrad, J.M., and Shen, M. 1996. 2-D frost action modeling using the segregation potential of soils. Cold Regions Science and Technology, **24**(3): 263-278.

Kujala, K. 1994. Frost heave calculation models, Finnish National Road Administration, R&D Unit Oulu, Finland. Research report 2/1994. 135p (in Finnish).

Kujala, K. 1997. Estimation of frost heave and thaw weakening by statistical analyses and physical models. *In* International Symposium on Ground Freezing and Frost Action in Soils. A.A. Balkema, Rotterdam, Netherlands, Luleå, Sweden, pp. 31-41.

Laba, J.T. 1975. Forces exerted on rigid retaining walls by a confined frozen soil layer. *In* 4th Southeast Asian Conference on Soil Engineering. Institute of Engineering, Malays, Kuala Lumpur, pp. 5-18.

Ladanyi, B. 1975. Bearing capacity of strip footings in frozen soils. Canadian Geotechnical Journal, **12**(3): 393-407.

Ladanyi, B. 2006. Creep of frozen slopes and ice-filled rock joints under temperature variation. Canadian Journal of Civil Engineering, **33**(6): 719-725.

Ladanyi, B., and Morel, J.-F. 1990. Effect of internal confinement on compression strength of frozen sand. Canadian Geotechnical Journal, **27**(1): 8-18.

Li, H.-S., Liu, Z.-L., and Zhu, Y.-L. 2002. Application of fracture mechanics of frozen soil to retaining wall stability analysis (in Chinese). Yantu Gongcheng Xuebao/Chinese Journal of Geotechnical Engineering, **24**(1): 69-69.

Li, Y.H., Wang, F., and Wang, H. 2010. Cell death along single microfluidic channel after freeze-thaw treatments. Biomicrofluidics, **4**(1): Article No. 014111. 014110 pp (digital article).

Ling, F., and Zhang, T. 2004. A numerical model for surface energy balance and thermal regime of the active layer and permafrost containing unfrozen water. Cold Regions Science and Technology, **38**(1): 1-15.

Mackay, J.R. 1983. Pingo growth and subpingo water lenses, western arctic coast, Canada. *In* 4th International Conference on Permafrost. National Academic Press, Fairbanks, AK, USA, pp. 762-766.

Mason, J.A. 1995. Effects of glacial-interglacial climate change on mass wasting, southeastern Minnesota. Ph.D. dissertation, The University of Wisconsin, Madison, United States.

Mazur, P. 1970. Cryobiology: the freezing of biological systems. Science, **168**(3934): 939-949.

McRoberts, E.C. 1973. Stability of slopes in permafrost. Ph.D. dissertation, University of Alberta, Canada.

McRoberts, E.C., and Morgenstern, N.R. 1974a. The stability of thawing slopes. Canadian Geotechnical Journal, **11**(4): 447-469.

McRoberts, E.C., and Morgenstern, N.R. 1974b. Stability of slopes in frozen soil, Mackenzie Valley, N.W.T. Canadian Geotechnical Journal, **11**(4): 554-573.

McRoberts, E.C., and Morgenstern, N.R. 1975. Pore water expulsion during freezing. Canadian Geotechnical Journal, **12**(1): 130-141.

McSaveney, M.J. 2002. Recent rockfalls and rock avalanches in Mount Cook national park, New Zealand. *In* Catastrophic landslides, effects, occurrence and mechanisms. Geological Society of America, Reviews in Engineering Geology, Volume XV, pp. 35–70.

Nater, P., Arenson, L.U., and Springman, S.M. 2008. Choosing geotechnical parameters for slope stability assessments in alpine permafrost soils. *In* 9th international conference on permafrost. University of Alaska, University of Alaska, Fairbanks, USA, pp. 1261-1266.

Neklyudov, V.S., Targulyan, Y.O., and Lolaev, A.B. 1992. Multifunctional combined foundations on permafrost soils (in Russian). Osnovaniya, Fundamenty i Mekhanika Gruntov(5): 26-28.

Neuber, H., and Wolters, R. 1977. Mechanical Behaviour of Frozen Soils under Triaxial Compression, Translation, Report NRC/CNR-TT-1902, National Research Council of Canada, Ottawa, Ontario, Canada.

Newman, G.P., and Wilson, G.W. 1997. Heat and mass transfer in unsaturated soils during freezing. Canadian Geotechnical Journal, **34**(1): 63-70.

Novikov, F.Y. 1980. Calculation of earth pressure on a retaining wall constructed on frozen ground. Soil Mechanics and Foundation Engineering, **17**(4): 146-152.

Parameswaran, V.R. 1980. Deformation behaviour and strength of frozen sand. Canadian Geotechnical Journal, **17**(1): 74-88.

Parameswaran, V.R., and Jones, S.J. 1981. Triaxial testing of frozen sand. Journal of Glaciology, **27**(95): 147-155.

Qi, J., and Ma, W. 2007. A new criterion for strength of frozen sand under quick triaxial compression considering effect of confining pressure. Acta Geotechnica, **2**(3): 221-226.

Razbegin, V.N., Vyalov, S.S., Maksimyak, R.V., and Sadovskii, A.V. 1996. Mechanical properties of frozen soils. Soil Mechanics and Foundation Engineering, **33**(2): 35-45.

Repetto-Llamazares, A.H.V., Høyland, K.V., and Kim, E. 2011. Experimental studies on shear failure of freeze-bonds in saline ice. Part II: Ice-ice friction after failure and failure energy. Cold Regions Science and Technology, **65**(3): 298-307.

Roggensack, W.D., and Morgenstern, N.R. Direct shear tests on natural fine-grained permafrost soils. *In* 3rd International Conference on Permafrost, Edmonton, Alberta, Canada. 10-13 July 1978 1978. National Reseach Council of Canada, pp. 728-735.

Sadovskii, A.V., Bondarenko, G.I., Tikhomirov, S.M., and Konstantinov, A.V. 1987. Freezing-together strength of sea ice and bottom soils in shelf zone. Soil Mechanics and Foundation Engineering, **24**(5): 189-193.

Sadovsky, A.V., Maksimyak, R.V., and Razbegin, V.N. State of the art: mechanical properties of frozen soil. *In* 5th International Symposium on Ground Freezing, Nottingham, England. 26-28 July 1988 1988. A.A. Balkema, pp. 443-463.

Sayles, F.H. Triaxial and creep tests on frozen Ottawa sand. *In* North American Contribution to the 2nd International Permafrost Conference 1973. National Academy of Sciences, pp. 384-391.

Sayles, F.H. 1974. Triaxial constant strain rate tests and triaxial creep tests on frozen Ottawa sand. CRREL Technical Report 253, U.S. Army Cold Regions Research and Engineering Laboratory (CRREL), Hanover, N.H., USA.

Semenov, N.G. 1967. Dam construction in permafrost regions (in Russian: Stroitel'stvo plotiny v raione vechnoi merzloty). Gidrotekhnicheskoe Stroitel'stvo, **9**: 14-15.

Sharratt, B.S. 1993. Freeze-thaw and winter temperature of agricultural soils in interior Alaska. Cold Regions Science and Technology, **22**(1): 105-111.

Sheng, D. 1994. Thermodynamics of freezing soils, theory and application. Ph.D. Dissertation, Luleå University of Technology, Finland.

Song, L. 1984. Measurement of mechanical properties of frozen soil using the single specimen method (in Chineese). Meitan Xuebao/Journal of the China Coal Society, **1**: 21-30.

Stoker, K.J.L. 1989. Active layer detachment slope failures on Fosheim Peninsula, Ellesmere Island, Northwest Territories. M.Sc. thesis, University of Toronto, Canada.

Taber, S. 1929. Frost heaving. Journal of Geology, **37**(5): 428-461.

Tharp, T.M. 1987. Conditions for crack-propagation by frost wedging. Geological Society of America Bulletin, **99**(1): 94-102.

Thirumala, S., and Devireddy, R.V. 2004. On the optimal rate of freezing native and artificial tissues. *In* 2003 MRS Fall Meeting, December 1-4, 2003. Materials Research Society, Boston, MA, United states, pp. 5-7.

Tsui, P.C. 1987. Geotechnical investigations of glaciotectonic deformation in central and southern Alberta. Ph.D. dissertation, University of Alberta, Canada.

Tsytovich, N.A. 1940. An investigation of elastic and plastic deformation of frozen ground (Issledovanie uprugikh i plasticheskikh deformatsii merzlykh gruntov: in Russian). Trudy, **10**: 5-36.

Tsytovich, N.A. 1975. The mechanics of frozen ground. Scripta Book, Washington, D.C.

Tsytovich, N.A., and Sumgin, M.I. 1959. Principles of mechanics of frozen ground = Osnovaniia mekhaniki merzlykh gruntov. U.S. Army Snow, Ice and Permafrost Research Establishment, Corps of Engineers, Wilmette, Ill.

Vangool, W.J. 1996. Foundations for permafrost and other problem soils. *In* 8th International Conference on Cold Regions Engineering. ASCE, Fairbanks, AL, USA, pp. 303-314.

Vasil'ev, I.M., Sinyakov, L.N., and Mel'nikov, V.A. 1988. Strength of thawed and frozen soils of dam cores under conditions of triaxial independent loading by tension and compression. Hydrotechnical Construction, **22**(1): 27-33.

Vyalov, S.S. 1965. Rheological properties and bearing capacity of frozen soils. United States Engineer Department, Cold Regions Research and Engineering Laboratory -- Translation: 219.

Vyalov, S.S., and Shusherina, Y.P. 1964. Resistance of frozen soils to triaxial compression. Translation from Merzlotnye Issledovaniya, No.4. Pages: 340-375, Defence Documentation Centre, Cameron Station, Alexandria, Virginia, USA.

Vyalov, S.S., Gorodetskii, S.E., Ermakov, V.F., Zatsarnaya, A.G., and Pekarskaya, N.K. 1969. Methods of Determining Creep, Long-Term Strength and Compressibility Characteristics of Frozen Soils, Report 0077-5606, NRC Institute for Research in Construction; National Research Council Canada.

Vyalov, S.S., Gmoshinskii, V.G., Gorodetskii, S.E., Grigorieva, V.G., Zaretskii, K., Pekarskaia, N.K., and Shusherina, Y.P. 1965. The strength and creep of frozen soils and calculations for ice-soil retaining structures. CRREL Translation 76, U.S. Army Cold Regions Research and Engineering Laboratory (CRREL), Hanover, N.H., USA.

Wang, J., Li, S., Zhou, G., Liu, Z., and Bie, X. 2006. Analysis of bearing capacity of pile foundation in high temperature permafrost regions with permafrost table descending (in Chinese). Yanshilixue Yu Gongcheng Xuebao/Chinese Journal of Rock Mechanics and Engineering, **25**(Suppliment 2): 4226-4232.

Weston, H.K., and Williams, T.R. 1986. Building foundation on thawed soil and permafrost. *In* 4th International Conference on Cold Regions Engineering. ASCE, Anchorage, AK, USA, pp. 93-105.

Williams, P.J., and Burt, T.P. 1974. Measurement of hydraulic conductivity of frozen soils. Canadian Geotechnical Journal **11**(4): 647-650.

Wong, L.C., and Haug, M.D. 1991. Cyclical closed-system freeze-thaw permeability testing of soil liner and cover materials. Canadian Geotechnical Journal, **28**(6): 784-793.

Yang, Y., Lai, Y., and Chang, X. 2010. Laboratory and theoretical investigations on the deformation and strength behaviors of artificial frozen soil. Cold Regions Science and Technology, **64**(1): 39-45.

2. Measuring pore-water pressure in partially frozen soils: theory and technical requirements

2.1 Introduction

There will be no geotechnical challenges during freezing and thawing or issues with pore ice development in soils if water does not occupy the pores of the soil. Engineers are interested in applied stresses (positive and negative pressures) to evaluate resistance and deformations of materials. Therefore, when water is present in the soil, it is important to first measure and analyze pore-water pressure within these soils to correctly understand their mechanics under applied loads and thermal gradients.

When a saturated coarse-grained soil freezes, the pore space gradually infills with ice; hence, its hydraulic and mechanical behavior changes due to the phase change of the pore-water into ice. The ice matrix increases the apparent cohesion and tensile strength and reduces compressibility and hydraulic conductivity of the soil and therefore the soil's behavior becomes more like a cemented soil. This analogy guides one to adapt the knowledge of measuring pore-water pressure in cemented soils for use in partially frozen soils. The challenges in measuring pore-water pressure in partially frozen soils are associated with:

1. Low hydraulic conductivity in the partially frozen state
2. Continuity and availability of the unfrozen water phase

3. Thermal effects
4. Existence of two solid phases (ice and soil grains)
5. Time and temperature dependency of the ice matrix stiffness
6. Melting of the ice phase under increase of effective stress or pore-water pressure
7. Ice formation under decrease of pore-water pressure in supercooled pore-water

This chapter outlines the theoretical support for a reliable technique and development of an instrument to measure pore-water pressure and its distribution in partially frozen soils in the laboratory, as well as, design of a Filter-less Rigid Piezometer (FRP) to implement these theories. The testing and measured results of the FRP are presented in the next chapter. Three conditions are assumed in the current research:

1. Soil temperatures are maintained close to, but below, 0^{o}C. It ensures a sufficient amount of unfrozen water exists in the partially frozen soil to satisfy the continuity of the water phase.
2. The applied total pressures are kept low, within the range of interest for geotechnical engineering applications. In this case pressure melting is minimal.
3. Laboratory prepared specimens with degree of saturation greater than 98% ± 2% are studied.

To address the challenges in measuring pore-water pressure in partially frozen soils, first the lessons learnt from measuring pore-water pressure in unfrozen soils are reviewed. Then, technical requirements for measuring pore-water pressures in partially frozen soils in the laboratory are discussed. The concluding remarks of these two sections are then used to guide the design and fabrication of Filter-less Rigid Piezometer (FRP) which is presented later. The small size of the sensing tip of the FRP allows measuring pore-pressure distribution at small intervals within the thin freezing or thawing fringes, which are 1 mm to 20 mm thick. This enhances understanding of the phenomenon occurring at this scale, as well as, enables measuring hydraulic gradients and material properties required for future analytical modeling. Further, it allows measuring pore-water pressure distribution within specimens (not only at their top or bottom) under various

loading, thermal, and drainage conditions to evaluate their constitutive and strength behavior in terms of effective stresses. The testing of FRPs and interpretation of the measured pore-water pressures are presented in chapter 3.

2.2 Lessons from measuring pore-water pressure in unfrozen soils

The analogy between freezing of pore-water that cements soil particles and transforms the soil into a rock-like material leads to adapting the knowledge of measuring pore-water pressure in cemented soils and rocks for use in partially frozen soils. Therefore, the rigidity requirements for the pore-water pressure measuring systems in cemented soils are adapted for the design of the FRPs. Further, compressibility of pore-fluid in soils is reviewed and new insights into total compressibility of pore fluids are presented. These insights aid interpretation of the measured pore-water pressures, as well as guide the selection of the fluid to be used in the piezometer (piezometer fluid). Moreover, the piezometer fluid is regarded as a "hydraulic fluid" and knowledge from machinery hydraulics are adapted to assist with its selection and specific details regarding the volume and geometry of the interface of the piezometer fluid and pore-fluid in the soil. It is further discussed that use of a filter can delay and alter the pore-pressure response of the piezometer, reduce its reliability, add to its flexibility, and cause loss of hydraulic connection between the piezometer fluid and the pore fluid in the partially frozen soil. This understanding aids the design of the FRP which is presented later.

2.2.1 Measurement of pore-water pressure in unfrozen soils

Since 1856 when Henry Darcy first introduced hydrogeology via conducting experiments on water flow through sand using standpipes in column tests (Bobeck 2004; Bobeck 2006; Darcy 1856) and since 1907, when installation of the first field standpipe in the Waghad dam (in India) was documented to check the phreatic surface (Penman 2002) for geotechnical evaluation of the dam, much advancement has been made to the design, manufacturing, and installation of piezometers, as well as to the interpretation of the measured data. Development of piezometers and methods for

measuring pore-water pressure and suction are reviewed by several authors (Bartholomew et al. 1987; Croney and Coleman 1960; Daehn 1963; Fredlund and Rahardjo 1993; Penman 2002; Peters and Long 1981; Ridley 2003). Commonly used methods for measuring pore-water pressure in geotechnical engineering are detailed by Dunnicliff and Green (1993). A relatively new technique using tensile strength of water has recently been used in suction probes (Guan and Fredlund 1997; Meilani et al. 2002; Ridley and Burland 1993; Ridley and Burland 1999; Zhang et al. 2008). Tensile strength of liquids was first measured by Berthelot (1850) and it is closely related to cavitation pressure (vapor pressure) and the fluid-solid interface characteristics (Ridley 2003). Mechanism of cavitation and the generation of tension in liquids have been reviewed elsewhere (Arakeri 1979; Sun et al. 2008; Trevena 1984; Washio et al. 2008). To the author's best knowledge, in all of the previous works, filters have been used to separate pore-water pressures from total pressures and the interface of the pore-fluid and the piezometer fluid (fluid inside the piezometer) is at or within the filter. Further, recent advancements emphasize on the rigidity of piezometers to correctly measure pore-water pressures. Later, it will be discussed how the removal of a filter and using miniature fiber optic sensors increases rigidity of the FRPs.

2.2.2 Transmission of pressure states in unfrozen soils

Several authors studied pressure transmission in soils (Barberis 1965; Biot 1956; Biot 1962; Gibson and Henkel 1954; Mayer and Habib 1955; Paton and Semple 1960). Theoretically, pressure states applied to a medium will transmit with the speed of mechanical waves (sound) in that medium. In a fully saturated soil contained within rigid boundaries, it is expected that pore-water pressures transmit with the speed of sound across the pore-water phase in the soil. In soils, pore-water flows under hydraulic gradients and therefore stress transmission is delayed when a volume of pore-water should be transferred to transfer the new state of the stresses and reach equilibrium. Barberis (1965) studied transmission of pressures in soils by conducting triaxial tests on sand, silt, and clay and concluded:

(1) Pressure states do not propagate instantly

(2) Propagation behavior depends on the permeability of the tested material: the lower the permeability, the greater the time needed to reach an equilibrium state of pore-water pressures throughout the sample

(3) The propagation speed varies directly with the change in pressure ($\Delta \boldsymbol{u}$) between the pressure applied on the top face of the sample and the previous internal water pressure

(4) Stable conditions are reached in a shorter time for positive (compressive) $\Delta \boldsymbol{u}$ than for negative $\Delta \boldsymbol{u}$

Further, he proposed an interpolation curve for pressure propagation in fluid filled soils:

$$\log \boldsymbol{u} = \log(\boldsymbol{u_\alpha} - \boldsymbol{\alpha}.\boldsymbol{t}) + \boldsymbol{e^{-\beta t}} \log \left(\frac{\boldsymbol{u_0}}{\boldsymbol{u_\alpha}}\right) \tag{2-1}$$

In which $\boldsymbol{u}$ is the pore-pressure after time $\boldsymbol{t}$, and $\boldsymbol{u_0}$ is the initial pore-water pressure in the sample. Barberis (1965) provided graphs to estimate $\boldsymbol{\alpha}$, $\boldsymbol{\beta}$, and $\boldsymbol{u_\alpha}$. Dunnicliff and Green (1993) summarized time lag effects on pore-pressure response of piezometers which depend to the pore-water volume transfer required to transfer the pressures. They also reviewed advantages and limitations of various geotechnical instruments and emphasized that 'reliability' is maximized by using the 'simplest instrument' that will do the measurement. Later, it will be discussed how the removal of the filter simplifies FRPs and increases their 'reliability', as well as reduces 'response time' when measuring pore-water pressures using FRPs.

2.2.3 Significance of rigidity of piezometer in correctly measuring pore-water pressures

A saturated soil consists of soil grains and water. If there are no soil grains, water will carry the entire load (like a ship floating on water). If there is no water, the soil skeleton will carry the entire applied load. Pore-pressure equations evaluate what portion of the load will be carried by the water phase when water is present and has not escaped from the voids between the soil grains. Knowledge of the pore-water pressure is essential to assess the 'flow' of water through a porous

material and to predict the 'effective stress' that controls its resistance and deformation. Therefore, measurement and having methods for estimating the pore-water pressure response to the applied loads are desirable. Piezometers were developed to measure these in-situ pore-water pressures. Pore-pressure equations, on the other hand, provide the estimation methods. Skempton (1948b) presented the first pore-water pressure equation for saturated unfrozen soils:

$$\boldsymbol{\Delta u = \Delta\sigma_3 + A(\Delta\sigma_1 - \Delta\sigma_3)} \tag{2-2}$$

Skempton (1954) further expanded Equation (2-2) for saturated and unsaturated unfrozen soils:

$$\boldsymbol{\Delta u = B[\Delta\sigma_3 + A(\Delta\sigma_1 - \Delta\sigma_3)]} \tag{2-3}$$

and:

$$\boldsymbol{\frac{\Delta u}{\Delta\sigma_1} = \bar{B} = B\left[1 - (1 - A)(1 - \frac{\Delta\sigma_3}{\Delta\sigma_1})\right]} \tag{2-4}$$

Where:

$\boldsymbol{\Delta u}$ = the excess pore-water pressure due to changes in principal stresses, $\boldsymbol{\Delta\sigma_1}$ and $\boldsymbol{\Delta\sigma_3}$

A, **B**, and $\boldsymbol{\bar{B}}$ are the Skempton's pore-water pressure parameters

In the transition from soil to rock, as the contacts between the grains grow, the contacts eventually reach diameters equal to the grain diameter. At this point, the pores vanish and the compressibility of the skeleton equals the compressibility of the solid phase (Figure 2-1). Hence, with growth of the solid phase, it carries a larger portion of the applied loads during undrained loading.

The "fluid substitution formula", relates the dry or drained bulk modulus $\boldsymbol{K}$ to the undrained (or saturated) modulus $\boldsymbol{K_u}$ by:

$$\boldsymbol{K_u = \frac{K}{1 - \alpha B}} \qquad \text{Gassmann (1951)} \tag{2-5}$$

Where:

B = Skempton's pore-pressure parameter (Berryman 2002; Carroll 1980)

α = the Biot-Willis total volume effective-stress coefficient (Berryman 2002; Biot and Willis 1957)

It can be seen that $\boldsymbol{K_u}$>$\boldsymbol{K}$. The added 'rigidity' in undrained loading is due to pore fluid rigidity that also contributes to the total stiffness of the soil mass. Further, this added rigidity depends on Skempton's pore-pressure parameter (**B**). The stress transfer between each phase depends on their relative stiffness. A flexible piezometer allows the release of pore-pressure and contributes to softening the fluid phase. In this case, the measuring device alters the quantity being measured. This effect is greater in cemented soils and rocks with stiff solid matrix as the matrix deformations under applied stresses do not closely follow the release or dissipation of pore-pressures to compensate for the released pressure within the liquid phase. This effect on pore-water pressure is more significant when the volume of unfrozen water available in the soil is small.

Wissa (1969) studied the effects of the rigidity of the measuring equipment on pore-water pressure response in cemented-soils during undrained shear using triaxial cell. He suggested an extension to the Skempton's pore-pressure equation (Skempton 1954) to incorporate the effects of the compressibility of the measuring equipment:

$$\boldsymbol{B} = \frac{\boldsymbol{\Delta u}}{\boldsymbol{\Delta \sigma}} = \frac{1}{1 + \boldsymbol{n}\frac{\boldsymbol{C_w}}{\boldsymbol{C_{sk}}}}$$ Bishop and Eldin (1950) and Skempton (1954) (2-6)

$$\boldsymbol{B} = \frac{\boldsymbol{\Delta u}}{\boldsymbol{\Delta \sigma}} = \frac{1}{1 + \boldsymbol{n}\frac{\boldsymbol{C_w}}{\boldsymbol{C_{sk}}} + \left(\frac{\boldsymbol{V_l}}{\boldsymbol{V_0}}\right)\left(\frac{\boldsymbol{C'_w}}{\boldsymbol{C_{sk}}}\right) + \left(\frac{\boldsymbol{C_l} + \boldsymbol{C_M}}{\boldsymbol{C_{sk}V_0}}\right)}$$ Wissa (1969) (2-7)

$\boldsymbol{C_w}$= the compressibility of the pore fluid

$\boldsymbol{C_{sk}}$= the compressibility of the mineral skeleton

$\boldsymbol{n}$= the porosity of the soil

$\boldsymbol{V_l}$= the volume of fluid in the pore-water pressure measuring lines (the volume of fluid in pipes and connections)

$\boldsymbol{V_0}$= the total volume of the test specimen

$\boldsymbol{C'_w}$= the compressibility of the fluid in the pore-water pressure measuring lines

$\boldsymbol{C_l}$= the compressibility of the pore-water lines which is equal to the change in internal volume of the lines per unit change in pressure

$\boldsymbol{C_M}$= the compressibility of the pore-pressure transducer which is equal to the change in volume for a unit change in pressure (i.e. required volume transfer of liquid to transfer unit pressure)

Wissa (1969) observed that for uncemented-soils the compressibility of the skeleton exceeds 10^{-3} cm^2/kgf (approximately 98 MPa^{-1}) under normal consolidation pressures. He observed the errors were less than 2% when comparing the theoretical pore-pressures (Equation (2-6)) with those obtained using either a null indicator or electric transducer and Equation (2-7). However, in cemented soils (such as soils stabilized using cement or lime), heavily over-consolidated soils, and dense sands at high consolidation pressures, Wissa (1969) reported that the compressibility of the soil skeleton can approach 10^{-4} cm^2/kgf (approximately 980 MPa^{-1}). In this case, the error in measuring pore-pressures can be greater than 15% when using a mercury null indicator and less than 7.5% when using an electric transducer. Wissa (1969) also noted the measurements are 'highly sensitive to leakage' (i.e. release of pore-pressure due to loss or transfer of pore-water).

To increase the accuracy of measuring pore-pressures in cemented-soils, Wissa (1969) suggested:

1. To use a transducer with low flexibility (compressibility of transducer less than $1.6 \times 10^{-5} cm^2/kgf$ or approximately 6.13 GPa^{-1})
2. To increase the volume of the test specimen, V_0 (it is not always feasible: it increases the time for consolidation because of the increased drainage path. It also requires

shearing specimens at a slower strain rate to ensure equalization of pore-water pressures during the test)

3. To decrease the volume of liquid in the pressure lines by reducing the length and diameter of the lines (total volume of liquid in the pore-pressure lines should be less than 3% of the pore volume in the test specimen)
4. To use a no-leak set up (by sealing the test specimen in a 0.04-cm thick rubber membrane and using no-volume change, low leakage valves in the pore-pressure lines)
5. To ensure saturation by measuring the pore-pressure response at several applied backpressures while keeping the effective consolidation pressure constant
6. To apply high consolidation pressure to prevent lateral surface drainage during the early stages of undrained shear (lateral surface drainage affects the stress-strain and strength behavior)

They reduced the errors to less than 1% when the first and the third recommendations were followed.

The analogy of pore-water turning into ice in freezing soils to cement a soil provides guidance to enhance our knowledge about measuring pore-pressure in partially frozen soils. Therefore the recommendations given by Wissa (1969) are used for design and testing of Filter-less Rigid Piezometer. In partially frozen soils with low hydraulic conductivity and small volume of available unfrozen pore-water, a 'rigid piezometer' is required to accurately measure changes in pore-pressures. A 'rigid piezometer' requires only a very small pore-fluid volume transfer to measure the pressures. The designed FRP requires only a volume transfer of approximately 416 $\mu m^3/kPa$ which is about 300 times less than the volume transfer required in the best electrical pressure sensors reported by McKim et al. (1976). The authors did not find other published work reporting volume change of the sensors in the literature pertaining to measurement of pore-water pressures in soils at subzero temperatures.

2.2.4 Rigidity of the piezometer fluid and pore-water

Even a small volume 'air bubble' significantly alters the compressibility of the pore fluid. The role of the piezometer fluid is to transfer pore-pressures to the transducer without affecting the pressures. The term *'hydraulic fluid'* is used in mechanical engineering and refers to the medium through which power is transferred. Hydraulic machines work more efficiently if the hydraulic fluid has 'low compressibility'. Other major properties of the hydraulic fluid for power transfer and control are 'fast air release' and 'low foaming tendency'. Air in a liquid can be in the form of '***dissolved air***' or '***entrained air***' (air bubbles of various sizes and foam). Totten et al. (1997) reviewed air entrainment and release in hydraulic fluids.

If there is no air in the liquid, the compressibility of the liquid is equal to its pure substance compressibility (primary compressibility). In contact with air, some of the air dissolves into the liquid or comes out of solution owing to thermal or pressure variations; this adds to the compressibility of the liquid (added secondary compressibility). However, at any specific pressure and temperature, only a limited amount of air can dissolve in a liquid. Therefore, the part of the entrained air that remains as air bubbles within the liquid follows the gas law and its volume changes when subjected to pressure or temperature changes. The pressure within air bubbles is in equilibrium with pressure in the liquid and the volume change of these air bubbles add to the compressibility of the liquid (added tertiary compressibility). Free air that can have independent pressure of the liquid is treated as an independent phase when considering the mechanics of a multi-phase medium.

The added secondary compressibility can be calculated using formulas given by Bishop and Eldin (1950) and Schwab and Köhler (2003) and it increases the compressibility of air-water mixture by approximately two orders of magnitude (Fredlund and Rahardjo 1993). Based on Boyle's law and Henry's law of solubility, Bishop and Eldin (1950) gave 'additional compressibility' of the pore-liquid that is operative until all of the free air is dissolved in water. Based on the work of Bishop and Eldin (1950), Schwab and Köhler (2003) expressed the compressibility of the pore air-water mixture as:

$$\boldsymbol{\beta = S\beta_w + \frac{1 - S + hS}{P}} \tag{2-8}$$

$\boldsymbol{\beta}$: Compressibility of air-water mixture (1/kPa)

$\boldsymbol{\beta_w}$: Compressibility of water (1/kPa)

$\boldsymbol{S}$: Degree of saturation

$\boldsymbol{h}$: Henry's volumetric coefficient of air solubility (Approximately 0.02 cm^3 of air per 1 cm^3 of water at room temperature)

$\boldsymbol{P}$: Environment pressure (absolute pressure, kPa)

To estimate the compressibility associated with the added tertiary compressibility, the ideal gas law can be used. The compressibility of an ideal gas is controlled by its absolute pressure and is independent of temperature:

$$\boldsymbol{\frac{PV}{T} = nR \Rightarrow V = \frac{nRT}{P}} \quad \text{ideal gas law} \tag{2-9}$$

$$\boldsymbol{\Delta\beta = \frac{1}{V} \times \frac{\partial V}{\partial P} = -\frac{1}{V}\frac{nRT}{P^2} = \frac{-P}{nRT} \times \frac{nRT}{P^2} = -\frac{1}{P}} \tag{2-10}$$

In which:

$\boldsymbol{\Delta\beta}$: Added tertiary compressibility in Pa^{-1}

$\boldsymbol{V}$: Volume of gas in m^3

$\boldsymbol{P}$: Absolute pressure of gas in Pa

$\boldsymbol{T}$: Temperature of gas in K

$\boldsymbol{n}$: Number of moles of gas

$\boldsymbol{R}$: Universal gas constant = 8.314472 $J \cdot K^{-1} \cdot mol^{-1}$

At 1 atmosphere pressure (101.325 kPa) the compressibility of air is about 9.87×10^{-6} Pa which is four orders of magnitude larger than that of water (4.6×10^{-10} Pa as given by Domenico and Mifflin (1965)). Therefore, air bubbles that do not dissolve in the fluid dramatically increase the compressibility of the gas-water mixture. Even though tertiary compressibility has the most effect on the total compressibility, it was not considered by Bishop and Eldin (1950) and Schwab and Köhler (2003).

The amount of entrained air in a liquid depends on the method of air entrainment, the method of measurement, the temperature of the liquid, and the applied pressure (Davidson and Amick 1956; Rowand Jr et al. 1973). Magorien (1980) reviewed the problems and sources of air contamination in hydraulic systems and provided guidelines to keep air out of hydraulic systems. Magorien (1980) emphasized to seal properly, use volume to flow ratio greater than 3, de-gas, use bleed points, use backpressure, and limit the amount of the flow. The guidelines are used in designing of FRPs.

Vegetable oils generally have less primary compressibility than mineral oils and can have compressibility close to that of water (Skinner 1918). Where a fluid of exceptionally high bulk modulus is required, mercury can be used as a hydraulic fluid in small, sealed systems. The isothermal bulk modulus of pure mercury at 20^{o}C and zero pressure is 25.1 GPa as compared to 2.18 GPa for water. Mercury and water are the only liquids whose bulk modulus is known with great accuracy (Hayward 1970). A detailed investigation comparing compressibility of mineral oil, water, and other hydraulic fluids, as well as, optimization of hydraulic fluids for use as 'piezometer fluid' is beyond the scope of this research and remains for future research.

In a saturated soil, some of the 'liquid water' turns into 'water vapor' during the stress wave transition period of an unloading scenario. Figure 2-2 shows how liquid water can turn into water vapor through reduction of ambient pressure at constant temperature. Further, dissolved air in water may come out of solution (release) when its pressure is reduced. Water vapor and the released air can create a 'gas bubble'. The result will be a more 'compressible' fluid. Further, this

'gas bubble' reduces the hydraulic conductivity of the soil for fluid flow and hence volume transfer of water required to transfer the new stress state is delayed (De Boer 2000; De Boer and Kowalski 1995; Schwab and Köhler 2003; Smeulders and Van Dongen 1997). The water vapor bubbles (or water vapor in the humid air bubble) may partially turn into liquid water after the wave transition period. The amount of water vapor as 'gas bubble' in pore-water depends on the vapor pressure of water, which is a thermodynamic property (depends on temperature and pressure). During loading, more of the water vapor turns into liquid water and hence increases the rigidity of the liquid, as well as, hydraulic conductivity of the soil for water flow, which lead to faster pressure equalization. Cavitatation in water in the form of 'water vapor bubbles' can be observed with the naked eye when water pressure approaches approximately -90 kPa (Fredlund and Rahardjo 1993). In unsaturated soils, the volume of the air bubbles increases with a reduction of the stress (similar to ideal gas law), hence it reduces the hydraulic conductivity of the soil and increases pressure equalization time. Figure 2-2 illustrates the general pressure-temperature diagram of pure substances. Based on Figure 2-2, it is expected that the vapor pressure of water decrease with decreasing temperature and that when water turns into ice its vapor pressure should suddenly drop.

The discussion on compressibility and air entrainment within the piezometer fluid and pore-water provides a background for interpretation of the measured pore-water pressures and selection of piezometer fluid presented in this thesis.

2.2.5 The role of a filter in a piezometer

Based on the classic geotechnical engineering literature, the roles of filters in piezometers are to:

1. separate the pore-pressure from the total pressure in a soil, by transmitting pressure to the transducer only through the fluid in the measuring system;
2. maintain the rigidity of the piezometer by eliminating (or minimizing) air from entering the measuring system (in addition to using a filter, flushing of the piezometer fluid is also required before each reading in some piezometer systems); and,

3. independently measure pore-air and pore-water pressures in an unsaturated soil, only when air and water pressures differ significantly. Generally, “low air entry” and “high air entry” filters are used to independently measure pore-air and pore-water pressures, respectively.

Continuity and hydraulic connection between the pore-water in the soil and the fluid that transmits pressure to the sensing element (transducer) in the piezometer is necessary to measure pore-water pressure correctly (Richards and Gardner 1936; Stannard 1992; Toker et al. 2004). If the fluid in the piezometer is separated from the pore-water phase with a continuous air phase, piezometer measures pore-air pressures. If the fluid in the piezometer is separated from the pore-water phase with an occluded ‘air bubble’ (discontinuous air phase), theoretically, the stabilized pressure in the air bubble and the water phase are not significantly different (provided temperature and volume are maintained constant under static loading) and the piezometer should measure the correct pore-water pressure. In reality, the volume of air bubbles changes with temperature (gas law), therefore a small fluctuation in temperature would fluctuate the occluded gas volume and thus the measured pore-pressures. Schwab and Köhler (2003) emphasize that even minor ‘gas bubbles’ change the properties of the pore fluid dramatically; the ‘gas bubbles’ counteract variations of external pressures by volume changes, thus causing local transient micro flow, which is further delayed by low hydraulic conductivity. The general consensus is that when air bubbles are present in the measuring system, the pore-water pressure measurements are erroneous. The air phase generally becomes continuous as the degree of saturation of soil is reduced to less than approximately 85% (Corey 1957). When the degree of saturation is above 90%, the air phase becomes occluded, and air flow is only by diffusion through the pore-water (Matyas 1966). This research is focused on soil specimens where the degree of saturation is above 98%.

A high air entry filter (usually a porous ceramic disk or cylinder with very fine pore size) allows the passage of water, but prevents the ‘*flow of free air’* into the measuring system. Filters are rated by their air entry value: the maximum matric suction that can be maintained across their surface. Air entry value depends on the pore size of the filter and the surface tension of the liquid used in

the measuring system (piezometer fluid) and changes slightly with temperature. Commonly, Kelvin's equation is used to calculate a theoretical air entry value for regular piezometers (piezometers with filter). By adopting Kelvin's equation:

$$\boldsymbol{Uc} = (\boldsymbol{u_a} - \boldsymbol{u_{mo}})_{\text{FRP}} = \frac{2\boldsymbol{T_s}}{\boldsymbol{R_s}} \tag{2-11}$$

Where:

$\boldsymbol{Uc} = (\boldsymbol{u_a} - \boldsymbol{u_{mo}})_{\text{FRP}}$: air entry value of the FRP

$\boldsymbol{u_a}$: air pressure

$\boldsymbol{u_{mo}}$: mineral oil pressure (pressure of oil in FRP)

$\boldsymbol{T_s}$: surface tension of the oil in FRP

$\boldsymbol{R_s}$: radius of curvature of the oil contractile skin or the radius of the transfer tube

The '*theoretical air entry value*', as well as, the measurement techniques for measuring its value, assume that '*flow of free air*' is '*physically permissible*' through a capillary tube; if there is no free air, or when there is no space for the free air to enter, '*flow of free air*' is not permissible.

Even a high air entry filter does not prevent '*diffusion*' of air into the piezometer fluid. Preferential solubility of different 'gas molecules' of air in water shows the diffused air will not be in the form of 'air bubbles' (that is free air as in a liquid-gas mixture) but is in the form of "gas in solution". Findings of Krzyzanowski and Wislicki (1973) and Konishi et al. (1990) confirm that the total gas in solution is a summation of independent solution of each gas in the liquid, which their proportionality changes with pressure, temperature, viscosity, liquid type, and gas type (Krzyzanowski and Wislicki 1973; Staeck 1987). Therefore, one may argue that air bubbles observed in suction devices used for measuring pore pressures in unsaturated soils came from micro-flow of 'free air', water (that has diffused gas), and water vapor in flexible measuring systems. There is also a possibility that the gas in solution may be released (because of agitation or increase in temperature) and coalesce into 'gas bubbles'. This air accumulates behind the filter and

introduces an error in the measured pore-water pressures (Bishop and Donald 1961). In a '*flexible*' pore-pressure measuring system, large volumes of fluid transfer are required to transfer pressures and this can cause 'agitation', as well as, 'free air' and 'dissolved air' flow. Therefore, it is concluded that in a flexible piezometer, regardless of the air entry value of the filter, the filter only delays air entrapment within the piezometer. Further, when air bubbles are trapped in the measuring system, the filter prevents their release into the soil and the bubbles should be released by other means such as flushing techniques (Fredlund and Rahardjo 1993).

In current geotechnical engineering practice, a high air entry filter is generally used to increase the range of negative pore-pressures that can be measured by a flexible or a more rigid piezometer. Regardless of the air entry value of the filter, a lower limit of -90 kPa applies when attempting to measure the pore-water pressure in unsaturated soils directly, limited by cavitation of water. Fredlund and Rahardjo (1993) reported a value of -101 kPa as the lower limit when they used high air entry filters. This limitation of direct control or measurement of pore-water pressure is commonly overcome by applying an axis-translation to the specimen as described by Hilf (1956). By applying a positive pore-pressure, water is forced not to cavitate, hence a continuous water phase (and less compressible) transfers the pressures to the sensing element (transducer). General consensus is that axis translation does not alter the mechanics of the multi-phase soil. However, in reality, when negative pore-pressures are applied to the water phase, volumetric ratio of gas to liquid in the pore space of soil is increased, hence, hydraulic conductivity of the soil for liquid flow is decreased. These processes further shift the predicted from the measured values of quantities that depend on hydraulic conductivity (for example discharge of the liquids through an unsaturated porous media, amount of frost heave, and pore-water pressure response measured by a flexible piezometer). Later, Guan and Fredlund (1997) used cyclic pre-pressurization up to 12,000 kPa to dissolve potential cavitation nuclei in the water in a suction probe to increase the sustainable tension of the water. They reported that their suction probe was able to measure matric suction up to 1250 kPa with satisfactory accuracy. They still used a 100 kPa ceramic disk for their suction probe. They also reported that their previous methods of measuring suction in unsaturated

soils gave lower or higher measured pore-pressures than those measured by their new suction probe. Further, they reported that equalization time for the suction probe was smaller than other methods and was in the order of 1 to 18 hours, whereas other methods required 5 hours to 7 days. The difference between the measured pressure values, as well as, the required equalization time of the various methods compared in Guan and Fredlund (1997) indicates that the reported measured values indeed reflect the response of the measuring instrument itself to the applied pressures as compared to the actual pore-pressures. Further, according to Toker et al. (2004) the capacity of these new-generation of tensiometers (Guan and Fredlund 1997; Ridley and Burland 1993) is still limited by the air entry pressure of their porous stone, but not the vapour pressure of water. They still would need to collect and flush the entrapped air bubbles out of the system. High air entry disks with a maximum air entry value of 1500 kPa are available (Fredlund and Rahardjo 1993). It is concluded that in the new generation of tensiometers, a more rigid system is used owing to pre-conditioned water and use of a smaller volume system. This leads to a faster response time and more accurate measurements. However, this temporal rigidity is lost by air entrapment. Similar to flexible piezometers, the filter only delays air entrapment in these measuring systems.

If piezometer fluid does not freely flow out of the piezometer under gravity or applied loads, and is not replaced with free air, there will not be a need for a filter to measure pore-water pressure accurately. As long as, the piezometer fluid is in intimate contact with the pore-water and pore-pressure is transmitted to the transducer only through the fluid in the measuring system. Using a rigid piezometer fluid, rigid parts, and a rigid transducer helps to achieve this goal. In addition, removal of the filter adds to the simplicity of the piezometer. Having fewer parts to malfunction or alter the quantity being measured makes the piezometer more reliable. Moreover, the porous membranes (filters or high air entry disks) used for piezometers generally have finer pores than the soil; they have lower hydraulic conductivity, as well as, can produce sharper meniscus curvatures between the piezometer fluid and the pore fluids; both of these differences can delay and alter pore-pressure response of the measuring device thus impacting the measured pore-pressure response.

2.3 Measuring pore-pressures in partially frozen soils

In this section, first it is discussed that continuity of unfrozen water is required for continuity of stresses within the continuum, for fluid flow within the porous media, and for hydraulic connection between fluid phases in the multi-phase media and in the measuring system for correctly measuring pore-pressures.

In addition, practical and experimental significance of conducting experiments on soils at subfreezing temperatures close to $0^{\circ}C$ and at low confining pressures are outlined. Then, shortcomings of the current methods for measuring pore-water pressures in partially frozen soils are summarized. In conclusion, the critical requirements for developing a rigid miniature piezometer for measuring pore-water pressures in partially frozen soils are presented.

2.3.1 Significance of continuity of unfrozen water phase

Continuity of phases is mathematically required for continuity of the stress tensor across the boundary and within the body of the porous media (De Buhan and Dormieux 1996). For example, the expressions for the static equilibrium state of an infinitesimal element of the material assumes continuity in stresses (Fung 1977). Further, if the phases are not continuous, they do not meet the definition of a continuum and the stress in one phase is dependent on that of the other phase(s).

Moreover, continuity is required to ensure fluid flows under head and thermal gradients. Further, the ‘continuity equations’ of water flow are used together with ‘force equilibrium equations’ to establish constitutive equations for the porous media (for consolidation) and are valid only if the continuity of the unfrozen water holds.

In addition, continuity and hydraulic connection of fluid phases in the soil and in the measuring system is necessary to measure pore-pressures properly. The issues with existence of a continuous or discontinuous air phase between the fluid phases in the soil and in the measuring system were previously discussed.

The amount of unfrozen water in a soil at subzero temperatures is strongly related to the fines content of the soil and to the geometry of the pore space, whereas the continuity of the water films mainly depends on the distribution of the fines that fill the pore space between the coarser soil particles (Konrad 1999). Continuous unfrozen water exists at the ice to soil interface (Anderson and Morgenstern 1973; Jellinek 1967) and at the grain boundaries in the ice (Barnes et al. 1971b), even at very low temperatures. However, the thickness of the water film should be enough to allow water to flow. Figure 2-3 shows the relationship between unfrozen water content, soil type, salinity, and thickness of the water film in soils at sub-zero temperatures. Experimental data by Yong (1965) show the unfrozen water content is also related to the initial water content (Figure 2-3.c) but this effect is less for silt compared to clay. It is expected this effect would be even less for sand.

Continuity of the pore-water phase can be confirmed through using continuity of electrical conductivity or by independently changing applied pore-water pressure and observing the measured pore-water pressure within the soil. Electrical confirmation may be considered superior because of the response delays in pore-pressure. However, electrical conductivity indeed confirms ion conductivity within the water film, not the flow of water. Further, the electrical resistance depends on the thickness of water film, salinity, and temperature. It is recommended that response in pore-pressure in response to independently applied backpressures be used to monitor the continuity of the water phase and water flow in a frozen soil.

2.3.2 Significance of experiments at subfreezing temperatures close to 0^{o}C and at low confining pressures

The practical needs for conducting experiments on soils at subfreezing temperatures close to 0^{o}C and at low confining pressures were discussed in Chapter 1.

From an experimental point of view, conducting experiments at subfreezing temperatures close to 0^{o}C ensures sufficient unfrozen water exists in the partially frozen soil to satisfy the continuity of the water phase. Moreover, conducting experiments at low pressures assures pressure melting has

a minimal impact on the measured pore-water pressures. Therefore, these two conditions not only are of prime practical importance in frozen ground engineering but also provide favorable experiment conditions for reliably measuring pore-water pressures in partially frozen soils.

2.3.3 Previous research on measuring pore-water pressure in soils at subfreezing temperatures

Measurement of pore-water pressures in freezing, thawing, and to some extent in frozen soils has been the subject of interest from the beginning of modern research in these fields (Arenson and Springman 2005b; Beskow 1935; Chamberlain 1981; Czurda and Schababerle 1988; Eigenbrod et al. 1996; Fukuda 1982; Fukuda 1983; Henry 1990; Ingersoll and Berg 1981; Knutsson et al. 1985; Konrad 1989; Konrad and Morgenstern 1981; McKim et al. 1976; McRoberts and Morgenstern 1975; Miyata et al. 1994; Nishimura et al. 1994; Nixon and Morgenstern 1974; Ogawa et al. 1991; Penner 1957; Penner 1958; Ruckli 1950; Rydén 1985; Taber 1929; Williams 1966; Yanagisawa and Yao 1985).

In all of the literature on laboratory measurement of pore-pressures in freezing and thawing soils to date, except for the work by Eigenbrod et al. (1996), the pore-water pressures were measured not at the advancing freezing or thawing fronts or within the frozen soil, but at the base or top of the soil samples at a stationary front. Eigenbrod et al. (1996) used porous plastic filter rings at the perimeter of the sample, 4 mm spacing along the height of the sample, and used a 50% alcohol solution to transfer pressures to transducers, which were attached to the filters. They measured pore-pressures between +44 kPa to -22 kPa. The soil used in their study was a clayey silt with LL=30%, PL=16%, 90% passing sieve # 200, and clay size fraction = 18.5%. The cooling plate (at -2^{o}C) in their experiments was at the bottom and the warming plate (0.8^{o}C to 1.0^{o}C) was at the top of the sample. They used a sample that was 70 mm high and 46 mm in diameter. It is perceived that the clayey silt used in their experiment at subfreezing temperatures close to 0^{o}C would have had a large amount of unfrozen water. The shortcomings of the work by Eigenbrod et al. (1996) are that they did not provide data on the unfrozen water content or confirmation of the

continuity of the water phase in their experiments. Further, they used an antifreeze (alcohol) in contact with partially frozen soil to measure pore-water pressures. It is perceived that using antifreeze may alter the freezing and pore-ice content of the partially soil and hence altering the quantity being measured.

Experiments on measuring pore-water pressures in soils at subfreezing temperatures close to $0^{o}C$ is of special practical importance in stability assessment of soil masses in permafrost regions. Use of pore-water pressures brings the advantages of using effective stresses and effective stress material properties. For the first time, Arenson and his co-researchers (Arenson 2002; Arenson and Springman 2005b; Arenson et al. 2004) attempted to measure pore-water pressures in natural permafrost samples in a triaxial cell. Nater et al. (2008) then used their results in an effective stress analysis for slope stability assessments in Alpine permafrost soils. They reported high air contents in their natural permafrost samples. They used the term '*effective shear strength properties*' as the required geotechnical parameters and adopted triaxial data published by Arenson et al. (2004) and Arenson and Springman (2005a; 2005b). In these experiments, Arenson (2002) used 2.9 mm thick brass filters (pore diameters of 0.8 mm) to assure drainage from the top and bottom platens in the triaxial cell. He used PVC pore-water tubes to transfer pressures to two (electrical) pore-pressure transducers that were kept at room temperatures. Further, he used antifreeze as the fluid in the measuring system. He argued "the pores within a frozen soil sample contain air and unfrozen water, which do not have to be interconnected. Therefore, only total stresses can be measured. However, the pore system, such as transducers, tubes and platens, are filled with antifreeze, and therefore air pressures acting at the top and the bottom of the sample can be measured during a test".

In the majority of the literature reporting on pore-water pressure measurements in freezing, thawing, and frozen soils, the measuring system used in unfrozen soft soils were used with frozen soils, without any modifications. In some cases, the only modification was limited to replacing the piezometer fluid with alcohol or glycol, both of which alter the freezing of water and hence the

quantity being measured. In all cases, a filter or ceramic disk was used and little or no attention was given to the essential 'rigidity' and 'continuity' requirements as discussed in the current work.

It was generally assumed that when the ceramic disk or filter is initially saturated before the experiment, the hydraulic connection between the piezometer fluid and the pore-water is established. This cannot be guaranteed in a soil at subfreezing temperatures. Further, all of the previous devices used for measuring pore-water pressure in freezing, thawing, and frozen soils have large sizes which are not suitable for measuring pore-water pressure distribution across freezing or thawing fringes at fine intervals. Moreover, at their best, the previous works have used electrical transducers, which require significant volume transfer to correctly measure pore-pressures and can be affected by electromagnetic interferences. Correct and accurate measurements are the prerequisite for correctly understanding the physics of freezing, thawing, and frozen soils, measuring material properties and stress gradients, and developing more efficient design procedures. Hence, highly controlled boundary conditions (leak free and constant temperature environment) and rigid small-size measuring systems are required to properly measure pore-pressures in soils at subfreezing temperatures in the laboratory.

2.4 Need for a miniature piezometer for measuring pore-water pressures in partially frozen soils

Based on the background and earlier discussions, small size piezometers are required to measure pore-water pressures in partially soil to satisfy:

1. The rigidity requirements
    - Low volume measuring instrument
    - Low volume expansion and contraction
    - Low volume transfer to accurately measure pressures
    - Low volume ratio between fluid in the piezometer and specimen

- Low volume ratio between the volume of oil required to transfer the pressures and the water available as unfrozen pore-water
- Low disturbance in the thermal, flow, and stress fields in the specimen
- Prevent piezometer fluid from being replaced by air when not using a filter

2. The need for measuring pore-pressure distribution at small intervals within the freezing or thawing fringes, which are 1mm to maximum 20 mm thick. To better understand the phenomenon occurring within these fringes, as well as, to measure stresses and material properties required for future modeling
3. The need for measuring pore-water pressure distribution within specimens (not only at their top or bottom) under various loading, thermal, and drainage conditions to evaluate constitutive and strength behavior of partially frozen soils in terms of effective stresses
4. The need for accurate measurements in the laboratory testing on specimen sizes normally used in geotechnical laboratories

2.5 Design of the filter-less rigid piezometer (FRP)

The review and discussions presented in previous sections led to the design of a Filter-less Rigid Piezometer (FRP) presented here and subsequent testing of FRPs presented in Chapter 3. The patent for this method of measuring pore-pressures is pending.

In FRPs, the interface of the piezometer fluid with the pore-water is within the soil (not at or within a filter), using a droplet injected into the soil through the tip of the FRP. The volume of the droplet is slightly greater than 4 times the volume that is required to transfer the pressures. The droplet also provides an oil cap for the tip of the PEEKSil^{TM} tube which prevents flow of free air into FRP. The oil-saturated soil around the tip of the FRP can be regarded as a filter for the FRP; the filter of the measuring device would have the same pore-size, hydraulic conductivity, and deformation characteristics as the soil itself.

Implementation of the theories and technical requirements for measuring pore-water pressure in partially frozen soils is presented here as a Filter-less Rigid Piezometer. In the following,

advantages of miniature fiber-optic pressure sensors and mineral oil for use in FRP are outlined. Then, the design and fabrication of the FRPs are provided.

2.5.1 Miniature fiber-optic pressure sensors

Fiber-optic pressure sensors (FOP sensors) of various size have been used in many engineering and medical applications owing to their intrinsic insensitivity to electromagnetic interferences (EMI), electric passivity, corrosion resistance, and long-term reliability, which give them unique benefits over capacitive or piezo-resistive sensors (Pinet et al. 2007). FISO Technologies Inc. has developed a variety of miniature FOP sensors by using white-light cross-correlator (Belleville and Duplain 1995) to measure the absolute cavity length of FISO's Fabry-Perot fiber-optic gauges. The length of the Fabry-Perot cavity changes with pressure with a sensitivity of ~2 nm/kPa (Pinet et al. 2007). The diameter of the sensing tip of the transducers is 515 μm. This requires only a volume transfer of approximately 416 $\mu m^3/kPa$ to transfer the pressures. This method (Belleville and Duplain 1995) provides high accuracy and reliable measurements. Each fiber-optic gauge comes with a 7-digit ID number which allows the signal conditioners to recognize the type and calibration of the gage. No additional tuning or calibration is required (FISO 2010). FISO developed silicon-based FOP-MIV pressure sensor originally for medical applications. Two models of FOP-MIV sensor are available; BA and PK models. The shield of the fiber optic wire is sealed to the Fabry-Perot tip in the PK model; hence, this model is favored to build a leak-free piezometer. Figure 2-4 illustrates the schematic of fiber-optic sensor model FOP-MIV-PK used in this research and the principle of white-light Fabry-Pérot interferometry technology developed by FISO Technologies Inc. Table 2-1 lists specifications of this sensor and Table 2-2 summarizes the specifications of the UMI8 unit used for data logging the FOPs.

2.5.2 Mineral oil in FRPs

McKim et al. (1976) compared several piezometer fluids for use in a 200 mm diameter tensiometer for measuring pore-water pressures in soils at subfreezing temperatures in remote areas. They reported that a negligible change in calibration is associated with interfacial effects of

a non-water internal fluid and pore-water. The calibration results presented in Chapter 3 agrees with their finding. Owing to their specific design, McKim et al. (1976) encountered problems with de-airing silicone oil and chose to use glycol (an antifreeze liquid) as the piezometer fluid.

In the current study, mineral oil was chosen primarily because it does not freeze at temperatures down to -30^{o}C, does not affect the freezing temperature of water, is not toxic, and does not change the chemistry of pore-water for the purpose of this research (for example as compared to alcohol or glycol). In addition, mineral oil improves the reliability of the measurements as a 'hydraulic fluid' owing to its high lubricating, low total compressibility, and fast air release properties compared to water. Table 2-3 lists some 'thermodynamic properties' of mineral oil and water as pure substances. The term 'mineral oil' is a generic term. The values marked with an asterisk (*) do not reflect the exact value of the property of the specific mineral oil that was used in this research (white mineral oil with Chemical Abstracts Service Registry Number 8042-47-5). They are reported for comparison only. The mineral oil used in this research was provided by Fisher Scientific and their manufacturer did not have the requested thermodynamic properties. Some physical and chemical properties of mineral oils are summarized by Godfrey and Herguth (1995).

The advantages of considering piezometer fluid as a hydraulic fluid were discussed earlier. Oils have long been the preferred *'hydraulic fluid'* in hydraulic machinery owing to 'low total compressibility', 'fast air release', 'low air entrainment', 'high lubricating properties', 'low freezing temperature', and 'low chemical reaction with container walls'.

Total compressibility as a summation of primary, secondary, and tertiary compressibilities was discussed earlier. In a study comparing flow of air bubbles in water and two lightweight mineral oils, Shollenberger et al. (2002) reported that average volumetric fraction of air bubbles in water were approximately 1.5 times that of air entrained in the light mineral oils at slow gas flow rates (approximately 10% air bubble in mineral oils as compared to about 15% air bubbles in water, on average). Davidson and Amick (1956) also compared air entrainment in water and in mineral oils and reported the volumes of 'static bubbles' were proportional to the surface tension and were

independent of the gas-flow rate at slow rates. The surface tension of water is about twice that of mineral oil (Table 2-3) and therefore it is expected to have approximately twice the volume of static air bubbles in water compared to mineral oil.

Approximately, 6% to 12% volumetric air can dissolve in mineral oil compared to 2% in water (Table 2-3). Owing to higher 'solubility' of air in mineral oil, the air in solution has a higher tendency to 'stay in solution' under agitation and thermal fluctuations when the volume of air is lower than the air saturation of the liquid.

Yamaguchi (1980a) compared the delay time to initiate cavitation (the time required for gas to come out of solution and appear as air bubbles that can be seen by the naked eye) in hydraulic fluids for stepwise reduction in pressure. He generated air bubbles using the 'shearing method' described by Yamaguchi (1980b) and found the delay time for water-glycol is approximately 10 times more than that of paraffinic mineral oil. The paraffinic oil had 8.8% dissolved air compared to only 2.2% dissolved air in water-glycol. The delay time for tap water with 2.5% dissolved air was 5 to 8 times more than that of paraffinic oil. The cavitation delay time is the time required for gas to come out of solution and create a bubble, '*if it must come out of solution to reach a more stable state*', and affects the '*response time*' when measuring pore-pressures during an unloading step. The mineral oil responds approximately 10 times faster than water-glycol in reaching stable pressure during unloading when secondary compression exists. This makes it more favorable as a piezometer fluid for measuring pore-pressures in partially frozen soils.

Even though the surface tension of mineral oil is about half of that of water, hence provides a lower air entry value as compared to water based on Kelvin's equation, and even though its primary bulk modulus is in the range of 60% to 90% of that of water (Table 2-3), it is still a superior 'piezometer fluid' compared to water as it improves rigidity and response time of FRPs:

1. It has approximately half the 'air entrainment' of water, hence has lower secondary and tertiary compressibility. Secondary and tertiary compressibility can increase the compressibility by 2 and 4 orders of magnitude, respectively.

2. It has lower vapor pressure (15 to 25 times less than that of water), hence can sustain higher negative pressures without cavitation.
3. Unlike water that requires pre-treatment (such as removal of impurities or pressurizing), untreated mineral oils can sustain large tensile stresses (Holl 1970; Nakai and Okino 1976; Washio et al. 1999; Washio et al. 2008). In one study, Nakai and Okino (1976) measured tensile stress in 10 untreated mineral oils used in journal bearings and reported tensile stresses up to -578 kPa.
4. It has 10 times faster air release and hence faster response time to reach equalization, when the air needs to come out of solution to reach a new thermodynamic equilibrium.
5. It has higher viscosity and thus is less prone to flow away from the tip of the FRP during micro-flow of fluids required to reach pressure equilibrium.
6. It provides a more rigid fluid to transfer the pressures in the measuring system, both in tension and compression, owing to its very low vapor pressure and high air solubility (3 to 6 times that of water).
7. It has high air solubility, hence, in '*nearly saturated soils where the amount of entrained air is small*', all of the entrained air would dissolve in the mineral oil (especially under backpressure) and no free air remains to contribute to the added secondary or tertiary compressibility. Further, if the amount of the dissolved air is less than the air saturation level of the mineral oil, the air has a tendency to stay in solution rather than '*coming out and going back into solution*' repeatedly with small fluctuations in pressure.
8. It has faster air release, hence, in '*unsaturated soils where the amount of entrained air is high*', if the air needs to come out of the oil so that the solution reaches a more stable thermodynamic state, it occurs approximately 10 times faster. This leads to faster response time. A droplet of oil provides a cap on the tip of the FRP, therefore, the interface of the piezometer fluid with the pore fluid is within the soil, not in the piezometer. Together with the rigid design of the FRP, this oil cap makes the flow of free air into the FRP physically impermissible. Futher, FRPs do not use a filter, therefore, the air released from solution will not be trapped inside the piezometer as entrained air.

9. It has high lubricating properties and hence less resistance in transferring pressures in PEEKSil^{TM} tube.

Mineral oils may have 'trace' solubility in water depending on their chemical formula. For the purpose of this research, it is assumed that heavy mineral oil is not soluble in water. A detailed investigation comparing compressibility and optimization of hydraulic fluids for use as 'piezometer fluid' is beyond the scope of this research and remains for future research.

2.5.3 Assembling of the filter-less rigid piezometer (FRP)

Guidelines by Wissa (1969) and Magorien (1980) were presented earlier and are used in the design of FRPs. The FRP presented here uses a fiber optic pressure sensor, mineral oil as the piezometer fluid, a PeekSil^{TM} tube, and low volume connectors to maximize the rigidity of the piezometer. A droplet of oil is created on the tip of the PeekSil^{TM} tube that is within the soil to provide intimate contact between the oil in FRP and unfrozen pore-water in the soil at subfreezing temperatures. The schematic of a FRP is shown in Figure 2-5. Forming uni-size droplets of high viscosity mineral oil on the tip of PeekSil^{TM} tubes ensures uniformity and continuity of fluid in the FRP. The droplet also provides an oil cap for the tip of the PEEKSil^{TM} tube which prevents flow of free air into the FRP. The volume of the droplet is about 4 times the volume required to transfer the pressures, which itself is a very small volume. The uni-size droplets are created by first applying a pressure to the oil between the two valves of FRP and then releasing the pressure into the soil specimen. Recommended droplet generating pressure is 200-300 kPa more than the maximum pressure the specimen would be tested at. This procedure should be repeated 4 times to ensure a proper volume of the droplet is available in the oil cap. The volume of the droplet also can be controlled by setting a constant flow rate on the syringe pump and injecting oil into the soil specimen for a controlled amount of time.

The design of FRP allows the sensing element (fiber-optic sensor) to be protected outside the testing cell and therefore the size of the probe that goes into the specimen is controlled only by the size of the selected PeekSil^{TM} tube. The PeekSil^{TM} tubes are high-quality tubes used for gas

chromatography. They provide a smooth internal surface (small resistance for oil flow), high rupture strength (several MPa), flexibility, chemically inertness, low thermal conductivity, and low thermal expansion coefficients. Two insulation boxes encapsulate the piezometers to minimize the effects of the ambient temperature fluctuations on the pore-pressure measurements. This design has the following advantages:

- Mineral oil used in the piezometer does not alter the freezing or thawing temperature of the soil and does not change phase at sub-zero temperatures down to -30^{o}C.
- Mineral oil provides a more rigid hydraulic fluid compared to water.
- The small diameter PeekSil^{TM} tubes (made from silica) impose minimal thermal and mechanical disturbance to the thermal and stress fields within the specimens.
- Minimal fluid volume transfer is required to transfer the pressures. It provides a rigid system with rapid response and reliable measurement of pore-pressure when little unfrozen water is available to transfer the pressures and hydraulic conductivity of the soil is low.
- The PeekSil^{TM} tubes can withstand high pressures without closing or undergoing excessive change in diameter.
- The cantilevered PeekSil^{TM} tubes are structurally flexible to follow soil deformations without closing up.
- The end tip of the PEEKSil^{TM} tube in the soil is surrounded by an uni-size droplet of oil to convey pore-pressures via intimate contact between piezometer fluid and unfrozen pore-water.
- The internal diameter of the PeekSil^{TM} tubes used in this research is 0.07 mm and can be selected in the range of 0.025 mm to 0.3 mm. FRP is a “filter-less” piezometer used for measuring pore-pressures in soils at subfreezing temperatures.
- The electrical and magnetic noises are avoided by using fiber-optic sensors.

- Fiber-optic sensors provide rapid response and require low fluid volume transfer to measure water pressure fluctuations. The pressure sensitivity of fiber-optic sensors is 2 nm/kPa (Pinet et al. 2007).

PEEKsil™ is polymer-sheathed fused silica tubing, developed by SGE Analytical Science Pty Ltd (SGE 2007), and is available in outside diameters of 1.59 mm, 0.79 mm, and 0.36mm. The sheathing polymer is PolyEther Ether Ketone (PEEK) that is mechanically strong. PEEKsil™ is used in applications where solvents must be pumped under high or low pressures with little flow resistance or possibility of contamination. Other uses of PEEKSil^{TM} tubes are in LC connecting lines, sample loops, and sample lines. The small size of the PEEKSil^{TM} tubes allows measurement of pore-water pressures at fine intervals, especially when studying ice lens formation in freezing soils. Table 2-4 lists some advantages of PEEKSil^{TM} tubing. Table 2-5 lists the parts used for fabricating one FRP. It should be noted that one syringe pump and one data logger also will be required to operate a set of FRPs.

2.6 Comparison of the pore-water pressure measurements using FRP and ordinary piezometers

Applicability of FRPs for measuring positive and negative pore-water pressures in a soil was confirmed via measuring pore-water pressures generated during shearing of a contractive and a dilative soil in triaxial testing, as well as, via measuring suction in an unsaturated soil.

2.6.1 Triaxial testing (comparison with electrical pressuremeter)

Three FRPs were installed within loose and dense sand specimens through the base of a triaxial testing apparatus (Figure 2-6). The specimens were sheared under undrained condition and the pore-water pressure response within the specimen and at its base were measured. Figure 2-7 shows photos of the two specimens after the tests. Figure 2-8 shows that the pore-water pressure response measured using FRPs (within and at the base of the specimens) coincide with the measured values using an electrical piezometer at the base of the specimens, in both positive and negative pore-

water pressures. For the dense sand specimen, Skempton pore-pressure parameters were $\boldsymbol{B}$= 0.96, $\boldsymbol{A_f}$ = -0.16, and $\boldsymbol{\bar{B}_f}$ = -0.15.

2.6.2 Suction in an unsaturated soil (comparison with tensiometer)

FRPs were used for measuring negative pore-water pressures in an unsaturated fine sand specimen. Grain size distribution of the sand used in this research is shown in Figure 2-9. A tensiometer model UMS T5-18 was used as the reference device. Figure 2-10 shows the tensiometer and datalogger used in this experiment. Suction was induced using a vacuum pump. The test results are shown in Figure 2-11. It is observed that the FRP and tensiometer give close results (difference less than 1 kPa) and show the same trend. More experiments using different soils and methods of inducing suction remain for future research.

2.7 Summary and conclusions

Lessons learned from measuring pore-water pressures in unfrozen soils and cemented soils, as well as, theory and technical requirements for measuring pore-water pressures in partially frozen soils were discussed. The concluding remarks of these discussions were then used to guide the design of a Filter-less Rigid Piezometer (FRP) presented in this chapter and subsequent testing of the FRPs and interpretation of the test results in the next chapter.

A flexible piezometer softens the pore fluid phase and hence alters the pressure being measured. Furthermore, in partially frozen soils where a small volume of unfrozen pore-water is available to transfer the pressures, rigid piezometers are required to accurately measure the pore-pressures.

Further insights into the governing role of tertiary compressibility of total compressibility of pore fluids were presented which were not considered in the previous soil mechanics literature. These considerations aid interpretation of the measured pore-pressures, as well as, guide the selection of piezometer fluid. Moreover, piezometer fluid was regarded as a “hydraulic fluid” and lessons learned from machinery hydraulics were adapted for the design of the FRPs.

The roles of filters in piezometers and conditions where a filter is not required, or should not be used, were discussed. The use of filter can delay and alter the pore-pressure response of the measuring device, reduce reliability, add to flexibility, and risk loss of hydraulic connection between the piezometer fluid and the pore fluid in soils at subfreezing temperatures. In FRPs, the interface of the piezometer fluid with pore-water is pushed into the soil, without having a filter in between, using a droplet injected into the soil through the tip of the FRP.

Continuity requirements of unfrozen water for continuity of stresses in continuum, fluid flow and constitutive equations, as well as, hydraulic connection between fluid phases in the soil and in the measuring system were reviewed. Further, practical and experimental significance of conducting experiments at subfreezing temperatures close to $0^{o}C$ and at low confining pressures were outlined.

The shortcomings of the current methods for measuring pore-water pressure in soils at subfreezing temperatures were summarized and the critical needs for developing a miniature piezometer for measuring pore-water pressure distribution in partially frozen soils were outlined. These measurements will be used to better understand the behavior of these soils as they freeze and thaw and when they are subjected to external loads. They also will be used to measure hydraulic conductivity and effective stress resistance and deformation material properties for future modeling.

The fundamental concepts discussed in this chapter enhance understanding and methods of measuring pore-pressures in multi-phase porous media.

2.8 Tables

Table 2-1. Specifications of FOP-MIV pressure sensor - Range R3 *(FISO 2005)*

Pressure range	−40 kPa to 1 MPa
Resolution	0.34 kPa
Accuracy	0.1%
Sensitivity thermal effect	0.15% /°C
Zero thermal effect	0.4 kPa /°C
Proof pressure	3 MPa
Operating temperature	−40°C to 50°C
Connector type	SC connector (other available)
EM/RF/MW susceptibility	Total immunity

Table 2-2. Specifications of UMI8 (FISO 2006)

Sampling rate	20 Hz
Switching time	150 ms
Averaging	1 to 500 samples
Precision	0.025% of full scale
Resolution	0.01% of full scale
Operating temperature	-20°C to 40°C
Communication	RS-232; USB
EM/RF/MW susceptibility	Total immunity

Table 2-3. Thermodynamic properties of mineral oil and water

Property	Heavy Mineral Oil	Water
Density (g/cc) @ 25^{o}C	0.8508 ± 0.0050 (Hamida 2006)	998.2 kg/m3 (Hamida 2006)
Kinematic viscosity (cSt) @ 40^{o}C	34.5	0.658
Air solubility (volumetric fraction)	CO_2: 0.841 @ 24-25^{o}C	CO_2: 0.759 @ 25^{o}C

Table 2-3. Thermodynamic properties of mineral oil and water

	O_2: 0.134 @ 24°C N_2:0.071 @ 22-22.5°C (Kubie 1927) * 6%-12% air (Blume 1976)* 8%-9% air (Godfrey and Herguth 1995)	O_2: 0.0283 - 0.0290 @ 25°C N_2: 0.0143 – 0.0150 @ 25°C (Seidell 1919) 2% air (Blume 1976)
Surface tension (mN/m) @ 25°C	34.3 ± 0.7 (Hamida 2006)	71.0 ± 1.4 (Hamida 2006)
Vapor pressure @ 57°C	n-Decane ($C_{10}H_{22}$): 1.3 kPa (Wilhoit et al. 1971) *	17.3 kPa (Wilhoit et al. 1971)
Vapor pressure @ 1°C	n-Decane ($C_{10}H_{22}$): 0.025 kPa extrapolated using Antonie constants given by Wilhoit et al. (1971) *	0.66 kPa (Wilhoit et al. 1971)
Tensile strength	For an untreated mineral oil: up to 578 kPa (Nakai and Okino 1976)	Untreated water 40-90 kPa Theoretical value: 50 MPa (Ridley 2003) Measured values: 25 MPa (static) (Briggs 1950) 1 MPa (dynamic) (Sedgewick and Trevena 1976) 13 MPa (dynamic) (Williams et al. 2005)
Bulk modulus of elasticity @ atmospheric pressure *[Isothermal bulk modulus of liquids is less than adiabatic (isentropic) bulk modulus (Hayward 1965)]*	(Adiabatic) 1.69 - 1.88 GPa @ 17.9°C for VG 46 mineral oil (Washio et al. 1994) * (Adiabatic) 1.57 – 1.83 GPA at 40°C for 4 paraffinic mineral oils (Mia and Ohno 2009)* (Isothermal) ~ 1.38 GPa @ 37.8°C for paraffinic mineral oil (Klaus and	(Isothermal) 2.15 GPa @ 16°C (Liu 2003) (Isothermal) 2.2 GPa @ 24°C (Bahadori and Vuthaluru 2009) (Isothermal) 2.17 GPa @ 25°C (Domenico and Mifflin 1965)

Table 2-3. Thermodynamic properties of mineral oil and water

	O'Brien 1964)*	
Isothermal bulk modulus of elasticity @ atmospheric pressure and 20°C Based on estimation method given by Hayward (1970) (±5% accuracy)	1.64 GPa	2.18 GPa

Table 2-4. Advantages of PEEKSil™ tubing (SGE 2007)

Robust Tubing	Pressure rated to 6000 and 10000 psi
Smooth Wall Surface	Exceptionally smooth surface, free of imperfections, which ensures excellent flow characteristics. Stainless steel, in contrast, has a very rough and pitted inner wall surface Far less likely to block compared to steel tubing
Solvent Compatibility	Effective pH range of 0-10, except for hydrofluoric acid
Inertness	Extremely low absorption
Precision of inside Diameter	± 1 micron to ± 5 micron
Inside diameter (I.D.)	25µm (± 1 micron) to 300µm (± 5 micron)
Ease of Connection	PEEKsil™ is inherently straight, but is very flexible (can be coiled), which makes connection between columns, detectors and injectors easier than with more rigid stainless steel tubing
Thermal conductivity	1.38 $Wm^{-1} K^{-1}$

Table 2-5. List of parts used for fabricating one FRP

Part/Model	Quantity	Manufacturer
Fiber-Optic Pressure sensor Model FOP-MIV-PK, range R3	1	FISO Technologies, Inc. http://www.fiso.com
PEEKSil™ Tube O.D.: 1.59 mm, I.D.: 0.07 mm, 10 cm long	1	SGE Analytical Science Pty, Ltd http://www.sge.com

Table 2-5. List of parts used for fabricating one FRP

Part/Model	Quantity	Manufacturer
O-ring for Fiber Optic cable, 1/16 in.	2	Swagelok http://www.swagelok.com
NTP brass union tee 1/16 in.	1	
NTP brass valve B-42F2, 1/8 in., 2500 psi	2	
NTP brass Zero Volume Reducing Union, 1/8 x 1/16 in.	6	
Steel tube, 1/8 in. O.D., 5 cm long	1	
Brass tube, 1/16 in. O.D., 1.5 cm long	2	

2.9 Figures

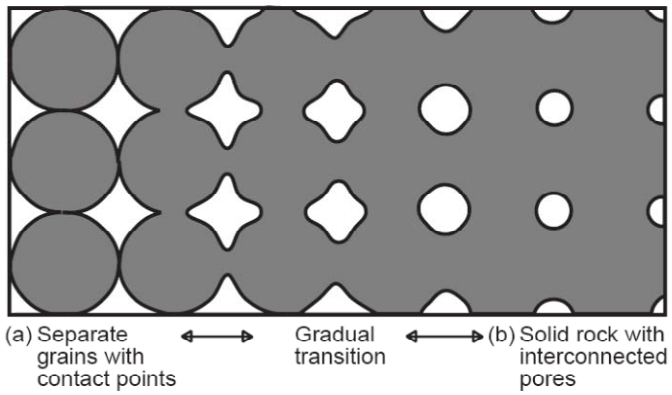

Figure 2-1. Schematic illustration of gradual transition in porous material from soils to rocks *(Lade and De Boer 1997)*

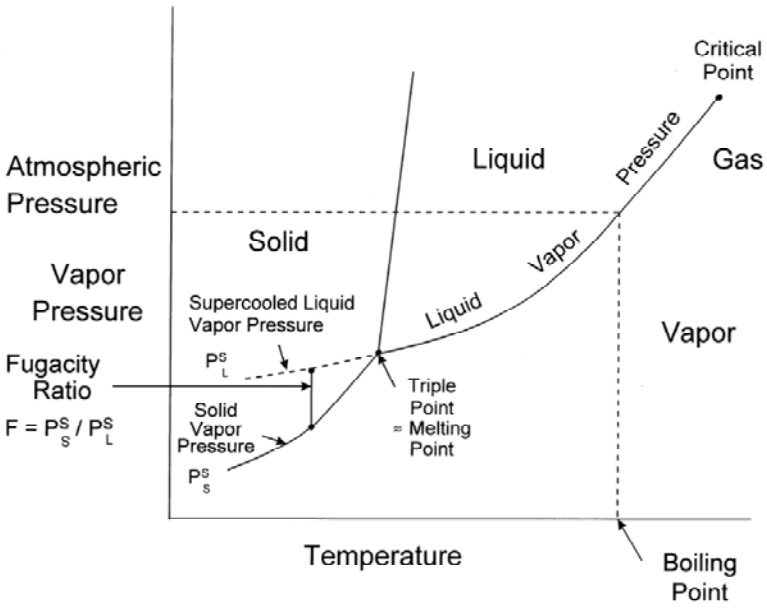

Figure 2-2. Pressure-temperature diagram of a pure substance (Sage and Sage 2000)

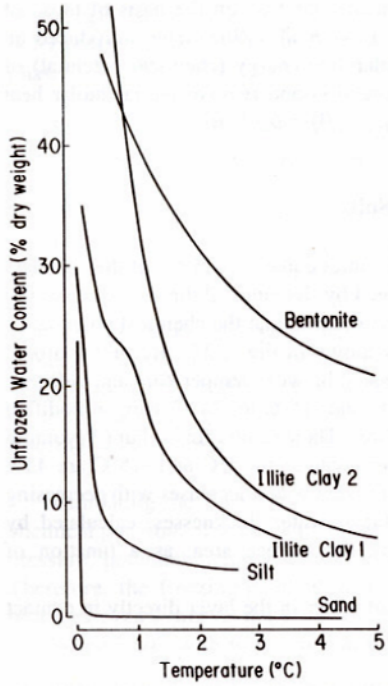

(a) Unfrozen water content for various soils at temperatures below 0°C (Williams 1988)

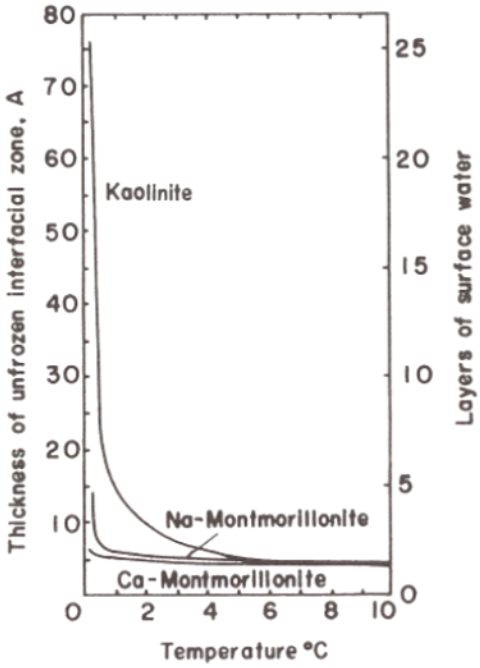

(b) Thickness of unfrozen water film versus temperature for three representative clays (Anderson and Morgenstern 1973; Nersesova and Tsytovich 1963)

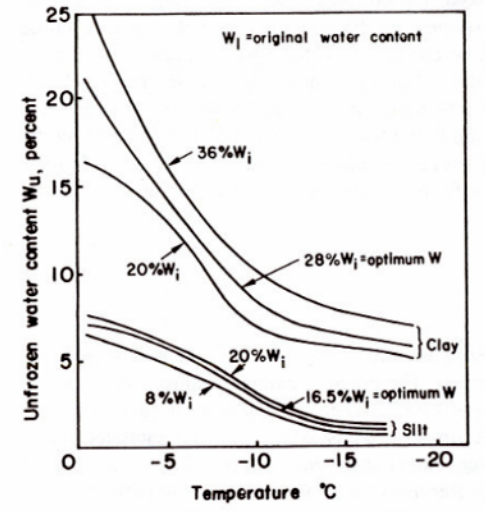

(c) Unfrozen water content in clay and silt at different initial water contents (Yong 1965)

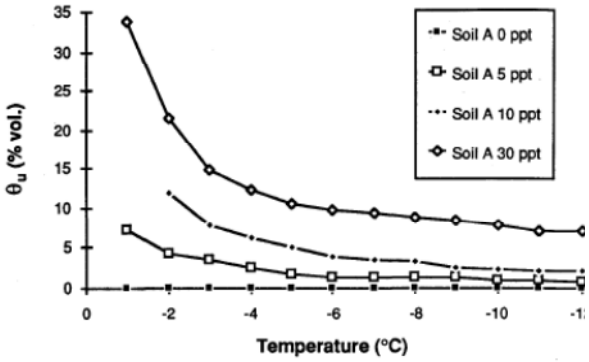

(d) Unfrozen water contents of fine uniform sand (soil A) at various degrees of salinity- TDR technique (Hivon and Sego 1995)

Figure 2-3. Unfrozen water in soils at subzero temperatures

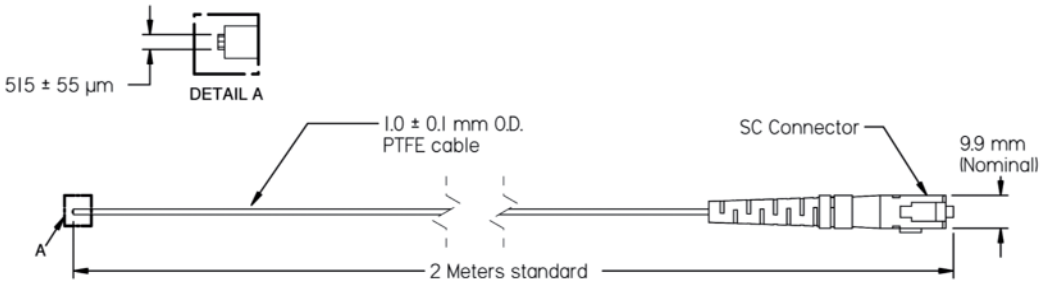

(a) Schematic of Fiber-optic sensor Model FOP-MIV-PK (FISO 2005)

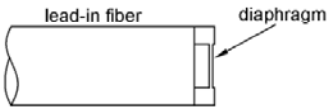

(b) Schematic of Fabry-Pérot cavity and flexible diaphragm (Cibula et al. 2009)

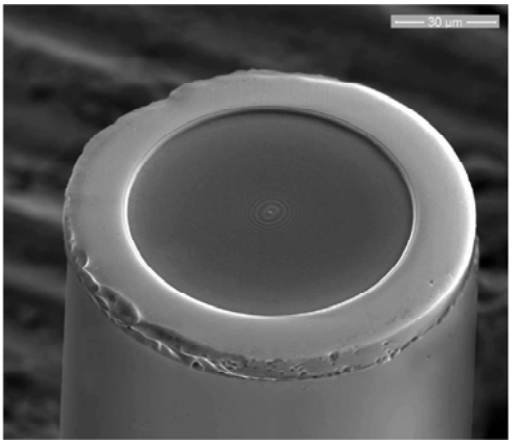

(c) Scanning Electron Microscope (SEM) photo of a typical fiber-optic sensor with a sensitivity of ~550 nm/bar (Cibula et al. 2009)

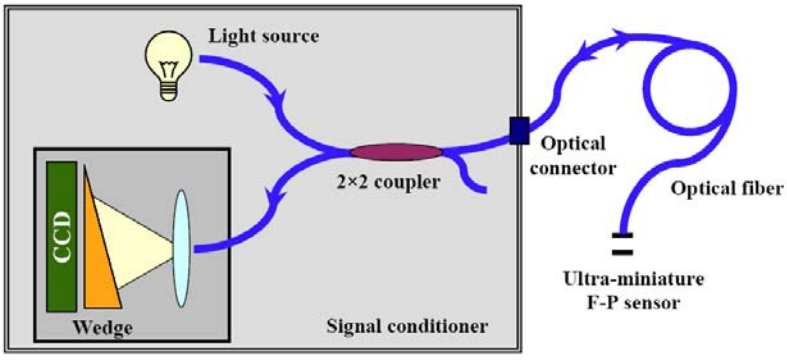

(d) Principle of operation of white-light Fabry-Pérot (F-P) interferometry technology (Pinet et al. 2007)

Figure 2-4. Schematic of fiber-optic sensor and principle of white-light Fabry-Pérot interferometry technology

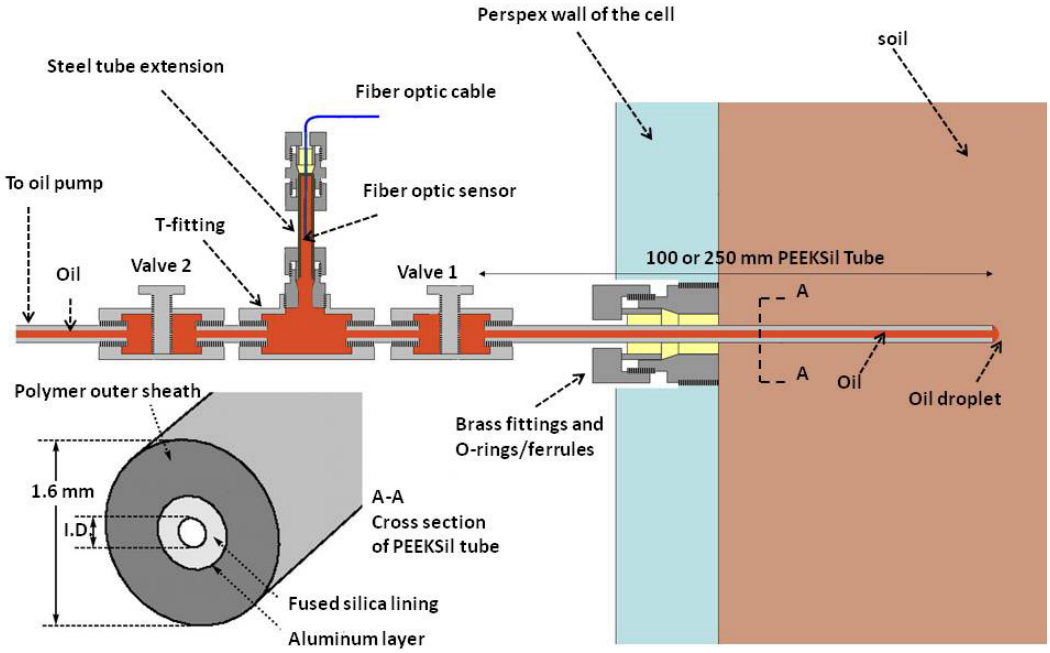

Figure 2-5. Schematic of a Filter-less Rigid Piezometer (FRP)-patent pending- cross section of PEEkSil™ tube is taken from SGE (2007)

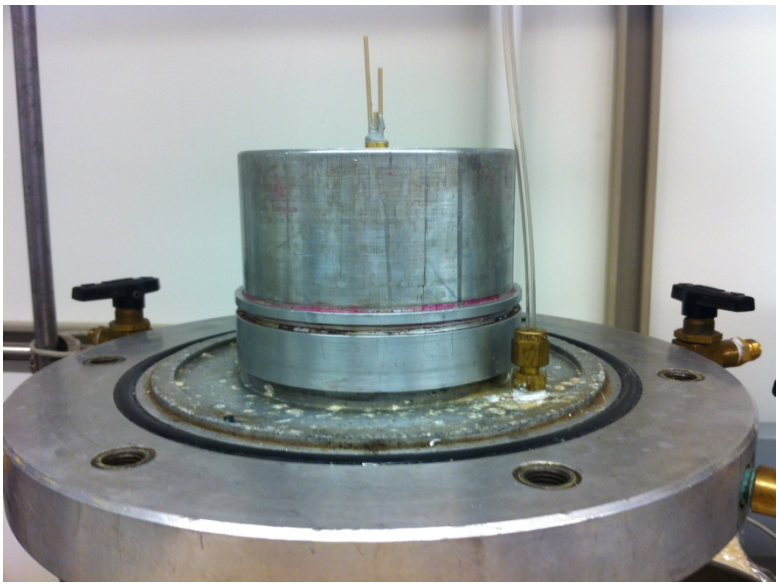

Figure 2-6. Feeding the tips of three FRPs into the specimen through the base of a triaxial apparatus

a- Bulging of the loose sand specimen

b- Development of visible shear plane in the dense sand specimen

Figure 2-7. Photos of the loose and dense sand specimens after undrained experiments

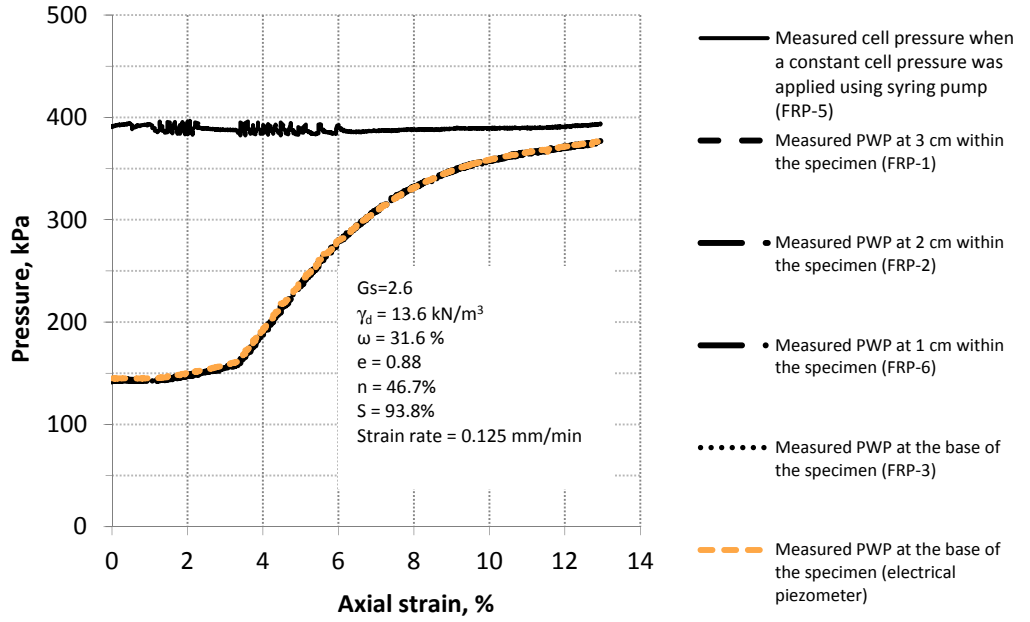

(a) Loose sand. The measurements coincide within ± 2 kPa difference.

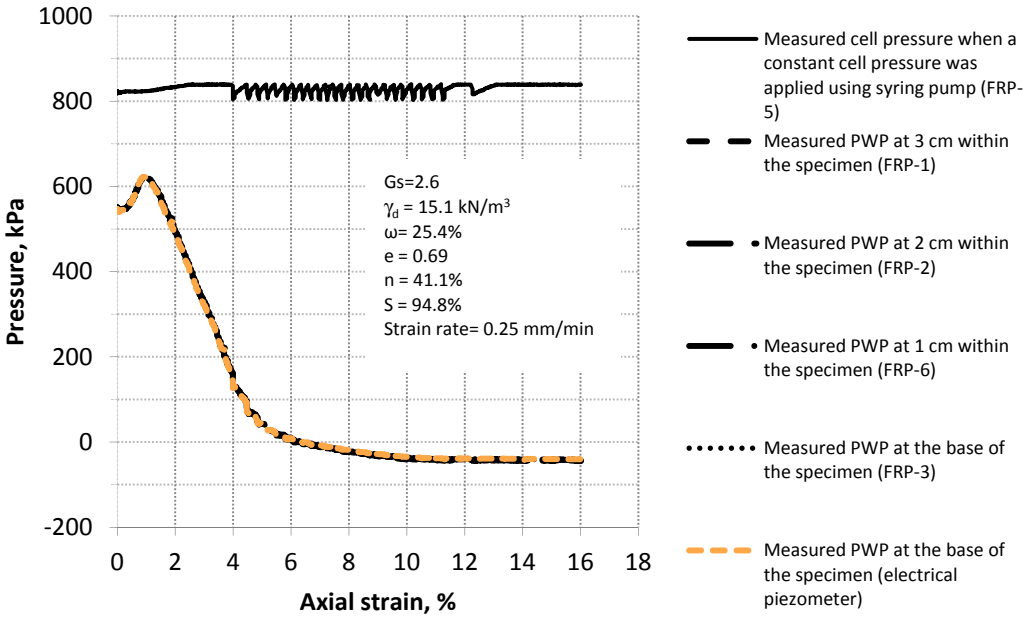

(b) Dense sand. The measurements coincide within ± 2 kPa difference.

Figure 2-8. Measured pore-water pressure response in loose and dense sand under undrained condition using FRPs and electrical piezometer

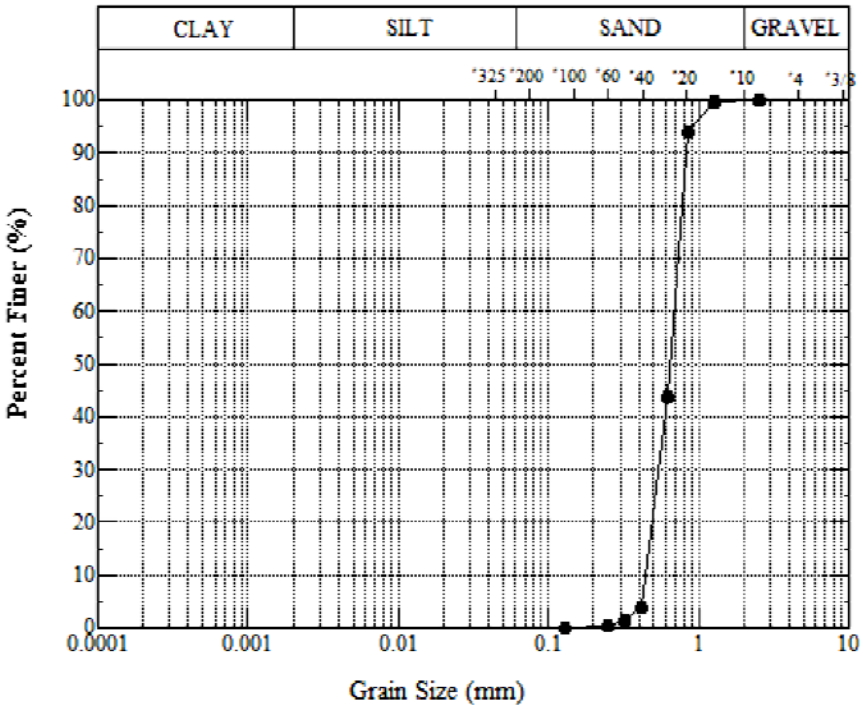

Figure 2-9. Grain size distribution of sand used in this research

Figure 2-10. Tensiometer model UMS T5-18 and Infield7 datalogger

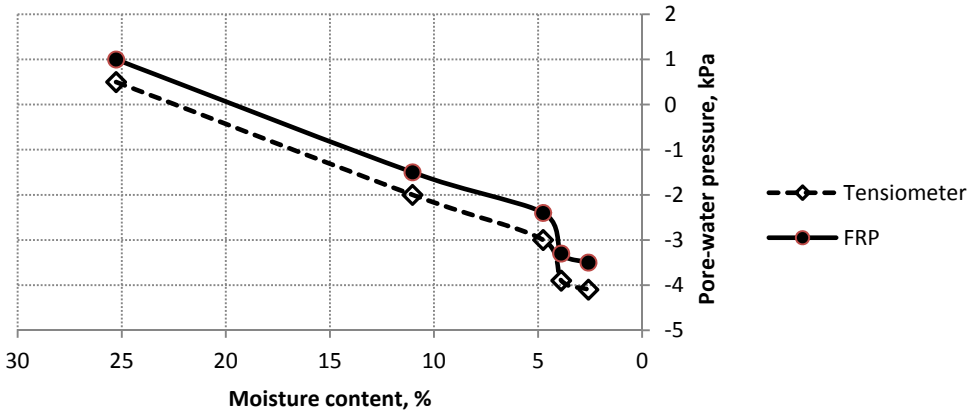

(a) Pore-water pressure as a function of moisture content in loose fine sand

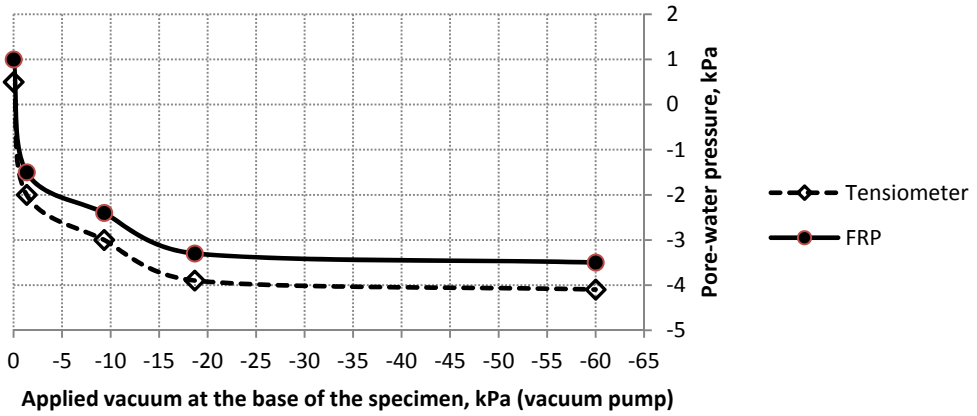

(b) Measured suction in loose fine sand as a function of the applied vacuum at the base

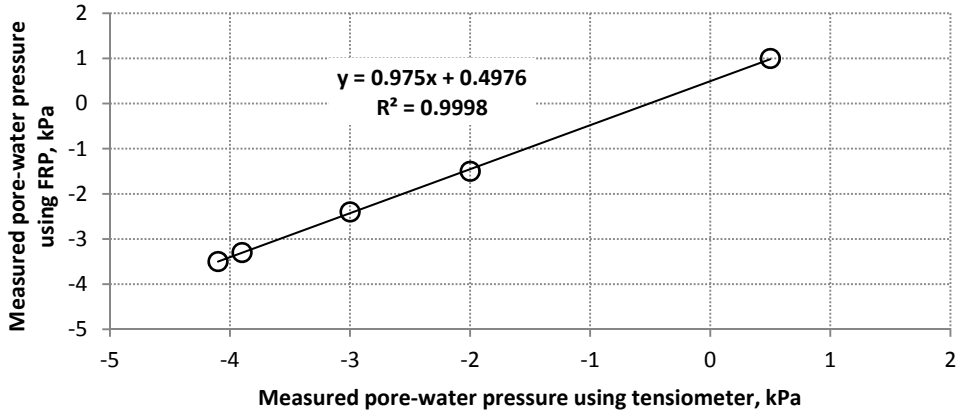

(c) Relationship between measured suction using Tensiometer and FRP

Figure 2-11. Pore-water pressure within a loose fine sand in response to applied vacuum at the base of the specimen

2.10 References

Anderson, D.M., and Morgenstern, N.R. 1973. Physics, chemistry, and mechanics of frozen ground : a review. *In* 2nd International Conference on Permafrost. National Academy of Science, Washington, D.C., Yakutsk, USSR, pp. 257-288.

Arakeri, V.H. 1979. Cavitation inception. Proceedings of Indian Academy of Sciences, Section C: Engineering Sciences, **2**(2): 149-177.

Arenson, L.U. 2002. Unstable alpine permafrost: a potentially important natural hazardPh.D. dissertation, Institute for Geotechnical Engineering Technische Wissenschaften ETH, Zurich, Switzerland.

Arenson, L.U., and Springman, S.M. 2005a. Triaxial constant stress and constant strain rate tests on ice-rich permafrost samples. Canadian Geotechnical Journal, **42**(2): 412-430.

Arenson, L.U., and Springman, S.M. 2005b. Mathematical descriptions for the behaviour of ice-rich frozen soils at temperatures close to 0 °C. Canadian Geotechnical Journal, **42**(2): 431-442.

Arenson, L.U., Johansen, M.M., and Springman, S.M. 2004. Effects of volumetric ice content and strain rate on shear strength under triaxial conditions for frozen soil samples. Permafrost and Periglacial Processes, **15**(3): 261-271.

Bahadori, A., and Vuthaluru, H.B. 2009. Prediction of bulk modulus and volumetric expansion coefficient of water for leak tightness test of pipelines. International Journal of Pressure Vessels and Piping, **86**(8): 550-554.

Baranov, I.J. 1964. Principles of geocryology. Technical Translation 1121. National Research Council of Canada.

Barberis, V. Transmission of pressure states in soils. *In* 6th International Conference on Soil Mechanics and Foundation Engineering, Montreal. 8-15 September, 1965 1965. University of Toronto Press, Montreal, pp. 156-160.

Barnes, P., Tabor, D., and Walker, J.C.F. 1971. The friction and creep of polycrystalline ice. Proceedings of the Royal Society of London, **A324**(1557): 127-155.

Bartholomew, C.L., Murray, B.C., Goins, D.L., and (U.S.), E.a.R.C. 1987. Embankment dam instrumentation manual. Bureau of Reclamation, Engineering and Research Center, Denver, Colorado.

Belleville, C., and Duplain, G. 1995. Fabry-Perot optical sensing device for measuring a physical parameter. US Patent 5,392,117. Institut National d'Optique and Ministere des Transports, Canada.

Berryman, J.G. 2002. Extension of poroelastic analysis to double-porosity materials: New technique in microgeomechanics. Journal of Engineering Mechanics, **128**(8): 840-847.

Berthelot, M. 1850. Sur quelques phénomenes de dilation forcée de liquids. Ann. De Chimie et de Physique, **30**: 232-239.

Beskow, G. 1935. Soil freezing and frost heaving with special applications to roads and railroads. *In* Swedish Geological Society, Series C, No. 375, 26th Year Book No. 3. Translated by J.O. Osterberg 1947, Technological Institute, Northwestern University, Evanston, Illinois.

Biot, M.A. 1956. Theory of propagation of elastic waves in a fluid-saturated porous solid. I. low-frequency range. The Journal of the Acoustical Society of America, **28**(2): 168-178.

Biot, M.A. 1962. Mechanics of deformation and acoustic propagation in porous media. Journal of Applied Physics, **33**(4): 1482-1498.

Biot, M.A., and Willis, D.G. 1957. The elastic coefficients of the theory of consolidation. Journal of Applied Mechanics **24**: 594-601.

Bishop, A.W., and Eldin, G. 1950. Undrained triaxial tests on saturated sands and their significance in the general theory of shear strength. Géotechnique, **2**(1): 13-32.

Bishop, A.W., and Donald, I.B. 1961. The experimental study of partly saturated soil in the triaxial apparatus. *In* 5th International Conference on Soil Mechanics and Foundation Engineering, Paris, France, pp. 13-21.

Blume, K. 1976. Problems caused by air in hydraulic systems (in German). Industrie-Anzeiger, **98**(16): 275-276.

Bobeck, P. 2004. Henry Darcy and the public fountains of the city of Dijon, Philadelphia, PA, pp. 37-50.

Bobeck, P. 2006. Henry Darcy in his own words. Hydrogeology Journal, 14(6): 998-1004.

Briggs, L.J. 1950. Limiting negative pressure of water. Journal of Applied Physics, 21(7): 721-722.

Carroll, M.M. 1980. Mechanical response of fluid-saturated porous materials. *In* 15th International Congress of Theoretical and Applied Mechanics. North-Holland Publication Co., Toronto, Canada, pp. 251-262.

Chamberlain, E.J. 1981. Frost susceptibility of soil, review of index tests. Monograph 81-2, U.S. Army Cold Regions Research and Engineering Laboratory (CRREL), Hanover, N.H., USA.

Chamberlain, E.J., Groves, E., and Perham, R. 1972. The mechanical behavior of frozen earth materials under high pressure triaxial test conditions. Géotechnique, **22**(3): 469-483.

Cibula, E., Pevec, S., Lenardili, B., Pinet, E., and Onlagi, D. 2009. Miniature all-glass robust pressure sensor. Optics Express, 17(7): 5098-5106.

Corey, A.T. 1957. Measurement of water and air permeability in unsaturated soil. Proceedings of the Soil Science Society of America Journal, **21**(1): 7-10.

Croney, D., and Coleman, J.D. 1961. Pore-pressure and suction in soil. *In* Conference on Pore-pressure and Suction in Soils. Butterworths, London.

Czurda, K.A., and Schababerle, R. 1988. Influence of freezing and thawing on the physical and chemical properties of swelling clays. *In* 5th International Symposium on Ground Freezing. A.A.Balkema, Nottingham, England, pp. 51-58.

Daehn, W.W. 1963. Development and installation of piezometers for measurement of pore-fluid pressures in earth dams. *In* Special Technical Publication No. 322. American Society for Testing and Materials (ASTM), Philadelphia, PA, United States, pp. 8-17.

Darcy, H. 1856. Les fontaines publiques de la ville de Dijon. Dalmont, Paris.

Davidson, L., and Amick, J.E.H. 1956. Formation of gas bubbles at horizontal orifices. American Institute of Chemical Engineers Journal, **2**(3): 337-342.

De Boer, R. 2000. Contemporary progress in porous media theory. Applied Mechanics Reviews, 53(12): 323-369.

De Boer, R., and Kowalski, S.J. 1995. Thermodynamics of fluid-saturated porous media with a phase change. Acta Mechanica, 109(1-4): 167-189.

De Buhan, P., and Dormieux, L. 1996. On the validity of the effective stress concept for assessing the strength of saturated porous materials: A homogenization approach. Journal of the Mechanics and Physics of Solids, **44**(10): 1649-1667.

Domenico, P.A., and Mifflin, M.D. 1965. Water from low-permeability sediments and land subsidence. Water Resources Research, **1**(4): 563-576.

Dunnicliff, J., and Green, G.E. 1993. Geotechnical instrumentation for monitoring field performance. Wiley, New York.

Eigenbrod, K.D., Knutsson, S., and Sheng, D. 1996. Pore-water pressures in freezing and thawing fine-grained soils. Journal of Cold Regions Engineering, **10**(2): 77-92.

FISO 2005. FOP-MIV pressure sensor datasheet, FISO Technologies Inc. Accessed online at www.fiso.com on Nov 10th, 2010.

FISO 2006. Universal multichannel instrument signal conditioner. FISO Technologies Inc.

FISO. 2010. FISO Technologies Inc, complete profile. Accessd online at http://www.ic.gc.ca/app/ccc/srch/nvgt.do?lang=eng&prtl=1&sbPrtl=&estblmntNo=123456192619&profile=cmpltPrfl&profileId=1861&app=sold on Nov 12, 2010 [online]. [cited Nov 12 2010].

Fredlund, D.G., and Rahardjo, H. 1993. Soil mechanics for unsaturated soils. Wiley, New York.

Fukuda, M. 1982. Experimental studies of coupled heat and moisture transfer in soils during freezing. *In* Contribution no. 2528 from Institute of Low Temperature Science, Hokkaido University, Sapporo, Japan, pp. 35-91.

Fukuda, M. 1983. The pore water pressure profile in porous rocks during freezing. *In* 4th International Conference on Permafrost. National Academy Press, Fairbanks, Alaska, U.S.A., pp. 322-324.

Fung, Y.C. 1977. A first course in continuum mechanics. Prentice-Hall, Englewood Cliffs, N.J.

Gassmann, F. 1951. Über die Elastizität poröser Medien (Elasticity of porous media). Vierteljahrsschrift der Naturforschenden Gesselschaft, **96**: 1-23. Translation available for download via "Stanford Exploration Project ". Accessed online on 28 Sep 2009 at http://sepwww.stanford.edu/sep/berryman/PS/gassmann.pdf.

Gibson, R.E., and Henkel, D.J. 1954. Influence of duration of tests at constant rate of strain on measured 'drained' strength. Géotechnique, **4**(1): 6-15.

Godfrey, D., and Herguth, W.R. 1995. Physical and chemical properties of industrial mineral oils affecting lubrication. Lubrication Engineering, **51**(6): 493-496.

Guan, Y., and Fredlund, D.G. 1997. Use of the tensile strength of water for the direct measurement of high soil suction. Canadian Geotechnical Journal, **34**(4): 604-614.

Hamida, T. 2006. Effect of ultrasonic waves on immiscible and miscible displacement in porous media. MSc Thesis, University of Alberta.

Hayward, A.T.J. 1965. Compressibility measurements on hydraulic fluids. Hydraulic Pneumatic Power, **11**(131): 642-646.

Hayward, A.T.J. 1970. How to estimate the bulk modulus of hydraulic fluids. Hydraulic Pneumatic Power, **16**(181): 28-32, 35-38, 40.

Henry, K.S. 1990. A case study of potential causes of frost heave. CRREL Special Report 90-9, U.S. Army Cold Regions Research and Engineering Laboratory (CRREL), Hanover, N.H., USA.

Hilf, J.W. 1956. An investigation of pore-water pressure in compacted cohesive soils. Ph.D. dissertation, University of Colorado at Boulder, Colorado, United States.

Hivon, E.G., and Sego, D.C. 1995. Strength of frozen saline soils. Canadian Geotechnical Journal, **32**(2): 336-354.

Holl, J.W. 1970. Nuclei and cavitation. Journal of Basic Engineering, Transactions of ASME, **D92**(4): 681-688.

Ingersoll, J., and Berg, R. 1981. Simulating frost action by using an instrumented soil column. Transportation Research Record, **809**: 34-42.

Jellinek, H.H.G. 1967. Liquid-like (transition) layer on ice. Journal of Colloid And Interface Science, **25**(2): 192-205.

Klaus, E.E., and O'Brien, J.A. 1964. Precise measurement and prediction of bulk-modulus values for fluids and lubricants. Transactions of American Society of Mechanical Engineers. Journal of heat transfer, **86**: 469-473.

Knutsson, S., Domaschuk, L., and Chandler, N. 1985. Analysis of large scale laboratory and in situ frost heave tests. *In* the 4th International Symposium on Ground Freezing A.A. Balkema, Sapporo, Japan, pp. 65-70.

Konishi, T., Baba, M., Deishi, S., and Takahashi, S. 1990. Diffusion mechanism of gases contained in oiles. 2nd report: study on diffusion of Nitrogen into/out of oil. Japanese Journal of Tribology, **35**(12): 1376-1383.

Konrad, J.-M. 1999. Frost susceptibility related to soil index properties. Canadian Geotechnical Journal, **36**(3): 403-417.

Konrad, J.M. 1989. Pore water pressure at an ice lens: its measurement and interpretation. Cold Regions Science and Technology, **16**(1): 63-74.

Konrad, J.M., and Morgenstern, N.R. 1981. The segregation potential of a freezing soil. Canadian Geotechnical Journal, **18**(4): 482-491.

Krzyzanowski, R., and Wislicki, B. 1973. Solubility of gases/air in mineral oils. (in Polish). Instytut Lotnictwa Prace, **53**: 45-63.

Kubie, L.S. 1927. The solubility of O2, CO2, and N2 in mineral oil and the transfer of carbon dioxide from oil to air. Journal of Biological Chemistry, **72**(2): 545-548.

Ladanyi, B., and Morel, J.-F. 1990. Effect of internal confinement on compression strength of frozen sand. Canadian Geotechnical Journal, **27**(1): 8-18.

Lade, P.V., and De Boer, R. 1997. The concept of effective stress for soil, concrete and rock. Geotechnique, **47**(1): 61-78.

Liu, H. 2003. Pipeline engineering. CRC Press.

Magorien, V.G. 1980. Keeping air out of hydraulic systems. Machine Design, **52**(18): 71-76.

Matyas, E.L. 1967. Air and water permeability of compacted soils. *In* Symposium on Permeability and Capillarity of Soils, Atlantic City.1966. American Society for Testing and Materials, pp. 160-175.

Mayer, A., and Habib, P. 1955. Note Sur Les Variations Des Sous-Pressions Dans Les Massifs A FàIble PerméAbilité. Géotechnique, **5**(2): 190 –193

McKim, H.L., Berg, R.L., McGaw, R.W., Atkins, R.T., and Ingersoll, J. 1976. Development of a remote-reading tensiometer/transducer system for use in subfreezing temperatures. *In* 2nd Conference on Soil-Water Problems in Cold Regions., Edmonton, Canada, pp. 31-45.

McRoberts, E.C., and Morgenstern, N.R. 1975. Pore water expulsion during freezing. Canadian Geotechnical Journal, **12**(1): 130-141.

Meilani, I., Rahardjo, H., Leong, E.-C., and Fredlund, D.G. 2002. Mini suction probe for matric suction measurements. Canadian Geotechnical Journal, **39**(6): 1427-1432.

Mia, S., and Ohno, N. 2009. Prediction of pressure–viscosity coefficient of lubricating oils based on sound velocity. Lubrication Science, **21**(9): 343-354.

Miyata, Y., Minami, Y., and Akagawa, S. 1994. Measuring unfrozen pore water pressure at the ice-lens forming front. *In* 7th International Symposium on Ground Freezing. A.A. Balkema, Nancy, France, pp. 157-162.

Nakai, M., and Okino, N. 1976. Tensile stress in journal bearings. Wear, **39**(1): 151-159.

Nater, P., Arenson, L.U., and Springman, S.M. 2008. Choosing geotechnical parameters for slope stability assessments in alpine permafrost soils. *In* 9th international conference on permafrost. University of Alaska, University of Alaska, Fairbanks, USA, pp. 1261-1266.

Nersesova, Z.A., and Tsytovich, N.A. 1966. Unfrozen water in frozen soils. *In* 1st International Conference on Permafrost, Purdue University, Lafayette, Indiana. 11-15 November 1963 1963. National Academy of Sciences, Washington, D.C., pp. 230-234.

Nishimura, T., Ogawa, S., and Fukuda, M. 1994. Effective stresses in unsaturated soils after freezing and thawing. *In* Proceedings of the 7th International Symposium on Ground Freezing, October 24, 1994 - October 28, 1994. A.A. Balkema, Nancy, Fr, pp. 121-128.

Nixon, J.F., and Morgenstern, N.R. 1974. Thaw-consolidation tests on undisturbed fine-grained permafrost. Canadian Geotechnical Journal, **11**(1): 202-214.

Ogawa, S., Nishimura, T., and Fukuda, M. 1991. Influence of freezing and thawing on suction of unsaturated soils. *In* 6th International Symposium on Ground Freezing. A.A. Balkema, Beijing, China, pp. 71–76.

Parameswaran, V.R. 1980. Deformation behaviour and strength of frozen sand. Canadian Geotechnical Journal, **17**(1): 74-88.

Paton, J., and Semple, N.G. 1961. Investigation of the stability of an earth dam subject to rapid drawdown including details of pore-pressure recorded during a controlled drawdown test. *In* Pore-pressure and Suction in Soils, Institution of Civil Engineers, England. 30 March 1960 1960. Butterworths, London, pp. 66-71.

Penman, A.D.M. 2002. Measurement of pore water pressures in embankment dams. Geotechnical News, **20**(4): 43-49.

Penner, E. 1957. Soil moisture tension and ice segregation. Highway Research Board, Washington, DC, Bulletin No. **168**: 50-64 (Also National Research Council, Canada, Division of Building Research, Research Paper 67).

Penner, E. 1958. Pressures developed in a porous granular system as a result of ice segregation, Highway Research Board, Washington, DC, Special Report No. **40**: 191-199 (Also National Research Council, Canada, Division of Building Research, Research Paper 81).

Peters, N., and Long, W.C. 1981. Performance monitoring of dams in Western Canada. *In* Water Science and Technology: Recent Developments in Geotechnical Engineering for Hydroprojects. ASCE, New York, NY, USA, pp. 23-45.

Pinet, E., Cibula, E., and Donlagic, D. 2007. Ultra-miniature all-glass Fabry-Perot pressure sensor manufactured at the tip of a multimode optical fiber. *In* Fiber Optic Sensors and Applications V, September 10, 2007 - September 12, 2007. SPIE, Boston, MA, United states, p. The International Society for Optical Engineering (SPIE).

Qi, J., and Ma, W. 2007. A new criterion for strength of frozen sand under quick triaxial compression considering effect of confining pressure. Acta Geotechnica, **2**(3): 221-226.

Richards, L.A., and Gardner, W. 1936. Tensiometers for Measuring the capillary tension of soil water. Journal of the American Society of Agronomy, **28**(5): 352-358.

Ridley, A.M. 2003. Recent developments in the measurement of pore water pressure and suction. Geotechnical News, **21**(1): 47-50.

Ridley, A.M., and Burland, J.B. 1993. A new instrument for the measurement of soil moisture suction. Géotechnique, **43**(2): 321-324.

Ridley, A.M., and Burland, J.B. 1999. Use of the tensile strength of water for the direct measurement of high soil suction: Discussion. Canadian Geotechnical Journal, **36**(1): 178-180.

Rowand Jr, H.H., Patula, R.J., and Sargent Jr, L.B. 1973. The evaluation of the air entraining tendency of fluids. Lubrication Engineering, **29**(11): 491-494.

Ruckli, R. 1950. Der Frost im Baugrund. Springer-Verlag, Vienna.

Rydén, C.G. 1985. Pore-pressure in thawing soil. *In* 4th International Symposium on Ground Freezing. A.A. Balkema, Sapporo, Japan, pp. 223-226.

Sage, M., and Sage, G. 2000. Vapor Pressure. *In* Handbook of property estimation methods for chemicals, CRC Press.

Schwab, R., and Köhler, H.J. 2003. Behaviour of near-saturated soils under cyclic wave loading. *In* Deformation Characteristics of Geomaterials. A.A. Balkema Publishers, Lyon, France, pp. 857-862.

Sedgewick, S.A., and Trevena, D.H. 1976. limiting negative-pressure of water under dynamic stressing. Journal of Physics D-Applied Physics, **9**(14): 1983-1990.

Seidell, A. 1919. Solubilities of inorganic and organic compounds. Van Nostrand, New York.

SGE 2007. PEEKSil™ tubing, SGE Analytical Science Pty Ltd. Accessed online at http://www.sge.com/uploads/Mq/1J/Mq1JWLIob1nMLVN6QSsYSw/PD-0230-Aw.pdf on July 20, 2007.

Shollenberger, K.A., Torczynski, J.R., and George, D.L. 2002. Gas distribution in air/water and air/oil bubble-column flows. *In* Proceedings of the 2002 ASME Joint U.S.-European

Fluids Engineering Conference. American Society of Mechanical Engineers, Montreal, pp. 641-648.

Skempton, A.W. 1948. The effective stresses in saturated clays strained at constant volume. *In* 7th International Congress for Applied Mechanics, pp. 378-392.

Skempton, A.W. 1954. Pore-pressure coefficients ***A*** and ***B***. Geotechnique, **4**(4): 143-147.

Skinner, S. 1918. Notes on lubrication [with discussion]. Proceedings of the Physical Society of London, **31**(1): 94-100.

Smeulders, D.M.J., and Van Dongen, M.E.H. 1997. Wave propagation in porous media containing a dilute gas-liquid mixture: Theory and experiments. Journal of Fluid Mechanics, 343: 351-373.

Staeck, D. 1987. Gases in hydraulic oils. (in German). Tribologie und Schmierungstechnik, **34**(4): 201-207.

Stannard, D.I. 1992. Tensiometers. Theory, construction, and use. Geotechnical Testing Journal, **15**(1): 48-58.

Sun, D.C., Wen, W., Zhiming, Z., Xiaoyang, C., and Meili, S. 2008. Theory of cavitation in an oscillatory oil squeeze film. Tribology Transactions, **51**(3): 332-340.

Taber, S. 1929. Frost heaving. Journal of Geology, **37**(5): 428-461.

Toker, N.K., Germaine, J.T., Sjoblom, K.J., and Culligan, P.J. 2004. A new technique for rapid measurement of continuous soil moisture characteristic curves. Géotechnique, **54**(3): 179-186.

Totten, G.E., Sun, Y.H., and Bishop Jr, R.J. 1997. Hydraulic fluids: foaming, air entrainment, and air release - a review. *In* International Off-Highway & Powerplant Congress & Exposition. SAE, Milwaukee, WI, USA, pp. 53-63.

Trevena, D.H. 1984. Cavitation and the generation of tension in liquids. Journal of Physics D: Applied Physics, **17**(11): 2139-2164.

Washio, S., Takahashi, S., Kanamitsu, M., and Yoshida, A. 1994. Measurement of thermodynamic quantities of mineral oil by laser interferometry. Proceedings of the Institution of

Mechanical Engineers, Part C: Journal of Mechanical Engineering Science, **208**(4): 267-274.

Washio, S., Takahashi, S., Uda, Y., and Sunahara, T. 1999. Observation of cavitation inception in hydraulic oil flow (in Japanese). Nihon Kikai Gakkai Ronbunshu, B Hen/Transactions of the Japan Society of Mechanical Engineers, Part B, **65**(633): 1643-1651.

Washio, S., Takahashi, S., Uemura, K., Iwamoto, T., and Ogata, T. 2008. Singular properties of flow separation as a real cause of cavitation inception. Proceedings of the Institution of Mechanical Engineers, Part C: Journal of Mechanical Engineering Science, **222**(4): 667-678.

Wilhoit, R.C., Zwolinski, B.J., and Estok, G.K. 1971. Handbook of vapor pressures and heats of vaporization of hydrocarbons and related compounds. Thermodynamics Research Center, Texas A&M University, College Station.

Williams, P.J. 1966. Pore-pressures at a penetrating frost line and their prediction. Géotechnique, **16**(3): 187-208.

Williams, P.J. 1988. Thermodynamic and mechanical conditions within frozen soils and their effects. *In* 5th International Conference on Permafrost. Tapir Publishers, Trondheim, Norway, pp. 493-498.

Williams, R.L., Williams, P.R., and Al-Hussany, A. 2005. The tensile strength of water as a function of temperature. *In* 2005 ASME Fluids Engineering Division Summer Conference. American Society of Mechanical Engineers, Houston, TX, United states, pp. 525-530.

Wissa, A.E.Z. 1969. Pore-pressure measurement in saturated stiff soils. Journal of the Soil Mechanics and Foundations Division, ASCE, **95**(SM4): 1063-1073.

Yamaguchi, A. 1980a. Cavitation in hydraulic fluids: Part 2. Delay time for stepwise reduction in pressure. Fluidics quarterly, **12**(3): 16-28.

Yamaguchi, A. 1980b. Cavitation in hydraulic fluids: Part 1. Inception in shear flow. Fluidics quarterly, **12**(3): 1-15.

Yanagisawa, E., and Yao, Y.J. 1985. Moisture movement in freezing soils under constant temperature condition. *In* 4th International Symposium on Ground Freezing. A.A. Balkema, Sapporo, Japan, pp. 85-91.

Yong, R.N. 1965. Soil suction effects on partial soil freezing. Highway Research Record, **68**: 31-42.

Zhang, M., Ng, C.W.W., and Chen, R. 2008. A suction probe for direct measurement of high matric suction. Yantu Gongcheng Xuebao/Chinese Journal of Geotechnical Engineering, **30**(8): 1191-1195.

3. Filter-less rigid piezometer for measuring pore-water pressures in partially frozen soils

3.1 Introduction

Measuring pore-water pressures in soils at subfreezing temperatures close to 0^{o}C is a major challenge due to phase change and uncertainties regarding continuity of liquid pore-water in these soils. Knowing how these pressures develop in a partially frozen soil will enhance our understanding of their behavior under applied loads, as well as, the behavior of soils during freezing and thawing. The theory and technical requirements for measuring pore-water pressure distribution in partially frozen soils and the design of the Filter-less Rigid Piezometer (FRP) for conducting these measurements in the laboratory are presented in Chapter 2. This chapter presents the testing of the FRP and testing equipments.

First, the testing equipment, specimen preparation procedure, and the calibration method are described. Then, effects of air-entrainment and de-saturation, pore-fluid temperature, and ambient temperature fluctuations on the interpretation of the measured pore-water pressures are studied. This is followed by examples of pore-water pressure response within a partially frozen soil at temperatures close to 0^{o}C and at low applied pressures within the range of interest for geotechnical engineering. Validity of the measurements and continuity of the unfrozen water phase are verified by applying different backpressures independent from the applied total pressures and measuring the pore-water pressure responses within the specimens. The partially frozen soil specimens in this

study are laboratory prepared saline sand specimens with degree of saturation above 98%. Extending the use of FRPs to other soil types and saturation levels and the study of the pore-water pressure response and stress transfer mechanism in partially frozen soils is beyond the scope of this research and remains for future research.

3.2 Materials and methods

3.2.1 Testing equipment

A modified Qiu and Sego cell (MQS cell) was used to calibrate the FR Piezometers and for measurements of pore-water pressures in both partially frozen and unfrozen specimens. The original Qiu and Sego cell is a large strain consolidation apparatus developed for research on mine tailings (Qiu and Sego 2001). The internal diameter of the cell is 10.16 cm and the specimen height can be up to 28 cm. The modifications consisted of using double O-rings to seal the specimen area from the air chamber at the perimeter of the loading piston; addition of the top drain for saturating the specimen, applying backpressures, and water intake and expulsion flow measurements using a syringe pump; mounting 8 RTDs and 5 FRPs through the cell wall; and improving thermal control and loading conditions. A paper-filter and a cloth-filter (to provide reinforcement for the filter paper) on top of the specimen prevent soil from moving into the top drain during consolidation and testing. The top porous stone is removed from the original design to allow for ease of saturating the specimen and thermal boundary control. Schematic of the MQS cell is illustrated in Figure 3-1.

Total stresses are applied to the specimen by changing the air pressure in the air chamber (Figure 3-1) and are controlled using two mechanical air pressure regulators. The use of two regulators provides enhanced control on the feed of air pressure from the compressor (less fluctuation). The backpressure is controlled using an ISCO pump model 500D (Teledyne Isco Inc. 2010). Table 3-1 summarizes specifications of this pump. Fluorescein dye is added to the pore-water used for specimen preparation and in the backpressure line to indicate if the water changes phase during testing. Use of Fluorescein dye as an indicator of phase change of pore-water in soils was first

described by Arenson and Sego (2006). The backpressure water is maintained at +0.5±0.1^{o}C using a separate temperature controlled bath.

A coil was placed around the cell wall and connected in series with the coolant line flowing to the bottom and top plates and this line was connected to a temperature controlled bath to maintain the specimen at the desired temperature during the experiments. The MQS cell and the instruments were all encapsulated in an insulated box to improve ambient temperature control. Krahn and Fredlund (1972) described a method for maintaining thermal fluctuations in the range of ±0.001^{o}C. Thermal control in the range of ±0.01^{o}C meets the current test program requirements.

3.2.2 Specimen preparation

Figure 3-2 shows the grain size distribution of the sand used in this research. It is the same material used as Soil A by Hivon and Sego (1995). Its physical, mechanical, and unfrozen water content as a function of salinity and temperatures were reported by Hivon and Sego (1995). Its grain size distribution is comparable to marine sands in the Beaufort Sea and similar to the sand reported on by Sego et al. (1982) and Sego and Chernenko (1984). Sand is an elastic material and is simple to work with, unlike clay and silt (due to their plastic behavior, ice lens formation, and ice structure). Further, sand-size particles are present in various mine tailings and their engineering behavior under conditions studied in this research is of practical significance for many engineering activities.

Saturated sand (boiled) was placed into the MQS cell using the fluviation technique. The saline pore-water was prepared by controlling the mass of NaCl (accuracy ±0.1 gram) and the volume of the de-aired distilled water (accuracy ± 50 ml) used for specimen preparation. The salinities are further controlled using a portable refractometer (Fisher Scientific. 2001). The accuracy of the refractometer used in this research is ± 1 ppt. De-aired distilled water was added (accuracy ± 0.1 ml) to compensate for water evaporated during boiling, whenever necessary, to maintain salinity at the desired level. To prepare a frozen saline sand specimen at desired temperature a rapid freezing and subsequent warming procedure was used which is described later in this section. As a routine

procedure in this study, the measuring system is calibrated at the beginning of each test and then the unfrozen specimen is consolidated to a desired level of effective stress before freezing the specimen. The measuring system is also calibrated at the end of each test for quality control purposes.

3.2.3 Calibration of the measuring system to account for the testing equipment compliance

Factory calibrations of FOP sensors are examined using an Omega portable pressure calibrator with built-in pressure pump model DPI 603 (OMEGA 2007). The accuracy of this calibrator is ± 0.75 kPa. An insulated box is used to minimize thermal effects. FOPs are zeroed to atmosphere before checking the factory calibrations.

The MQS cell is used to calibrate the FRPs and also for conducting pore-pressure measurements in the specimens. For calibration of the FRPs, the water level in the cell is kept above the sand specimen (FRPs are calibrated after the specimen is placed in the cell). FRPs are calibrated in loading and unloading by changing pressure in the air chamber. The whole system is thus calibrated which accounts for the testing equipment compliance, specimen preparation, and other boundary conditions. The system is calibrated twice: once with the top drain closed (case 1: rigid), and once with the top drain open (case 2). In case (2), the syringe pump is connected to the top drain and pressure is measured while it maintains a zero flow rate into the cell. In this case, the syringe pump is calibrated together with the rest of the instruments in the testing equipment, thus, accounting for the accumulated system imperfections. Further, the delivered backpressure on the specimen applied via the syringe pump is also calibrated using the same FOP that measures pressure in the air chamber by connecting that FOP to the bottom of the MQS cell. As all of the FRPs and the syringe pump are calibrated against ‘air chamber pressure’, all pressures are measured using the air chamber pressure as the reference.

The calibration of the FRPs, as well as, the response of the FRPs to independent change of total pressure (air chamber pressure) and backpressure are checked before and after each test to

evaluate the quality of the measurements and tightness of the system to water and air. Ambient temperature is also closely monitored and controlled. Further, clogging of the PEEKSil^{TM} tubes is evaluated by checking the flow of internal oil in the tubes before and after each test.

3.2.4 Air entry value of FRPs

Generally, Kelvin's equation (Thomson 1871) is used to calculate a theoretical air entry value for piezometers with filters (Dunnicliff and Green 1993; Fredlund and Rahardjo 1993). A new approach was used in this research to assess the air entry value of the FRPs based on the concept of 'permissibility of air entry' provided in Chapter 2. An FRP was connected to an air chamber such that the tip of the PEEKSil^{TM} tube was held upward and an oil droplet was generated on the tip of the FRP before applying 1 MPa air pressure. This pressure was maintained for two hours with 5 cycles of lowering pressure to approximately 200 kPa and then raising it to 1 MPa. Then, the FRP was connected to the bottom of a cylinder full of water and the oil was injected from the FRP into the water by applying oil pressure to the FRP through valve 2 (Figure 3-3). While the injected oil was rising to the surface of the water it was visually examined (with naked eye) for release of air bubbles.

3.2.5 Effects of air-entrainment and desaturation on the calibration of FRPs

First, FRPs were calibrated using only de-aired water in the MQS cylinder. Then a 1.5 cm air cap was placed between the water and the loading piston and the FRPs were calibrated again. The same experiment was conducted using hydraulic oil at temperatures above and below 0^{o}C.

Further, to evaluate the effects of desaturation on the measured pore-water pressures, a saturated sand specimen was placed in the cell and the FRPs responses were measured. First, a 1.5 cm 'water cap' was placed above the sand and a calibration was carried out. Then, the specimen was de-saturated by draining water from the specimen and then re-flooding the specimen with water. Volumetric air to water ratio was 0.23 after de-saturation. Volumetric change in the water content was measured by measuring the difference between volumes of the drained water and the water

required to fill the pore space in sand at the same effective stress level (80 kPa). Again, a 1.5 cm 'water cap' was placed above the desaturated sand and a calibration was carried out. The data logging was conducted using 5 second intervals to allow time for manual application of pressure in the air chamber. Effects of desaturation on 'pressure response' and 'pressure equalization time' of the specimen in both loading and unloading were studied using FRPs

3.2.6 Effects of pore-fluid temperature on the calibration of FRPs

There were concerns that the amount of the load transferred to the specimen is affected by the cell (or pore-fluid) temperature and that the calibration at a temperature above 0^{o}C might not be applicable for experiments at temperatures below 0^{o}C. To quantitatively investigate the effects of cell temperature, as well as, to be able to calibrate at subzero temperatures, a glycol-water mix was used in the MQS cell.

In the first set of the experiments, only glycol-water mix was placed in the MQS cell and the response of the FRPs to *'applied air chamber pressures'* (transferred to glycol-water through loading piston) were measured at various positive and negative temperatures. In the second set of the experiments, sand saturated with glycol-water was placed in the MQS cell and pre-consolidated to 300 kPa, then it was unloaded at a predefined set of total and backpressures. This time responses of FRPs to *'applied backpressures'* were measured at various positive and negative temperatures. The total pressure (air chamber pressure) was accordingly changed to maintain a constant effective stress and minimize piston displacements.

3.2.7 Effects of ambient temperature fluctuations on measured pressures

To measure pore-pressures accurately where a limited amount of water is available to transfer pore-pressures, the piezometer system needs to be as rigid as possible (Chapter 2). However, rigidity of the measuring system makes it sensitive to thermal fluctuations. Thermally induced volume fluctuations may cause pressure fluctuations throughout the measuring system and specimen. To quantify these thermal effects on the measurements, the measuring system was subjected to thermal fluctuations and its response was recorded. Two setups were used for this

purpose: an open system and a closed system. In the open system, FRP-4 was open to the MQS cell (valve 1 was open and valve 2 was closed, Figure 3-3). The temperature of the saturated sand specimen in the MQS cell was maintained above 0^{o}C and there was a water cap above the sand. A constant pressure was applied in the air chamber. In the closed system, both valves of FRP-3 were closed. This simulates the extreme condition when no unfrozen water exists in the specimen and there is no (micro) flow. Both open and closed systems were subjected to the same thermal fluctuations and responses of the FRPs were measured.

3.2.8 Rapid freezing and subsequent warming of the specimens

To produce a frozen saline sand specimen at subzero temperatures, the specimen is first rapidly frozen using a constant flow of liquid nitrogen through the bottom cooling plate of the MQS cell and venting it to the air (at this stage the coil surrounding the cell is not connected to the coolant line). The temperature at the top of the specimen (19 cm to 21 cm high) drops to below -14^{o}C within five hours of cooling with nitrogen. The time required to freeze the specimen depends on the flow of nitrogen, specimen height, salinity, initial temperature of the specimen, and insulation of the cell. The minimum temperature measured within the specimen was about -57^{o}C. Rapid freezing using temperatures down to -180^{o}C was used in the initial trials; however, it was modified to avoid damages to the FRPs and minimize temperature extremes. The procedure rapidly freezes the saline sand in an upward freezing direction. To enhance freezing, the cell was insulated and the specimen was first cooled to +2^{o}C prior to opening the flow of nitrogen. Uni-directional rapid upward freezing prevents salt rejection and non-uniform salinity distribution within the prepared specimen (Hivon and Sego 1995). After the specimen is frozen, it is warmed uniformly to -10^{o}C and then to the desired test temperature, always from colder to warmer temperatures. During the warming phase, a backpressure using saline water is applied to the top drain of the cell. The backpressure line is kept unfrozen using a separate temperature controlled glycol bath. For checking whether the backpressure line at the top of the specimen is open (not frozen or otherwise clogged), a 10 ml/min flow is applied to the backpressure line using the syringe pump. When the backpressure line is open, water flows into the cell (and loading piston moves upwards) without

building up more than about 5 kPa in excess of the applied total pressure (air chamber pressure). After this observation, the syringe pump is set to maintain a constant backpressure. This control is performed several times during the warming phase to ensure the specimen can intake or reject water. An example of desaturation of a specimen during the warming phase and gradual change of pore-pressures from a negative value to the applied backpressure is presented in the results and discussion sections.

3.2.9 Continuity of pore-water and validity of the measured pore-pressures in partially frozen saline sand specimens

Continuity of water phase in partially frozen soil specimens is checked by applying backpressures independent of the applied total pressure and measuring the corresponding pore-water pressure response. The water phase is considered continuous if the measured pore-water pressures reflect the applied backpressures. Continuity of water phase cannot always be guaranteed in a soil at subfreezing temperatures even at temperatures close to 0^{o}C. An example is demonstrated in which the specimen was originally saturated; however, desaturation and discontinuity of water phase was induced during warming the specimen from about -30^{o}C to -3.90^{o}C. The pore-water pressure response of this specimen during saturation, when it was connected to a backpressure for continuity test, is presented later.

3.2.10 Pore-water pressure response of a partially frozen saline sand specimen to undrained loading

An unfrozen saline sand specimen containing 30±1 ppt NaCl in the pore fluid and consolidated at 70 kPa effective stress was first rapidly frozen using liquid nitrogen (upward freezing) and then warmed to -2.07 ± 0.04 °C, while given access to water (backpressure of 50 kPa). Then pore-water pressures were measured within the specimen while it was subjected to five loading and unloading cycles in undrained conditions (top drain of the MQS cell was closed).

3.2.11 Effect of lateral load transfer to the cell wall on the measured B-bars in the MQS cell

It is speculated that due to the shear resistance between the specimen and the inside surface of the wall of the MQS cell, the transferred total stress to the base of the specimen would be less than the applied total stress at the top, and hence, the calculated B-bar would be less than the actual value.

A total pressure cell was placed at the base of the MQS cell at the bottom of the specimen to measure transferred total pressure to the base. The voltage output of the load cell was calibrated using the applied air chamber pressure while the MQS cell was filled with deaired water.

A saline sand specimen (30±1 ppt), 11.1 cm in height and 10.2 cm in diameter, was prepared according to the method previously described in this research. Pore-water pressure response and transferred total stress to the base of the specimen were measured before freezing the specimen at +6.7^{o}C, at three temperatures below 0^{o}C (-4.6^{o}C, -3.4^{o}C, and -2.2^{o}C), and again in thawed specimen at +5.0^{o}C. During warming of the partially frozen specimens to the experiment temperatures no access to water was provided.

Using simplifying assumptions, one can quantify the magnitude of the difference between the actual and measured B-bar:

$\bar{\boldsymbol{B}}$: Actual (corrected) pore-pressure parameter of the specimen

$\bar{\bar{\boldsymbol{B}}}$: Apparent (without correction) pore-pressure parameter of the specimen

$\Delta\boldsymbol{\sigma_T}$: Change in total stress at the top of the specimen

$\Delta\boldsymbol{\sigma_B}$: Change in total stress at the bottom of the specimen

$\Delta\boldsymbol{\sigma_x}$: Change in total stress at distance x downward from the top of the specimen

$\Delta \boldsymbol{u_x}$: Change in pore-water pressure at distance x from the top of the specimen at infinitesimal time t after applying the change of total stress to the top of the specimen (before equalization of the pore-water pressures)

$\Delta \boldsymbol{u_{eq}}$: Change in pore-water pressure within the specimen after equalization

H: Height of the specimen

$$\Delta \boldsymbol{u_x} = \overline{\boldsymbol{B}}.\Delta \boldsymbol{\sigma_x} \tag{3-1}$$

$$\Delta \boldsymbol{u_{eq}} = \frac{\int_0^{\boldsymbol{H}} \Delta \boldsymbol{u_x}\,.\,\mathrm{dx}}{\int_0^{\boldsymbol{H}} \mathrm{dx}} = \Delta \boldsymbol{\sigma_T}.\overline{\overline{\boldsymbol{B}}} \tag{3-2}$$

If $\Delta \boldsymbol{\sigma_T}$ is potentially uniformly reduced along the height of the specimen to $\Delta \boldsymbol{\sigma_B}$ and $\overline{\boldsymbol{B}}$ is uniform within the specimen:

$$\Delta \boldsymbol{\sigma_x} = \Delta \boldsymbol{\sigma_T} - \left(\frac{\Delta \boldsymbol{\sigma_T} - \Delta \boldsymbol{\sigma_B}}{\boldsymbol{H}}\right).\mathrm{x} \tag{3-3}$$

$$\Delta \boldsymbol{u_x} = \overline{\boldsymbol{B}}\left[\Delta \boldsymbol{\sigma_T} - \left(\frac{\Delta \boldsymbol{\sigma_T} - \Delta \boldsymbol{\sigma_B}}{\boldsymbol{H}}\right).\mathrm{x}\right] \tag{3-4}$$

$$\Delta \boldsymbol{u_{eq}} = \frac{\int_0^{\boldsymbol{H}} \overline{\boldsymbol{B}}\left[\Delta \boldsymbol{\sigma_T} - \left(\frac{\Delta \boldsymbol{\sigma_T} - \Delta \boldsymbol{\sigma_B}}{\boldsymbol{H}}\right).\mathrm{x}\right].\mathrm{dx}}{\int_0^{\mathrm{H}} \mathrm{dx}}$$
$$= \frac{\overline{\boldsymbol{B}}}{\boldsymbol{H}} \int_0^{\boldsymbol{H}} \left[\Delta \boldsymbol{\sigma_T} - \left(\frac{\Delta \boldsymbol{\sigma_T} - \Delta \boldsymbol{\sigma_B}}{\boldsymbol{H}}\right).\mathrm{x}\right].\mathrm{dx} = \overline{\boldsymbol{B}}\left(\frac{\Delta \boldsymbol{\sigma_T} + \Delta \boldsymbol{\sigma_B}}{2}\right) \tag{3-5}$$

$$\overline{\boldsymbol{B}}\left(\frac{\Delta \boldsymbol{\sigma_T} + \Delta \boldsymbol{\sigma_B}}{2}\right) = \Delta \boldsymbol{\sigma_T}.\overline{\overline{\boldsymbol{B}}} \tag{3-6}$$

$$\overline{\boldsymbol{B}} = \frac{2\overline{\overline{\boldsymbol{B}}}.\Delta \boldsymbol{\sigma_T}}{\Delta \boldsymbol{\sigma_T} + \Delta \boldsymbol{\sigma_B}} \tag{3-7}$$

Hence the value of $\overline{\boldsymbol{B}}$ depends on the value of the ratio of $\Delta \boldsymbol{\sigma_B}/\Delta \boldsymbol{\sigma_T}$. If $\Delta \boldsymbol{\sigma_B}$=0, then $\overline{\boldsymbol{B}}$ =2 $\overline{\overline{\boldsymbol{B}}}$**.**

3.3 Results

3.3.1 Calibration of the measuring system

FOPs, FRPs, and the syringe pump were calibrated according to the methods described earlier. Figure 3-4 shows the calibration of a FOP sensor model FOP-MIV-PK. The calibration curves for FRP-3 and syringe pump are shown in Figure 3-5 and Figure 3-6. The correlation coefficients are close to unity and show slightly better correlation when the top drain is closed. The delivered backpressure on the specimen applied by the syringe pump was also calibrated and the calibration curve is shown in Figure 3-7.

3.3.2 Air entry value of FRPs

The experiment for determining air entry value of FRPs showed that air pressure up to 1 MPa did not induce visually detectable 'air bubble' in the oil in the FRP.

3.3.3 Effects of air-entrainment and desaturation on the calibration of FRPs

To investigate the effects of air-entrainment on the measured pore-pressures, calibration of FRPs when the MQS cell is filled with either de-aired water or hydraulic oil were compared with the cases when an air cap is placed over the water or the hydraulic oil (Figure 3-8 to Figure 3-10). Further, effects of specimen desaturation on 'pressure response' and 'pressure equalization time' of the specimen were studied using FRPs and the procedure described earlier. The measured pressures using FRP-3 are shown in Figure 3-11 to Figure 3-13 for the saturated case and in Figure 3-14 to Figure 3-16 for the unsaturated case. The influence of specimen desaturation on calibration curves of the FRPs is shown in Figure 3-17.

3.3.4 Effects of pore-fluid temperature on the calibration of FRPs

Response of FRPs to the 'applied total pressure' (first set of experiments) and to the 'applied backpressures' (second set of experiments) were measured at various cell (pore-fluid)

temperatures. The results of the first and the second set of the experiments are shown in Figure 3-18 and Figure 3-19, respectively.

3.3.5 Effects of ambient temperature fluctuations on measured pressures

Figure 3-20 shows the FRP responses to thermal fluctuations in open and closed measuring systems. It shows that for ±0.23^{o}C fluctuation in ambient temperature, pressure measured in closed system fluctuated ± 95 kPa whereas it fluctuated only ± 4 kPa in the open system.

3.3.6 Continuity of pore-water and validity of the measured pore-pressures in partially frozen saline sand specimens

Figure 3-21 shows pore-water pressure response in a "nearly saturated" partially frozen overconsolidated saline sand specimen (estimated degree of saturation $\boldsymbol{S_r} = 98\% \pm 2\%$) subjected to change in the applied backpressure while the total stress was kept constant. The continuity of pore-water pressures in the specimen at -1.62^{o}C is shown in Figure 3-21.a. Figure 3-21.b shows that the pore-water pressures measured 10 minutes after application of each loading step coincide with the applied backpressures on the specimen.

Continuity of the water phase cannot always be guaranteed in a partially frozen soil even at subfreezing temperatures close to 0^{o}C. Figure 3-22 shows an example of pore-water pressure response of an unsaturated saline sand specimen at -3.90^{o}C when it was connected to the backpressure for continuity test. The response of FRPs shown in Figure 3-22 reflects the measured pore-water pressures during gradual saturation of the specimen after it was connected to the backpressure port.

3.3.7 Pore-water pressure response within a partially frozen saline sand specimen to undrained loading

Figure 3-23 shows an example of the pore-water pressure response of partially frozen saline sand subjected to five undrained loading and unloading cycles. Based on Figure 3-23.b, $\overline{\boldsymbol{B}}$ for this specimen is 0.35 during the first loading cycle and 0.34 during the first unloading cycle.

3.3.8 Effect of lateral load transfer to the cell wall on the measured B-bars in the MQS cell

Figure 3-24 shows the calibration of total pressure cell. The transferred total and effective stresses to the base of the specimen in the partially frozen and unfrozen states are shown in Figure 3-25. Pore-water pressures in response to the applied total stresses to the partially frozen specimen at -2.2^{o}C are shown in Figure 3-26.

3.4 Discussion

3.4.1 Role of filters, air entry value, and rigidity of the piezometers

Commonly, Kelvin's equation is used to calculate a theoretical air entry value for ordinary piezometers (piezometers with filters). In this case, for $\boldsymbol{T_s}$= 34.3 mN/m and $\boldsymbol{R_s}$=0.035 mm, $\boldsymbol{Uc}$ = 2.0 kPa is calculated for FRPs. With water (surface tension $\boldsymbol{T_s}$= 0.075 N/m) the 'theoretical air entry value' is $\boldsymbol{Uc}$ = 4.3 kPa. However, the experiment conducted in the current chapter showed that even air pressures up to 1 MPa did not create visual air bubbles in the FRPs.

The '*theoretical air entry value*', as well as, the measurement techniques used for measuring its value (Fredlund and Rahardjo 1993), assume that '*flow of free air*' is 'physically permissible' through a capillary tube; if there is no free air, or when there is no space for the free air to enter, this kind of flow (flow of free air) is not permissible. Owing to the rigidity of the FRPs and the geometry of the oil droplet at the tip of the FRP, '*flow of free air*' into the FRP is not physically permissible. Only a very small volume transfer (416 $\mu m^3/kPa$) is required to transmit pressures to the fiber optic pressure sensors in the FRPs (Chapter 2) (Kia et al. 2011).

The amount of air going into or coming out of the piezometer fluid (which could be water, oil, alcohol, or any other hydraulic fluid) is time dependent. Depending on the engineering application, this time dependency may be ignored or taken into consideration (Fredlund and Rahardjo 1993). FOPs can be read at time intervals as fast as once per 0.01 second and are factory calibrated to negative pressures of -40 kPa. The FRPs, as used in the MQS cell, have an equalization time in the

range of 1 second to 10 minutes in saturated and unsaturated sands (Figure 3-12 to Figure 3-16) compared to 1 hour to 7 days (Guan and Fredlund 1997) for piezometers and suction probes that use high air entry ceramics.

The filter can be eliminated if oil does not flow out of PEEkSoil tube under gravity (which is achieved through its adhesion, higher viscosity of mineral oil as compared to water, and upward direction of the tip of the FRP) or under the applied loads (which is achieved through the rigid design of the piezometer). The oil-saturated soil around the tip of the PEEKSil^{TM} tube can be regarded as a filter for the FRP; the filter of the measuring device would have the same pore-size, hydraulic conductivity, and deformation characteristics as the soil itself. In this case, even if some soil enter the PEEKSil^{TM} tube, continuity of liquid phases is maintained provided a proper diameter of PEEKSil^{TM} tube is selected either by using a diameter that is smaller than the smallest particle in the soil, or large enough to ensure continuity of the liquid phase around a particle in the PEEKSil^{TM} tube.

It is difficult to maintain a 'saturated specimen' under high air pressure over an extended test time. When a high air pressure is sustained in an air chamber for a prolonged period of time, eventually some air leaks or diffuses into the specimen due to imperfect equipment, workmanship, and procedures. This can be monitored by watching for any deviation in calibration curves before and after each experiment, increase in the response time of the FRPs to independent changes of backpressures, and showing equalization patterns that are characteristic of unsaturated specimens. This is discussed later. Further, air diffusion into the specimen can be minimized by shortening the experiment duration and duration with high air pressures in the air chamber, increasing the number of O-rings that seal around the loading piston, or completely replace the pneumatic loading system with a hydraulic loading system. It is also suggested to use hard metal alloys instead of Perspex as the material for the cell wall to minimize the chance of the wall getting scratched by the sand particles.

3.4.2 Calibration of the measuring system

Figure 3-4 shows the calibration of one of the FOP sensors model FOP-MIV-PK used to monitor the air chamber pressures. The curve shows a linear correlation and both the correlation factor and the slope of the line are close to unity. The intercept of the curve is less than the accuracy of the FOP sensor. The factory calibration and accuracy of the FOP sensors were thus confirmed.

The FRP calibrations all show linear response to the applied loads. The calibration curves for FRP-3 and the syringe pump are shown in Figure 3-5 and Figure 3-6. The correlation coefficients were close to unity and show slightly better correlation coefficients in case (1) as compared to case (2), owing to the rigidity of the system when the syringe pump is not connected to the cell (top drain is closed). FRPs measure a higher pore-pressure during an unloading step compared to a loading step. The difference in loading and unloading curves is discussed later and is attributed to the effects of the loading piston interface with the pore-water and tensile strength of the pore-water. The calibration shown in Figure 3-6 is for the pressure measured using the syringe pump in response to an applied pressure in the air chamber under condition of 'zero flow'. This is useful especially during freezing and thawing experiments, when a water supply at a constant backpressure is applied. The calibration of the syringe pump shown in Figure 3-7 shows the delivered pressure to the specimen when a specific pressure is applied on the syringe pump and is useful for measuring the pore-water pressure response to an independent change of applied backpressure.

3.4.3 Effects of air-entrainment and desaturation on the calibration of FRPs

Calibration and pore-pressure response of FRPs when the cell is filled with either de-aired water or hydraulic oil are compared with the cases when an air cap is placed over water or hydraulic oil in Figure 3-8 to Figure 3-10. These observations aid interpretation of the measured data, recognition of patterns of pore-pressure response when the specimen desaturates, and evaluation

of thermal effects on the results from the test program described in this research. By comparing Figure 3-8 to Figure 3-10 it is observed that:

1. In both de-aired water and hydraulic oil, the loading curves are above Y = X whereas the unloading curves tend to be below Y = X. This means for the same applied pressure in the air chamber, the FRPs measure a slightly smaller value in loading and slightly higher value in unloading. One may associate this to the frictional forces developed at the interface between the inside of the PEEKSil^{TM} tube and the internal mineral oil during micro flow of mineral oil when transferring pressures to FOP. In unloading, the pressures are delayed, therefore, it takes time for pressure to release and FRPs show a slightly higher pressure. This is further discussed later and it is concluded that it is associated to interfacial effects between the loading piston and the fluid in the cell. No matter the reason for this observed behavior, the calibration of FRPs converts the measured value to the applied air chamber pressure when all measurements are conducted using the same equalization time.
2. In both de-aired water and hydraulic oil, placing an air cap between the loading piston and the liquid in the cell (changing the interface between the loading piston and the liquid in the cell with air) results in a calibration curve that coincides with Y = X line, for both loading and unloading at both positive and negative temperatures.
3. In loading, the calibration curve is almost parallel to Y = X, whereas in unloading it deviates from Y=X. However, when an air cap is present between the loading piston and the liquid in the cell, both loading and unloading curves are parallel to (coincide with) Y = X.
4. Decreasing temperature of the hydraulic oil from +6.89^{o}C to -2.98^{o}C increased the differences between loading and unloading curves (Figure 3-9 and Figure 3-10). When loading, the colder temperature shifted the calibration curve to the left by 28 kPa, on average. However, the graph remained almost parallel to Y= X in loading. This shows colder temperatures do not change the slope of the calibration curve appreciably, during loading. One may attribute this shift to higher friction between the mineral oil and the

internal wall of the PEEKSil^{TM} tube at colder temperatures. When unloading, the effect of the colder temperature was that the angle of the unloading curve increased compared to the Y=X line. One may attribute this behavior to the increase in viscosity (due to cooling) and resistance of mineral oil to flow out of the PEEKSil^{TM} tubes. However, adding an air cap between the piston and the oil resulted in the data corresponding to Y = X line. Further, this deviation is observed 'only in unloading'. Therefore, this behavior is attributed to the lower vapor pressure and higher tensile strength of colder "hydraulic oil" which results in higher adhesion to the loading piston (i.e. higher interface effect).

5. The unloading curve when the cell is filled with hydraulic oil is to the right of the curve for when the cell is filled with de-aired water and has a higher slope. Following the same argument, this behavior is attributed to lower vapor pressure of the hydraulic oil and shows a higher loading piston-liquid interface effect.

These observations (effects of an air interface between the loading piston and the liquid in the cell) explain the effects of desaturation of sand on the calibrations curves shown in Figure 3-17. It can be observed that for the unsaturated case, both loading and unloading curves moved towards the Y = X line, and became almost parallel to Y = X. This is similar to when an air cap was placed between the loading piston and de-aired water or hydraulic oil. Loading and unloading curves are still slightly to the left and right of the Y = X, respectively. The volumetric air to water ratio in the specimen was 0.23 after desaturation and a water cap (which also may contained air) was between the piston and the specimen.

Further, comparison of the measured pore-pressure response and the trend of equalization of the pore-pressures in a saturated sand specimen (Figure 3-11 to Figure 3-13) with that in an unsaturated sand specimen (Figure 3-14 to Figure 3-16) shows that:

1. In saturated sand, after the application of each '*loading step*', the measured pore-water pressure first increases quickly and then gradually till it reaches the equilibrium state, whereas, for unsaturated sand, after the first increases, the measured pressure gradually decreases till it reaches the equilibrium state.

2. In saturated sand, after the application of each '*unloading step*', the measured pore-water pressure rapidly decreases, becoming more gradual as it nears the equilibrium state, whereas, in unsaturated sand, after the first decrease, the measured pressure gradually increases until it reaches the equilibrium state.
3. The required time to reach pore-water pressure equalization in the unsaturated sand is longer than in saturated sand. Based on the equalization times shown in Figure 3-14 to Figure 3-16, allowing 10 min for equalization before recording the data provides sufficient time for equalization even when the specimen is unsaturated. It should be noted that this is the response time of the 'specimen' within the testing system to reach its equilibrium of pressures. The response time of the FOPs is only 0.01 second.

Even though the process of replacing dissolved and entrained air in water with water vapor (by boiling water) theoretically reduces the air content of the pore fluid in the soil to 0%, however, due to small cavities on the surface of the loading piston and trapped air under the piston, some air may still be present. Further, during the process of water expulsion and cell shrinkage during freezing and subsequent water intake and cell expansion during thawing, the specimen may become unsaturated because of impeded water intake due to low permeability of soil at subfreezing temperatures and the imperfect sealing of the connections. Imperfect sealing of connections allows air to leak or diffuse into the specimen especially when a relative vacuum is created in the specimen due to the warming induced expansions. The amount of air leaking or diffusing through a seal depends to the type of seal, pressure gradient, and time. The amount of air entering the specimen due to these imperfections is usually low and is assumed to go into solution under the applied backpressures in this research.

3.4.4 Effects of pore-fluid temperature on the calibration of FRPs

Using Figure 3-18 and Figure 3-19 it is observed that:

1. Decrease of cell temperature (pore-liquid temperature) does not affect the FRP response to the 'applied backpressures' whereas it shifts the calibration curve to the left, in both glycol-water and hydraulic oil, when pressures are transferred to the liquid by the loading

piston (i.e. 'applied air chamber pressure'). It is concluded that this effects is associated with the medium transferring the pressures to the liquid in the cell, i.e. the loading piston.

2. The rate by which the slope of the calibration lines changes with cell temperature is negligible and ranges from -0.002 to 0.006, based on Figure 3-18.a. It is also observed that the coldest and warmest data points when using glycol-water mix are off the fitted line. It is perceived that these two data points are affected by tiny amounts of air coming out of solution as these two measurements were conducted after 48 and 64 hours of allowance for thermal equalization, whereas the other data points were measured after 24 hours allowance for thermal equalization between data measurements. Insufficient data were available for hydraulic oil to reach similar conclusions and the trend shown by hydraulic oil may indeed reflect air coming out of solution, or show a fluid-dependence. The very low correlation coefficient is an indicator that the slope of the correlation lines is not influenced by the cell temperature. It is concluded that when the objective of the measurement is to measure change in pore-water pressure (Δu) to change in total pressure ($\Delta \sigma_t$), for example when estimating b-bar, the cell temperature do not have a significant effect on the results as only the 'slopes' of the calibration lines are used.
3. The rates by which the intercept of the calibration lines changes with cell temperature is in the range of -3.65 kPa/^{o}C to -3.75 kPa/^{o}C, for glycol-water and hydraulic oil, respectively. It also shows the same trend for both glycol-water and hydraulic oil (Figure 3-18.b). One may conclude that the influence is a result of the friction between the loading piston and the cell wall. However, previous observations showed that placing an air cap between the liquid in the cell and the loading piston diminished the effects of cell temperature. One may also conclude that the air may create an independent phase in the pore space of liquid molecules and transfer pressures to the sensing element. However, based on the background theory discussed in Chapter 2, existence of an independent air phase requires it to exist as a "continuous entrapped air phase" having air pressure independent of water pressure, not as "air in solution".

3.4.5 Effects of the system compliance on the measured pore-pressures

Effects of compliance of the testing equipment on the measured pore-water pressures in the laboratory have been studied by several authors and some attempted to calculate corrections for the measured pore-water pressures (Gibson 1963; Haeri and Shakeri 2010; Martin et al. 1978; Tokimatsu 1990; Wissa 1969). In the current research, the calibration procedure accounts for the accumulated system imperfections (including flexibility, frictions, and response time) all through the calibration factors. The whole system (FR Piezometers as installed in the MQS cell) is thus calibrated. Further, time lag associated with measuring system is minimized in FRPs owing to their '*simplicity*' and '*rigid design*'. Simplicity of instruments maximizes reliability of the measurements based on the guidelines given by Dunnicliff and Green (1993).

The observed cell temperature effects, desaturation effects, and delayed unloading response are all influenced by the interface of the loading piston with the pore-liquid. Figure 3-27 illustrates how water is lifted from its free surface due to its tensile strength and adhesion to steel. The same phenomenon occurs during an unloading scenario. Tensile strength of liquids is closely related to cavitation pressure (vapor pressure) and the fluid-container interface characteristics (Ridley 2003). The mechanism of cavitation and the generation of tension in liquids have been reviewed elsewhere (Arakeri 1979; Sun et al. 2008; Trevena 1984; Washio et al. 2008). A reduction in temperature causes vapor pressure to decrease; hence, tensile strength of the liquid and its adhesion to the loading piston is increased. The delayed separation of the liquid from the piston, delays pressure equalization in the sand specimen. FRPs with their fast response time measure the real time change in the pore-fluid pressures.

No matter the reason for the observed behavior being caused by desaturation or the delayed unloading response, the calibration of FRPs converts the measured value to the applied air chamber pressure when all measurements are conducted using the same equalization time in the MQS cell. It was decided to allow 10 minutes for pressure equalization in specimens for the current test program. It is further concluded that when the objective of the measurement is to measure change in pore-water pressure (Δu) to change in total pressure ($\Delta \sigma_t$), for example when estimating B-bar, the cell temperature does not affect the results because only the 'slopes' of the

correlated response lines are considered. Further investigation on the effects of the system compliance on the measured pore-water pressures is beyond the scope of this research and remains for future research.

3.4.6 Effects of ambient temperature fluctuations on the measured pressures

Figure 3-20 shows the thermally induced fluctuations on the response of the FRPs. For ±0.23^{o}C fluctuation in ambient temperature FRP-3 fluctuated ± 95 kPa (both valves of FRP-3 were closed) whereas FRP-4 fluctuated only ± 4 kPa (FRP-4 was open to the cell). Based on these observations, if the thermal fluctuations are maintained below ±0.01^{o}C (which is also the accuracy level of RTDs for temperature measurement), the fluctuations in measured pressures will be less than ± 5 kPa in the extreme case of no flow (closed system) and less than ± 0.2 kPa (theoretically) with free flow or access to water. Considering the '*simplicity*' of the FRPs, it is concluded that at temperatures close to 0^{o}C where greater amounts of unfrozen water exists and unfrozen water can flow in partially frozen soil, the accuracy of FRPs is the same as FOP sensors. The accuracy of FOP sensors is ± 1 kPa. It should be also noted that FOP sensors are thermally compensated.

3.4.7 Continuity of pore-water and validity of the measured pore-pressures in partially frozen saline sand specimens

Ice-poor soils will de-saturate during warming and partial thaw, because during phase change the water occupies 90% of its volume in the frozen state. This can result in negative pore-water pressures. If backpressure with liquid water is not maintained (for example due to ice-blockage of the top drain in MQS cell) or delayed (low hydraulic conductivity of frozen soil) for prolonged periods, then air may enter the specimen. An example of this suction and pore-pressure transition from negative to positive with gradual saturation during application of backpressures is shown in Figure 3-22 for a partially frozen saline sand specimen (30±1 ppt salinity). In an attempt to minimize the possible micro-cracking of the specimen due to change in effective stress, both backpressure and total stress are changed (almost equal amount) during each loading and

unloading steps in the experiment shown in Figure 3-22. It is seen that FRP-4 measures a negative pore-pressure about -100 kPa (which is also the cavitation pressure of water) and then by saturation, owing to the application of backpressure, reaches the same pressure. The soil at FRP-3 location is partially unsaturated and follows the 'total pressure' and not the backpressure trend, till about 45 minutes has passed (consider the 'pattern' of increase of pressure during the loading steps which portrays a pattern for an unsaturated specimen), and then gradually reaches saturation and shows a trend of pressure equalization similar to a saturated soil. The FOPs are factory calibrated only to -40 kPa and no warranty is provided below -40kPa. However, our experience with positive pressures shows linear response of FOPs (Figure 3-4). FOPs are rated to withstand positive pressures up to 3 MPa according to factory specifications. Further, experience with FRPs subjected to negative pressures down to -150 kPa showed the calibration did not change compared to FRPs that did not experience these high negative pressures. However, pressures higher than 3 MPa failed several FOPs during this research program. High pressures can occur during a rapid freezing (using liquid nitrogen). One way to dampen these high pressures is to open the back valve of the FRPs to an oil filled flexible plastic tubing during rapid freezing (temporary increasing the flexibility of FRPs) and sustain a positive pressure on the line after warming to ensure the intimate contact of the piezometer fluid and unfrozen pore-water and then close the back valve before measuring the internal pore-pressures. High pressures also can be managed by controlling the rate of cooling through adjusting the rate of nitrogen flow into the freezing plate. The later method is preferred and was used for the subsequent experiments.

It should be noted that validity of pore-water pressure measurements depends on the continuity of pore-water phase which depends to the amount and distribution of unfrozen pore-water. The frozen saline sand at 30±1 ppt salinity and -3.90^{o}C has volumetric unfrozen water content $\boldsymbol{\theta_u} = 13.9\%$ whereas at -2^{o}C it has $\boldsymbol{\theta_u} = 23.4\%$. The distribution and amount of salt in a frozen soil and its temperature affect its volumetric unfrozen water content (Hivon and Sego 1995) and hydraulic conductivity. The uniformity, speed, and direction of freezing affect the distribution of salt in the specimen. Natural permafrost soils commonly have a non-uniform salt distribution and

if they are ice-poor, they will reach an unsaturated state during warming. Figure 3-21 shows the pore-water pressure response of a nearly saturated saline sand specimen at -1.62°C that was subjected to change in the applied backpressure while the total stress was kept constant. The FRP response was linear related to backpressure; the slope was close to unity and the intercepts were 1 to 2 kPa in loading and 1 to 6 kPa in unloading. The fluctuations in the measured pressures are attributed to the thermal fluctuations (± 0.15 °C) in this 'nearly saturated' specimen.

3.4.8 Pore-water pressure response of a partially frozen saline sand specimen to undrained loading

Figure 3-23.a shows an example of the pore-water pressure response of partially frozen saline sand subjected to five undrained loading-unloading cycles. Saline sand at 30±1 ppt NaCl and consolidated at 70 kPa effective stress was first rapidly frozen using liquid nitrogen (upward freezing) and then warmed to -2.07 ± 0.04 °C, while given access to water. Then it was subjected to undrained loading and unloading cycles. The loading steps in the first cycle are in 50 kPa steps, whereas in the subsequent cycles they are in 100 kPa steps. The response of FRPs after 10 minutes for each loading step were plotted to measure Skempton pore-water pressure parameter, $\overline{B}$ (Figure 3-23.b). The temperature of the specimen was kept constant with fluctuations in the range of ± 0.01°C during each cycle. As it can be observed in Figure 3-23.b, $\overline{B}$ for this specimen is about 0.35 at -2.01°C in the first loading cycle and 0.34 in the first unloading cycle. In comparison, Veyera et al. (1992) reported $\overline{B}$ parameter, in the range of 1.00 to 0.51, as a function of effective confining pressure (86-690 kPa) and relative density (6-85%) for two saturated unfrozen sands in reloading. Further experiments and interpretation of pore-water pressures in a partially frozen soil are presented in Chapter 4, where the low $\overline{B}$ values are attributed to void ratio of the sand specimen, ice content, ice temperature, and degree of saturation.

3.4.9 Effect of lateral load transfer to the cell wall on the measured B-bars in the MQS cell

It is observed that the output voltage of the total pressure cell show a linear response to the applied pressures (Figure 3-24). When calibrating total pressure cell in the MQS cell, the effects of the piston friction is automatically incorporated in the calibration factors.

The transferred total and effective stresses to the base of the specimen in the partially frozen and unfrozen states are shown in Figure 3-25. Figure 3-25.a shows that a higher percentage of the total stress is transferred to the base under colder temperatures (-4.6^{o}C and -3.4^{o}C compared to -2.2^{o}C) which is the opposite of the expected behavior (i.e. colder ice should develop a stronger bond to the cell wall and hence reduce the total stress transferred to the base of the specimen). Further, it is observed that the transferred total stress to the base is reduced in the thawed specimen compared to the unfrozen specimen before conducting the test. This behavior is due to the desaturation induced by warming of the specimen while its water-intake line may get blocked due to freezing of the water line. Figure 3-25.b shows the results when stress transferred via pore-water is discounted from the total stress transfer. In several data points with the same effective stress but at different temperature, the transferred effective stress is almost the same. Even though Figure 3-25.b may provide insights into lateral earth pressure coefficients to be used with effective stresses, it is difficult to use this graph to quantify the effects of these load transfers on the measured pore-water pressures because various factors are involved (for example: de-saturation during freezing, warming, and thawing processes of ice-poor soils which impacts the compressibility of the liquid phase that transfers the pore-water pressures). The study of the distribution of the load transfer to the cell wall along its height is beyond the scope of the current research and remains for future research.

Pore-water pressures in response to the applied total stresses to the partially frozen specimen at -2.2^{o}C are shown in Figure 3-26. Based on this graph: $\Delta\boldsymbol{\sigma_B} = 0.9529\ \Delta\boldsymbol{\sigma_T}$, therefore using Equation (3-7) $\overline{\boldsymbol{B}} = 1.02418\ \overline{\overline{\boldsymbol{B}}}$. The correction is about 2.4% and the corrected

$\overline{\boldsymbol{B}} = 1.02418\ (0.8253) = 0.8452$. This case is an extreme condition in which the partially frozen soil desaturated during warming (was not given access to water during warming). An immense effort has been invested in experiments described in Chapter 4 to assure high degrees of saturation of the specimens (via giving access to water during warming and applying backpressure) and therefore the resulted error in calculation of B-bars without applying a correction factor would be less than 2.4%.

3.5 Summary and conclusions

The importance of measuring pore-water pressures in partially frozen soils subjected to independent change of backpressure and total stress is that the effective stress concept in partially frozen soils can be examined and verified. For the first time, examples of the measured pore-water pressure response to independent changes in both total stress and backpressures were presented, as well as, the Skempton's pore-pressure parameter B-bar ($\overline{\boldsymbol{B}}$) for partially frozen saline sand. Validity of the measurements were verified by observing that the measured pore-water pressures closely reflect the independent change of backpressures applied to the partially frozen saline sand specimens. Further experiments and interpretation of pore-water pressures in a partially frozen soil are presented in Chapter 4. More presentation of data and interpretation of the mechanical behavior of partially frozen soils in light of effective stress concept will be presented in the near future.

Testing of FRP and interpretation of the measured pore-pressures using FRPs for measuring pore-water pressures in partially frozen soils in the laboratory were discussed. Further, effects of air-entrainment, de-saturation, pore-fluid temperature, ambient temperature fluctuations, and testing system compliance on the interpretation of the measured pore-water pressures were studied. The calibration method used in this research compensates for a majority of the testing equipment imperfections.

It was also demonstrated that the interface characteristics between the loading piston and the pore-liquid has a determining effect on the delayed response in the unloading scenarios, as well as, on

the effects of de-saturation, air-entrainment, and pore-fluid temperature on the measured pore-pressures, and is a function of tensile strength and adhesion of the pore-fluid to the loading piston. Further study of this matter was not within the scope of the current research and remains for future research.

The fundamental concepts discussed in this chapter enhance the understanding and method of measuring pore-pressures in multi-phase porous media. FRP may also have application in measuring pore-water pressures in stiff clays and also in liquefaction assessment under dynamic loading, owing to its rigidity (only very small volume transfer of liquid is required to transfer the pressures) and high frequency data logging (time intervals as small as 0.01 sec).

3.6 Tables

Table 3-1. Specifications of ISCO pump model 500D syringe pump (Teledyne Isco Inc. 2010)

Flow Range (ml/min)	0. 001 – 204
Flow Accuracy	0.5% of the set point
Pressure Range (psi)	10 - 3,750
Pressure Accuracy	0.1% FS
Operating temperature	5 - 40° C Ambient

3.7 Figures

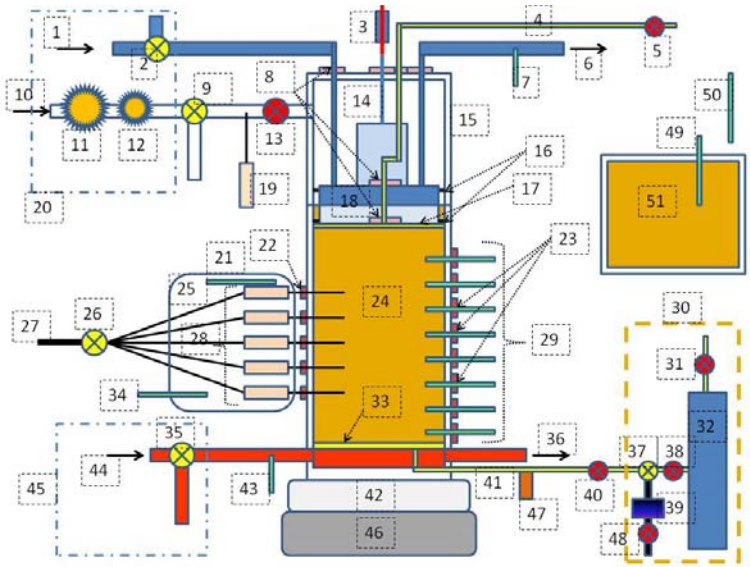

Legend

1 Inflow of glycol from the thermally controlled bath to top plate
2 3-way valve for directing glycol to the cell or to the bath
3 LVDT
4 Upper drain/backpressure application tube
5 Open-close valve
6 Outflow of glycol to the bath from top plate
7 RTD # 307
8 O-ring and vacuum grease sealing for air tight connections
9 3-way valve on air pressure line
10 Connected to air compressor
11 High air pressure dial gage and regulator
12 Low air pressure dial gage and regulator
13 Open-close valve on air pressure line
14 Rod connecting piston and LVDT
15 Air chamber
16 O-ring and Vacuum grease sealed loading piston (air and water tight)
17 Filter paper+ cloth filter
18 Loading piston and cooling/warming plate
19 FOP # 7 to measure air pressure in the chamber
20 Instruments in lab room space (temp = 21^{o}C, not insulated) enables changing pressures without the need to open the cold room door (better thermal control of specimen)
21 Insulation box for FRPs
22 Brass ferrule for FRP connections to the cell- NTP fittings (1/16")
23 Brass ferrule for RTD connections to the cell- NTP fittings (1/8")
24 Specimen
25 RTD # 106 (E) attached to FOP # 1
26 Multi-way valve for saturating oil-line in the FOPs
27 To oil reservoir pressurized using syringe pump
28 A set of 5 FRPs
29 RTD # 201 to 208 (fed into the specimen)
30 Insulation box for the syringe pump
31 Open-close valve for filling the syring pump with de-aired water
32 Syringe pump with water in the reservoir (half full)
33 Porous stone filter
34 RTD # 107 (F), in the air in the FRP insulation box
35 3-way valve on the inflow to the bottom plate
36 Outflow of the glycol line connected to the bottom plate
37 3-way valve to apply pressure to either oil reservoir or to the specimen (switch between oil and water)
38 Open-close valve on the syringe pump. Allows filling the pump reservoir or applying pressure on the line
39 Oil over water reservoir with air vent (saturating oil line)
40 Open-close valve on the bottom drain of the MQS cell
41 Bottom drain of the MQS cell
42 Base of the MQS cell
43 RTD # 308
44 Inflow of glycol from the thermally controlled bath to bottom plate
45 Instruments in lab room space (temp = 21^{o}C, not insulated) enables changing pressures without the need to open the cold room door
46 Scale for automatic mass measurements
47 Electrical pressuremeter
48 Open-close valve for the oil saturating line
49 RTD # 105 (inside the Dummy cell at its wall)
50 RTD # 103 (B) (in the larger insulation box)
51 Dummy cell

Figure 3-1. Schematic of Modified Qiu-Sego large strain consolidation cell

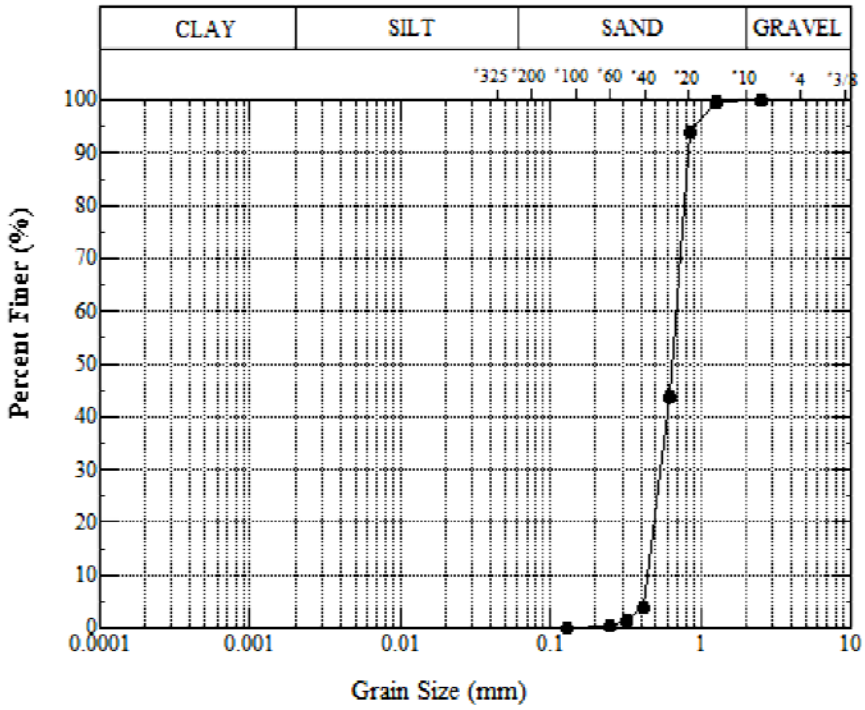

Figure 3-2. Grain size distribution of sand used in this research

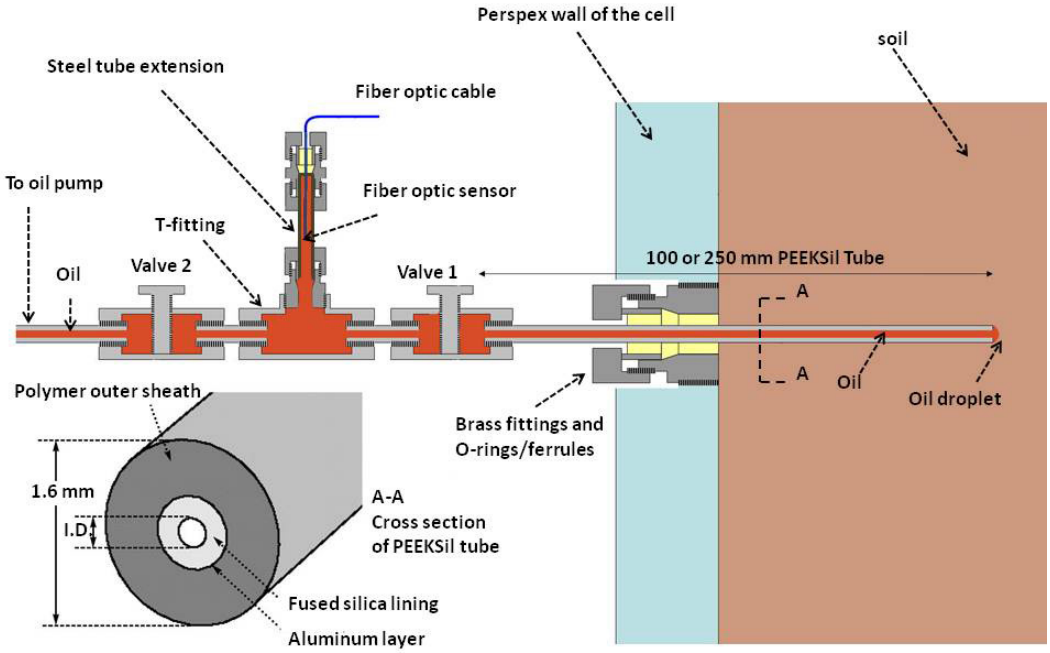

Figure 3-3. Schematic of a Filter-less Rigid Piezometer (patent pending)- cross section of PEEkSil™ tube is taken from SGE (2007)(same as Figure 2-5)

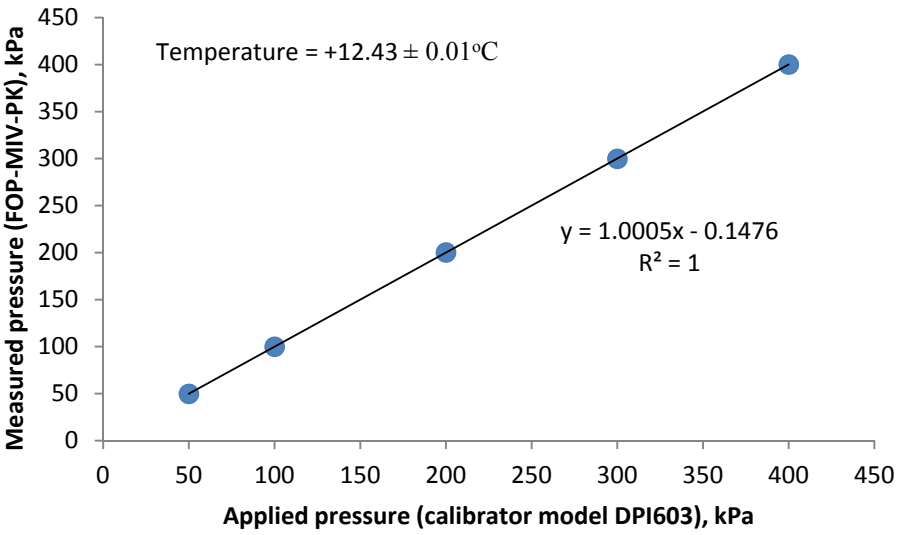

Figure 3-4. Calibration of FOP sensor model FOP-MIV-PK

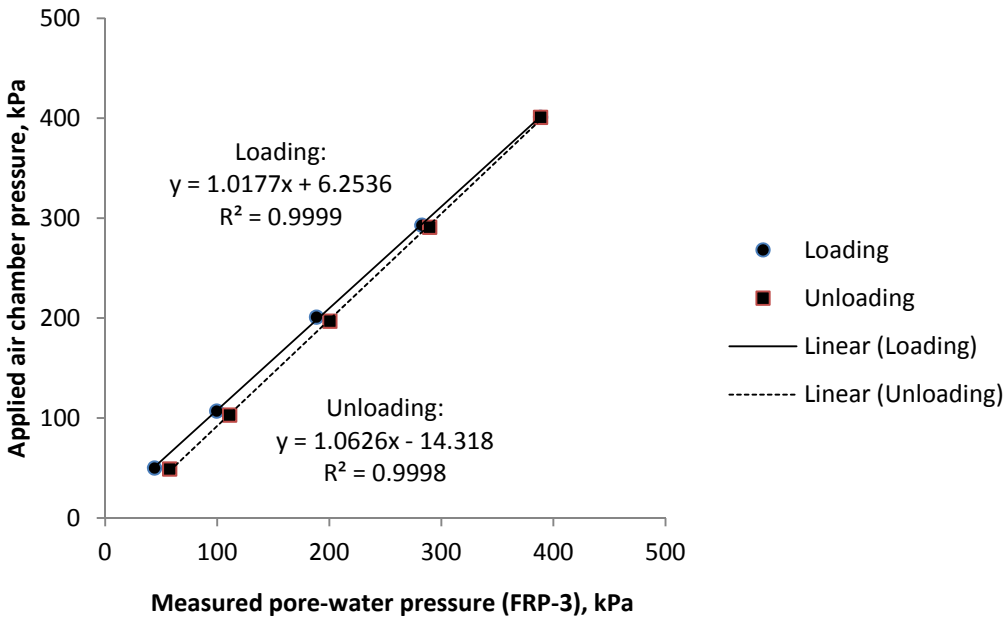

(a) top drain closed (rigid system)

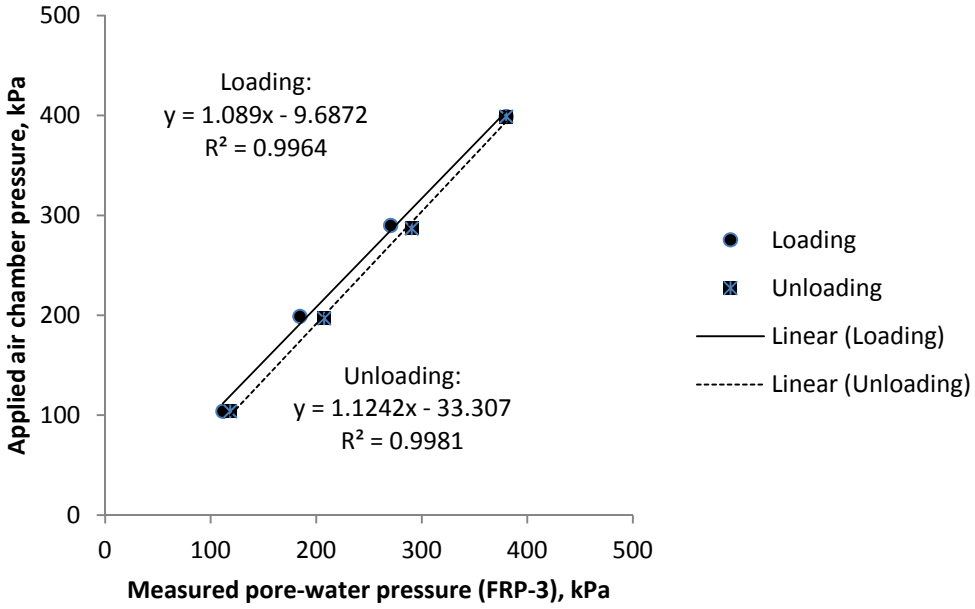

(b) top drain open (calibrated together with the syringe pump)

Figure 3-5. Calibration of FRP-3 in the MQS cell

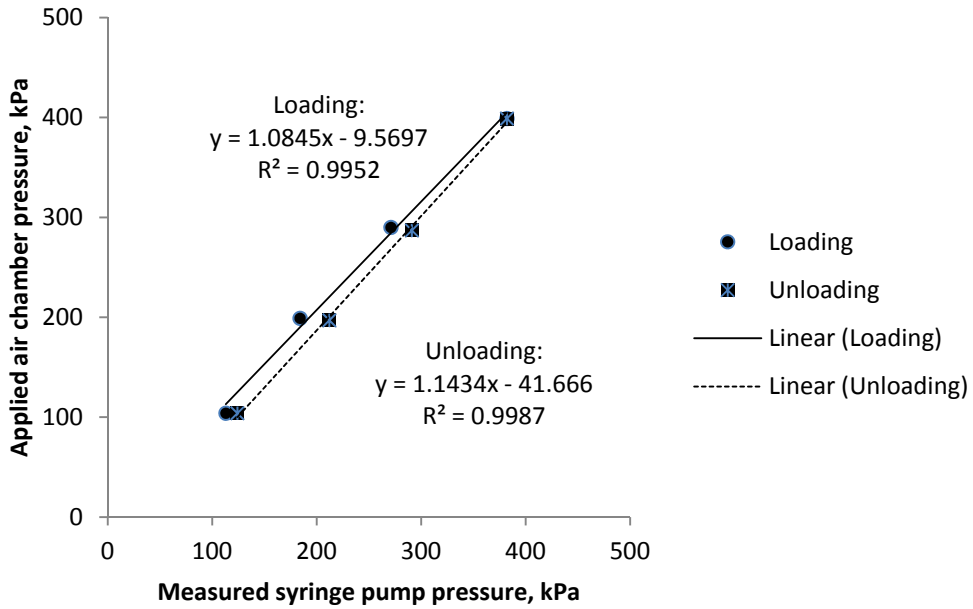

Figure 3-6. Calibration of syringe pump connected to backpressure line in the MQS cell (calibrated together with FRPs)

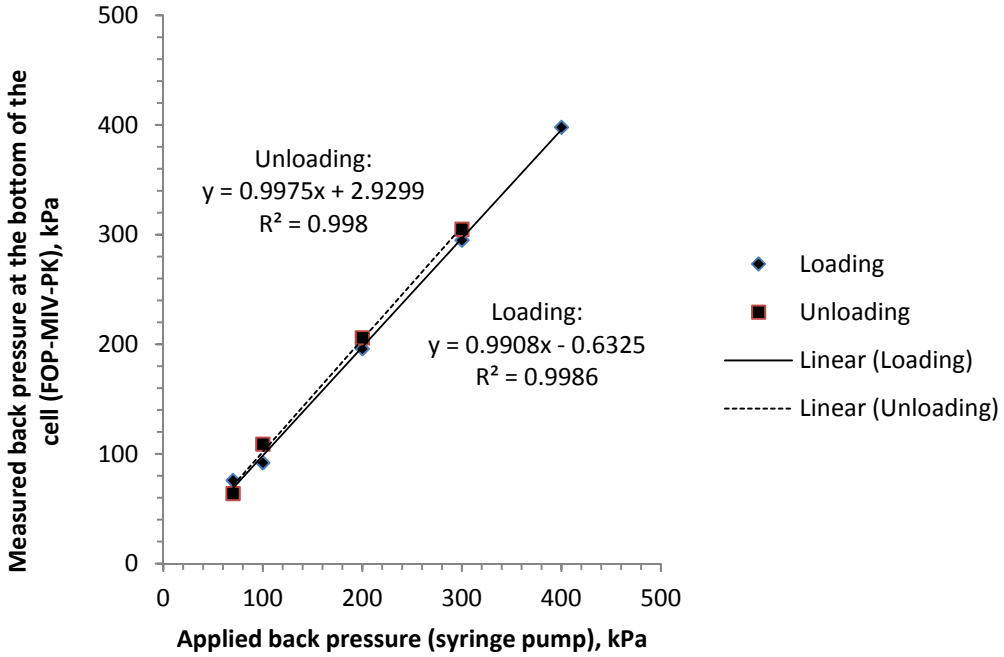

Figure 3-7. Delivered backpressure at the bottom of the MQS cell (measured 10 minutes after the application of each loading step on the syringe pump)

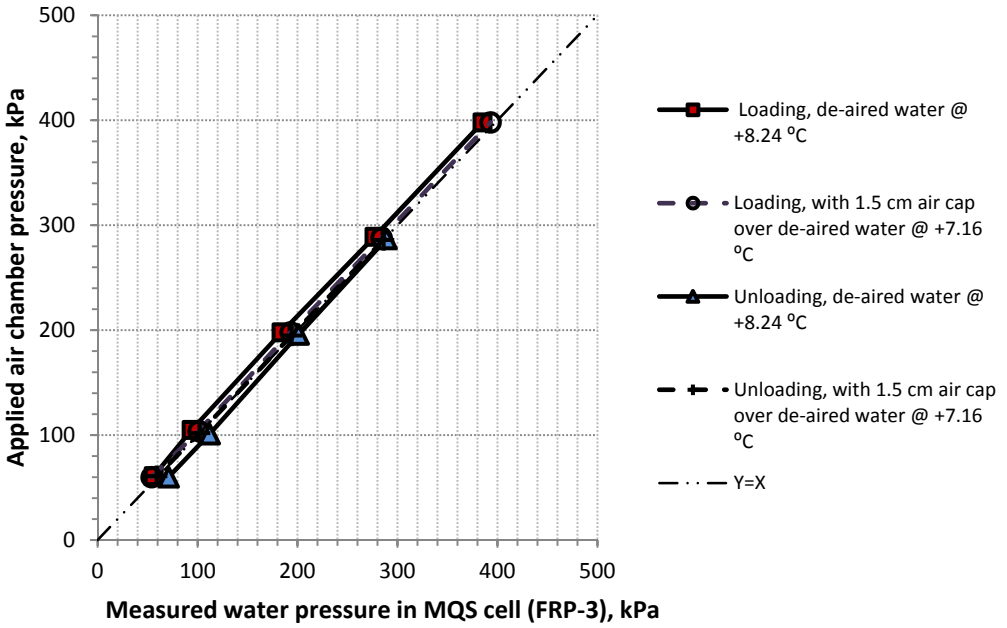

Figure 3-8. FRP response to the applied air chamber pressure when de-aired water is placed in the MQS cell at positive temperatures, with and without an air cap between the loading piston and the water

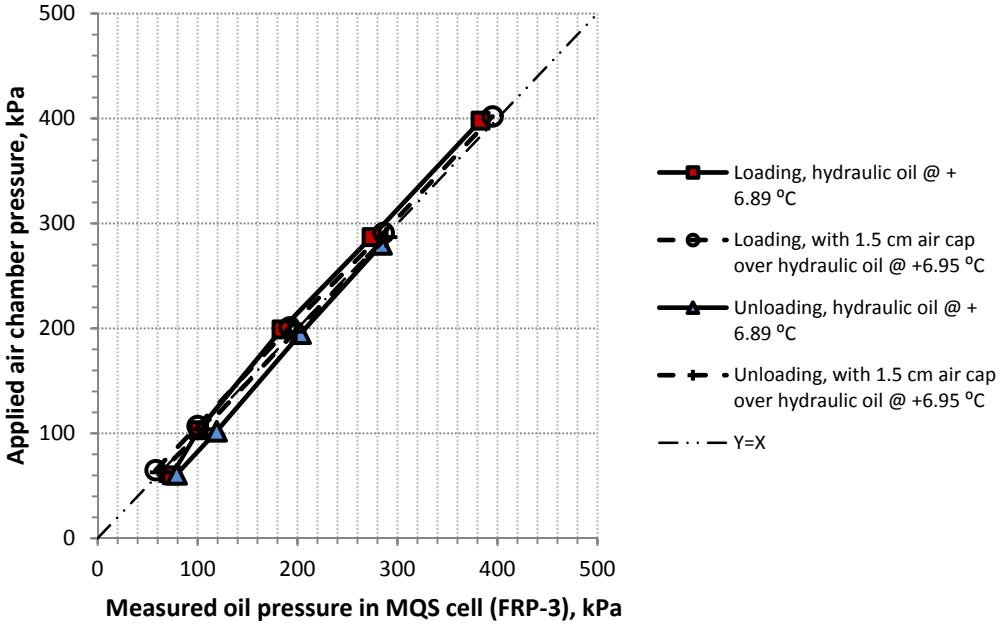

Figure 3-9. FRP response to the applied air chamber pressure when hydraulic oil is placed in the MQS cell at +6.9°C, with and without an air cap between the loading piston and the oil

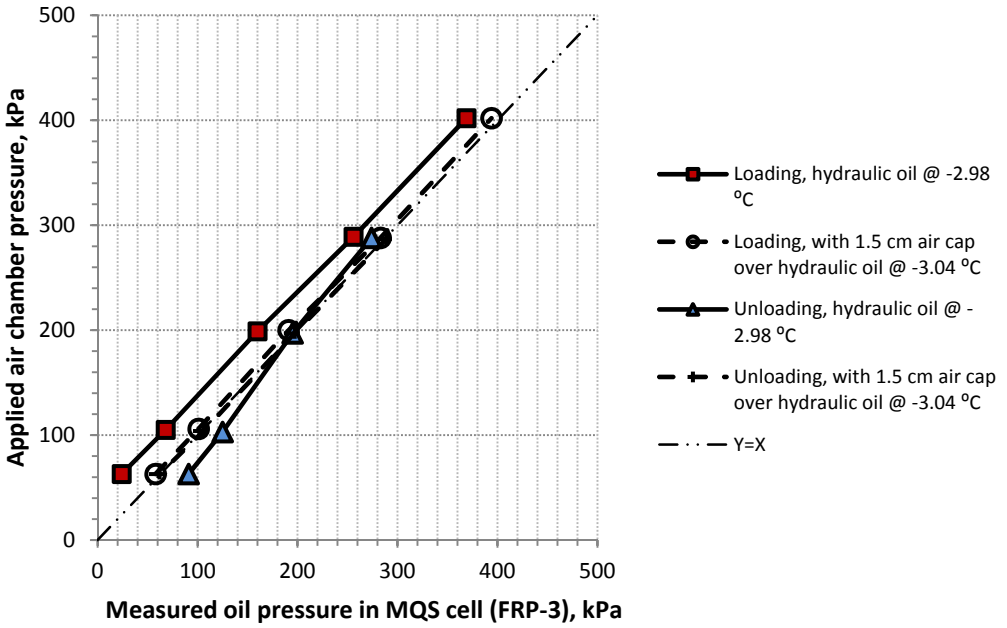

Figure 3-10. FRP response to the applied air chamber pressure when hydraulic oil is placed in the MQS cell at -3°C, with and without an air cap between the loading piston and the oil

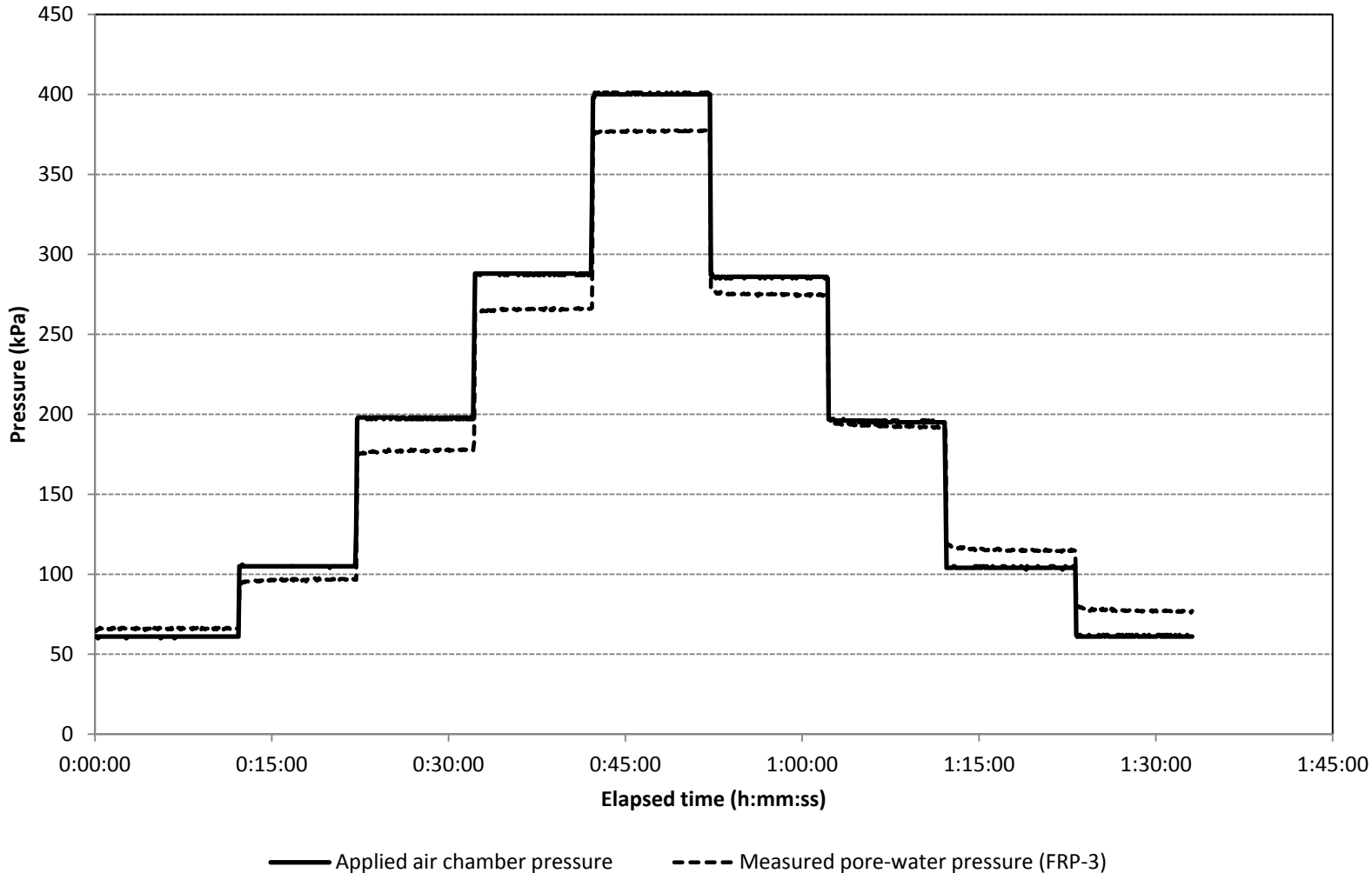

Figure 3-11. Pore-water pressure response in saturated sand in loading and unloading scenarios during calibration (with 1.5 cm water cap above sand)

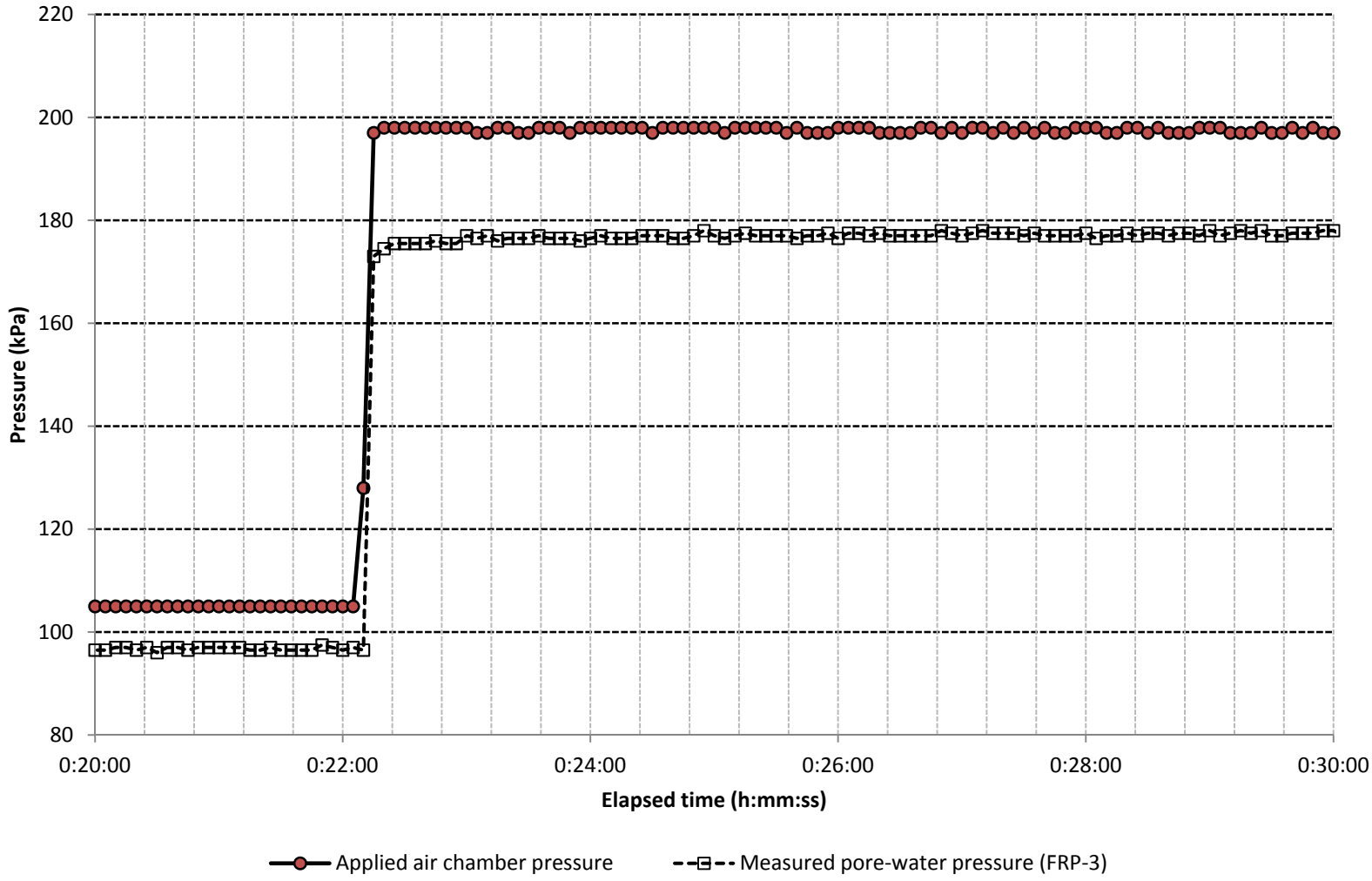

Figure 3-12. Trend of pore-water pressure equalization in 'saturated sand' in a 'loading step', measured by FRP-3 during calibration (with 1.5 cm water cap above sand)

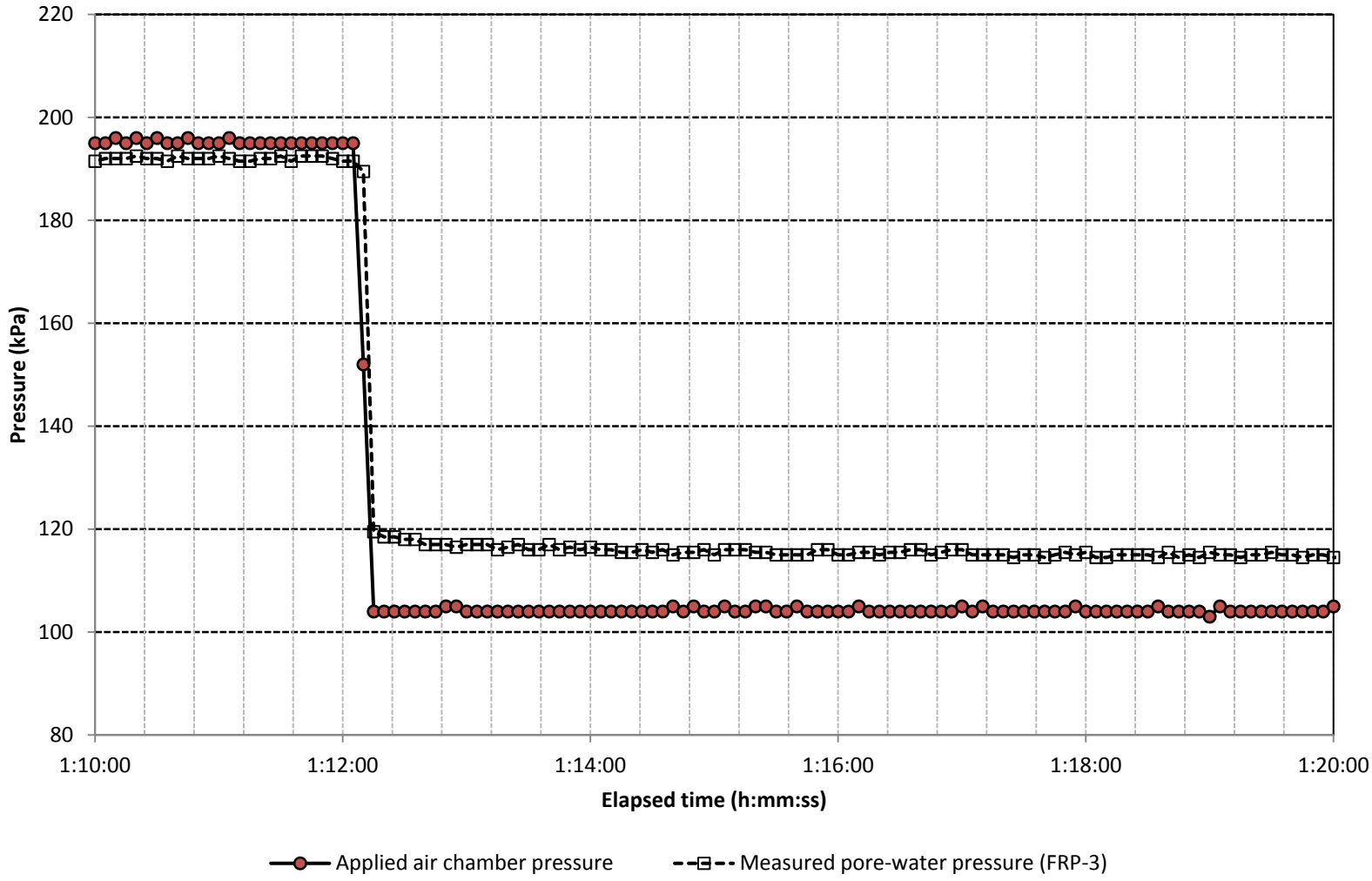

Figure 3-13. Trend of pore-water pressure equalization in 'saturated sand' in an 'unloading step', measured by FRP-3 during calibration (with 1.5 cm water cap above sand)

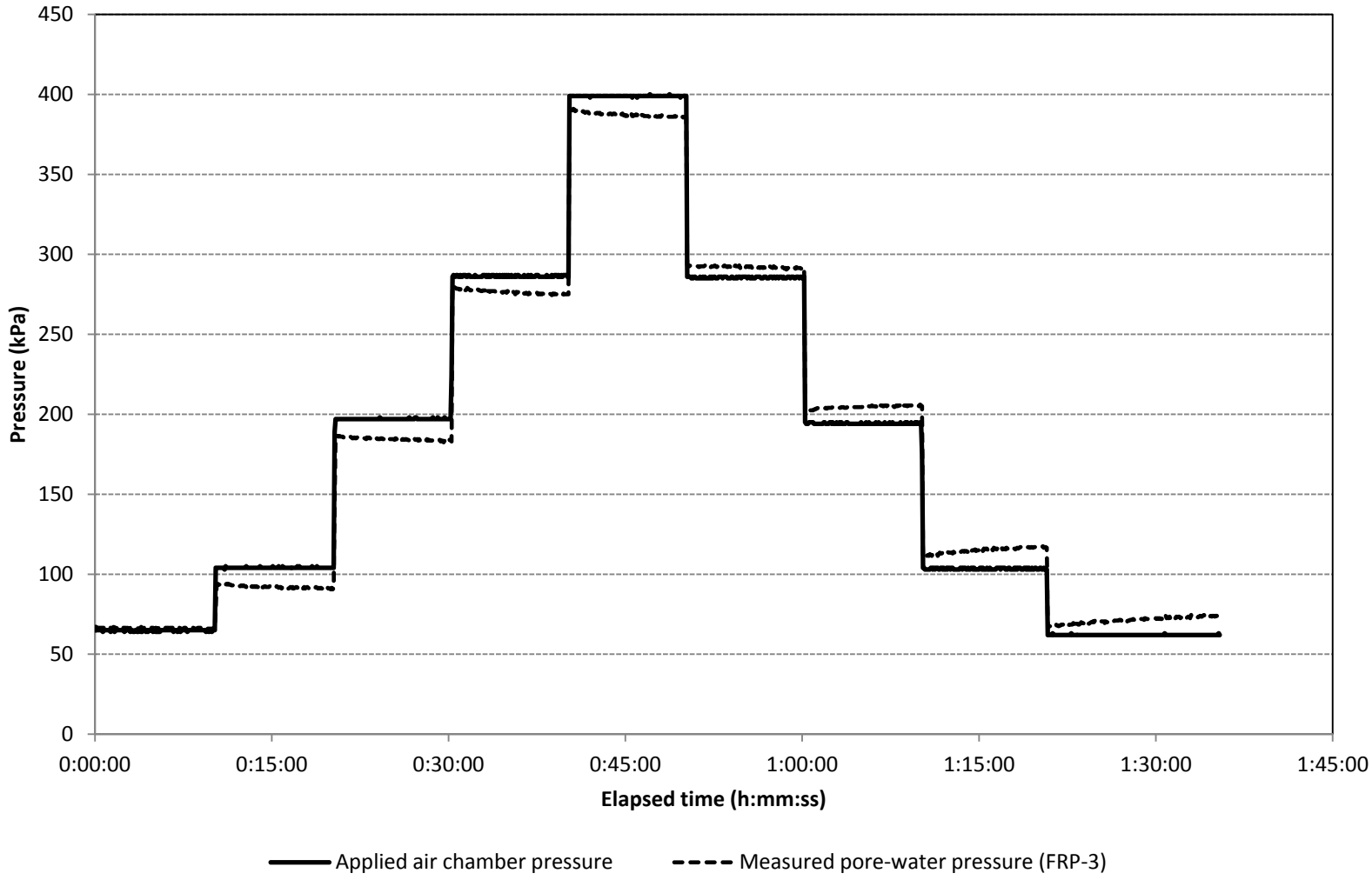

Figure 3-14. Pore-water pressure response in 'unsaturated sand' in loading and unloading scenarios during calibration (with 1.5 cm water cap above sand)

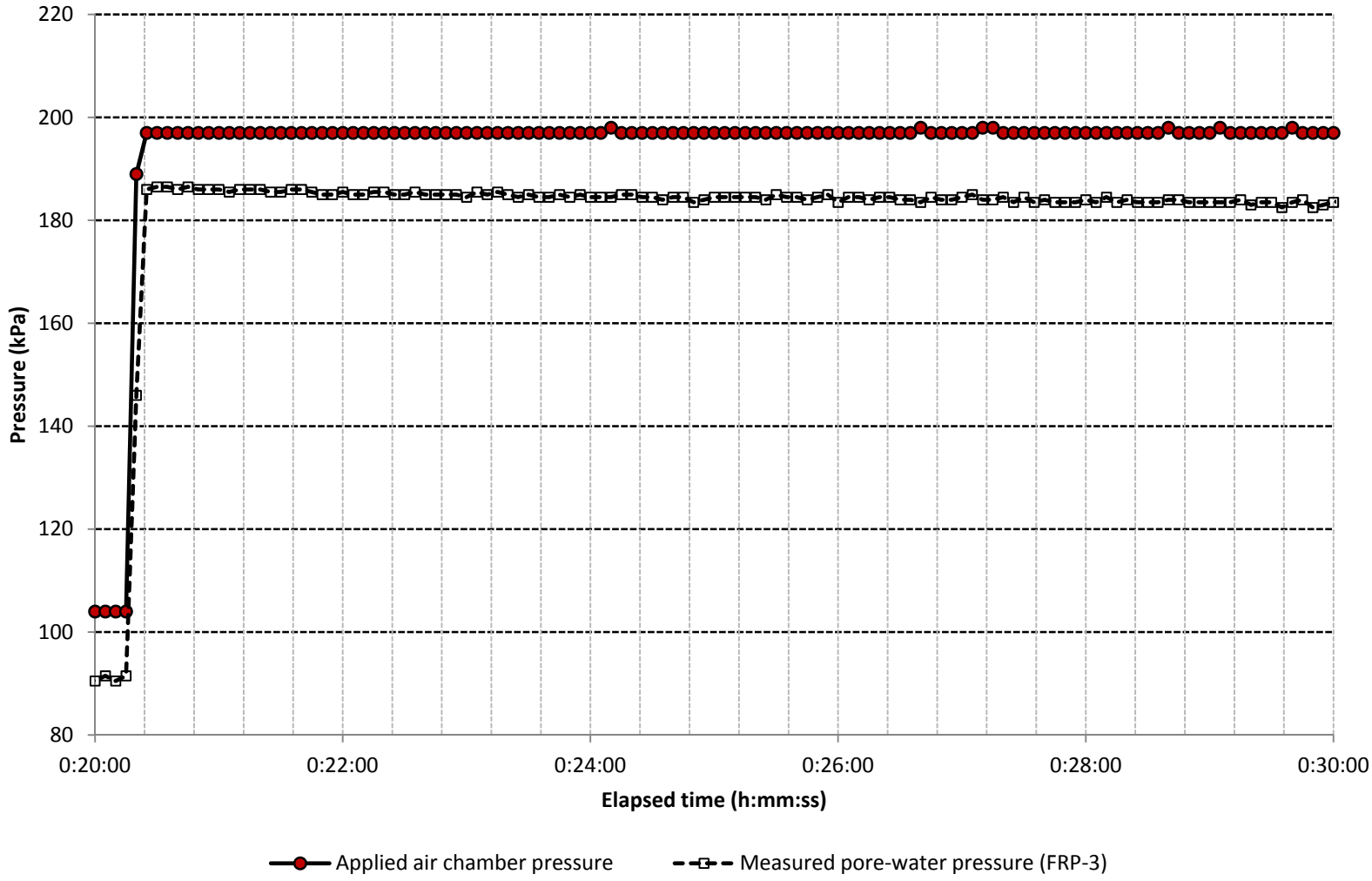

Figure 3-15. Trend of pore-water pressure equalization in 'unsaturated sand' in a "loading step", measured by FRP-3 during calibration (with 1.5 cm water cap above sand)

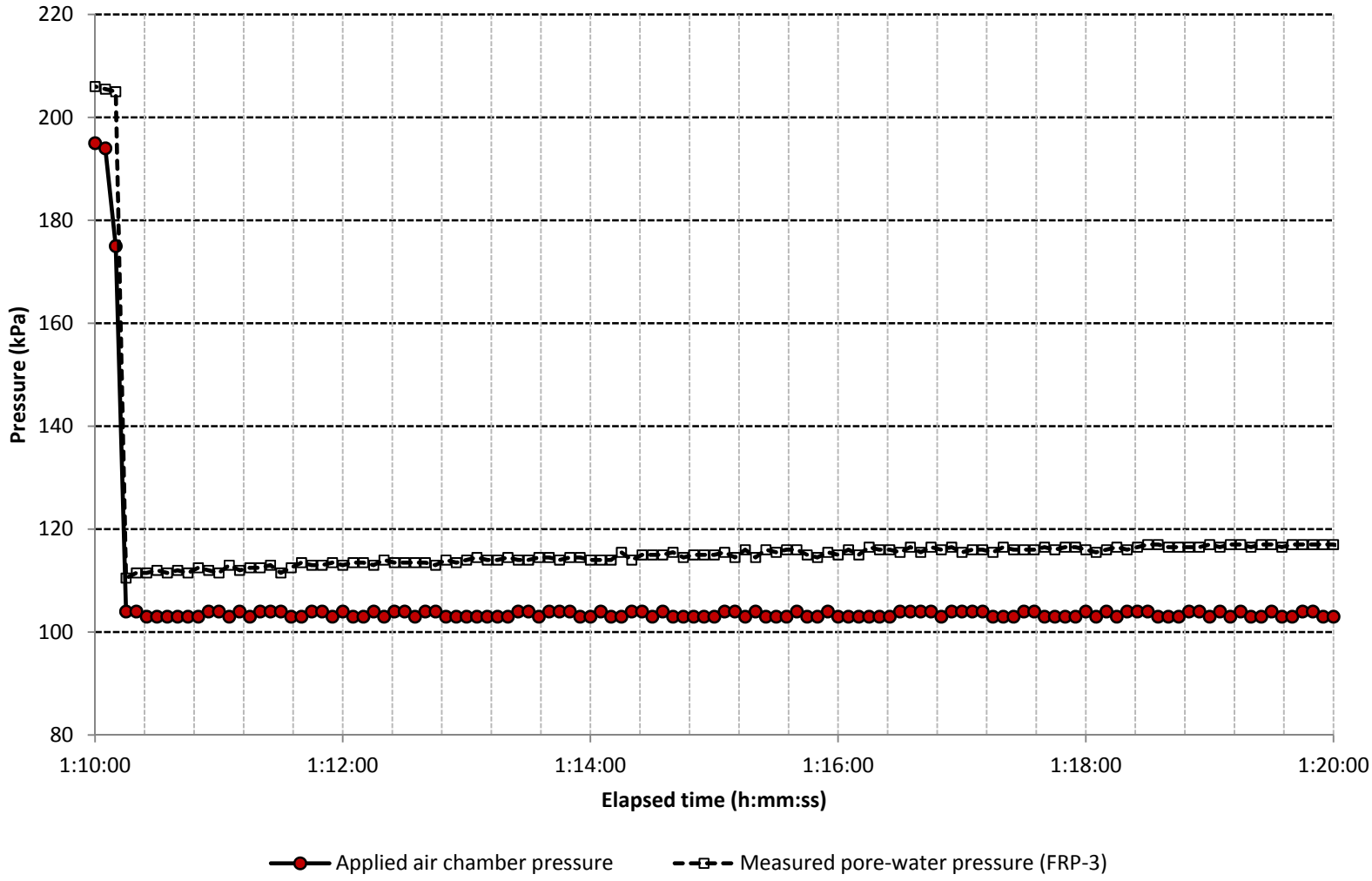

Figure 3-16. Trend of pore-water pressure equalization in 'unsaturated sand' in an "unloading step", measured by FRP-3 during calibration (with 1.5 cm water cap above sand)

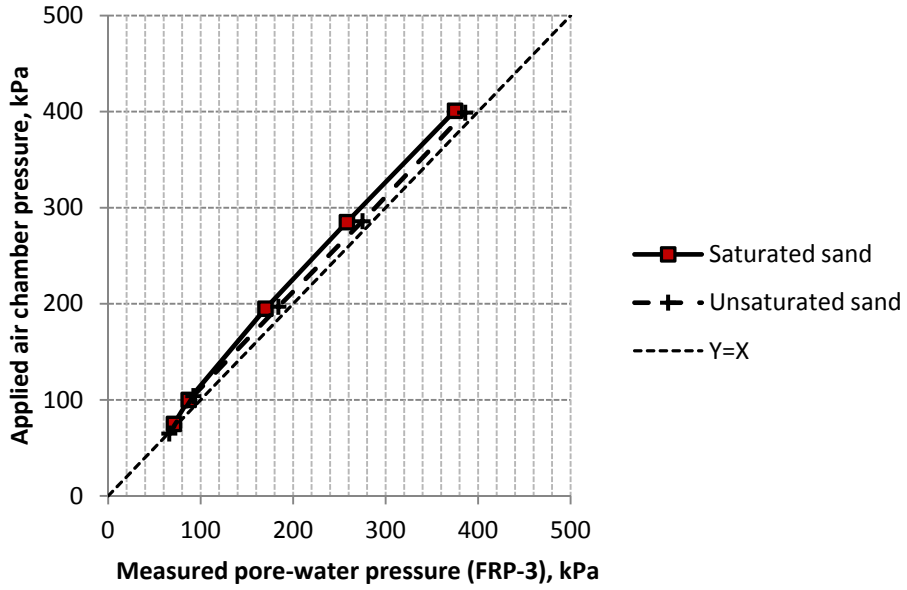

(a) loading

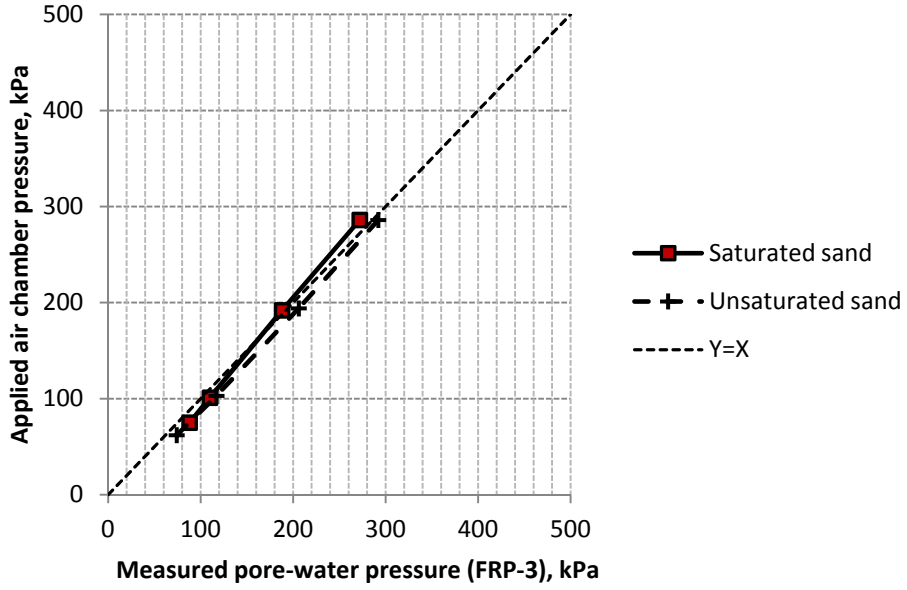

(b) unloading

Figure 3-17. Effect of desaturation of specimen on the calibration of FRPs in loading and unloading: the curves move towards and get parallel to Y=X line

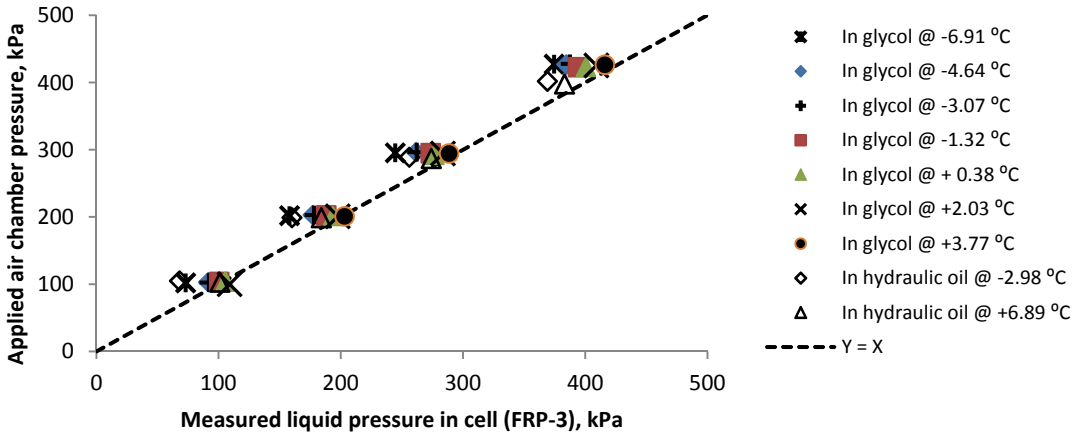

(a) Shift of the calibration data points to the left with reduction of the cell temperature

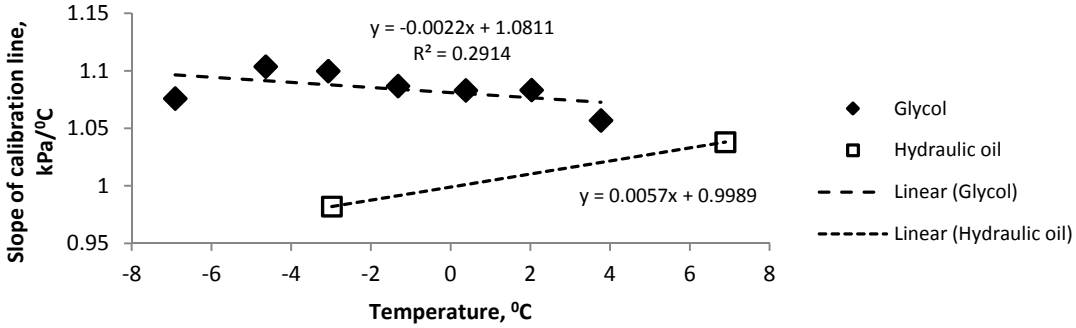

(b) Influence of the cell temperature on the slope of the fitted calibration lines

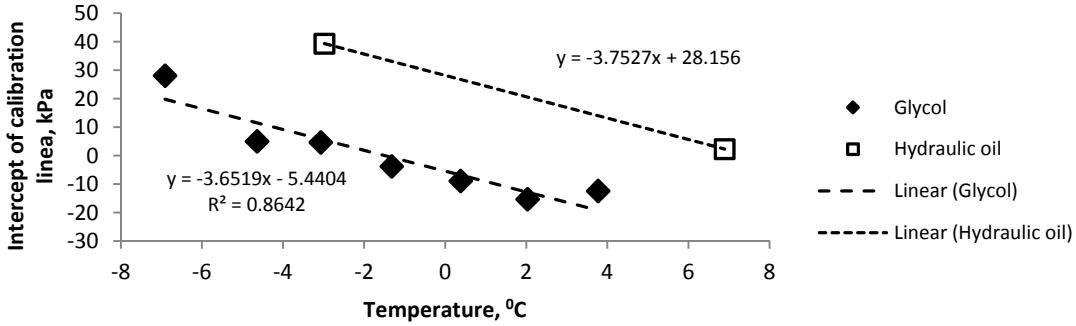

(c) Influence of the cell temperature on the intercept of the fitted calibration lines

Figure 3-18. Influence of cell temperature on measured FRP response to the applied air chamber pressure when either glaycol-water mix or hydraulic oil is placed in the MQS cell

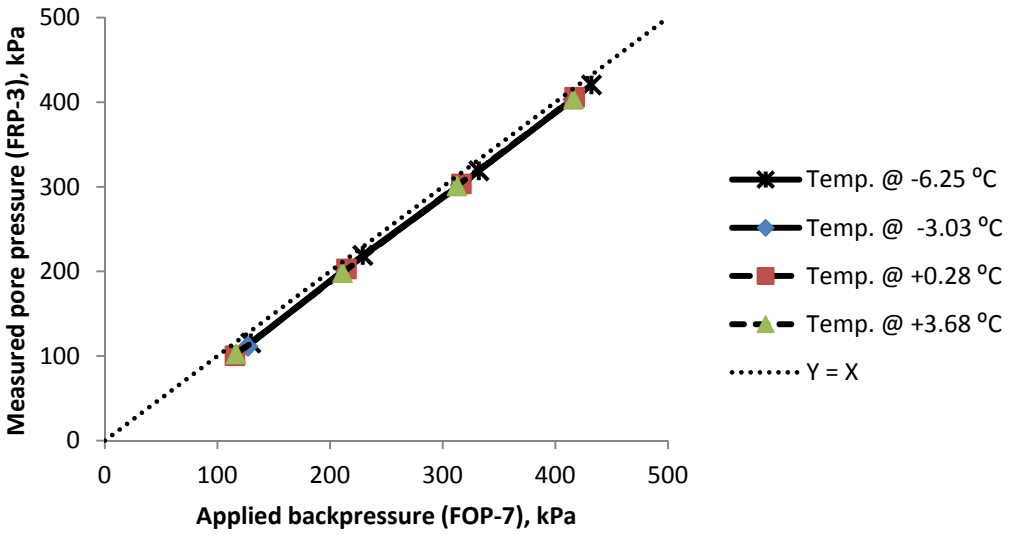

(a) Loading

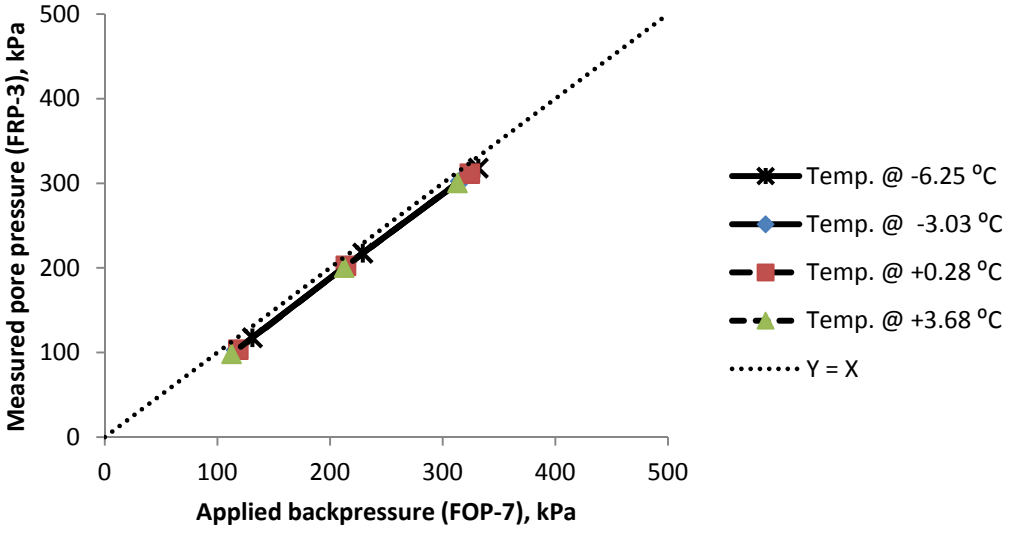

(b) Unloading

Figure 3-19. Influence of the cell temperature on measured FRP response to the applied backpressure when glaycol-water saturated sand is placed in the MQS cell

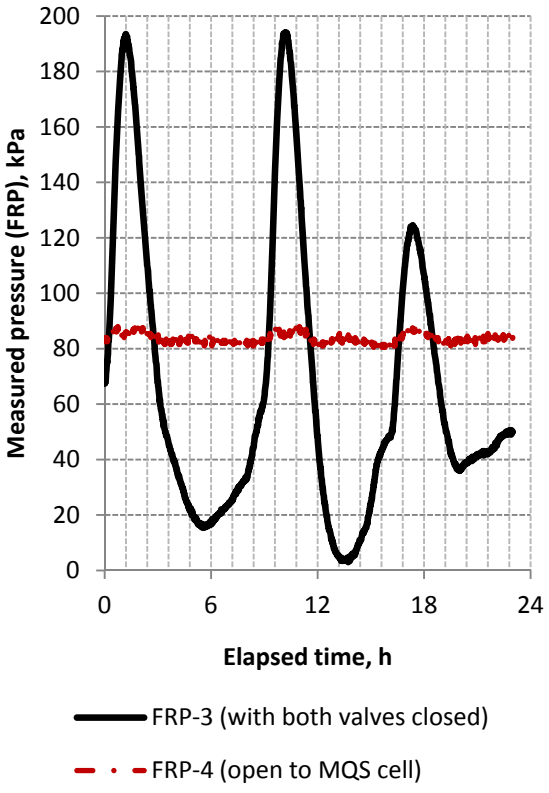

(a) FRP response to ambient temperature fluctuations

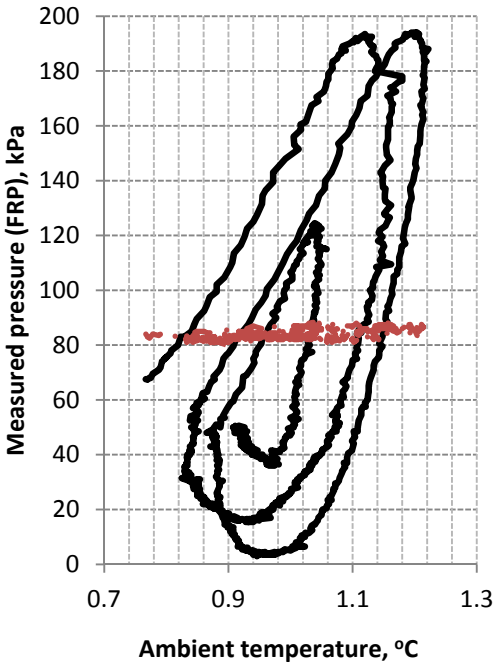

Fluctuations:
FRP 3 = ± 95 kPa
FRP 4 = ± 4 kPa
Ambient temperature = ± 0.23 °C

(b) Thermally induced fluctuations in measured pressures by FRPs

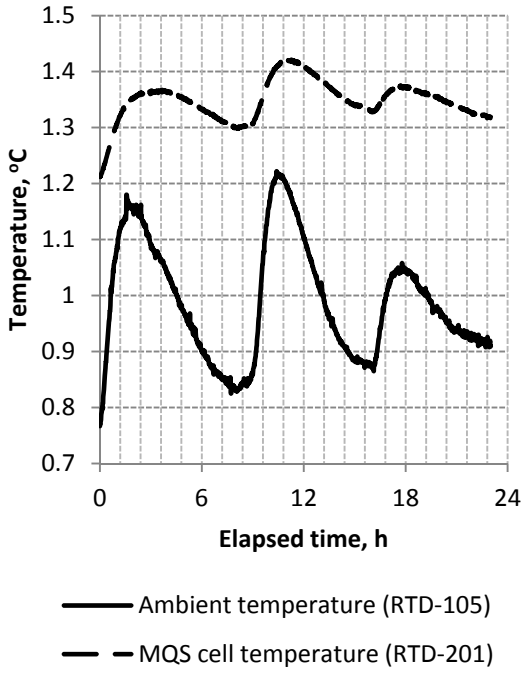

(c) Temperature fluctuation

Figure 3-20. Effects of ambient temperature fluctuations on FRP response

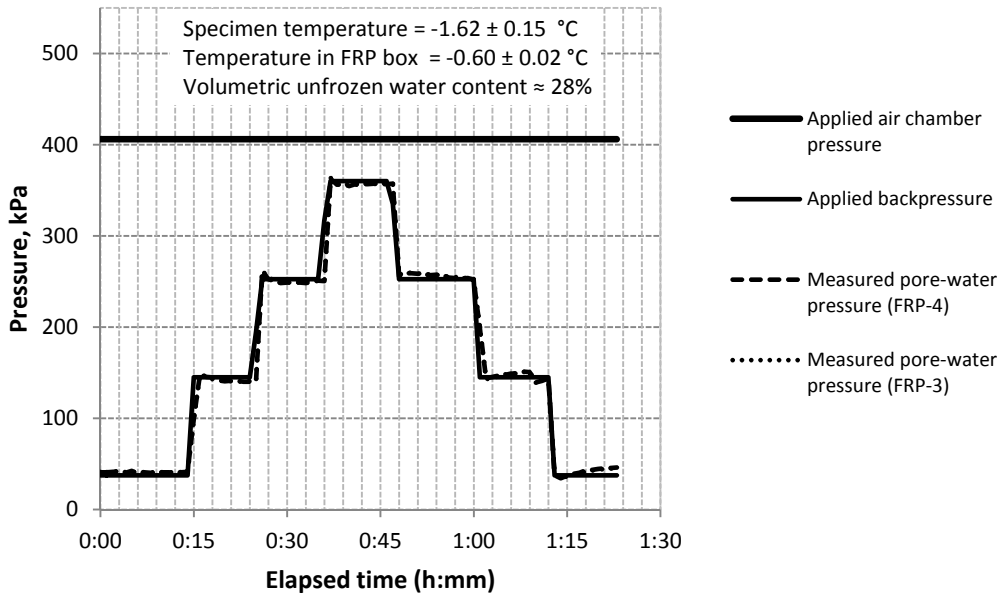

(a) Continuity of pore-water pressures in a "nearly saturated" partially frozen OC sand

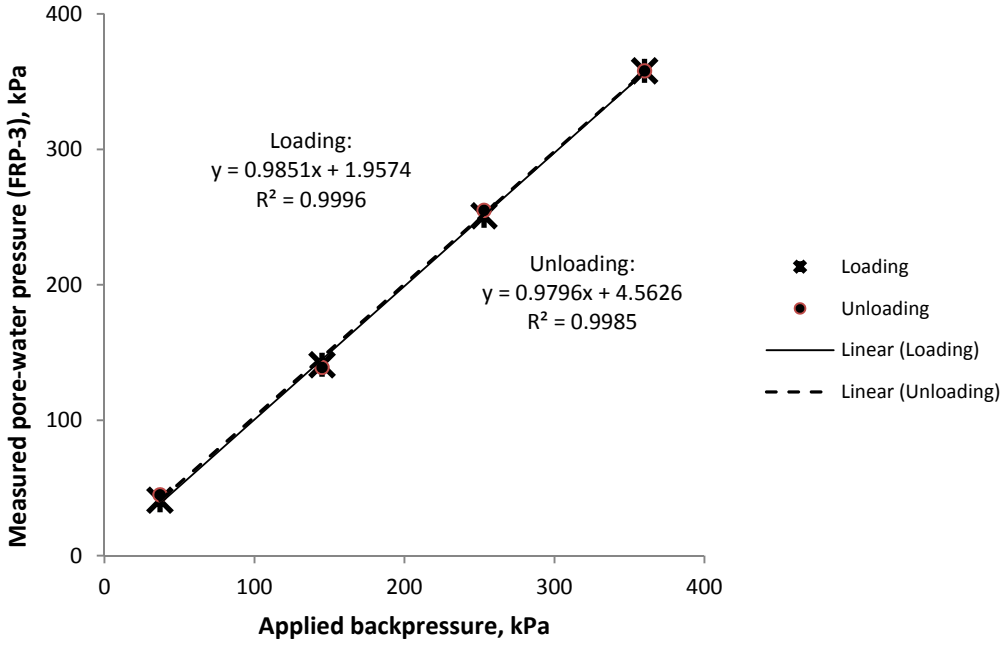

(b) Response of FRP-3 to change in the applied backpressure measured 10 minutes after application of each loading step

Figure 3-21. Pore-water pressure response in a "nearly saturated" partially frozen OC sand subjected to change in the applied backpressure while total stress is kept constant

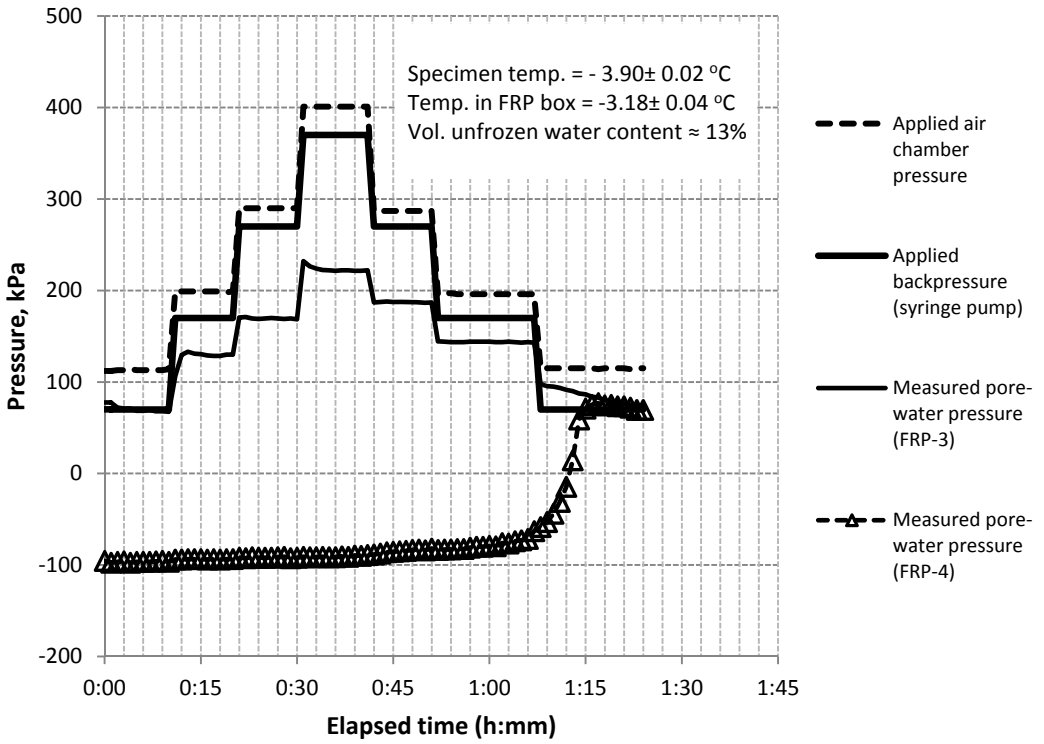

Figure 3-22. Pore-water pressure response during gradual saturation of an unsaturated partially frozen saline sand at -3.90°C during a backpressure test to examine the continuity of pore-water pressures

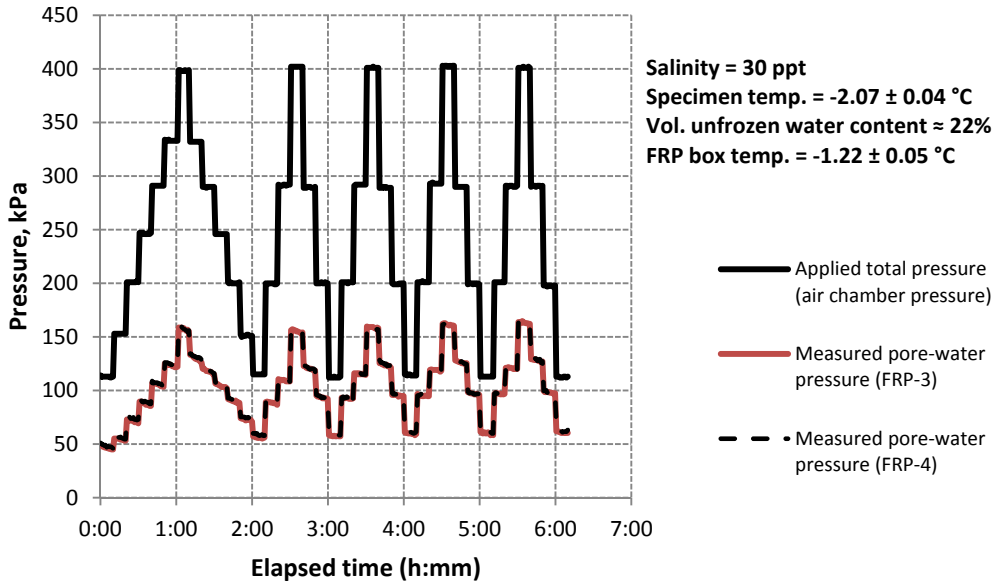

(a) Pore-water pressure response of partially frozen saline sand subjected to repeated undrained loading and unloading

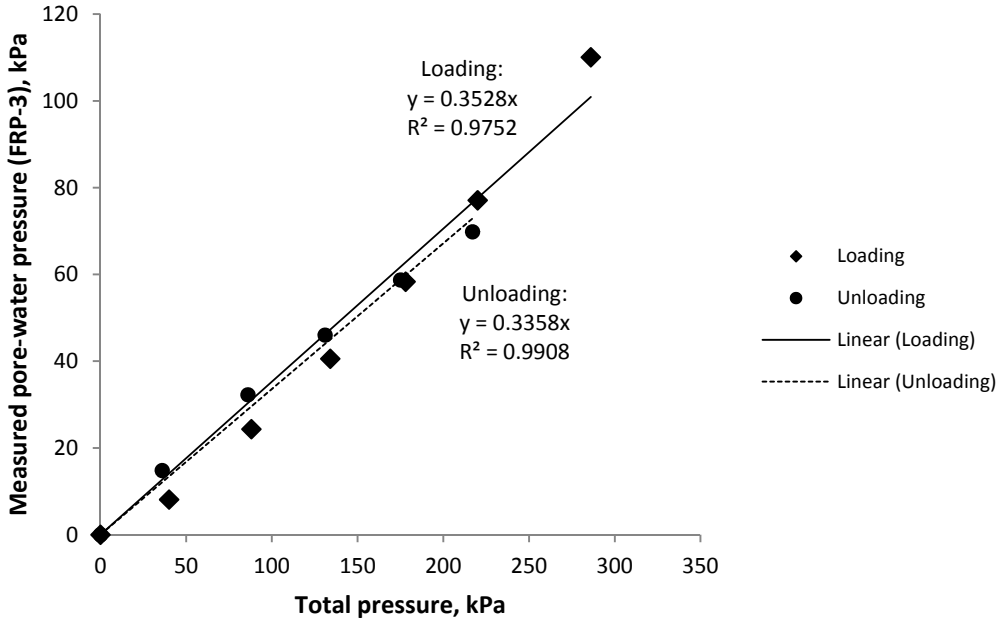

(b) Pore-water pressure response of partially frozen saline sand to an undrained loading, measured 10 minutes after application of each loading-unloading step in the first loading-unloading cycle

Figure 3-23. Pore-water pressure response of partially frozen saline sand (30±1 ppt salinity) subjected to repeated undrained loading and unloading

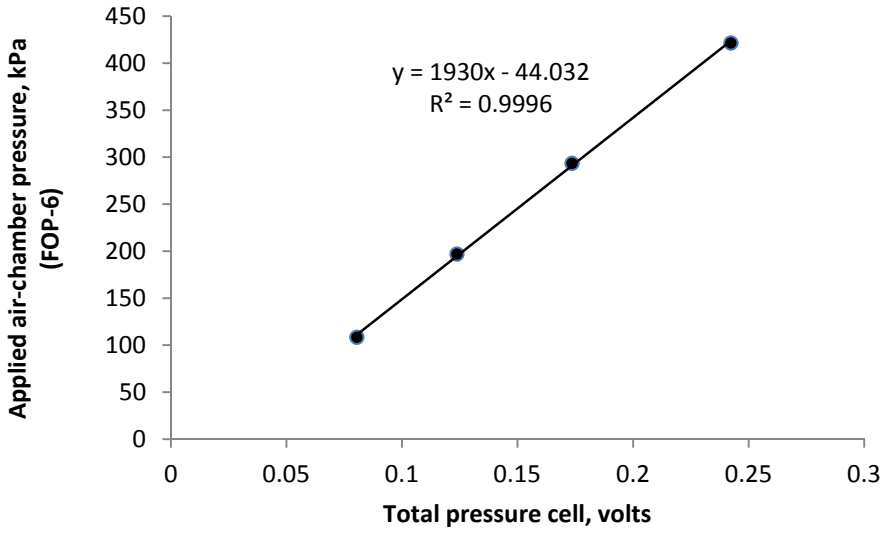

Figure 3-24. Calibration of the total pressure cell in the MQS cell

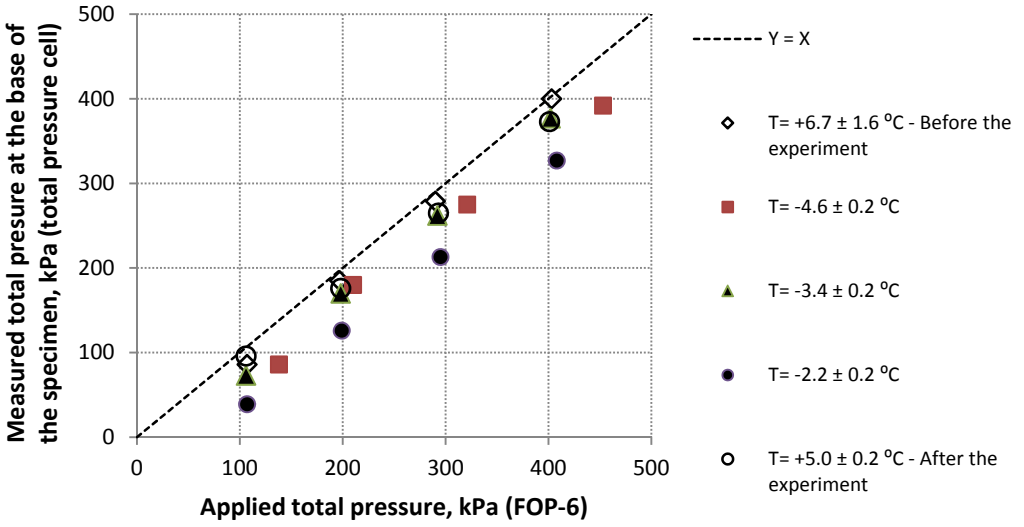

(a) Total stress transfer to the base of the specimen

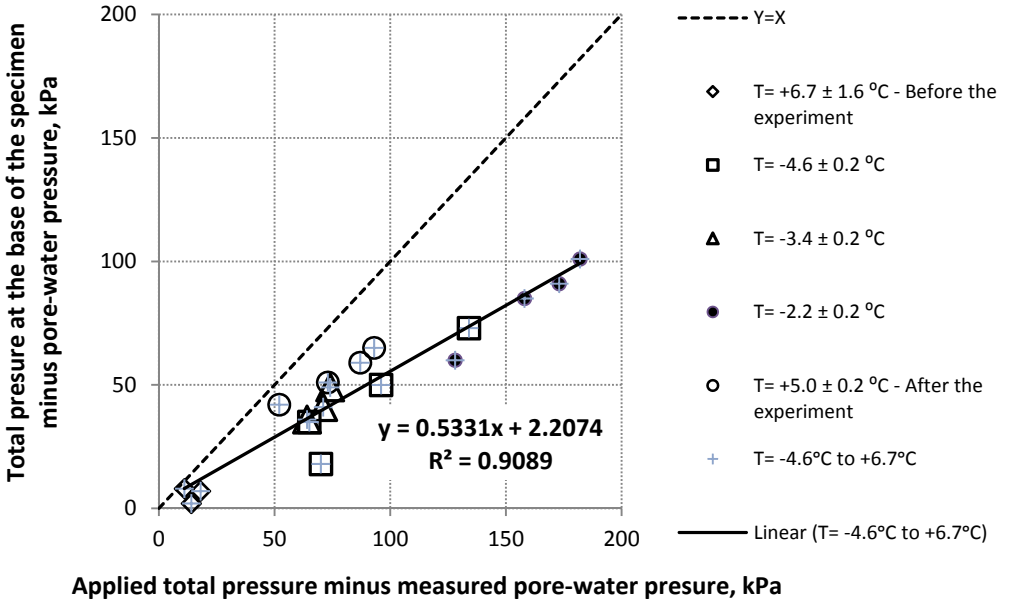

(b) Effective stress transfer to the base of the specimen

Figure 3-25. Total and effective stress transfer to the base of the saline sand specimen (30±1 ppt NaCl) at temperatures between -4.6°C to +6.7°C

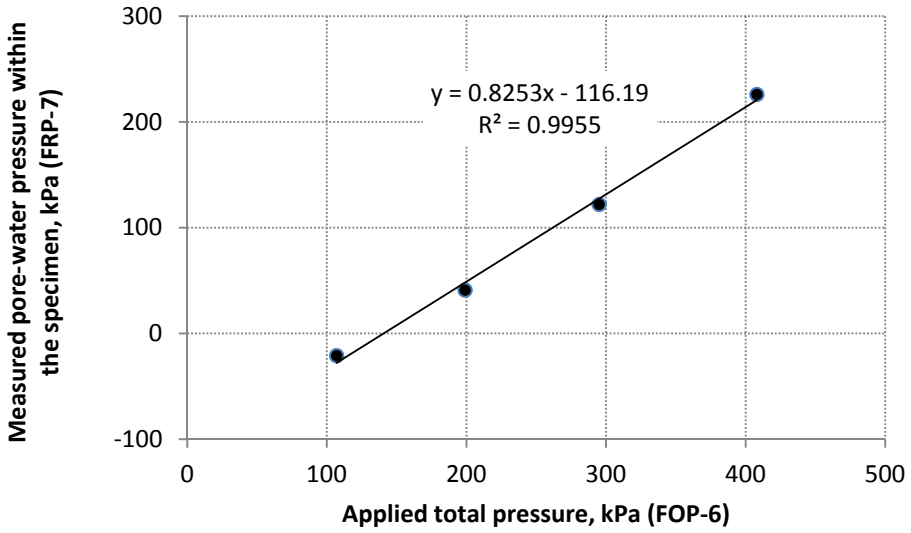

(a) Pore-water pressure response

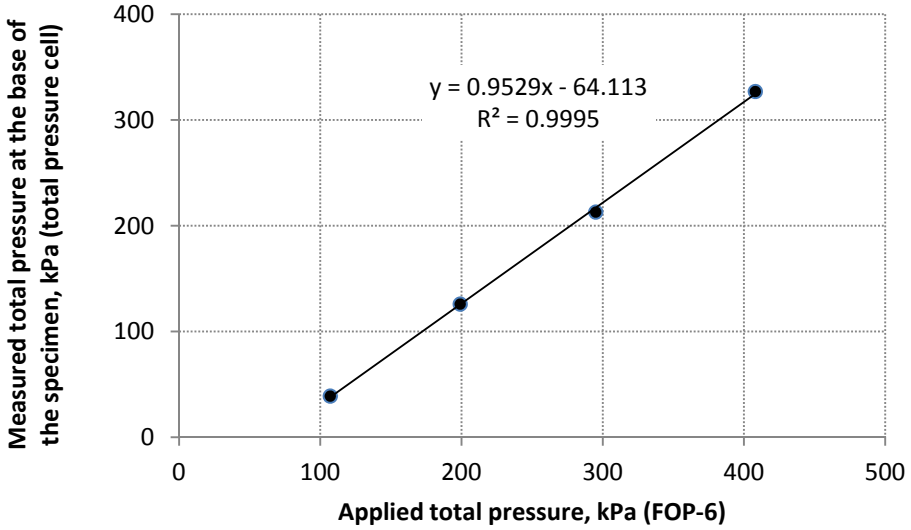

(b) Applied total stress at the top and bottom of the specimen

Figure 3-26. Applied total stress at the ends and the measured pore-water pressure response within a partially frozen saline sand specimen (30±1 ppt NaCl) at -2.2±0.2°C

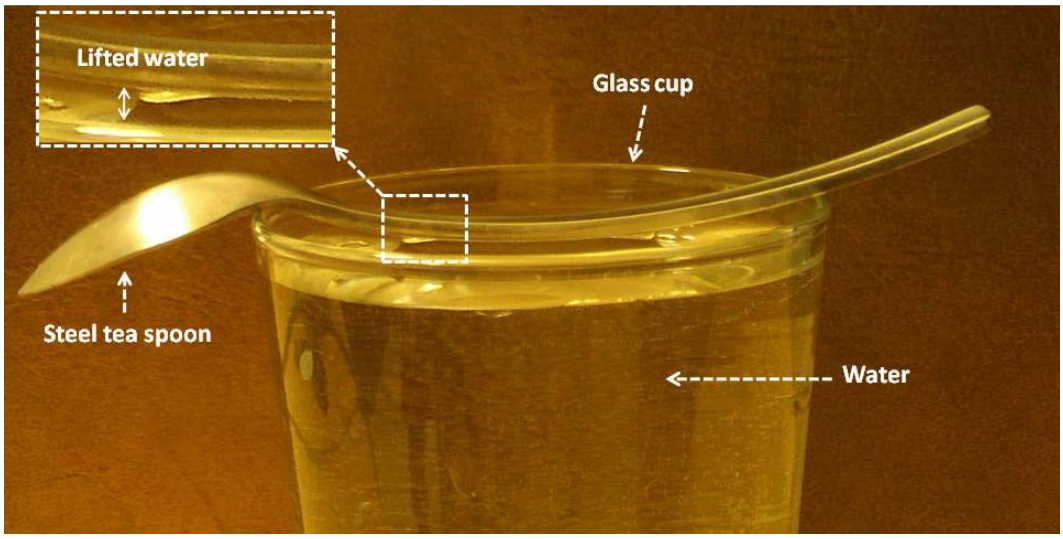

Figure 3-27. Water is lifted from its free surface owing to its tensile strength and adhesion to steel

3.8 References

Arakeri, V.H. 1979. Cavitation inception. Proceedings of Indian Academy of Sciences, Section C: Engineering Sciences, **2**(2): 149-177.

Arenson, L.U., and Sego, D.C. 2006. The effect of salinity on the freezing of coarse-grained sands. Canadian Geotechnical Journal, **43**(3): 325-337.

Dunnicliff, J., and Green, G.E. 1993. Geotechnical instrumentation for monitoring field performance. Wiley, New York.

Fisher Scientific. 2001. Operation manual for handheld refractometers for saltwater/brine with automatic temperature compensation, Catalog Number 13-946-27. Fisher Scientific

Fredlund, D.G., and Rahardjo, H. 1993. Soil mechanics for unsaturated soils. Wiley, New York.

Gibson, R.E. 1963. An analysis of system flexibility and its effect on the time lag in pore water pressure measurements. Geotechnique, **13**(1): 1-11.

Guan, Y., and Fredlund, D.G. 1997. Use of the tensile strength of water for the direct measurement of high soil suction. Canadian Geotechnical Journal, **34**(4): 604-614.

Haeri, S.M., and Shakeri, M.R. 2010. Effects of membrane compliance on pore water pressure generation in gravelly sands under cyclic loading. Geotechnical Testing Journal, **33**(5): 375-384.

Hivon, E.G., and Sego, D.C. 1995. Strength of frozen saline soils. Canadian Geotechnical Journal, **32**(2): 336-354.

Krahn, J., and Fredlund, D.G. 1972. Total, matric and osmotic suction. Soil Science, **114**(5): 339-348.

Martin, G.R., Finn, W.D.L., and Seed, H.B. 1978. Effects of system compliance on liquefaction tests. Journal of the Geotechnical Engineering Division, ASCE, **104**(4): 463-479.

OMEGA. 2007. Portable pressure calibrators with built in pressure pump. Accessed online at http://www.omega.com/pptst/DPI603.html on Nov 14, 2007 [online].

Qiu, Y., and Sego, D.C. 2001. Laboratory properties of mine tailings. Canadian Geotechnical Journal, **38**(1): 183-190.

Ridley, A.M. 2003. Recent developments in the measurement of pore water pressure and suction. Geotechnical News, **21**(1): 47-50.

Sego, D.C., and Chernenko, D. 1984. Confining pressure influence on the strength of frozen saline sand. *In* 3rd International Specialty Conference on Cold Regions Engineering, Northern Resource Development. Canadian Society for Civil Engineering, Edmonton, Alberta, Canada, pp. 565-578.

Sego, D.C., Shultz, T., and Banasch, R. 1982. Strength and deformation behavior of frozen saline sand. *In* 3rd international symposium on ground freezing. US Army Cold Regions Research and Engineering Laboratory, Hanover, NH, pp. 11-17.

Sun, D.C., Wen, W., Zhiming, Z., Xiaoyang, C., and Meili, S. 2008. Theory of cavitation in an oscillatory oil squeeze film. Tribology Transactions, **51**(3): 332-340.

Teledyne Isco Inc. 2010. D-series pumps, installation and operation guide. Accessed online at http://www.isco.com/products/products3.asp?PL=1051020 on Nov 12, 2010.

Thomson, W. 1871. On the equilibrium of vapour at a curved surface of liquid. The London, Edinburgh and Dublin Philosophical Magazine and Journal of Science, **42**(282): 448-452.

Tokimatsu, K. 1990. System compliance correction from pore-pressure response in undrained cyclic triaxial tests. Soils and Foundations, **30**(2): 14-22.

Trevena, D.H. 1984. Cavitation and the generation of tension in liquids. Journal of Physics D: Applied Physics, **17**(11): 2139-2164.

Veyera, G.E., Charlie, W.A., Doehring, D.O., and Hubert, M.E. 1992. Measurement of the pore-pressure parameter C less than unity in saturated sands. Geotechnical Testing Journal, **15**(3): 223-230.

Washio, S., Takahashi, S., Uemura, K., Iwamoto, T., and Ogata, T. 2008. Singular properties of flow separation as a real cause of cavitation inception. Proceedings of the Institution of Mechanical Engineers, Part C: Journal of Mechanical Engineering Science, **222**(4): 667-678.

Wissa, A.E.Z. 1969. Pore-pressure measurement in saturated stiff soils. Journal of the Soil Mechanics and Foundations Division, ASCE, **95**(SM4): 1063-1073.

4. Pore-water pressure response in a partially frozen soil

4.1 Introduction

This chapter provides a step toward establishing effective stress analysis and design in partially frozen soils by independently measuring pore-water pressure and total stress, as well as, estimating the stress distribution between the ice matrix, soil matrix, and unfrozen water phase in a partially frozen soil. Modern soil mechanics owes its beginning to the introduction of the concept of effective stress; the stress that governs deformation and strength of a soil mass. In an effective stress analysis, effective stresses and effective stress material properties are used. These properties, unlike total stress material properties, are stress and stress path independent, are measured at well-distinguishable steps during the test, and have less uncertainty (scatter) due to the method of identification and measurement. Therefore, identical results (with narrow scatter) are obtained by others when they use these methods. Owing to the higher confidence in determining material properties, factors of safety (costs) are selected and used efficiently, which leads to optimized design to minimize risks. Establishing the effective stress concept for partially frozen soils is the prerequisite for extending the critical states soil mechanics and limit states design to frozen ground engineering.

It is necessary to first determine how much of the applied loads are carried by each phase (mineral soil, water, and ice) to quantify effective stresses and effective stress material properties in a

partially frozen soils and its behavior under applied loads. Thus, stress transfer mechanics in partially frozen soils and the role of pore-water pressure coefficients in determining stress transfer in unfrozen soils will be reviewed in the following subsections. The major technical obstacles in setting up the effective stress principle in soils at subfreezing temperatures have been:

(1)- Difficulty with conducting reliable and accurate measurements of unfrozen pore-water pressure distribution within soils at subfreezing temperatures

(2)- Lack of data on continuity of unfrozen water within soils at subfreezing temperatures

A summary of previous research and technical requirements for measuring pore-water pressures in soils at subfreezing temperatures, as well as, a reliable method for measuring pore-water pressure within partially frozen soils is presented in Chapter 2. This chapter presents continuity of unfrozen water phase within a partially frozen soil and pore-water pressure response to undrained loading via independently changing applied backpressure and total pressure in uniformly prepared partially frozen saline sand specimens. First-time measurements of pore-pressure distribution within a partially frozen soil under applied loads are presented and compared to that in the unfrozen soil. Thus, by assuming superposition, stress distribution between the ice matrix, soil matrix, and unfrozen water phase are determined via measurements of Skempton's pore-pressure coefficient B-bar ($\bar{B}$) for pore-water and pore-ice. Saline sand specimens at 30±1 ppt NaCl were used in this study. Sand was used as it is generally considered to have a linear elastic soil skeleton.

It is also shown that the change in Terzaghi's effective stress under undrained loading is not zero; hence, frictional resistance is not zero under undrained conditions in partially frozen sand due to the stiffer solid phase. Study of the effective stress and strain paths under undrained and drained consolidation of a partially frozen soil is not in the scope of the current research and will be presented in a separate manuscript.

4.1.1 Stress transfer mechanics in unfrozen soils: role of pore-water pressure coefficients

A saturated soil consists of soil grains and water. If there are no soil grains, water will carry the entire applied load (similar to the case of a ship floating on water). If there is no water, the soil skeleton will carry the entire applied load. Pore-pressure equations evaluate what portion of the load will be carried by the water phase when water is present between the soil grains. Knowledge of the pore-water pressure is essential to assess the flow of water through a porous material and to predict the effective stress that controls its resistance and deformation. Therefore, estimating the excess pore-water pressure in response to the applied loads is desirable. Pore-pressure equations are developed to give estimates of excess pore-pressures under applied loads in field applications and to simplify numerical analysis using the effective stress approach. Fluids have no shear resistance and flow when they are subjected to pressure gradients. Skempton (1948b) presented the first pore-water pressure equation for 'saturated' soils (at constant temperature):

$$\boldsymbol{\Delta u = \Delta\sigma_3 + A(\Delta\sigma_1 - \Delta\sigma_3)} \tag{4-1}$$

Skempton (1954) further introduced pore-pressure coefficient $\boldsymbol{B}$ and expanded Equation (4-1) to Equation (4-2) for 'saturated and unsaturated' soils:

$$\boldsymbol{\Delta u = B[\Delta\sigma_3 + A(\Delta\sigma_1 - \Delta\sigma_3)]} \tag{4-2}$$

Further:

$$\frac{\boldsymbol{\Delta u}}{\boldsymbol{\Delta\sigma_1}} = \bar{\boldsymbol{B}} = \mathbf{B}\left[\frac{1-(1-\mathbf{A})(1-\mathbf{K})}{1-\mathbf{B}(1-\mathbf{A})(1-\mathbf{K})}\right] \quad \text{(Bishop 1954)} \tag{4-3}$$

Where:

$\boldsymbol{\Delta u}$ = the excess pore-water pressure due to changes in principal total stresses, $\Delta\sigma_1$ and $\Delta\sigma_3$ (kPa)

A, **B**, and $\bar{\boldsymbol{B}}$ = the Skempton's pore-water pressure coefficients

$\mathbf{K}$ = Lateral earth pressure coefficient

Pore-pressure coefficient $\boldsymbol{B}$ was originally introduced to represent desaturation effects. Fredlund and Rahardjo (1993) introduced separate $\boldsymbol{B}$ pore-pressure coefficients for air and water phases in an unsaturated soil. Later in this chapter, separate $\overline{\boldsymbol{B}}$ pore-pressure coefficients will be introduced for water and ice phases. Unlike separate $\boldsymbol{B}$ coefficients for separate phases, separate $\overline{\boldsymbol{B}}$ coefficients for each phase have a physical meaning; they define what percentage of the total load is carried by each phase. Various extensions to Equation (4-2) and Equation (4-3) have been used in soil mechanics for:

- Controlling staged construction of embankments
- Stability analysis of earth dams during rapid draw down
- Predicting deformations of footings under loads
- Calculating effective stress when carrying out numerical analysis

It should be noted that Equation (4-1) for Skepton's $\boldsymbol{A}$ pore-pressure parameter was derived for the specific case of triaxial compression tests ($\boldsymbol{\sigma_2 = \sigma_3}$ and $\boldsymbol{\sigma_1}$is vertical), under conditions of 'no water content change', and it assumes no volume change, linear elasticity, and superposition.

Skempton's pore-water pressure coefficient $\overline{\boldsymbol{B}}$ has been termed differently for various boundary conditions representing practical situations:

- $\boldsymbol{C = \overline{B}}$ for undrained loading in the oedometer (no lateral strains, K_0 loading) (Lambe and Whitman 1969)
- $\boldsymbol{D = \overline{B}}$ for undrained loading in uniaxial loading (lateral strains permitted) (Lambe and Whitman 1969)
- $\boldsymbol{B = \overline{B}}$ for isotropic loading (K = 1)
- $\boldsymbol{r_u = \overline{B}}$ for field condition (field $\overline{\text{B}}$) in general triaxial loading ($\boldsymbol{\sigma_2 \geq \sigma_3}$ and $\boldsymbol{\sigma_1}$ can have any direction) and permitted lateral strains, 'partial drainage', and volume change. Pore-pressure coefficient r_u (commonly known as 'pore-pressure ratio') was first introduced

by Bishop and Morgenstern and is extensively used for field control of staged construction of large embankments (Bishop and Morgenstern 1960)

The $\boldsymbol{C}$ coefficient is less than $\boldsymbol{B}$ coefficient for identical soils and is generally used for (Veyera et al. 1992):

- Predicting saturation state
- Estimating changes in effective stress during loading
- Predicting blast-induced liquefaction

Generally, value of Skempton's $\boldsymbol{B}$ pore-pressure coefficient is used as a measure to determine degree of saturation of specimens in the laboratory testing (Bishop and Henkel 1962; Chaney et al. 1979; Lee et al. 1969; Wissa 1969). However, for an unfrozen soil this coefficient is a function of several soil parameters:

$$\boldsymbol{B} = \frac{1}{1 + \boldsymbol{n} \times \boldsymbol{S_r}\left(\frac{\boldsymbol{C_w}}{\boldsymbol{C_d}}\right) + \left(\frac{\boldsymbol{n}}{\boldsymbol{C_d} \times \boldsymbol{P_a}}\right)(1 - \boldsymbol{S_r})} \qquad \text{(Lade and Hernandez 1977)} \qquad (4\text{-}4)$$

Where:

$\boldsymbol{n}$: Porosity of the soil,

$\boldsymbol{C_d}$: Compressibility of the soil matrix (1/kPa)

$\boldsymbol{C_w}$: Compressibility of the pore-water (1/kPa)

$\boldsymbol{P_a}$: Absolute pressure in the pore fluid (kPa), and

$\boldsymbol{S_r}$: Degree of saturation

In addition to soil parameters, the effects of testing equipment can be far more important on the measured pore-water pressures (Lade and Hernandez 1977). In a partially frozen soil, ice content and structure, as well as, time and temperature dependency of the ice matrix stiffness also

influence ***B*** (Chapter 2). System compliance and other factors affecting pore-water pressure measurements in partially frozen soil specimens are studied in Chapter 3.

To verify saturation in very stiff soils, general practice is to determine ***B*** at several successively higher backpressures while keeping the effective consolidation pressure constant. A measured ***B*** value that is 'constant' and independent of the magnitude of the backpressure indicates full saturation (Lee et al. 1969; Wissa 1969). ***B*** values for different types of soil at full and nearly saturation are presented by Black and Lee (1973). However, increasing backpressure in a partially frozen soil at temperatures close to 0^{o}C may decrease the ice fraction of the soil and hence alter the measurements.

When best practice laboratory procedures are used to produce saturated specimens, generally specimens with a degree of saturation above 98% are produced. To generate ideal saturation conditions in the laboratory, generally high backpressures (for example 1 MPa reported by Mesri et al. (1976)) are applied to these nearly saturated soil or rock specimens. By applying high backpressures, air bubbles dissolve in water, up to approximately 2% volumetric (Blume 1976), and water is forced not to cavitate, hence a less compressible pore-fluid transfers the pressures. Further insights into compressibility of pore-fluid in a soil and its role on the measured pore-water pressures are discussed in Chapter 2. Hence, backpressure can be used as a measure of compressibility of pore-fluid to replicate realistic field conditions with nearly saturated soils at the same degree of saturation. In these nearly saturated soils air content in the soil does not create an independent continuous phase. The replication is not 100% accurate. However, it is a practical measure to make estimations for quantitatively understanding the behavior of partially frozen soils in this study. The air phase generally becomes continuous as the degree of saturation is reduced to less than approximately 85% (Corey 1957; Sparkes 1963). Water phase in clay generally becomes discontinuous and does not flow if the degree of saturation is less than 50% (Barden 1965; Wroth and Houlsby 1985). Gilbert (1959) showed that for Vicksburg silty clay the air phase is continuous at moisture content 4% below the optimum moisture content and discontinuous at moisture content 3% above the optimum moisture content. When the degree of saturation is above 90%, the

air phase becomes occluded, and air flow is only via diffusion through the pore-water (Matyas 1966). It should be noted that if the water or air phase is not continuous, it cannot be treated as an independent phase (Fung 1977; Gonzalez and Stuart 2008). The soil specimens in the current study are laboratory prepared saline sand specimens with initial degree of saturation greater than 99.9%. Degree of saturations remained above 98% throughout the experiments, evaluated by balance of water inflow and outflow and deformations of the specimens. Further, comparison of the calibration curves before and after the experiments (unfrozen state) is used as an indicator of the quality of the measurements by quantifying the effects of air diffusion into the specimens on the pore-water pressure measurements (Chapter 3).

In addition to determining stress ratio between solid and liquid phase, pore-pressure coefficients also have application as a failure criterion. Baxter et al. (2010) showed that Skempton's $\overline{\boldsymbol{A}}$ pore-pressure coefficient (Skempton 1954) can be used as a failure criterion for weakly cemented unfrozen soils. This may have application in warm permafrost soils where the ice matrix provides a weak cementation to the soil particles.

4.1.2 Stress transfer mechanics in soils at subfreezing temperatures

Ladanyi and Morel (1990) provided a summary of stress-transfer mechanics in soils at subfreezing temperatures under deviatoric stresses based on the previous research by Ladanyi (1974; 1981; 1985):

(1) When a strain history is applied to an unfrozen soil, its effective stresses are forced to follow a well-defined path. The strain path in principal strain space is uniquely related to the stress path in the principal stress space

(2) When a strain history is applied to a frozen soil with no water phase, the effective stress path followed by the soil skeleton will be the same as that in the same soil but unfrozen. The soil is regarded as the same soil when its density, degree of consolidation, and water content are the same. Therefore, at any strain, the stress tensor in the pore-ice equals to the difference between the

applied stress tensor and the effective stress tensor in the soil skeleton. The pore-ice can temporarily sustain not only hydrostatic but also deviatoric stresses (unlike water).

(3) Where ice and water phases coexist in the soil pores in a partially frozen soil, a stress change in one phase is reflected by an equal change in the other phase, their difference remaining constant under isothermal conditions.

Based on this proposed stress transfer mechanics, the stress changes in the pore-ice can be predicted under the conditions of consolidated undrained (constant volume) triaxial tests at constant confining pressures. Following the same line of reasoning, Ladanyi and Morel (1990) reported that they theoretically evaluated and experimentally confirmed the effect of internal stresses on the strength under compression of dense, particulate, ice-saturated sand, subjected to dilatancy-hardening. However, they did not carry out pore-water pressure measurements within the soils at subfreezing temperatures. Further, their concluding summaries do not consider time and temperature dependency of the ice matrix stiffness and the time dependent proportionality of ice and water pressures.

In this chapter, after describing the testing methods and experiments for conducting B-bar tests and undrained warming, method for estimating stress in pore-ice is described. Effects of preconsolidation, backpressure, and temperature on pore-water pressure response to undrained loading in partially frozen and unfrozen saline sand specimens under conditions of low confining pressures and backpressures are studied. The temperatures were maintained at subfreezing temperatures close to 0^{o}C in partially frozen specimens. These conditions resemble near surface soil conditions of interest for geotechnical engineering in permafrost regions. Maintaining temperatures close to, but below, 0^{o}C ensures sufficient unfrozen water can exist in the partially frozen soil for continuity of the water phase. Further, in conditions of low applied total pressures and backpressures, pressure melting of ice is minimized (Chapter 2). For the temperature range of -1^{o}C to -5^{o}C, a pressure in the range of 9 MPa to 55 MPa is required for pressure melting of polycrystalline ice (Barnes et al. 1971a). Bragg and Andersland (1981) reported that compressive

forces between sand particles and pore ice at points of contact induce pressure melting. Ma et al. (1999) found that at confining stresses in the range of 1 MPa (for frozen silty clay) to 5 MPa (for frozen fine sand), and at temperatures in the range of -2^{o}C to -15^{o}C, the strength of the frozen soils decreased with increasing confining pressure owing to pressure melting caused by high contact pressures. The applied pressures in the current study are kept below 0.5 MPa, which is 10 times less than the reported value for pressure that cause contact pressure melting in non-saline frozen fine sand. To the author's best knowledge, to this date there is no reported method to accurately quantify points of contact pressure melting in a partially frozen saline soil. The author perceives that in partially frozen saline sand some of the fragile ice matrix will break and may melt and the water from pressure melting will freeze back to reach thermodynamic equilibrium should the thermodynamic conditions after pressure melting and release of high contact pressures dictate so. A further investigation in this regard remains for future research.

Validity of the measurements and continuity of the unfrozen water phase are verified by independent change of backpressure. Further, generated pore-water pressures during undrained warming were studied, as well as, pore-water pressure response to undrained loading within partially frozen and unfrozen specimens at various temperatures. These observations were used to study the role of ice fraction and ice melt on the stress transfer mechanics and generated pore-water pressures in partially frozen specimens.

4.2 Methods and experiments

Testing equipment and materials, as well as, procedures for specimen preparation, calibration, rapid freezing, and subsequent warming of the specimens are the same as described in Chapter 3. Figure 4-1 illustrates the Modified Qiu-Sego large strain consolidation apparatus (MQS cell) and Figure 4-2 shows the grain size distribution of the sand used in this research. A total of 14 set of partially frozen and unfrozen experiments were conducted with each set including up to a maximum of 19 B-bar tests. Data affected by leaking, excessive desaturation or diffusion of air into the specimen, thermal fluctuations, or discontinuous unfrozen water phase were not used.

Representative data of the best quality experiments are presented in this chapter. Reviewing the results of the experiments shows that the experiments show similar general trends. Factors affecting the measurements or causing erratic observations are discussed later in this chapter and recommendations for improved measurements are provided. Table 4-1 summarizes properties of the specimens used in experiments number 12 (unfrozen) and experiment number 14 (partially frozen) presented in this chapter. Both specimens had salinity of 30±1 ppt NaCl. Initial degree of saturation is estimated to be greater than 99.9% in freshly placed, previously boiled sand specimens.

4.2.1 Calibration

Calibration of the measuring system (FRPs as installed in the MQS cell while specimen is in the cell) before and after each experiment was conducted and interpreted according to the guidelines given in Chapter 3 as a measure for quality control of the experiments.

4.2.2 Validity of the measured pore-water pressures within partially frozen saline sand specimens

Continuity of water phase in partially frozen soil specimens is checked by applying backpressures independent of the applied total pressure and measuring the corresponding pore-water pressure response. The water phase is considered continuous if the measured pore-water pressures reflect the applied backpressures and all FRPs show the same trend of pore-pressures within the specimen.

4.2.3 Effects of preconsolidation on pore-water pressure response to undrained loading in unfrozen saline sand specimens

Specimens were first consolidated under drained conditions for a minimum of 11 hours. Then, $\overline{B}$-tests were conducted on preconsolidated unfrozen specimen by applying stepwise air pressures in the air chamber of the MQS cell under undrained conditions (drain valves closed) during loading and subsequent unloading in the range of 100 kPa to 450 kPa. The pore-water pressure

response of the specimen to the applied vertical loads was measured by FRPs. After each $\overline{\boldsymbol{B}}$-test, the specimen was consolidated at a higher effective preconsolidation pressure, and then unloaded to a predefined initial backpressure and total stress and allowed pressures to equalize for a minimum of 60 minutes before conducting the next $\overline{\boldsymbol{B}}$-test.

In several cases, $\overline{\boldsymbol{B}}$ values were measured at several initial backpressures (keeping the initial effective stress relatively constant) to quantify the effects of "near saturation conditions" at low backpressures. For this purpose, after each $\overline{\boldsymbol{B}}$-test, the top drain was connected to a higher backpressure, as well as, a higher initial total stress was applied to minimize the change in initial effective stress before conducting the next $\overline{\boldsymbol{B}}$-test.

Pore-water pressure responses during loading, unloading, and repeated loading and unloading were measured using 10 sec intervals and responses after 10 minutes of application of each loading step were plotted against total pressures (air chamber pressures). $\overline{\boldsymbol{B}}$ was determined as the slope of the linear fit for each loading and unloading cycle. It was observed that bilinear regressions provided better correlation coefficients than linear fits for loading cases in overconsolidated specimens. For bilinear fits, two separate lines were fitted through the measured data points. It was observed that the inflection point of the bilinear fit approximates the preconsolidation pressure plus initial backpressure for that experiment. Therefore, a primary and a secondary pore-water pressure response can be identified, for total stresses lower and higher than the total stress at the perceived inflection point. Therefore, primary (initial) and secondary $\overline{\boldsymbol{B}}$s were determined as the slope of each line:

$$\begin{aligned} \boldsymbol{u} &= \overline{\boldsymbol{B}}_i.\boldsymbol{\sigma} + \boldsymbol{u_{0i}} \quad \text{for primary response} \\ \boldsymbol{u} &= \overline{\boldsymbol{B}}_s.\boldsymbol{\sigma} + \boldsymbol{u_{0s}} \quad \text{for secondary response} \end{aligned} \tag{4-5}$$

In which:

$\boldsymbol{u}$: measured pore-water pressure (kPa)

$\boldsymbol{\sigma}$: applied total pressure (air chamber pressure, kPa)

$\overline{\boldsymbol{B}}_i$ and $\overline{\boldsymbol{B}}_s$: slopes of the primary and secondary response lines (fitted), respectively

$\boldsymbol{u_{0i}}$ and $\boldsymbol{u_{0s}}$: intercept of the lines fitted to the primary and secondary pore-water pressure responses, respectively (kPa)

Loading steps were conducted using 25 kPa intervals to better define the inflection points of the bilinear pore-water pressure response of the preconsolidated specimens. Unloading steps were conducted in 50 kPa intervals.

4.2.4 Effects of preconsolidation on pore-water pressure response to undrained loading in partially frozen saline sand specimens

The same procedure used for unfrozen specimens was used to conduct $\overline{\boldsymbol{B}}$-tests for partially frozen specimens at various preconsolidation levels and constant subfreezing temperature. In an attempt to reach the same level of preconsolidation void ratios as the unfrozen specimens, preconsolidation at predefined initial backpressures and total stresses were conducted for a minimum of 48 hours before each $\overline{\boldsymbol{B}}$-test in partially frozen specimens, in addition to the initial preconsolidation of the unfrozen specimen before freezing. In addition to $\overline{\boldsymbol{B}}$-tests in the partially frozen state, $\overline{\boldsymbol{B}}$-tests were also conducted before freezing the specimen, as well as, after the specimen was thawed. Similar to unfrozen case, it was also observed that pore-water pressure response of the overconsolidated partially frozen specimens is bilinear. Loading steps were conducted in 50 kPa intervals to shorten experiment duration.

4.2.5 Effects of warming on pore-water pressures in a partially frozen saline sand specimen

An overconsolidated partially frozen saline sand specimen (***OCR***=12) at subfreezing temperatures close to 0^oC was subjected to undrained warming at constant total pressures while pore-water pressures were measured. Then, the specimen was subjected to a predefined backpressure (194 ± 5kPa) for 60 minutes before conducting a $\overline{\boldsymbol{B}}$-test. These $\overline{\boldsymbol{B}}$-tests were conducted in one loading and

unloading cycle as described before. After the last unloading step of each $\bar{\boldsymbol{B}}$-test, the specimen was subjected to a warming cycle while the drain valves remained closed. This procedure was also continued for two temperatures above 0°C so that the net change in pore-water pressure coefficient due to change in ice fraction and temperature can be separated from the response of the soil specimen in the MQS cell.

4.2.6 Estimating pore-ice pressures and role of pore-ice pressure cut-offs

Pore-pressure coefficient $\bar{\mathbf{B}}$ is calculated by measuring pore-water pressure under undrained condition. This coefficient defines what percentage of the load is carried by the water phase under undrained condition and what percentage is carried by the solid phase. Via measuring $\bar{\mathbf{B}}$ in partially frozen and unfrozen specimens under undrained loading and assuming superposition, stress carried by the ice can be calculated:

$$\frac{\boldsymbol{\Delta u_{ice}}}{\boldsymbol{\Delta \sigma_1}} = \bar{\boldsymbol{B}}_{\boldsymbol{ice}} = \bar{\boldsymbol{B}}_{\boldsymbol{Water,Unfrozen}} - \bar{\boldsymbol{B}}_{\boldsymbol{Water,Partially\ frozen}} \tag{4-6}$$

Where:

$\boldsymbol{\Delta u_{ice}}$ = the excess pressure in pore-ice due to changes in principal total stresses, $\Delta\sigma_1$ and $\Delta\sigma_3$ (in kPa)

$\bar{\boldsymbol{B}}_{\boldsymbol{ice}}$ = pore-ice pressure coefficient

$\bar{\boldsymbol{B}}_{\boldsymbol{Water,Unfrozen}}$ = pore-water pressure coefficient measured in unfrozen state

$\bar{\boldsymbol{B}}_{\boldsymbol{Water,Partially\ Frozen}}$ = pore-water pressure coefficient measured in partially frozen state

Needle-like ice structure in partially frozen saline sand specimens were observed by Arenson and Sego (2006). Figure 4-3 shows a schematic of the pore-ice matrix, consisting of contact-ice and needle-ice, in partially frozen saline sand. When the partially frozen saline sand specimen is undisturbed before applying further consolidation, the fragile needle-like ice structure has very low stiffness and sustains negligible pressure; therefore $\bar{\boldsymbol{B}}_{\boldsymbol{ice}} \approx 0$ and it is 'assumed' that negative

values of $\bar{B}_{ice}$ do not exist when the specimen is subjected to positive pressures. The author calls this lower limit of $\bar{B}_{ice}$ in compression 'pore-ice pressure cut off'. It should be noted that ice can sustain tensile stresses (for example when pore-ice resists specimen dilation) and therefore negative ice pressures are possible. It is necessary that both partially frozen and unfrozen sand specimens have the same initial void ratio for Equation (4-6) to be valid. This condition is required to assume that the soil matrix carries the same amount of stress in both partially frozen and unfrozen states (Ladanyi and Morel 1990). During the experiments conducted in this research, the same levels of void ratios were not achieved by consolidating the partially frozen specimens at the same effective preconsolidation pressures applied to unfrozen specimens even though the subfreezing temperatures were close to 0^{o}C and up to 4 times the consolidation time was allowed. Therefore, fitted graphs were used to make comparison between measured B-bars in partially frozen and unfrozen states at the same void ratios.

In addition to the necessity of comparing B-bars at the same initial void ratios, it is deemed necessary to consider variables that might affect the pore-pressure measurements such as soil history (preconsolidation stress and void ratio) and initial loading conditions (initial backpressure and total stress). To simplify the process of comparing B-bars in partially frozen and unfrozen specimens having only void ratio as the variable, it is necessary to keep the 'other variables' constant so that their effects are eliminated. Alternatively, one may use interpolated values at constant values of these 'other variables'.

Variable selection is the process of selecting which independent (predictor) variables (including transformed variables) from possible candidates should appear in the final regression model. Stepwise regression procedures are semi-automated processes of building a regression model (or "fine tuning" existing models) by successively adding or removing variables based solely on the p-values of the estimated coefficients. The p-value, commonly used in 'statistical significance testing', is the probability of obtaining a 'test statistic' at least as extreme as the observed one, assuming the 'null hypothesis' is true. In variable selection case, the null hypothesis is that there is no relationship between measured phenomena. When the p-value is less than the 'significance

level', the null hypothesis is rejected and the result is said to be 'statistically significant' (unlikely to have occurred by chance). A significance level of 0.1 deems as extraordinary any result that is within the 10% of possible results under the null hypothesis.

Stepwise variable selection technique in Oakdale Engineering Datafit software (Oakdale Engineering 2008) was used for data mining and automated multiple variable regression for finding the best regression curves. It was found that only initial condition variables (initial void ratio and initial backpressure) met significance level of 0.1 for entry into the model and soil history variables met significance level of 0.2 for experiments on unfrozen sand specimens.

4.3 Results

4.3.1 Calibration

Figure 4-4 compares the calibration curves before and after two of the partially frozen experiment during loading with durations of 259 and 633 hours. It is observed that the slope of the calibration curves did not change significantly and the difference in the slopes of the calibration curves were 1.3% and 1.8% for the 259 hours and 633 hours experiments, respectively.

4.3.2 Validity of the measured pore-water pressures within partially frozen saline sand specimens

Figure 4-5 shows pore-water pressure response to independent change of total pressures and backpressures within a nearly saturated partially frozen saline sand specimen (30±1 ppt NaCl) at $-3.22 \pm 0.03^{o}C$. All FRPs except FRP-5 show the same trend and reflect the applied backpressures. By further warming the specimen to $-3.0 \pm 0.03^{o}C$, measurements from FRP-5 too coincided with the rest of the FRPs.

4.3.3 Effects of preconsolidation on pore-water pressure response to undrained loading in the unfrozen saline sand specimen

Table 4-2 summarizes the measured B-bars from linear regressions on the measured pore-water pressure response to undrained loading-unloading scenarios at various initial conditions in the unfrozen saline sand specimen. Table 4-3 summarizes the primary and secondary B-bars of the loading steps for the same experiments. An example of the pore-water pressure response in a loading-unloading scenario is shown in Figure 4-6. Effects of preconsolidation and backpressure on linear and bilinear pore-water pressure responses in the overconsolidated unfrozen saline sand specimen are represented in Figure 4-7 and Figure 4-8, respectively.

4.3.4 Effects of preconsolidation on pore-water pressure response to undrained loading in the partially frozen saline sand specimen

Table 4-4 summarizes the measured B-bars from linear regressions on the measured pore-water pressure response within the partially frozen saline sand specimen that was subjected to loading-unloading scenarios at various initial conditions. Table 4-5 summarizes the primary and secondary B-bars of the loading steps for the same experiments. Where validity of the measured pore-water pressures was questionable, the data have been shaded. When the data points for each B-bar did not correlate, those B-bars were not considered in averaging. These erratic observations are further discussed later in this chapter under ice blockage due to collapse and deformation of fragile ice structure under loads in partially frozen saline sand. An example of pore-water pressure response in a loading-unloading scenario is shown in Figure 4-9 at -2.88 ± 0.02^{o}C. Figure 4-10 shows that the effects of preconsolidation and backpressure on the primary and secondary pore-water pressures within the partially frozen experiment are similar to that of the unfrozen experiment (Figure 4-8).

4.3.5 Effects of warming on pore-water pressures in the partially frozen saline sand specimen

Pore-water pressure response to undrained warming of the partially frozen saline sand specimen is shown in Figure 4-11. Data was collected at 10 sec intervals however plotted data is from 2 hours intervals. Decrease of pore-water pressure ($\boldsymbol{\Delta u}$) during undrained warming is shown in Figure 4-12 for this specimen and the results are tabulated in Table 4-6. A regression in the form of Equation (4-7) correlates this decrease in pore-water pressures as a function of initial gravimetric ice content and its decrease:

$$\boldsymbol{\Delta u} = \text{a}.\boldsymbol{\omega_i^{\text{b}}}(\boldsymbol{\Delta\omega_i})^{\text{c}} \tag{4-7}$$

Where:

$\boldsymbol{\omega_i} = \frac{\boldsymbol{M_i}}{\boldsymbol{M_s}}$: initial gravimetric ice content

$\boldsymbol{M_i}$: mass of ice (kg)

$\boldsymbol{M_s}$: mass of soil particles (kg)

$\boldsymbol{\Delta\omega_i}$: decrease in initial gravimetric ice content

a , *b*, and *c* are regression coefficients. Regression coefficients are presented in Table 4-7 using data from Table 4-6.

To account for the interface effects due to warming of the cell and the pore-fluid (Chapter 3) and estimate net change in pore-water pressure decrease by only the soil behavior, a term for temperature increment can be added to Equation (4-7):

$$\boldsymbol{\Delta u} = a.\boldsymbol{\omega_{\text{i}}^{b}}(\boldsymbol{\Delta\omega_i})^{c} + d.\boldsymbol{\Delta T}^{\text{e}} \tag{4-8}$$

Where:

$\boldsymbol{\Delta T}$: temperature increment

And *a* to *e* are regression coefficients. Regression coefficients are presented in Table 4-8 for data from Table 4-6. Figure 4-13 shows effects of the specimen temperature (after it was warmed) on its pore-water pressure response to undrained loading and unloading during $\overline{\boldsymbol{B}}$-tests. Table 4-9 summarizes the B-bars at different temperatures from this experiment.

4.3.6 Ice-blockage and anomaly in the measured pore-water pressures within saline sand specimens at subfreezing temperatures

Questionable data have been shaded in Table 4-4 and Table 4-5. It was observed that the faulty readings occur gradually and generally after additional consolidation. The FRPs measuring discontinuous pore-pressures show deviation from the rest of the FRPs, irregular B-bar values (too low or too high), or low correlation coefficient in measured pore-pressures. Further, those FRPs do not pass the backpressure continuity test. Disturbing the deformation field within the specimen by repeated loading and unloading or further consolidation and warming the specimen restored continuity of the pore-water phase. Figure 4-14 shows examples of continuous and discontinuous hydraulic connection of the pore-water phase and FRPs in a partially frozen saline sand specimen during $\overline{\text{B}}$-tests.

4.3.7 Pore-ice pressures

Figure 4-15 compares consolidation behavior of the partially frozen and unfrozen saline sand specimens studied in this chapter. The figure shows only the results from the consolidation steps in unfrozen and partially frozen experiments. Figure 4-15 shows that the same levels of void ratios were not achieved in this partially frozen specimen subjected to the same Terzaghi effective consolidation pressures as the unfrozen specimen even though additional consolidation time was allowed.

To estimate stress in ice phase at each consolidation level, first a regression model for interpolating $\overline{\boldsymbol{B}}$ in the unfrozen saline sand specimen in terms of initial void ratio and backpressure was established. Datafit software (Oakdale Engineering 2008) was used to fit a 2D polynomial

regression on data tabulated in Table 4-2 that resulted in Equation (4-9) with coefficient of multiple determination R^2= 0.878:

$$\bar{\boldsymbol{B}} = a + b.\boldsymbol{e_i} + c.\boldsymbol{e_i^2} + d.\boldsymbol{e_i^3} + e.\boldsymbol{u_i} + f.\boldsymbol{u_i^2} + g.\boldsymbol{u_i^3} \quad (4\text{-}9)$$

Where:

$\boldsymbol{e_i}$: initial void ratio

$\boldsymbol{u_i}$: initial backpressure

a to *g* are regression coefficients presented in Table 4-10

Then, the predicted $\bar{\mathbf{B}}$ values within the unfrozen specimen were compared to the measured $\bar{\boldsymbol{B}}$ values within the partially frozen specimen at 100 kPa backpressure and various initial void ratios (Figure 4-16). Actual measured $\bar{\boldsymbol{B}}$ values within the partially frozen specimen were used because sufficient data at 100 kPa backpressure were available. Pore-ice pressure coefficient ($\bar{\boldsymbol{B}}_{\boldsymbol{ice}}$) was evaluated using superposition (Figure 4-16).

4.4 Discussion

4.4.1 Calibrations

The slope of the calibration curves did not significantly change before and after the two sets of partially frozen experiments (Figure 4-4) and the differences in the slopes of the calibration curves were 1.3% and 1.8% at 259 hours and 633 hours of experiments, respectively. Each of these experiments included several B-bar tests, consolidation, undrained warming, and creep tests. During undrained warming (usually last steps in the experiments) specimens experienced large negative pressures (up to -100 kPa) for extended periods. Fredlund and Rahardjo (1993) showed that when suctions are maintained for extended periods, some air will eventually diffuse or leak into the specimen. It is possible that some air had diffused into the specimens during the undrained warming steps. The calibration curves before and after the experiments remained almost identical in unfrozen experiments with only deviations in the range of the accuracy of the measurements. It

is recommended that a hydraulic system for loading replace the pneumatic loading system in the MQS cell for future research.

4.4.2 Continuity and validity of the measured pore-water pressures in partially frozen saline sand specimens

Figure 4-5 shows the measured pore-water pressure response to independent change of total pressure and backpressure within a nearly saturated partially frozen saline sand specimen (30±1 ppt NaCl pore-water salinity) at -3.22 ± 0.03^{o}C. The measured pore-water pressures at various elevations within the partially frozen specimen show the same trends and almost coincide, except for FRP-5. By further warming the specimen to -3.0 ± 0.03^{o}C, response of FRP-5 too coincided with the rest of the FRPs. Further, the pore-water pressures show minute fluctuations upon change of backpressure or total pressure. After equalization (within a maximum of 10 minutes) they correlate with the applied backpressures. This confirms continuity of the stress in pore-water phase and hydraulic connection of the FRP fluid and pore fluid. With further consolidation of the specimen, the hydraulic connection of some FRPs and the pore-water phase was lost and the measured pore-pressures became erratic (shaded results in Table 4-4 and Table 4-5). This is discussed further under ice-blockage and anomalies in the measured pore-water pressures later in this chapter.

4.4.3 Effects of preconsolidation on pore-water pressure response to undrained loading in the unfrozen saline sand specimen

It was observed that preconsolidation causes two effects on pore-water pressure response:

(a) Bilinear response of pore-water pressures with an inflection point that is related to the preconsolidation pressure and pore-water pressure at low backpressures

(b) Reduction of $\bar{B}$

Figure 4-6 compares bilinear versus linear regression for an overconsolidated unfrozen sand specimen. It is seen that bilinear regressions (Table 4-3) show better correlation coefficients than

linear regressions (Table 4-2). Further, both regression types show that B-bar decreases with increasing overconsolidation or decreasing backpressures (Figure 4-7 and Figure 4-8). In addition, B-bar values are generally higher during unloading than loading steps (Table 4-2). With increasing preconsolidation pressure, the primary and the secondary pore-water pressure coefficients ($\overline{\boldsymbol{B}}_{\boldsymbol{i}}$ and $\overline{\boldsymbol{B}}_{\boldsymbol{s}}$) remained 'almost' constant or decreased 'slightly'. The primary responses at various overconsolidation values (outline markers in Figure 4-8.a) coincided on a shared primary response line whereas secondary responses (solid markers in Figure 4-8.a) almost stayed parallel with $\overline{\boldsymbol{B}}_{\boldsymbol{s}}$ greater than $\overline{\boldsymbol{B}}_{\boldsymbol{i}}$. The inflection point of each graph approximated the effective overconsolidation pressure plus pore-water pressure. Hence, the overall $\overline{\boldsymbol{B}}$ (linear $\overline{\boldsymbol{B}}$) was reduced by increasing preconsolidation pressure and decreasing void ratio due to the 'position of the inflection point'. Position of the inflection point defines how much each of $\overline{\boldsymbol{B}}_{\boldsymbol{i}}$ or $\overline{\boldsymbol{B}}_{\boldsymbol{s}}$ contributes to the overall $\overline{\boldsymbol{B}}$. With increasing backpressure, primary B-bar values were increased whereas secondary B-bar values almost remained constant or showed a slight increase (Figure 4-8.b); therefore the deviation angle between secondary and primary response lines (the smaller angle of the two angles) became smaller (i.e. $\overline{\boldsymbol{B}}_{\boldsymbol{i}}$ approached $\overline{\boldsymbol{B}}_{\boldsymbol{s}}$). Again, the inflection point of each graph approximated the effective preconsolidation pressure plus pore-water pressure. It should be noted that $\overline{\boldsymbol{B}}_{\boldsymbol{i}}$ indeed reflects a reloading state, whereas, $\overline{\boldsymbol{B}}_{\boldsymbol{s}}$ indeed reflects a loading state, and therefore $\overline{\boldsymbol{B}}_{\boldsymbol{i}}$ are generally expected to be less than $\overline{\boldsymbol{B}}_{\boldsymbol{s}}$. However, with increased backpressure, $\overline{\boldsymbol{B}}_{\boldsymbol{i}}$ approached $\overline{\boldsymbol{B}}_{\boldsymbol{s}}$.

In the following paragraph, Equation (4-4) for Skempton's $\boldsymbol{B}$ pore-pressure coefficient has been interchangeably used for Skempton's $\overline{\boldsymbol{B}}$ coefficient to make qualitative comparisons only. One may attempt to qualitatively describe the behavior discussed in the previous paragraph using Equation (4-4): by increased backpressure (pore-water pressure), $\boldsymbol{S_r}$ approaches unity and compressibility of the pore-water reaches the compressibility of 100% saturated water, and therefore the differences in the ratio of pore-pressures in specimens having different backpressures will be minimized. To better understand the physics of the behavior, two important pore-water pressures should be noted for any given preconsolidation:

(1) $\boldsymbol{u_{inflection}}$: pore-water pressure at which the inflection point between primary and secondary responses occurs

(2) $\boldsymbol{u_{equalization}}$: pore-water pressure at which $\boldsymbol{\bar{B}_i}$ approaches $\boldsymbol{\bar{B}_s}$

These two pore-water pressures are not equal and also are different for different preconsolidation values. Therefore, a different mechanism than simply reaching full saturation of a specimen is involved. The sand skeleton has two different compressibilities at effective stresses lower and higher than its effective preconsolidation pressur as shown by examples of $\boldsymbol{e - log\acute{\sigma}}$ graphs for Cambra sand presented by Lade et al. (2006). Considering these two compressibilities, it is perceived that $\boldsymbol{u_{inflection}}$ approximates the pore-water pressure that if subtracted from the total pressure at the inflection point gives the maximum effective stress that the specimen has experienced before. At effective stresses higher then preconsolidation pressure, soil skeleton has a higher compressibility; hence for the same compressibility of water, $\frac{C_w}{C_d}$ will have a higher value which results in a higher $\bar{\mathbf{B}}_{\boldsymbol{s}}$. At higher backpressures, compressibility of water is increased by orders of magnitude (Chapter 2) and water starts to dominate the load bearing. At $\boldsymbol{u_{equalization}}$, the role of lower and higher stiffness in soil matrix is diminished and $\boldsymbol{\bar{B}_i}$ approaches $\boldsymbol{\bar{B}_s}$. It should be noted that both $\boldsymbol{\bar{B}_i}$ and $\boldsymbol{\bar{B}_s}$ are increased by increasing backpressures. However, $\boldsymbol{\bar{B}_i}$ is increasing at a faster rate than $\boldsymbol{\bar{B}_s}$. This cannot be explained by considering different compressibilities for primary and secondary consolidation; $\boldsymbol{C_d}$ is smaller during reloading than in virgin loading, therefore for the same $\Delta\boldsymbol{C_w}$, the corresponding $\Delta(\frac{C_w}{C_d})$ is larger, hence the corresponding $\Delta\boldsymbol{\bar{B}}$ is smaller.

It also cannot be simply explained by $\boldsymbol{S_r}$, and assuming a specific amount of un-dissolved air goes into solution as this behavior is observed within the 'primary response zone' and is related to the preconsolidation pressure and stress-strain history of the specimen. It is hypothesized that this is related to the fact that $\boldsymbol{\bar{B}_i}$ values are measured during reloading, for a range of deformations that have undergone a loading and unloading history. It is hypothesized that this takes the pore-fluid through a specific path of thermodynamic conditions in which a higher amount of gas (original un-

dissolved air and added water vapor) or the same amount of gas but with higher portion of water vapor exists in pore-fluid and the same amount of reloading will bring it back to the virgin thermodynamic state. This might be explained if we consider that some of the free occluded gas may go into a 'dead' state, at which it is effectively trapped or absorbed between soil particles or is dissolved in water, with a lower tendency to turn back to gaseous state than water turning into water vapor. We call this hypothesized state as 'apparent secondary desaturation effect' because by application of higher backpressures it diminishes, as well as, the effect is analogous to de-saturation; Mohr-Coulomb failure line for overconsolidated soils has a cohesion intercept, analogously, desaturation adds a cohesion intercept to the Mohr-Coulomb failure criterion that its value is proportional to matric suction in the soil (Fredlund and Morgenstern 1977). Evidence that may support this hypothesis is that vapor pressure for liquid water is about 100 kPa. However, a sudden drop in vapor pressure is expected as liquid transforms to a solid (Figure 4-17). The existence of a semi-solid phase of water may explain suction pressures of 200 kPa to1500 kPa in unsaturated soils. This range of suctions add a cohesion intercept in the range of 57 kPa to 430 kPa to shear strength of the saturated soil when it de-saturates (assuming $\boldsymbol{\phi^b}$=16^o, $\boldsymbol{\phi^b}$ = friction angle with respect to matric suction (Fredlund and Rahardjo 1993)). Further investigation to evaluate this hypothesis is required.

Therefore, under undrained loading, when the specimen undergoes larger strains than it has experienced before, the effective stress (frictional resistance) is decreased at a faster rate. This faster rise in pore-water pressure may cause effective stress to approach zero on some internal locations and lead to instability.

The author did not find any published work on the bilinear response of pore-water pressures during undrained loading under laterally confined deformations but during shearing in triaxial cells. Sánchez and Sagaseta (1981) and Balasubramaniam and his colleagues (1989; 2007) reported bilinear pore-water pressure response during shearing of soft clay specimens under triaxial undrained loading conditions. By considering these previous research, a second hypothesis is suggested; the inflection point might reflect a critical state. In fact, $\overline{\boldsymbol{B}}_{\boldsymbol{i}}$ and $\overline{\boldsymbol{B}}_{\boldsymbol{s}}$ may reflect initial

and incremental $\boldsymbol{A}$ pore-pressure coefficients, $\boldsymbol{A_i}$ and $\boldsymbol{A_s}$, observed by Sánchez and Sagaseta (1981) who reported bilinear effective stress paths, with a well-defined break point, in undrained triaxial tests in soft clays (Figure 4-18). They reported that this shape of the effective stress path was irrespective of the stress history. They further reported that a clear break point was observed in tests that were conducted using triaxial equipments with smooth, lubricated platens together with using axial drains along the specimen (Sánchez et al. 1979) and was not observed in regular triaxial tests with rough base. They attributed this observation to the lack of uniformity of the stress and strain fields in the specimens associated with rough base in standard triaxial tests. Balasubramaniam and his coworkers (1989; 2007) also reported bilinear relationship between $\frac{\boldsymbol{u}}{\boldsymbol{P_0}}$ and $\boldsymbol{K_c} = \boldsymbol{\eta} = \frac{\boldsymbol{q}}{\boldsymbol{p}}$, in which $\boldsymbol{u}$ is the pore-water pressure under undrained shear in a triaxial test, $\boldsymbol{P_0}$ is the pre-shear isotropic consolidation pressure, $\boldsymbol{q} = \frac{\sigma_1 - \sigma_3}{2}$ and $\boldsymbol{p} = \frac{\sigma_1 + \sigma_3}{2}$ are the shear and mean normal stresses during the triaxial tests. For preparing their anisotropically consolidated specimens, they unloaded specimens after the initial isotropic consolidation so that the overconsolidation stress ratio, $\boldsymbol{\eta_a}$, ranged from 0 to 0.75. They observed that the second linear part of the normalized pore-pressure response for their anisotropically consolidated samples were parallel to that of isotropically and normally consolidated samples and had a slope of about 0.52 (Figure 4-19). Mesri and Ali (1999) too observed that in the compression range beyond preconsolidation pressure ($\boldsymbol{\sigma_p'}$) (i.e. normally consolidated state) the ratio of $\frac{(\Delta u)_f}{\sigma_{vc}'}$ remained constant and independent of $\boldsymbol{\sigma_{vc}'}$ (effective vertical consolidation pressure) in their fully saturated overconsolidated Boston Blue clay samples.

4.4.4 Effects of preconsolidation on pore-water pressure response to undrained loading in the partially frozen saline sand specimens

Overconsolidation and backpressures had the same effects on pore-water pressure response in partially frozen specimens (Figure 4-10) compared to those described earlier for unfrozen specimens (Figure 4-8). Stress transmission parameter, $\boldsymbol{\tilde{\tilde{B}}}$**,** defined in Equation (4-10), ranged

from 0.1 to 0.5 with an average of 0.3 for both the partially frozen and unfrozen experiments (Table 4-2 to Table 4-5) for tests in which both a primary and a secondary B-bar were calculated.

$$\tilde{\bar{B}} = \frac{(\bar{B}_s - \bar{B}_i)}{\bar{B}} \tag{4-10}$$

Furthermore, all B-bars in partially frozen specimens are less than unity except anomalies that are discussed later. However, $\bar{B}$, $\bar{B}_i$, and $\bar{B}_s$ are generally smaller in the partially frozen state than unfrozen state under similar conditions due to existence of pore-ice which carries a portion of the stresses as presented earlier. Furthermore, the unloading curve is more separated from the loading curve for the partially frozen state than unfrozen state (Figure 4-6 and Figure 4-9) due to the temperature effects on the interfacial characteristics of the loading piston and specimen as outlined in Chapter 3. Moreover, it is expected that the ice phase (which has plastic behavior) will carry less load as it unloads than it does during loading compared to elastic sand particles. Further discussions related to these observations are presented later.

4.4.5 Effects of warming on the measured pore-water pressures in a partially frozen saline sand specimen

Figure 4-11.a shows the pore-water pressure response within a partially frozen saline sand specimen during five undrained warming steps. The initial pore-water pressures were 172 to 206 kPa (Table 4-6). The pore-water pressures dropped sharply (34 to 283 kPa for increments of +0.76 to +2.53^{o}C) within 4 to 16 hours after the application of the warmer temperatures and then remained relatively constant.

For partially frozen specimens, the pore-water pressure decrease during each step is related to initial ice content and ice content decrease during that step. These two parameters are related to the initial temperature, and the latter is also related to the temperature increment (Figure 4-12). This relationship is simplified as Equation (4-7) in which, for the sand, the calibration coefficients show a negative c-value for the power of $\Delta\omega_i$ (ice content decrease) and a positive b-value for the power of ω_i (initial ice content). The average size of pores filled with water is smaller in a coarse

grained granular soil at subfreezing temperatures than the unfrozen soil because solid ice reduces the average water-filled pore size. Hence, greater suctions can be generated in a partially frozen soil due to desaturation compared to the same unfrozen soil having the same grain size distribution and void ratio. Moreover, the higher the ice content, the smaller the average pore size, hence the higher will be the generated suctions. Further, the more ice turns into water, the lower will be the degree of saturation (because volume of water is about 9% less than that of the same mass of ice that turns into water), and hence a greater suction is expected. However, the more ice turns into water, the larger the average pore size; hence the generated suction may reduce. For the coarse grained soil used in this experiment, the effect of pore size becoming larger (due to ice melt) is higher. Hence, *b* has a positive value and *c* has a negative value (Table 4-7) in Equation (4-7).

In Chapter 3, using a glycol-water mixture and mineral oil in the MQS cell, it was shown that warming the pore fluid affects the interface properties of the loading piston and the pore-fluid such that at warmer temperatures a higher pore-water pressure is measured when the specimen undergoes a change in effective stress. Equation (4-8) incorporates interface effects due to temperature increments. The coefficient of regression c approaches zero (Table 4-8) in Equation (4-8) because the new term for the temperature increment is also responsible for the ice content decrease; hence a new set of correlation coefficients are fitted for the combined effects. It should be noted that correlation coefficients in Table 4-7 and Table 4-8 are derived based on a small database of measured values in Table 4-6. For more accurate evaluations it is suggested to produce and use a larger database which was not within the scope of this research.

For unfrozen specimens, there were also decreases in pore-water pressure due to thermal expansion of the cell during undrained warming.

Pore-water pressure distribution within the specimen during undrained warming from -3.11^{o}C to -2.35^{o}C (Figure 4-11.b) shows that the measured pore-water pressures using FRP-3 to FRP-5 coincide and follow the same pattern shown in Figure 4-11.a while FRP-1 and FRP-2 show an anomaly. However, after about 24 hours from the start of the warming phase, the measured pore-

water pressure using FRP-1 suddenly drops and coincides with FRP-3 to FRP-5. Data from FRP-2 showed the same pattern after about two hours of warming in the subsequent step. It is concluded that the hydraulic discontinuity between FRP-1 and FRP2 and the rest of the FRPs was due to a local ice blockage. With increasing temperature and reduction in the ice content the hydraulic connection and transfer was re-established. Pore-water pressures coincided within 20 seconds after hydraulic connection was restored.

Induced pore-water pressures due to undrained heating in 'unfrozen soils' had been studied by several pioneers (Agar et al. 1983; Campanella and Mitchell 1968; Mitchell 1976; Morgenstern 1981). Via experiments on Alberta oil sands at elevated temperatures (up to 300^{o}C) and high pressures (up to 30 MPa), Morgenstern (1981) introduced pore-pressure parameter $\boldsymbol{B_t}$ to account for the changes in pore-water pressure due to undrained heating. Agar et al. (1983) provided a formulation for $\boldsymbol{B_t}$ that incorporated the undrained thermal expansion coefficients of mineral grains and soil mass, undrained coefficient of compressibility of the soil mass, and thermal volume change due to mineral grain structure collapse. Evaluation of $\boldsymbol{B_t}$ and material properties that affect its value in partially frozen soils were not in the scope of the current research and remain for future research.

4.4.6 Effects of specimen temperature on pore-water pressure response to undrained loading in a partially frozen saline sand specimen

Figure 4-13.a shows that at warmer temperatures a greater portion of the load is carried by the pore-water phase when loading saline sand specimen under underained conditions, irrespective of the presence of pore-ice in the specimen, within the range of temperatures tested in the MQS cell. However, when pore-ice is present in the specimen, this effect is more evident, as is demonstrated by the greater slope of its correlation line (Figure 4-13.b). When ice content is reduced or ice temperature is increased, ice matrix stiffness is reduced; hence, the ratio of the striffness of the fluid phase to the stiffness of the solid phases is increased. Therefore, pore-water will carry a higher portion of the load. In addition to the role of the ice content and temperature, when the

temperature of the pore-water is increased, a higher pore-water pressure is measured in FRPs that are associated with interfacial effects in the MQS cell as described in Chapter 3. To estimate the change in pore-ice pressure due to warming, one can differentiate Equation (4-6) with respect to temperature (T):

$$\frac{\partial \overline{B}_{ice}}{\partial T} = \frac{\partial \overline{B}_{Water,Unfrozen}}{\partial T} - \frac{\partial \overline{B}_{Water,Frozen}}{\partial T} \tag{4-11}$$

From Figure 4-13.b , $\frac{\partial \overline{B}_{ice}}{\partial T} = 0.384 - 0.0733 = -0.0349/\,^{o}\text{C}$. The values of $\frac{\partial \overline{B}_{ice}}{\partial T}$ depend on several factors (salinity, void ratio, degree of saturation, initial backpressure, etc). Evaluation of these factors was not in the scope of this research.

Even though establishing an interpolation model to estimate B-bars at subzero temperatures from B-bars at room temperature is appealing, it was not attempted in this research as pore-water pressure response in a partially frozen soil depends on several factors (such as ice content, soil type, void ratio, ice structure, salinity, time, and temperature) and only with large databases of test results could such models be developed. It is also perceived that the curve relating temperature and B-bar flattens at temperatures close to room temperature and it might be necessary to conduct the experiments at temperatures closer to 0^{o}C. Establishing such correlations was not within the scope of this research.

4.4.7 Ice-blockage and anomaly in the measured pore-water pressures within the saline sand specimens at subfreezing temperatures

Study of the primary and secondary pore-water pressures provides further insights into understanding pore-water pressure response of partially frozen soils as well as an additional test for checking validity of and a tool for detecting anomalies in the measured pore-water pressures.

Three categories of anomalies were observed:

1. Some FRPs did not show the same patterns or values as the rest of the FRPs under independent application of total pressure and backpressures or during undrained warming

(for example FRP-5 in Figure 4-5, FRP-1 and FRP-2 in Figure 4-11.b, and FRP-2 in Figure 4-14.b)

2. Secondary B-bars greater than unity were observed (2nd and 3rd cycles of B-bar tests when σ_p= 239 kPa, Table 4-5)
3. Small correlation coefficients for the same FRPs that did not conform with the rest of the FRPs and showed too low or too high B-bars (Table 4-4 and Table 4-5).

These anomalies were not observed during unfrozen experiments (Table 4-2 and Table 4-3) or at the beginning of the partially frozen experiments. In partially frozen experiments, one or all of the anomalies appeared after the specimens underwent additional consolidation (for data in Table 4-4 after σ_p=137 kpa) and first appeared at FRPs that were near the top of the specimen in the MQS cell (FRP-1 and FRP-2). Then, with further consolidation and elapsed time additional FRPs showed anomalies (for data in Table 4-5 after $\boldsymbol{\sigma_p}$=239 kPa).

A negative B-bar implies that pore-water pressure decreased with increasing total pressure whereas a B-bar greater than unity implies that pore-water pressure increases beyond the increase in total pressure. Needle-like ice structure in partially frozen saline sand specimens were observed by Arenson and Sego (2006). Preliminary experiments in Chapter 3 confirmed that the saline ice forms a porous ice structure through which unfrozen saline water is hydraulically continuous. This initial hydraulic continuity is lost at higher consolidation levels due to breakage of fragile needle-like ice structure in partially frozen saline sand specimens. At higher void ratio, when the partially frozen saline sand has not been disturbed, the fragile ice structure provides a porous, less stiff solid phase. When the stress level of consolidation is increased, the fragile ice-needles break and may melt and reglatiate together in response to local stresses. This may result in (1) an increase or decrease of pore-water pressure associated with ice-melt and refreeze, and (2) a more rigid, less permeable ice matrix. The less porous ice results in lower hydraulic conductivity and due to heterogeneity it could cause local ice-blockages and hydraulic discontinuity. Further, the decreased void ratio during consolidation is due to brine water being expelled from the specimen; it is perceived that the remaining water (liquid water and ice) is less saline. The reduced salinity

results in reduced unfrozen water content in saline sand (Hivon and Sego 1995). The resulted lower hydraulic conductivity and lower unfrozen water content can cause discontinuity in hydraulic connection of the pore-water phase and the FRPs. This behavior was observed at temperatures colder than -2.6^{o}C but was not observed at temperatures warmer than -1.8^{o}C for experiments on sand with 30±1 ppt salinity and consolidation pressure of 330 kPa.

Secondary B-bars greater than unity (2nd and 3rd cycles of B-bar tests when $\boldsymbol{\sigma_p}$= 239 kPa, Table 4-5) might also be attributed to low hydraulic conductivity and localized pressure induced by regelation of water. Water from ice-melt caused by localized high stresses at higher consolidation levels may turn into ice again to reach a new thermodynamic equilibrium. Another hypothesis is that a mechanism similar to pore-water generation in 'sensitive soils' may take place in which $\boldsymbol{A}$ pore-pressure coefficients greater than unity are observed (Skempton 1954). It should be noted that for $\boldsymbol{B}$ = 1, from Equation (4-1):

$$\frac{\boldsymbol{\Delta u}}{\boldsymbol{\Delta \sigma_1}} = \bar{\boldsymbol{B}} = \boldsymbol{A} + \frac{\boldsymbol{\Delta \sigma_3}}{\boldsymbol{\Delta \sigma_1}}(1 - \boldsymbol{A}) = \boldsymbol{A} + \boldsymbol{K}(1 - \boldsymbol{A}) \tag{4-12}$$

Whereas from Equation (4-3):

$$\frac{\boldsymbol{\Delta u}}{\boldsymbol{\Delta \sigma_1}} = \bar{\boldsymbol{B}} = \left[\frac{1 - (1 - \mathbf{A})(1 - \mathbf{K})}{1 - (1 - \mathbf{A})(1 - \mathbf{K})}\right] = 1.0 \tag{4-13}$$

For $\boldsymbol{\phi'} = 30^{o}$, Jâky's formula (Jâky 1944) yields $\boldsymbol{K_0} = 0.5$. With $\boldsymbol{A}$ = 1.5 for a sensitive soil (Skempton 1954), Equation (4-12) yields $\bar{\boldsymbol{B}}$ = 1.25. For a maximum observed $\bar{\boldsymbol{B}}$ = 1.7 (Table 4-5) using $\boldsymbol{K_0} = 0.5$ results an $\boldsymbol{A}$ = 2.4. When a soil element is unevenly consolidated ($\boldsymbol{K_c} \neq 1$), it exhibits a cross-anisotropic behavior. In this case principal directions of stresses and strains will coincide only if they also coincide with the orthotropic axes otherwise normal stresses will produce shear distortions within the soil (Sánchez and Sagaseta 1981). With breakage of the needle-like ice it is hypothesized that some shear distortions may occur which induce excess pore-water pressures. Anisotropy of (partially) frozen soils has been studied by several authors (Lai et al. 2009; Razbegin et al. 1996; Vyalov et al. 1990).

Lowering temperature in a 'near saturated' partially frozen sand increases pore-ice that has a higher volume than the pore-water turned into pore-ice, hence, it increases the degree of saturation of the soil. Additional freezing can impose pressures higher than total stress to the hydraulically discontinuous unfrozen brine pockets or oil droplets that become encapsulated with ice. Unlike soil, ice can sustain tensile stresses; hence, the encapsulated brine pocket or oil droplet can have a higher pressure than the applied total pressure on the specimen.

Regular responses were restored after the (partially) frozen specimens were warmed (Table 4-9) or when the deformation field within the partially frozen specimen was disturbed by repeated loading and unloading or further consolidation (for data in Table 4-5 after $\boldsymbol{\sigma_p}$=330 kPa) by melting or micro-cracking of local ice blockages, respectively. Further experiments are planned for future research that will use imaging techniques in a special cell to study the change in ice structure under loading and its effects on the measured pore-water pressures.

4.4.8 Pore-ice pressures

It is required that both the (partially) frozen and unfrozen sand specimens have the same strain history to assume the soil matrix carries the same amount of stress in both the (partially) frozen and unfrozen states (Ladanyi and Morel 1990). Even though the subfreezing temperatures were close to 0^oC and up to four times the time for consolidation was allowed for the partially frozen specimen compared to unfrozen specimens, the same void ratios were not achieved under the same applied Terzaghi effective preconsolidation pressures (Figure 4-15). Therefore interpolation was used to compare the results at the same void ratios. However, many factors affect pore-water pressure coefficients as discussed earlier. A proper variable selection process is required to balance between interpolation model simplicity and quality of the fit. The model is desired to be as complete and realistic as possible, and to include any predictor variable that is related to the response variable. In contrast, it is desirable to include as few predictor variables as possible to avoid "over-fitting" of the model. Generally, past experience or theory provides good direction; however, there are also methods to help with the decision process. Data mining techniques (Florin 2011; MacLennan et al. 2009; Myatt and Johnson 2009; Odom and Henson 2002; Witten et al.

2011) can be used to understand data, to decide which variables should be studied for modeling the behavior of the system, and to aid decision making especially when huge amount of data need to be handled or high levels of complexity are involved in the behavior of the systems. Examples of such situations are when data are acquired at high frequencies or many parameters are measured. These techniques have been used in several recent geotechnical engineering studies (Alavi and Gandomi 2011; Baykasoglu et al. 2009; Dyminski et al. 2008; Smith 2009; Tinoco et al. 2009; Villwock et al. 2007). It is perceived that these techniques will have application in permafrost engineering due to the added complexity of time and temperature dependency of the mechanical behavior of freezing, thawing, and frozen soils. It is necessary to have a large database of measured behaviors and parameters affecting them to best utilize these techniques. Matlab software (Mathworks 2011) provides a comprehensive toolbox for complicated data mining tasks. In this research, the 'stepwise variable selection technique' in Oakdale Engineering DataFit software (Oakdale Engineering 2008) was used for data mining. Further, the automated multiple variable regression capability in DataFit was used for finding the best regression curves. It was found that only initial condition variables (initial void ratio and initial backpressure) met significance level of 0.1 for entry into the model and soil history variables met significance level of 0.2 for experiments on unfrozen sand specimens and therefore were not used in the regressions. Therefore Equation (4-9) was fitted to the data.

Interpolated B-bars from the unfrozen experiments were compared with measured B-bars from the partially frozen experiments at the same initial void ratios and initial backpressure (Figure 4-16) to evaluate pore-ice pressure coefficients ($\overline{\boldsymbol{B}}_{\boldsymbol{ice}}$). Figure 4-16 shows that for this saline sand specimen having initial salinity of 30±1 ppt NaCl, pore-ice pressure coefficient increased at a rate 10 times faster than the rate at which the void ratio decreased at temperature of -2.94 ± 0.18^{o}C. In the beginning of the experiment the ice structure is not disturbed and the stress is almost zero in pore-ice in the fragile needle-ice matrix. Further consolidation and changes in the structure of the ice matrix contribute to it becoming more rigid and allowing it to carry a higher portion of the applied loads.

At any pressure level ice will creep over time which accelerates by increasing temperature (Barnes et al. 1971a; Glen 1955; Hooke et al. 1980; Sego and Morgenstern 1983). When strains are maintained constant, or when other phases contribute to transferring loads, the creep in ice shows as stress relaxation (Razbegin et al. 1996; Vyalov and Oun 1991; Zaretsky and Fish 1996). The stress relaxation in the ice phase results in pressure redistribution in the multi-phase partially frozen soil and decrease in the internal ice pressure. At higher pressures, ice melt will also reduce pressure in the ice phase. Creep of polycrystalline fresh-water ice (Ashby and Duval 1985; Sinha 1978) and saline ice (Cole 1995) show a simple thermo-rheological behavior; different temperature creep curves can be shifted horizontally into one master curve in terms of a reduced time using a time-temperature shift factor (Ashby and Jones 1998; Roman 2003; Roman et al. 1994; Vyalov and Roman 1991). Therefore it might be possible to estimate pore-ice pressure at various temperatures and elapsed time by conducting a limited number of experiments. These effects were not in the scope of this research and remain for future research.

4.4.9 Effective stress during undrained loading

In both unfrozen and partially frozen specimens, $\bar{\boldsymbol{B}}$ values (Lambe and Whitman's $\boldsymbol{C}$ pore-water pressure coefficient) less than unity were measured at various preconsolidation levels in nearly saturated sand specimens ($\boldsymbol{S_r}$ greater than 98%) and decreased with increasing effective preconsolidation pressure. $\bar{\boldsymbol{B}}$ less than unity indicates that effective stress is not zero under undrained loading. This finding is explained through stiffness ratio of the phases and is supported by previous literature.

Pore-pressure coefficient $\boldsymbol{B}$ less than unity in 'saturated soils and rocks' is reported in the literature (Black and Lee 1973; Eigenbrod and Burak 1990; Fragaszy and Voss 1986; Lee et al. 1969; Mesri et al. 1976). Pore-pressure coefficient $\boldsymbol{C}$ less than unity in 'saturated sands' is reported by Zaretskii et al. (1991) and Veyera et al. (1992). In all cases, $\boldsymbol{B}$ or $\boldsymbol{C}$ decreased with increasing effective consolidation stress and increasing relative density. Eigenbrod and Burak (1990) also observed that $\boldsymbol{B}$ decreased with increasing stress levels applied to a thinly-interbedded 'varved clay'.

Eigenbrod and Burak (1990) reported $\boldsymbol{B}$ coefficient, in the range of 0.98 to 0.08, as a function of effective consolidation stress (25-450 kPa) for interbedded 'varved clay' during loading and unloading scenarios. Veyera et al. (1992) reported $\boldsymbol{C}$ coefficient, in the range of 1.00 to 0.51, as a function of effective consolidation stress (86-690 kPa) and relative density (6-85%) for two 'saturated sands' during reloading. In this work, $\boldsymbol{C}$ coefficient values in the range of 0.92 to 0.47 during loading (reloading-loading indeed) and 0.96 to 0.53 during unloading were measured for the unfrozen saline sand specimens, and in the range of 0.86 to 0.51 during loading (reloading-loading indeed) and 0.86 to 0.54 during unloading were measured for the partially frozen specimens under effective consolidation stresses in the range of 67 to 330 kPa.

It should be noted that $\frac{C_w}{C_d}$ is never zero; therefore the theoretical value of the $\boldsymbol{B}$ pore-water pressure coefficient is always less than unity (Equation (4-4)) but approaches unity at high backpressure levels in soft soils. Further, for identical soils, the $\boldsymbol{C}$ coefficient is always less than $\boldsymbol{B}$ coefficient (Veyera et al. 1992).

Values less than unity for $\boldsymbol{B}$ or $\overline{\boldsymbol{B}}$ indicate that changes in effective stress are not zero during undrained loading in saturated soils when the solid skeleton has 'appreciable stiffness' compared to the pore-fluid. Hence, in addition to altering hydraulic continuity and conductivity in soils, the axis translation technique alters the ratio of pore-fluid compressibility to solid-phase compressibility, hence, altering the mechanical behavior of the soil.

4.4.10 Effects of B-bar less than unity on frictional resistance

Bishop and Eldin (1950) reported that even a too small to be measured deviation from fully saturated state can change the compressibility of the pore-liquid by orders of magnitude and can cause appreciable measurable frictional resistance. Even in initially fully saturated samples if the pore-water pressure during shear reaches large negative values small bubbles of water vapor and air freed from solution form which result in a more compressible pore-liquid. During undrained loading of a 'saturated soft clay', the change in effective stress is zero and a zero friction angle is measured. The true internal friction angle is not zero for clays and is in the range of 10^o to 32^o

(Hvorslev 1937; Skempton 1948a). Golder and Skempton (1948) reported that unlike soft to stiff 'fissured' clays, friction angle in 'fully saturated' silts, silt-stone, and shales was not close to zero during undrained loading and was in the range 0^o to 38^o. Bishop and Eldin (1950) state that "this unexpected result was attributed to dilatancy, although no fully satisfactory explanation was given, and this led Skempton (1948c) to omit dilatant soils from his theoretical analysis of the changes in pore-water pressure during shear". The high values of measured friction angle (up to 38^o) was attributed primarily to (Bishop and Eldin 1950):

1. Departure from the constant-volume condition that is normally assumed in undrained tests on fully saturated samples (due to the compressibility of the pore-water)
2. Incomplete saturation or entrapped air (compressible unsaturated soil)
3. Generation of negative pore-water pressures during shear, of sufficient magnitude to cause cavitation, which leads to formation of 'voids filled with water vapor and gas' that were freed from solution (compressible unsaturated soil)

Therefore, when $\overline{\mathbf{B}} < 1.0$, effective friction angle greater than zero can be measured during an undrained shear test.

Several authors studied the frictional behavior of frozen soils and ice in uniaxial, triaxial, and direct shear tests (Alkire and Andersland 1973; Andersland and Alnouri 1970; Arenson and Springman 2005b; Bragg and Andersland 1981; Chamberlain et al. 1972; Fish and Zaretsky 1998; Goughnour and Andersland 1968; Ho et al. 1996; Neuber and Wolters 1977; Parameswaran and Jones 1981; Qi and Ma 2007; Repetto-Llamazares et al. 2011; Roggensack and Morgenstern 1978; Sadovskii et al. 1987; Sayles 1973; Sayles 1974; Song 1984; Tsytovich 1975; Vyalov and Shusherina 1964; Vyalov et al. 1965; Yang et al. 2010). In all of these studies, the frictional resistance is attributed to dilatancy of frozen soil and the frictional nature of the soil matrix. Except the works by Arenson and his coworkers (Arenson 2002; Arenson and Springman 2005a; Nater et al. 2008), all of the previous research on frictional resistance of (partially) frozen soils were limited to 'total stress friction angle'. The method of measuring pore-water pressure used in

the current research differs from that used by Arenson and his coworkers and is described in Chapter 2.

In partially frozen sand $\bar{B}$ is less than unity due to the stiffer solid phase. Therefore the change in effective stress under undrained loading is not zero; hence frictional resistance is not zero under undrained conditions.

4.5 Conclusions

First time measurements of Skempton's B-bar coefficient in a partially frozen soil under laterally confined conditions and at various initial void ratios were presented and compared with the unfrozen state. Thus, by assuming superposition, stress distribution between soil matrix, pore-ice, and unfrozen pore-water were evaluated. Pore-ice pressure coefficient ($\bar{B}_{ice}$) increased at a rate more than 10 times faster than the rate of void ratio decrease in the saline sand specimen having initial salinity of 30±1 ppt NaCl and at -2.94 ± 0.18°C. Effects of pore-ice structure, pore-ice pressure cut off, stress relaxation in pore-ice, and ice-melt on pore-ice pressures were discussed.

First time measurements of pore-water pressure distribution within a partially frozen soil during undrained warming were presented. It was shown that the pore-water pressures dropped sharply (up to 283 kPa for 0.76°C warming) within the first 4 hours of application of the warmer temperatures. Correlation models were suggested to predict induced pore-pressures associated with undrained warming.

Further, the decrease rate of the load bearing of ice matrix with increasing temperature was evaluated for an overconsoliated partially frozen saline sand specimen at subfreezing temperatures close to 0°C. For this specimen, $\frac{\partial \bar{B}_{ice}}{\partial T} = -0.0349/\,^{o}C$ was estimated.

It was further observed that preconsolidation causes two effects on pore-water pressure response in both partially frozen and unfrozen specimens: (a)- bilinear response of the pore-water pressures with an inflection point at a total stress that approximates the preconsolidation pressure plus pore-water pressure, and (b)- reduction of $\bar{B}$. With increasing preconsolidation pressure, the primary

pore-water pressure coefficient ($\overline{\boldsymbol{B}}_i$) and the secondary pore-water pressure coefficient ($\overline{\boldsymbol{B}}_s$) remained 'almost' constant or 'slightly' decreased. With increasing backpressure, $\overline{\boldsymbol{B}}_i$ increased whereas $\overline{\boldsymbol{B}}_s$ almost remained constant or only slightly increased (i.e. $\overline{\boldsymbol{B}}_{\boldsymbol{i}}$ approached $\overline{\boldsymbol{B}}_{\boldsymbol{s}}$). It was also hypothesized that the inflection point might reflect a critical state and that $\overline{\boldsymbol{B}}_{\boldsymbol{i}}$ and $\overline{\boldsymbol{B}}_{\boldsymbol{s}}$ may reflect initial and incremental $\boldsymbol{A}$ pore-pressure coefficients, $\boldsymbol{A}_{\boldsymbol{i}}$ and $\boldsymbol{A}_{\boldsymbol{s}}$, observed by Sánchez and Sagaseta (1981) for unfrozen soft clay specimens. It was further observed that $\overline{\boldsymbol{B}}$ values in the partially frozen state were smaller than that in unfrozen state due to the contribution of the ice matrix in load bearing.

Validity of the measured pore-water pressures within partially frozen saline sand specimens and their anomalies were discussed. Further, it was shown that the change in effective stress under undrained loading is not zero when the solid phase has appreciable stiffness relative to the fluid phase; hence, frictional resistance is not zero under undrained conditions in partially frozen sand.

4.6 Tables

Table 4-1. Summary of the properties of the unfrozen and partially frozen specimens compared in this research

	Unfrozen specimen (Exp. No. 12)	Frozen specimen (Exp. No. 14)
Dry mass of sand (gr)	2441.3	2317.5
Initial height of the specimen (mm)	201.3	191.7
Initial void ratio at zero surcharge	0.772	0.777

Table 4-2. Summary of pore-water pressure response to undrained loading-unloading within an unfrozen saline sand specimen (linear regression)

σ_p (kPa)	σ_i (kPa)	u_i (kPa)	e_p	e_i	Loading/ Unloading	$\bar{B}$						Average correlation coefficient
						FRP-1	FRP-2	FRP-3	FRP-4	FRP-5	Average	
67	101	79	0.7420	0.7439	**L**	0.8733	0.8763	0.8852	0.8816	0.8914	0.88156	0.9979
					U	0.9077	0.9115	0.8935	0.8966	0.9016	0.9022	0.9995
133	100	75	0.7329	0.7342	**L**	0.683	0.7001	0.6879	0.6875	0.6961	0.69092	0.9859
					U	0.7788	0.7727	0.768x	0.764	0.7699	0.7714	0.998
133	100	79	0.7328	0.7340	**L**	0.7366	0.7527	0.7465	0.7414	0.7483	0.7451	0.9957
					U	0.8341	0.8229	0.8212	0.8152	0.824	0.8235	0.9986
133	149	125	0.7327	0.7336	**L**	0.7924	0.8017	0.8074	0.7997	0.7989	0.8000	0.9973
					U	0.8751	0.8538	0.8777	0.8645	0.8666	0.8675	0.9995
228	101	78	0.7267	0.7282	**L**	0.5489	0.547	0.5521	0.5502	0.5591	0.5515	0.9855
					U	0.638	0.644	0.6256	0.6255	0.6356	0.6338	0.9942
228	101	81	0.7267	0.7283	**L**	0.6015	0.615	0.612	0.6094	0.6163	0.6108	0.9905
					U	0.6939	0.6901	0.6923	0.6816	0.6916	0.6899	0.9951
228	100	59	0.7267	0.7278	**L**	0.6563	0.6672	0.6801	0.6727	0.6697	0.6692	0.9951
					U	0.7478	0.7378	0.7405	0.7303	0.737	0.7387	0.9968
228	151	135	0.7267	0.7278	**L**	0.7312	0.7354	0.7471	0.7387	0.7373	0.7379	0.9968
					U	0.8106	0.815	0.8234	0.8128	0.8107	0.8145	0.9996
228	201	186	0.7267	0.7278	**L**	0.8034	0.7928	0.7797	0.7758	0.7866	0.7876	0.9985
					U	0.8522	0.8347	0.84	0.8409	0.8489	0.8434	0.9992
330	101	78	0.7214	0.7234	**L**	0.4695	0.4671	0.4769	0.4738	0.4816	0.4738	0.9974
					U	0.5591	0.5477	0.529	0.5394	0.5386	0.5428	0.9916
330	149	135	0.7214	0.7243	**L**	0.6796	0.6929	0.7301	0.7226	0.7158	0.7082	0.9961
					U	0.7503	0.7827	0.7936	0.7783	0.7763	0.7762	0.9982
330	200	185	0.7214	0.7239	**L**	0.7608	0.7486	0.7583	0.7561	0.7652	0.7578	0.9983
					U	0.7928	0.8099	0.8189	0.825	0.8275	0.8148	0.9996
330	250	246	0.7214	0.7241	**L**	0.8373	0.8154	0.8161	0.8098	0.8366	0.823	0.9994
					U	0.9129	0.8694	0.8804	0.8586	0.8804	0.8803	0.9999
330	299	291	0.7214	0.7242	**L**	0.7517	0.8067	0.8618	0.863	0.8905	0.8348	0.9969
					U	0.9556	0.9556	0.8889	0.9111	0.9333	0.9289	1

σ_p: effective overconsolidation pressure, σ_i: initial total pressure, u_i:initial backpressure, e_p: overconsolidation void ratio (minimum void ratio the specimen has experienced before), e_i: initial void ratio, $\bar{B}$: Skempton's pore-water pressure coefficient, L: during loading, U: during unloading

Table 4-3. Summary of primary and secondary pore-water pressure response to undrained loading within an unfrozen saline sand specimen (bilinear regression)

σ_p (kPa)	σ_i (kPa)	u_i (kPa)	e_p	e_i	Response Type	$\bar{B}$						Average correlation coefficient
						FRP-1	FRP-2	FRP-3	FRP-4	FRP-5	Average	
67	101	79	0.7420	0.7439	**Primary**	NA	NA	NA	NA	NA	NA	NA
					Secondary	0.8932	0.9014	0.9151	0.9126	0.9151	0.9075	0.9991
133	100	75	0.7329	0.7342	**Primary**	0.535	0.5395	0.5197	0.5388	0.5548	0.536	0.9967
					Secondary	0.7802	0.8181	0.8179	0.8409	0.8052	0.8062	0.9935
133	100	79	0.7328	0.7340	**Primary**	0.6641	0.6723	0.6164	0.6321	0.7003	0.657	0.998
					Secondary	0.7888	0.8181	0.8202	0.8061	0.8068	0.808	0.9969
133	149	125	0.7327	0.7336	**Primary**	0.7079	0.704	0.7328	0.7247	0.7125	0.7164	0.9992
					Secondary	0.8773	0.8839	0.8574	0.8587	0.8775	0.871	0.9997
228	101	78	0.7267	0.7282	**Primary**	0.4949	0.4891	0.4833	0.489	0.5003	0.4913	0.999
					Secondary	0.7686	0.738	0.7956	0.7835	0.7742	0.772	0.9979
228	101	81	0.7267	0.7283	**Primary**	0.5392	0.5494	0.5462	0.5527	0.5635	0.5502	0.9984
					Secondary	0.7975	0.8097	0.7759	0.7666	0.7852	0.787	0.9997
228	100	59	0.7267	0.7278	**Primary**	0.6018	0.6051	0.6232	0.6174	0.6151	0.6125	0.9997
					Secondary	0.764	0.7606	0.7704	0.7557	0.7739	0.7649	0.9988
228	151	135	0.7267	0.7278	**Primary**	0.6949	0.6906	0.7325	0.7139	0.711	0.7086	0.997
					Secondary	0.8	0.8333	0.7667	0.7667	0.8	0.7933	1
228	201	186	0.7267	0.7278	**Primary**	0.7964	0.7825	0.7773	0.7728	0.7808	0.782	0.998
					Secondary	NA	NA	NA	NA	NA	NA	NA
330	101	78	0.7214	0.7234	**Primary**	0.4695	0.4671	0.4769	0.4738	0.4816	0.4738	0.9974
					Secondary	NA	NA	NA	NA	NA	NA	NA
330	149	135	0.7214	0.7243	**Primary**	0.6796	0.6929	0.7301	0.7226	0.7158	0.7082	0.9961
					Secondary	NA	NA	NA	NA	NA	NA	NA
330	200	185	0.7214	0.7239	**Primary**	0.7608	0.7486	0.7583	0.7561	0.7652	0.7578	0.9983
					Secondary	NA	NA	NA	NA	NA	NA	NA
330	250	246	0.7214	0.7241	**Primary**	0.8373	0.8154	0.8161	0.8098	0.8366	0.823	0.9994
					Secondary	NA	NA	NA	NA	NA	NA	NA
330	299	291	0.7214	0.7242	**Primary**	0.7517	0.8067	0.8618	0.863	0.8905	0.8348	0.9969
					Secondary	NA	NA	NA	NA	NA	NA	NA

σ_p: effective overconsolidation pressure, σ_i: initial total pressure, u_i:initial backpressure, e_p: overconsolidation void ratio (minimum void ratio the specimen has experienced before), e_i: initial void ratio, $\bar{B}$: Skempton's pore-water pressure coefficient

Table 4-4. Summary of pore-water pressure response to undrained loading and unloading within a partially frozen saline sand specimen (linear regression)

T (°C)	σ_p (kPa)	σ_i (kPa)	u_i (kPa)	e_p	e_i	Loading/ Unloading	$\bar{B}^*$ FRP-1	FRP-2	FRP-3	FRP-4	FRP-5	Average	Average correlation coefficient
Unfrozen state before freezing the specimen:													
+3.44	**67**	129	89	0.7441	0.7445	**L**	0.9087	0.9042	0.9059	0.9095	0.9151	0.9087	0.994
						U	0.8521	0.8616	0.8448	0.8313	0.8378	0.8455	0.999
+3.53	**67**	128	107	0.7421	0.7433	**L**	0.8677	0.8563	0.8686	0.8766	0.8753	0.8689	0.9976
						U	0.8968	0.8968	0.8895	0.881	0.8931	0.8914	0.9994
Frozen state after rapid freezing and subsequent warming:													
-2.91	**67**	128	102	0.7368	0.7377	**L**	0.8186	0.8353	0.8205	0.8197	0.8178	0.8224	0.9959
						U	0.8449	0.835	0.8552	0.8447	0.849	0.8458	0.9989
Cycle 1 of 3 repeated undrained loading-unloading:													
-2.88	**137**	130	100	0.7323	0.7332	**L**	0.6691	0.677	0.6699	0.659	0.667	0.6684	0.984
						U	0.6923	0.5767	0.6912	0.6807	0.6859	0.6654	0.9946
Cycle 2 of 3 repeated undrained loading-unloading:													
-2.88	**137**	130	96	0.7318	0.7326	**L**	0.693	0.7284	0.7004	0.7005	0.6935	0.7032	0.9891
						U	0.7217	0.6024	0.7141	0.7065	0.7188	0.6927	0.9954
Cycle 3 of 3 repeated undrained loading-unloading:													
-2.87	**137**	130	99	0.7315	0.7325	**L**	0.7036	0.7102	0.7097	0.7083	0.6997	0.7063	0.9964
						U	0.7424	0.5463	0.7323	0.7213	0.7378	0.696	0.9894
Cycle 1 of 4 repeated undrained loading-unloading:													
-2.89	**239**	130	98	0.7291	0.7317	**L**	0.8601	0.8375	0.8515	0.8509	0.8559	0.8512	0.9966
						U	0.8448	0.1988	0.8317	0.8314	0.8489	0.7111	0.9311
Cycle 2 of 4 repeated undrained loading-unloading:													
-2.90	**239**	130	112	0.7291	0.731	**L**	0.8573	0.3887	0.8248	0.8454	0.8435	0.7519	0.9422
						U	0.878	0.0256	0.8829	0.8613	0.8729	0.7041	0.9886
Cycle 3 of 4 repeated undrained loading-unloading:													
-2.90	**239**	130	112	0.7291	0.7308	**L**	0.8917	0.0816	0.8662	0.8712	0.8699	0.7161	0.8476
						U	0.8981	0.0277	0.8983	0.8747	0.8845	0.7167	0.986
Cycle 4 of 4 repeated undrained loading-unloading:													
-2.91	**239**	130	112	0.7291	0.7309	**L**	0.8597	0.0192	0.8409	0.8418	0.8557	0.6834	0.8166
						U	0.8951	0.0231	0.9046	0.8844	0.9035	0.7221	0.9954
Increased initial backpressure:													
-2.93	**239**	179	151	0.7291	0.7305	**L**	0.8203	0.0108 ***-0.6868***	0.809	0.8015	0.8175	0.8121	0.9982
						U	0.7604	0.0281 ***0.8843***	0.7363	0.7463	0.7542	0.7493	0.9904
Increased initial backpressure:													
-2.99	**239**	279	260	0.7289	0.7297	**L**	0.8409	0.0002 ***-0.0007***	0.5996	0.7771	0.8224	0.76	0.9882
						U	0.8705	0.0094 ***-0.6892***	0.6347	0.8002	0.8416	0.7867	0.9975
Cycle 1 of 2 repeated undrained loading-unloading:													
-3.12	**332**	130	99	0.7251	0.727	**L**	0.0021 ***-0.3517***	0 ***-0.0002***	0.515	0.5148	0.5171	0.5156	0.9982
						U	0.0013 ***-0.0526***	0.0029 ***-0.4386***	0.547	0.5442	0.5557	0.549	0.99
Cycle 2 of 2 repeated undrained loading-unloading:													
-3.11	**332**	130	95	0.7251	0.727	**L**	- 0.0029 ***-0.4344***	- 0.0047 ***-0.6922***	0.5492	0.5515	0.5532	0.5513	0.9994
						U	0.0029 ***-0.4382***	0.0075 ***-0.7026***	0.5762	0.5635	0.5797	0.5731	0.9914

T (°C)	σ_p (kPa)	σ_i (kPa)	u_i (kPa)	e_p	e_i	Loading/ Unloading	$\bar{B}$ *						Average correlation coefficient
							FRP-1	FRP-2	FRP-3	FRP-4	FRP-5	Average	

T: $specimen\ temperature$, σ_p: effective overconsolidation pressure, σ_i: initial total pressure, u_i:initial backpressure, e_p: overconsolidation void ratio (minimum void ratio the specimen has experienced before), e_i: initial void ratio, $\bar{B}$: Skempton's pore-water pressure coefficient

* Second numbers after the $\bar{B}$ (in ***Italic Bold*** style in shaded area) are the correlation coefficient of the regression line reported for erratic values

Table 4-5. Summary of primary and secondary pore-water pressure response to undrained loading within a partially frozen saline sand specimen (bilinear regression)

T (°C)	σ_p (kPa)	σ_i (kPa)	u_i (kPa)	e_p	e_i	Loading/ Unloading	$\bar{B}$ *						Average correlation coefficient
							FRP-1	FRP-2	FRP-3	FRP-4	FRP-5	Ave.	
Unfrozen state before freezing the specimen:													
+ **3.44**	**67**	129	89	0.7441	0.7445	**Primary**	NA	NA	NA	NA	NA	NA	NA
						Secondary	0.9513	0.9451	0.9529	0.9595	0.957	0.9532	0.9978
+ **3.53**	**67**	128	107	0.7421	0.7433	**Primary**	NA	NA	NA	NA	NA	NA	NA
						Secondary	0.8908	0.8766	0.89	0.8986	0.8957	0.8904	0.9983
Frozen state after rapid freezing and subsequent warming:													
-2.91	**67**	128	102	0.7368	0.7377	**Primary**	NA	NA	NA	NA	NA	NA	NA
						Secondary	0.8691	0.8618	0.8478	0.8411	0.8418	0.8523	0.9978
Cycle 1 of 3 repeated undrained loading-unloading:													
-2.88	**137**	130	100	0.7323	0.7332	**Primary**	0.4949	0.5247	0.4657	0.4755	0.4951	0.4912	0.9993
						Secondary	0.8187	0.8287	0.8272	0.8202	0.823	0.8236	0.9976
Cycle 2 of 3 repeated undrained loading-unloading:													
-2.88	**137**	130	96	0.7318	0.7326	**Primary**	0.6122	0.0816	0.6327	0.5714	0.5918	0.498	1
						Secondary	0.7853	0.7788	0.7849	0.787	0.7726	0.7817	0.9962
Cycle 3 of 3 repeated undrained loading-unloading:													
-2.87	**137**	130	99	0.7315	0.7325	**Primary**	0.5625	0.5833	0.625	0.5833	0.6042	0.5917	1
						Secondary	0.7637	0.7686	0.7507	0.7661	0.7502	0.7598	0.9976
Cycle 1 of 4 repeated undrained loading-unloading:													
-2.89	**239**	130	98	0.7291	0.7317	**Primary**	0.8142	0.7631	0.8138	0.8142	0.8142	0.8039	0.9952
						Secondary	0.9556	0.9333	0.8667	0.8667	0.9111	0.9067	1
Cycle 2 of 4 repeated undrained loading-unloading:													
-2.90	**239**	130	112	0.7291	0.731	**Primary**	0.8049	0.0493 ***0.3068***	0.7802	0.8093	0.7926	0.7967	0.9999
						Secondary	1.2857	1.25 ***-1***	1.2143	1.1786	1.25	1.2321	1
Cycle 3 of 4 repeated undrained loading-unloading:													
-2.90	**239**	130	112	0.7291	0.7308	**Primary**	0.8272	-0.0291 ***-0.893***	0.8383	0.8296	0.8065	0.8254	0.9995
						Secondary	1.7	1.7 ***-1***	1.6	1.65	1.6	1.6375	1
Cycle 4 of 4 repeated undrained loading-unloading:													
-2.91	**239**	130	112	0.7291	0.7309	**Primary**	0.8418	-0.0315 ***-0.9012***	0.8751	0.8399	0.8439	0.8502	0.9998
						Secondary	0.7895	0.4474 ***-1***	0.8158	0.8158	0.8684	0.8224	1
Increased initial backpressure:													
-2.93	**239**	179	151	0.7291	0.7305	**Primary**	0.8007	0.0098 ***-0.5247***	0.791	0.785	0.7987	0.7939	0.9982
						Secondary	NA	NA	NA	NA	NA	NA	NA
Increased initial backpressure:													
-2.99	**239**	279	260	0.7289	0.7297	**Primary**	0.8409	0.0002 ***-0.0007***	0.5996 -0.9531	0.7771	0.8224	0.8135	0.9999
						Secondary	NA	NA	NA	NA	NA	NA	NA
Cycle 1 of 2 repeated undrained loading-unloading:													
-3.12	**332**	130	99	0.7251	0.727	**Primary**	0.0021 ***-0.3517***	0 ***-0.0002***	0.515	0.5148	0.5171	0.5156	0.9982
						Secondary	NA	NA	NA	NA	NA	NA	NA
Cycle 2 of 2 repeated undrained loading-unloading:													
-3.11	**332**	130	95	0.7251	0.727	**Primary**	-0.0029 ***-0.4344***	-0.0047 ***-0.6922***	0.5492	0.5515	0.5532	0.5513	0.9994

T: $specimen\ temperature$, σ_p: effective overconsolidation pressure, σ_i: initial total pressure, u_i:initial backpressure, e_p: overconsolidation void ratio (minimum void ratio the specimen has experienced before), e_i: initial void ratio, $\bar{B}$: Skempton's pore-water pressure coefficient

* Second numbers after the $\bar{B}$ (in ***Italic Bold*** style in shaded area) are the correlation coefficient of the regression line reported for erratic values

Table 4-6. Decrease of pore-water pressure in saline sand specimen due to undrained warming

Total pressure (σ), kPa	Initial pore-water pressure (u_i), kPa	Initial temperature (T), °C	Temperaure increment (ΔT), °C	Initial gravimetric ice content (ω_i)*, %	Gravimetric ice content decrease ($\Delta\omega_i$), %	Pore-water pressure decrease (Δu), kPa	Predicted Δu from Equation (4-7)	Predicted Δu from Equation (4-8)
231	205	-3.11	0.76	11.63	2.29	283	283	272
224	172	-2.34	0.93	9.30	4.85	175	175	190
227	192	-1.38	0.88	4.27	4.26	64	64	57
228	203	-0.48	2.53	No ice	No ice	57	No ice	57
228	206	+2.05	1.67	No ice	No ice	34	No ice	32

* Interpolated using a 10th order polynomial regression on data provided by Hivon (1991)

Table 4-7. Regression coefficients for Equation (4-7) using data in Table 4-6

Regression coefficient	Value (double precision)
a	13.15651354
b	1.332832776
c	-0.243427774
Coefficient of Multiple Determination (R^2) = 1.0	

Table 4-8. Regression coefficients for Equation (4-8) using data in Table 4-6

Regression coefficient	Value (double precision)
a	3.225614502
b	1.79158017
c	5.52615E-11
d	15.86903758
e	1.38524336
Coefficient of Multiple Determination (R^2) = 0.9914	

Table 4-9. Summary of pore-water pressure response to undrained loading and unloading within a partially frozen saline sand specimen subjected to undrained warming and subsequent back-pressuring before each $\overline{B}$-test

T (°C)	σ_p (kPa)	σ_i (kPa)	u_i (kPa)	e_p	e_i	Loading/ Unloading	$\overline{B}$ *						Average correlation coefficient
							FRP-1	FRP-2	FRP-3	FRP-4	FRP-5	Average	
-2.35	332	228	191	0.7249	0.7261	L	0.5071	0.0061 ***-0.747***	0.5192	0.5014	0.5032	0.5077	0.9976
						U	0.5842	0.0079 ***-0.7919***	0.586	0.5839	0.5918	0.5865	0.9993
-1.39	332	227	190	0.7247	0.7258	L	0.5828	0.5808	0.5769	0.5791	0.5789	0.5797	0.9983
						U	0.638	0.6198	0.6236	0.6221	0.6337	0.6274	0.9982
-0.48	332	225	196	0.7247	0.7258	L	0.6381	0.65	0.6283	0.6383	0.6344	0.6378	0.9994
						U	0.6834	0.6756	0.6736	0.6631	0.6815	0.6754	0.9976
2.05	332	231	199	0.7247	0.7261	L	0.7511	0.7492	0.7291	0.7312	0.7431	0.7407	0.9947
						U	0.779	0.761	0.753	0.756	0.7683	0.7634	0.9976
3.73	332	229	195	0.7247	0.7265	L	0.8057	0.8116	0.7838	0.7957	0.7913	0.7976	0.9952
						U	0.8234	0.8132	0.7969	0.7885	0.8089	0.8062	0.9989

T: $specimen\ temperature$, σ_p: effective overconsolidation pressure, σ_i: initial total pressure, u_i:initial backpressure, e_p: overconsolidation void ratio (minimum void ratio the specimen has experienced before), e_i: initial void ratio, $\overline{B}$: Skempton's pore-water pressure coefficient

***** Second numbers after the $\overline{B}$s (in ***Italic Bold*** style in shaded area) are the correlation coefficient of the regression line reported for erratic values

Table 4-10. Correlation coefficients for Equation (4-9)

Regression coefficient	Value (double precision)
a	-8851.966428
b	36155.79327
c	-49242.51222
d	22364.37715
e	0.000724643
f	9.23539E-06
g	-2.38135E-08

4.7 Figures

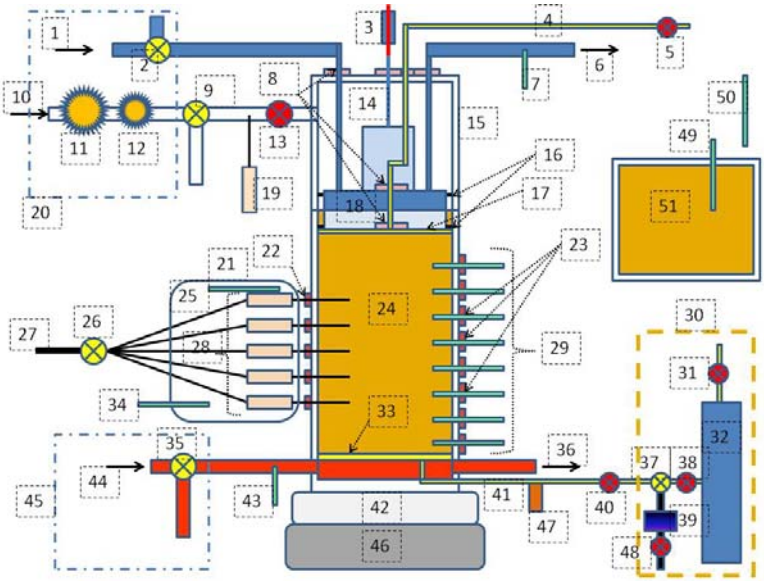

Legend

1 Inflow of glycol from the thermally controlled bath to top plate
2 3-way valve for directing glycol to the cell or to the bath
3 LVDT
4 Upper drain/backpressure application tube
5 Open-close valve
6 Outflow of glycol to the bath from top plate
7 RTD # 307
8 O-ring and vacuum grease sealing for air tight connections
9 3-way valve on air pressure line
10 Connected to air compressor
11 High air pressure dial gage and regulator
12 Low air pressure dial gage and regulator
13 Open-close valve on air pressure line
14 Rod connecting piston and LVDT
15 Air chamber
16 O-ring and Vacuum grease sealed loading piston (air and water tight)
17 Filter paper+ cloth filter
18 Loading piston and cooling/warming plate
19 FOP # 7 to measure air pressure in the chamber
20 Instruments in the laboratory space (temp = 21°C, not insulated) enables changing pressures without the need to open the cold room door (better thermal control of specimen)
21 Insulation box for FRPs
22 Brass ferrule for FRP connections to the cell- NTP fittings (1/16")
23 Brass ferrule for RTD connections to the cell- NTP fittings (1/8")
24 Specimen
25 RTD # 106 (E) attached to FOP # 1
26 Multi-way valve for saturating oil-line in the FOPs
27 To oil reservoir pressurized by syringe pump
28 A set of 5 FRPs
29 RTD # 201 to 208 (fed into the specimen)
30 Insulation box for the syringe pump
31 Open-close valve for filling the syring pump with de-aired water
32 Syringe pump with water in the reservoir (half full)
33 Porous stone filter
34 RTD # 107 (F), in the air in the FRP insulation box
35 3-way valve on the inflow to the bottom plate
36 Outflow of the glycol line connected to the bottom plate
37 3-way valve to apply pressure to either oil reservoir or to the specimen (switch between oil and water)
38 Open-close valve on the syringe pump. Allows filling the pump reservoir or applying pressure on the line
39 Oil over water reservoir with air vent (saturating oil line)
40 Open-close valve on the bottom drain of the MQS cell
41 Bottom drain of the MQS cell
42 Base of the MQS cell
43 RTD # 308
44 Inflow of glycol from the thermally controlled bath to bottom plate
45 Instruments in the laboratory space (temp = 21°C, not insulated) enables changing pressures without the need to open the cold room door
46 Scale for automatic mass measurements
47 Electrical pressuremeter
48 Open-close valve for the oil saturating line
49 RTD # 105 (inside the Dummy cell at its wall)
50 RTD # 103 (B) (in the larger insulation box)
51 Dummy cell

Figure 4-1. Schematic of Modified Qiu-Sego large strain consolidation apparatus (chapter 3)

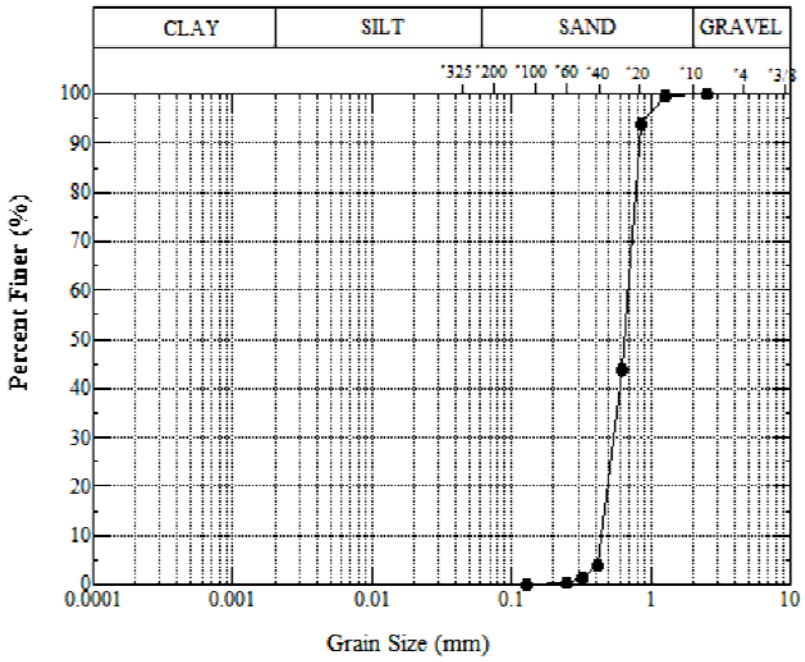

Figure 4-2. Grain size distribution of sand used in this research

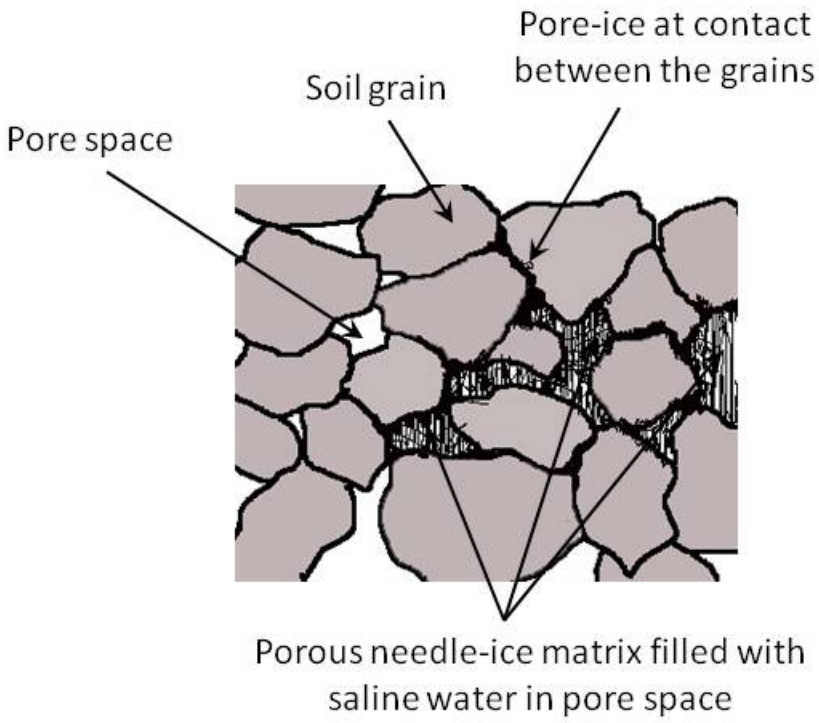

Figure 4-3. Schematic of the pore-ice matrix (contact-ice and needle-ice) in a partially frozen saline coarse grained soil based on research reported by Arenson and Sego (2006)

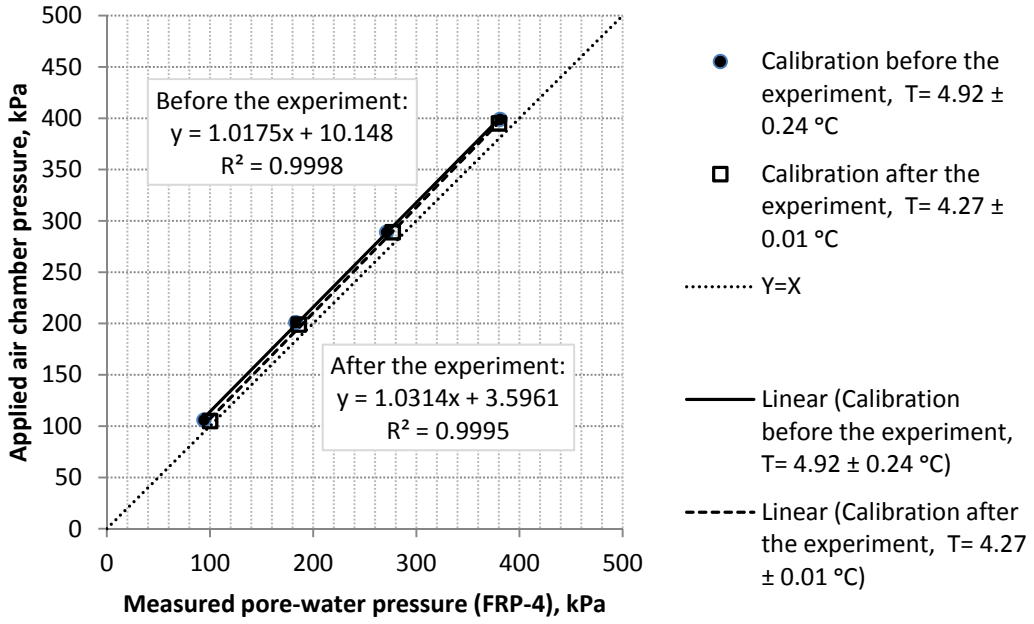

(a) Total duration of the experiment between the two calibrations = 259 hours

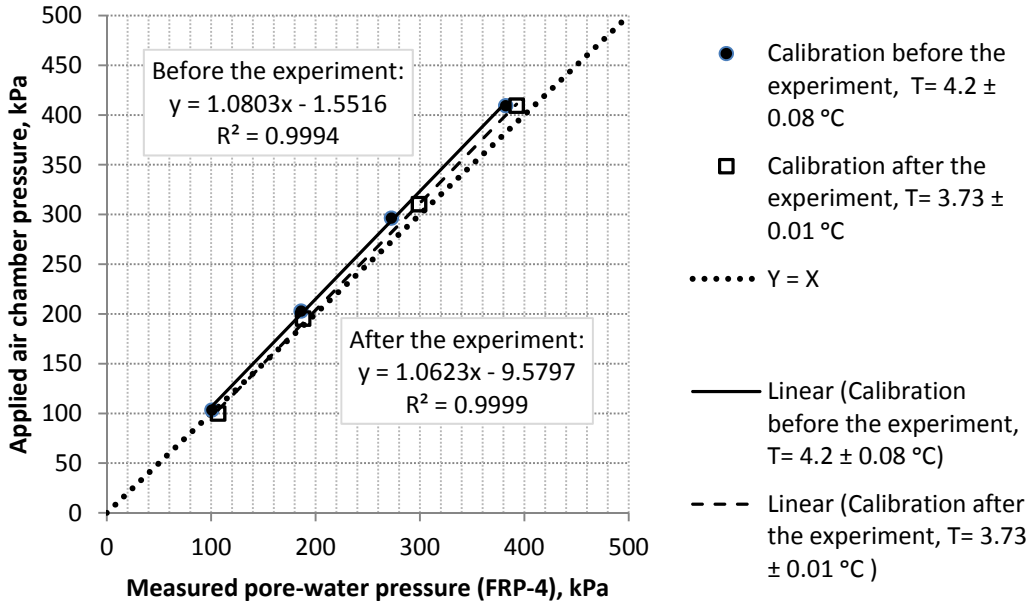

(b) Total duration of the experiment between the two calibrations = 633 hours

Figure 4-4. Comparison of calibration curves (during loading) before and after two of the partially frozen experiments

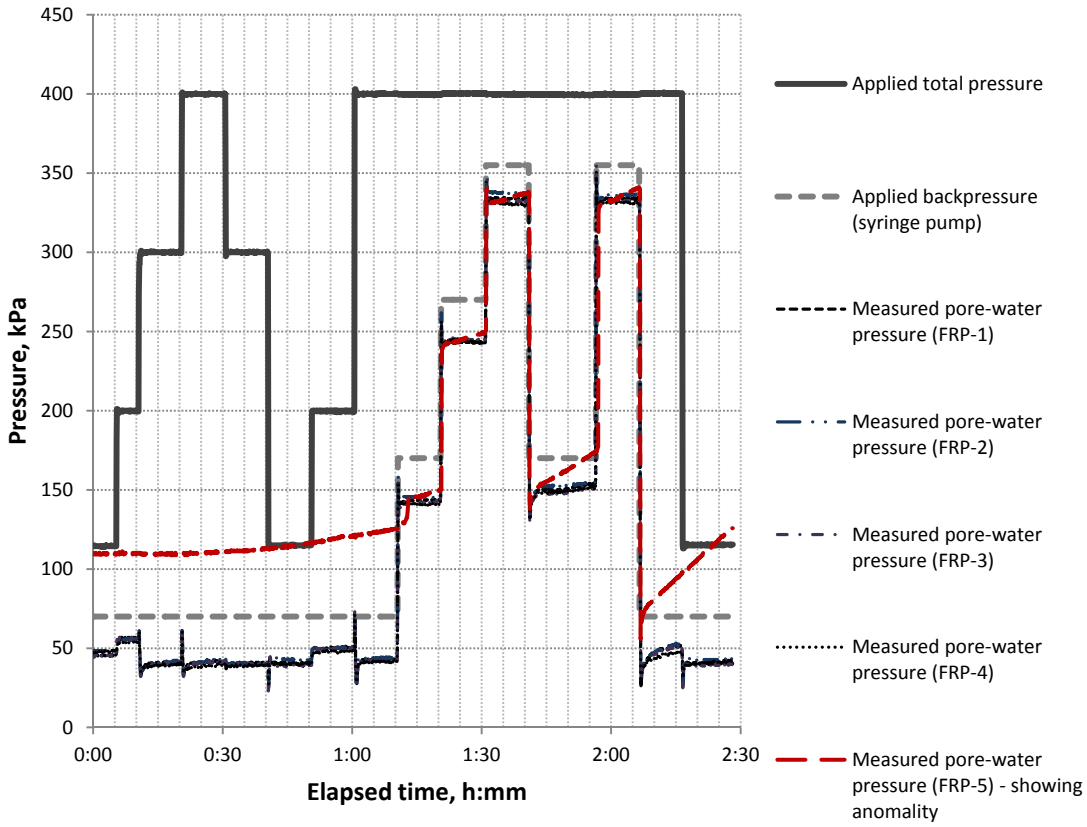

Figure 4-5. Pore-water pressure response to independent change of total pressure and backpressure within a nearly saturated partially frozen saline sand specimen (30±1 ppt NaCl) at -3.22 ± 0.03°C

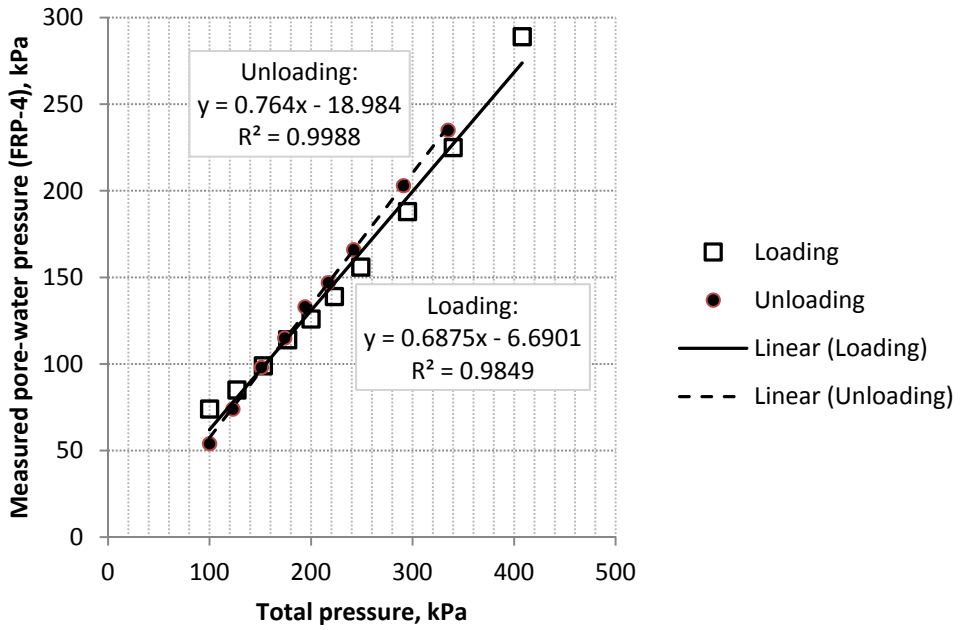

(a) Pore-water pressure response in an undrained loading-unloading cycle (linear regression)

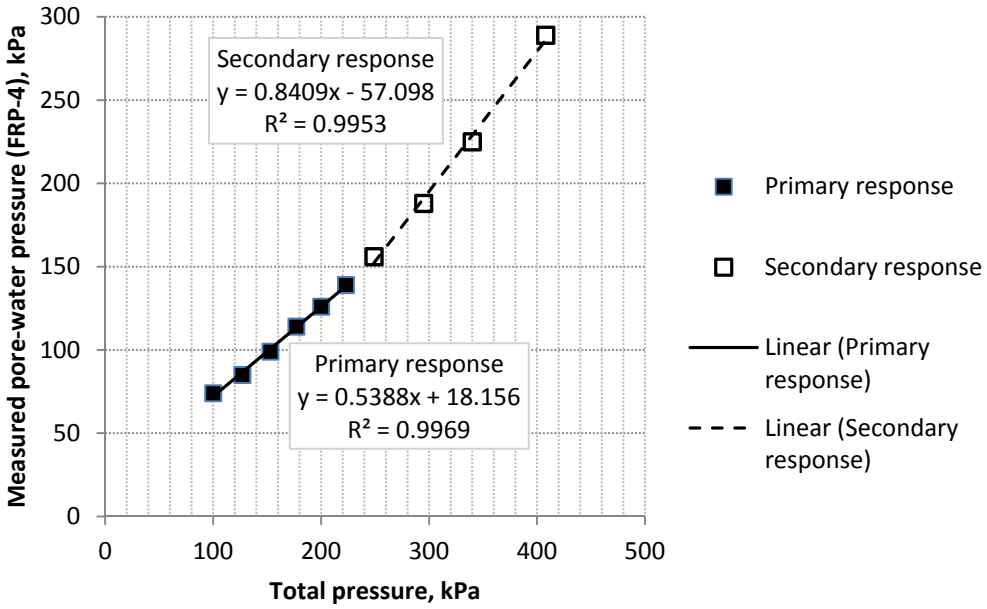

(b) Primary and secondary pore-water pressure responses during undrained loading (bilinear regression)

Figure 4-6. An example of pore-water pressure response in an overconsolidated unfrozen saline sand specimen ($\boldsymbol{\sigma_p}$ = 133 kPa, $\boldsymbol{u_i}$= 74 kPa)

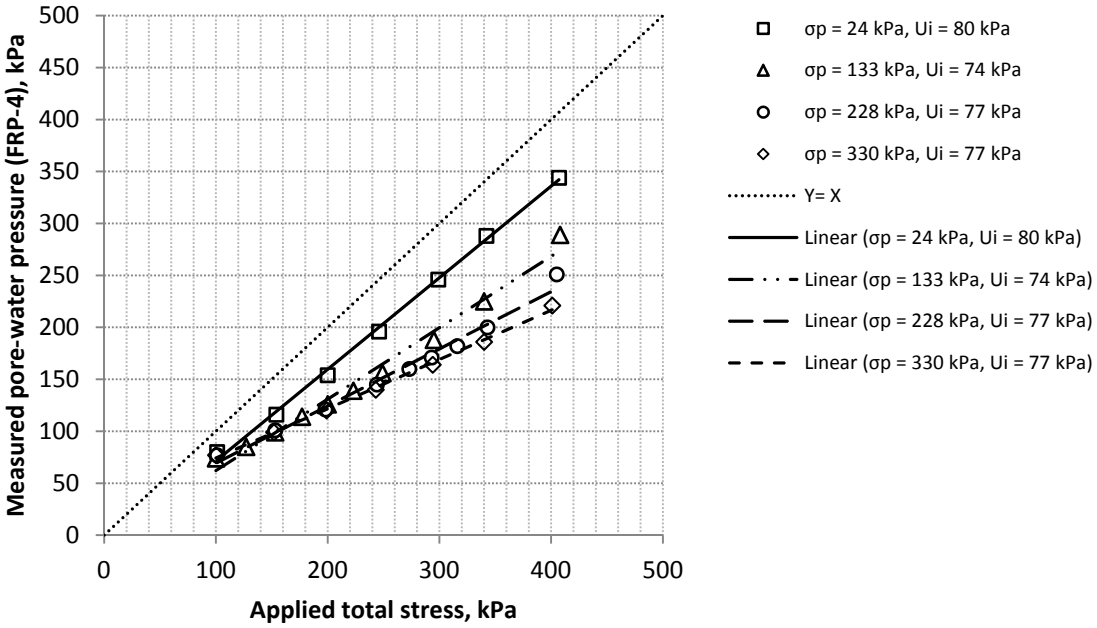

(a) Effect of preconsolidation pressure

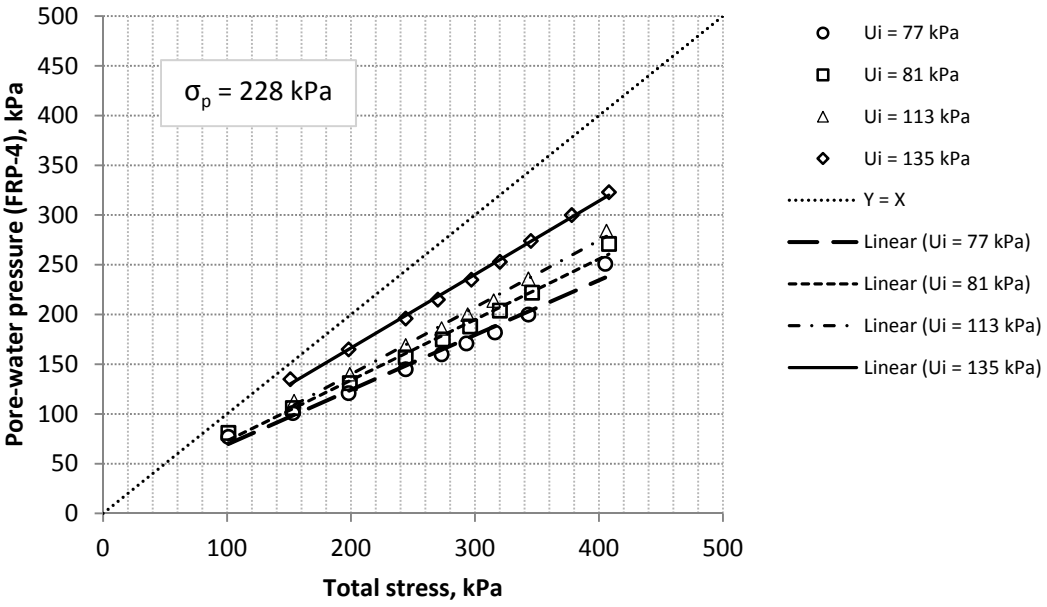

(b) Effect of backpressure

Figure 4-7. Effects of preconsolidation and backpressure on pore-water pressure response in an overconsolidated unfrozen saline sand specimen (linear regression)

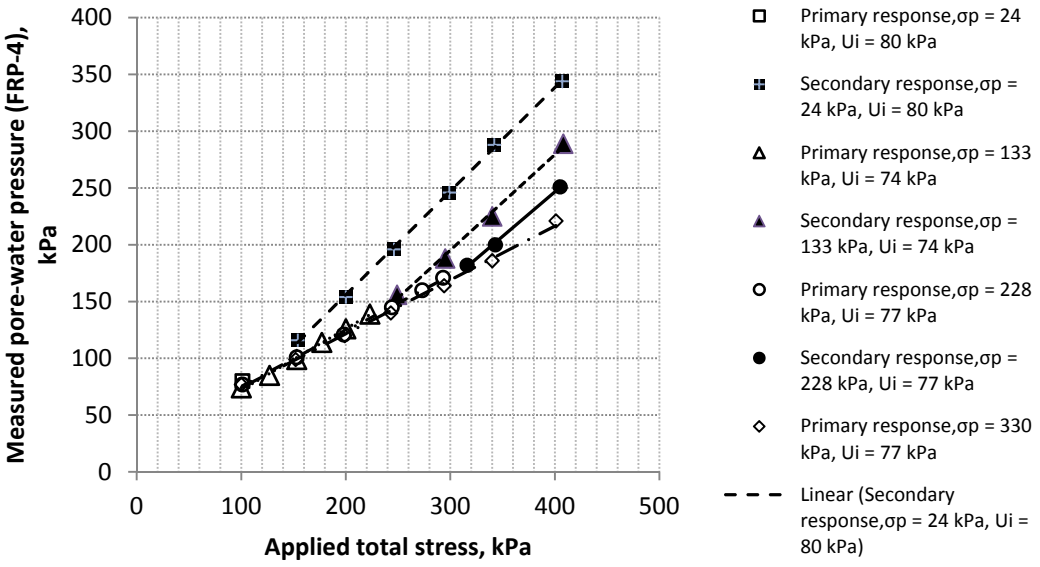

(a) Effect of preconsolidation pressure

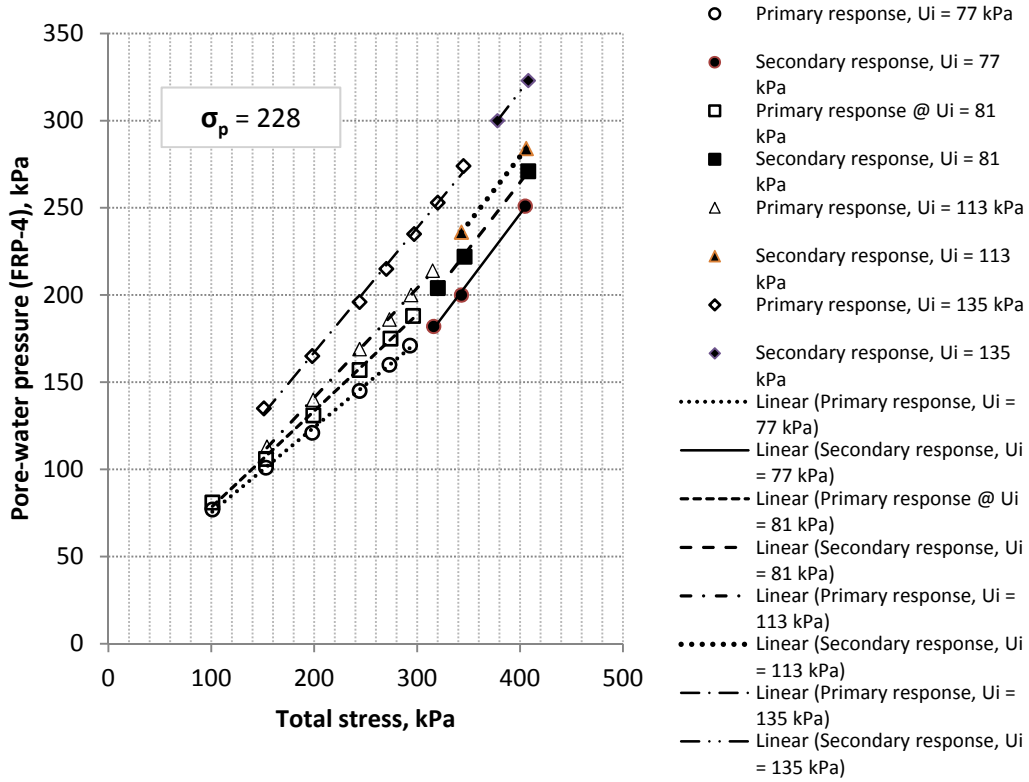

(b) Effect of backpressure

Figure 4-8 Effects of preconsolidation and backpressure on primary and secondary pore-water pressures in an overconsolidated unfrozen saline sand specimen (bilinear regression)

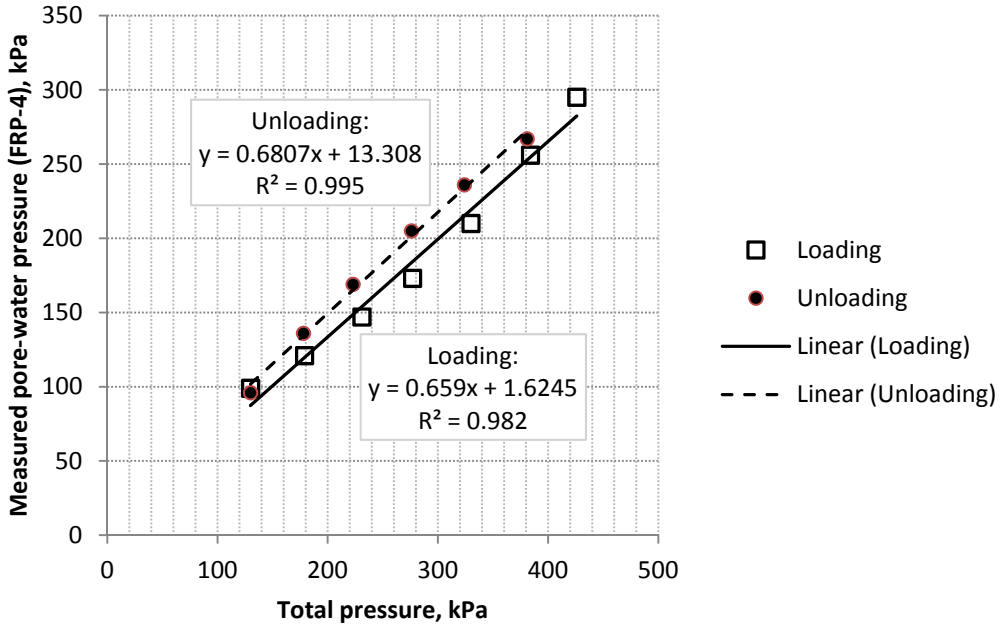

(a) Pore-water pressure response in an undrained loading-unloading cycle (linear regression)

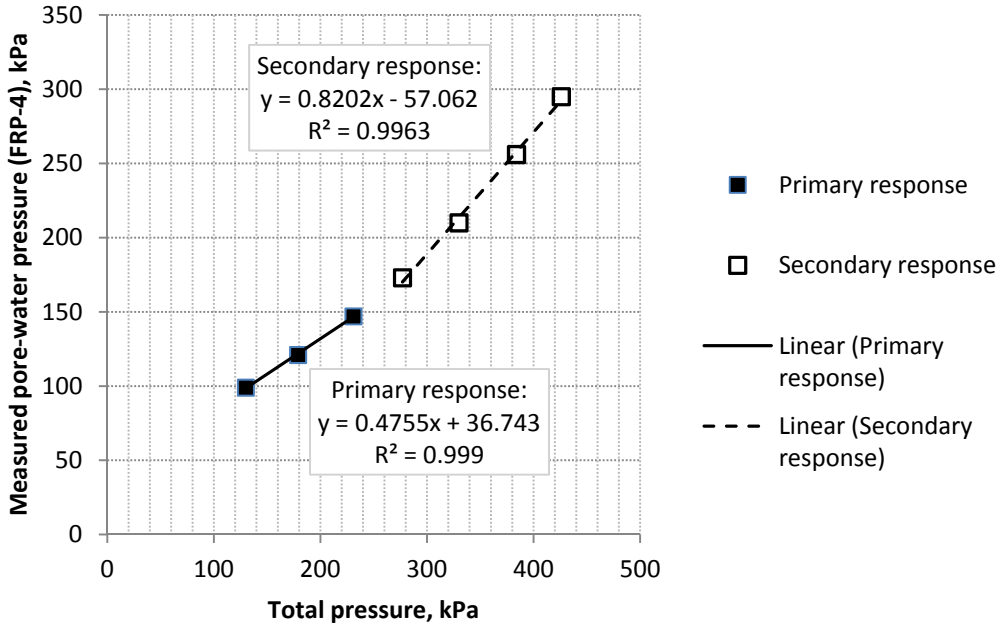

(b) Primary and secondary pore-water pressure responses during undrained loading (bilinear regression)

Figure 4-9. An example of pore-water pressure response in an overconsolidated 'frozen' saline sand specimen (σ_p = 137 kPa, u_i = 100 kPa, T = -2.88±0.02°C)

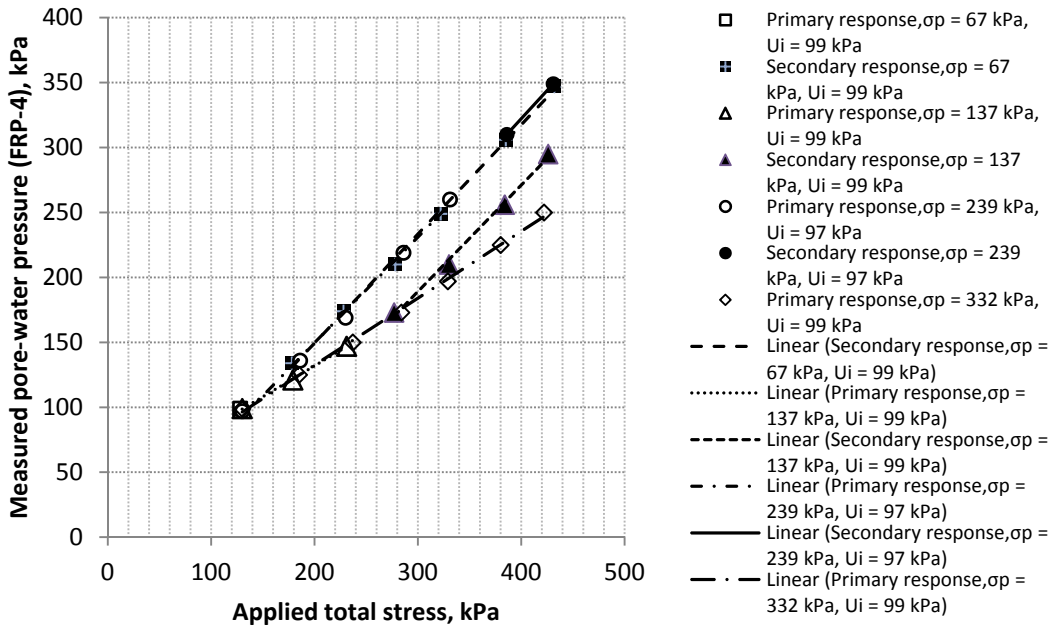

(a) Effect of preconsolidation pressure

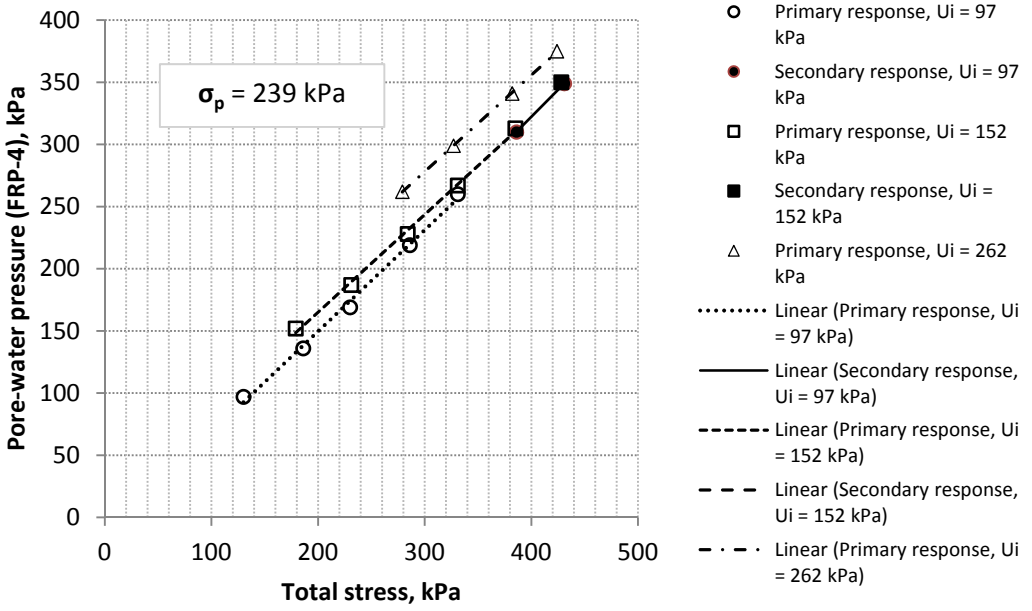

(b) Effect of backpressure

*Figure 4-10 Effects of preconsolidation and backpressure on primary and secondary pore-water pressures in an overconsolidated partially frozen saline sand specimen at 30±1 ppt salinity (**T** = -2.94 ± 0.05°C)*

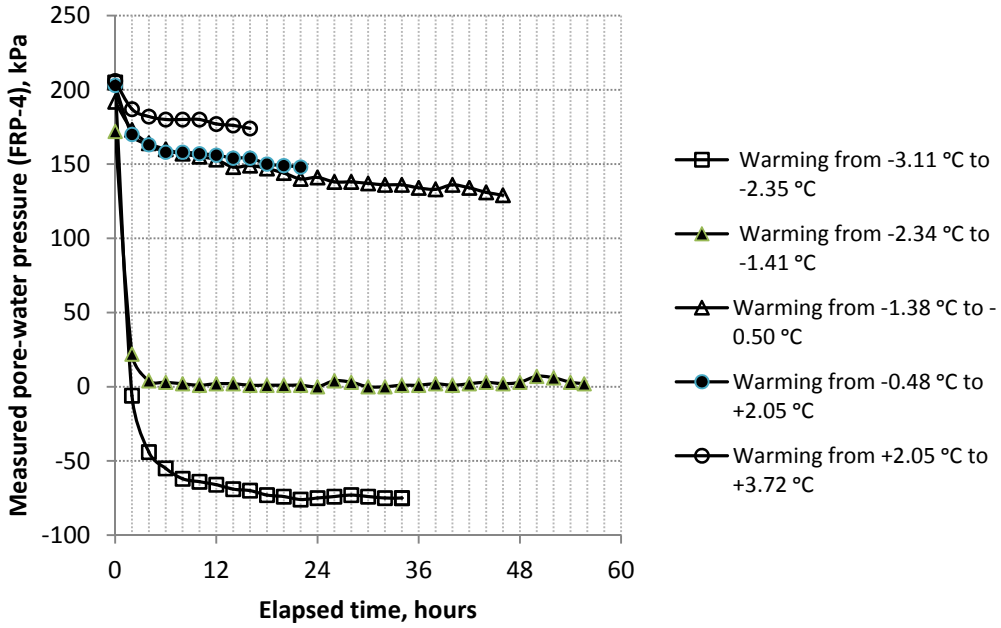

(a) Pore-water pressure response to undrained warming steps (FRP-4)

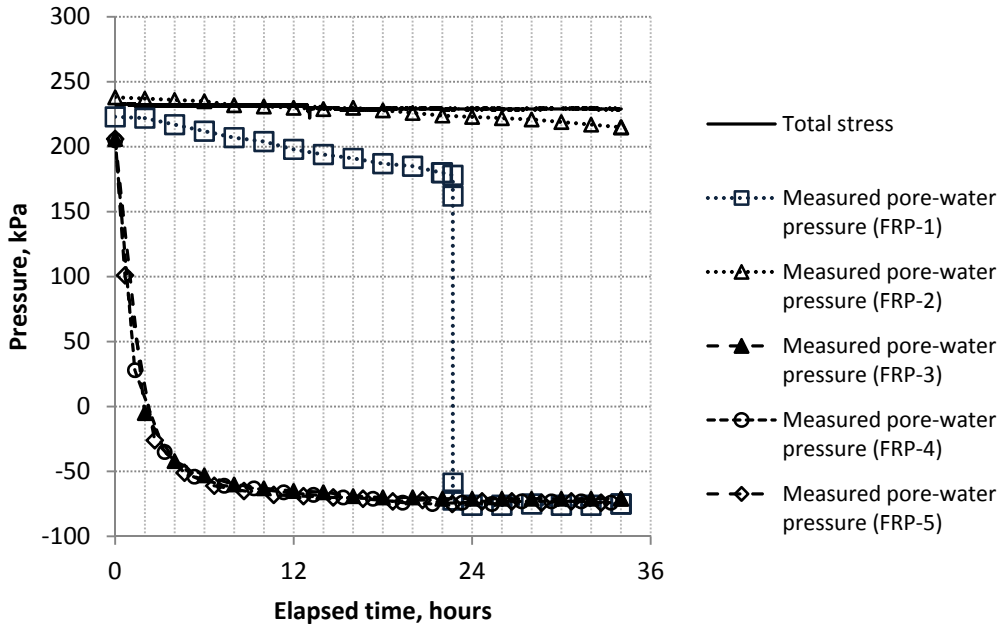

(b) Pore-water pressure response of all FRPs to undarined warming from -3.11°C to -2.35°C

Figure 4-11. Pore-water pressure response to undrained warming within a partially frozen saline sand specimen (σ_p = 332 kPa, salinity = 30±1 ppt NaCl)

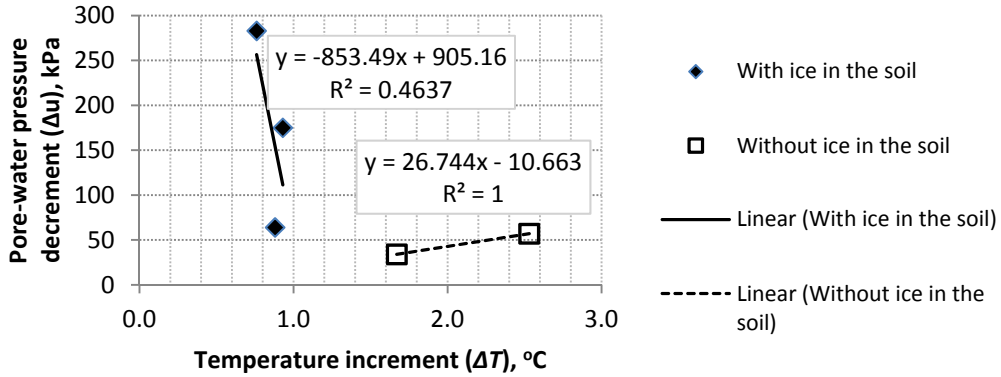

(a) Decrease in pore-water pressure versus temperature increment

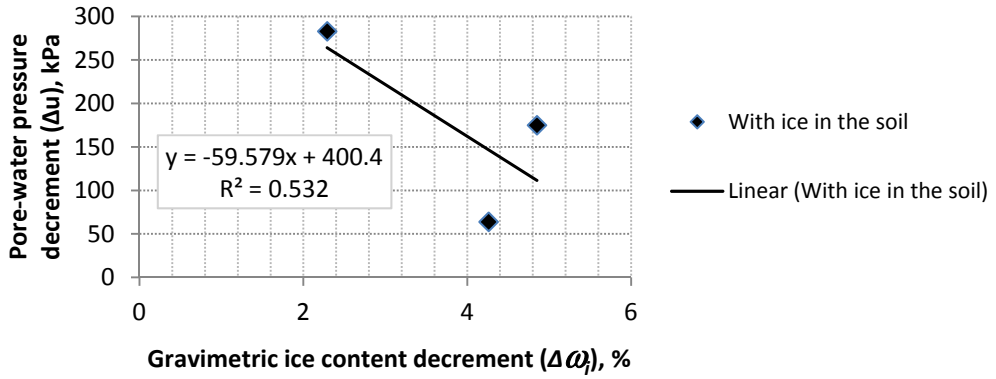

(b) Decrease in pore-water pressure versus decrease in gravimetric ice content

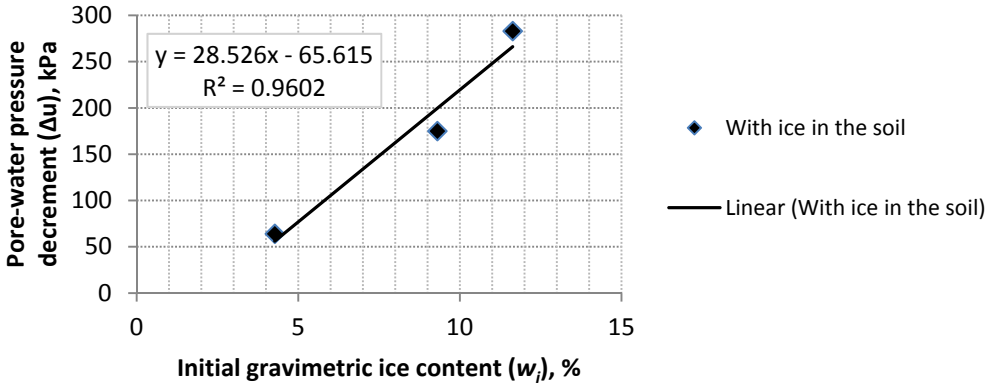

(c) Decrease in pore-water pressure versus initial gravimetric ice content

Figure 4-12. Decrease of pore-water pressure in a saline sand specimen during undrained warming as a function of temperature increment, gravimetric ice content decrease, and initial temperature

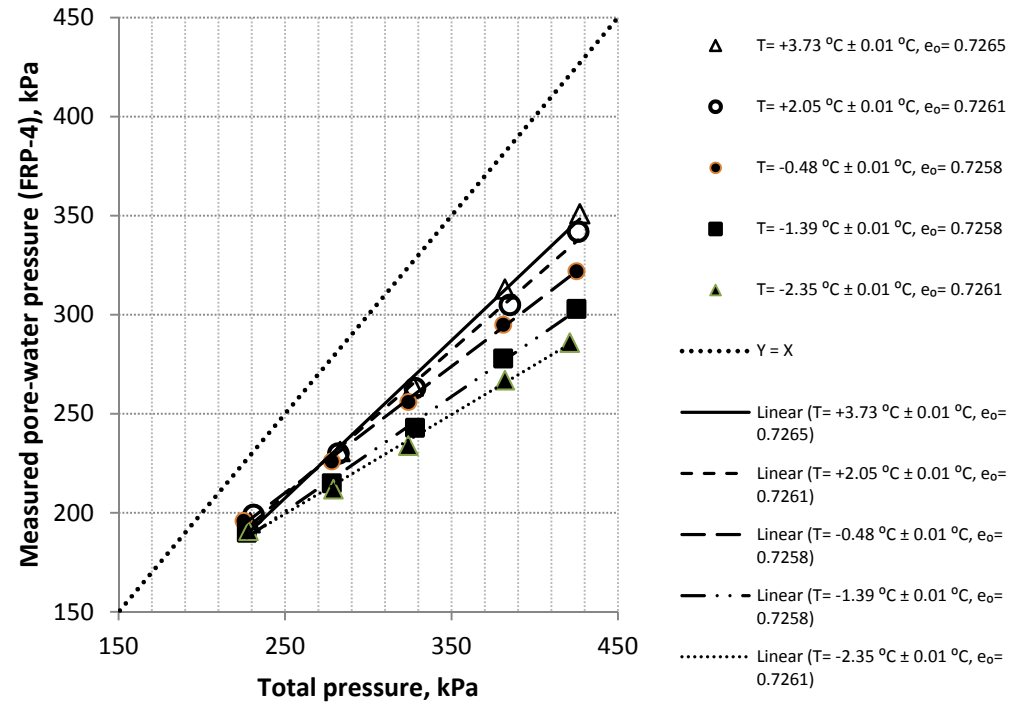

(a) Effects of temperature on pore-water pressure response to undrained loading within the specimen

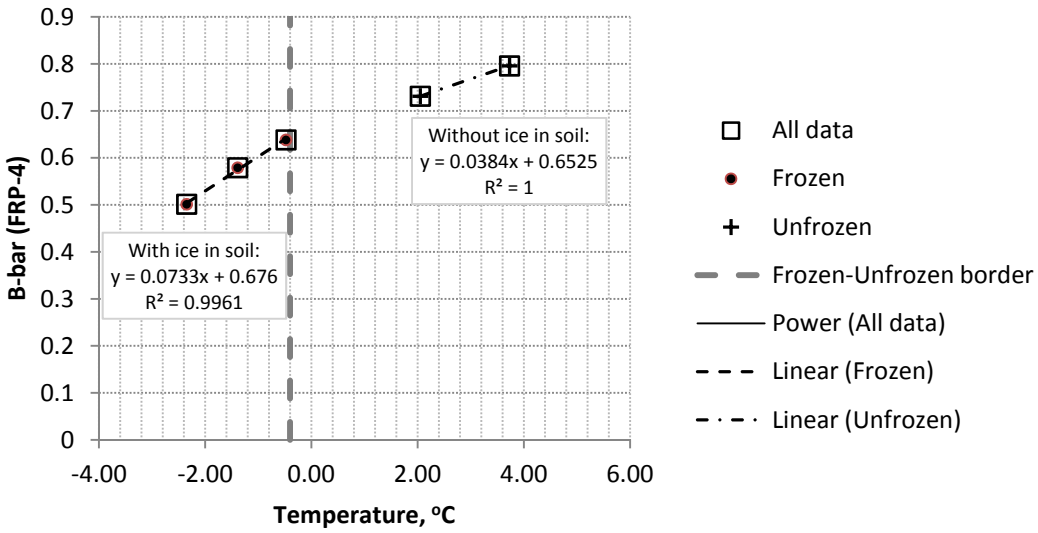

(b) Effects of specimen temperature on measured B-bars with and without pore-ice within the specimen

Figure 4-13. Effects of specimen temperature on pore-water pressure response to undrained loading within a saline sand specimen

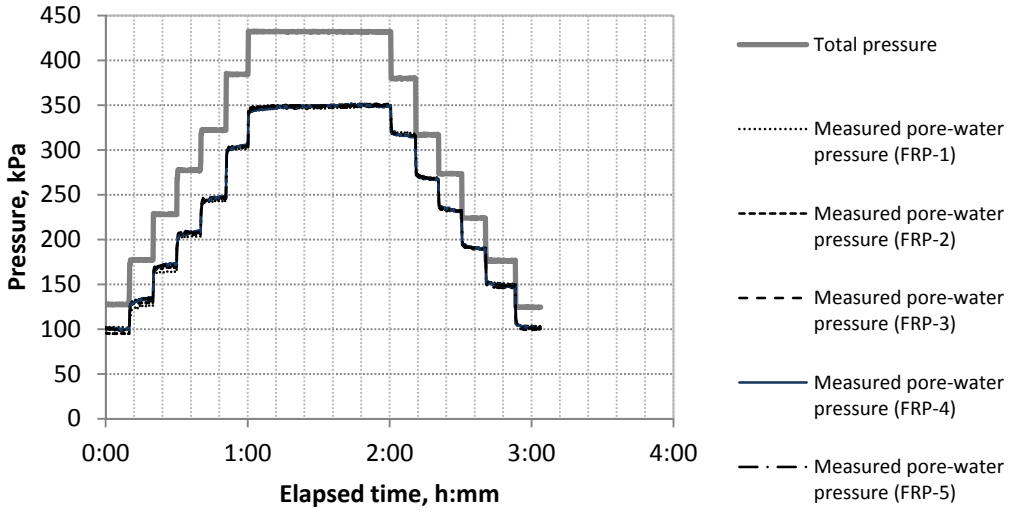

*(a) All FRPs show a continuous hydraulic connection (σ_p= 67 kPa, **T**=-2.91±0.02°C)*

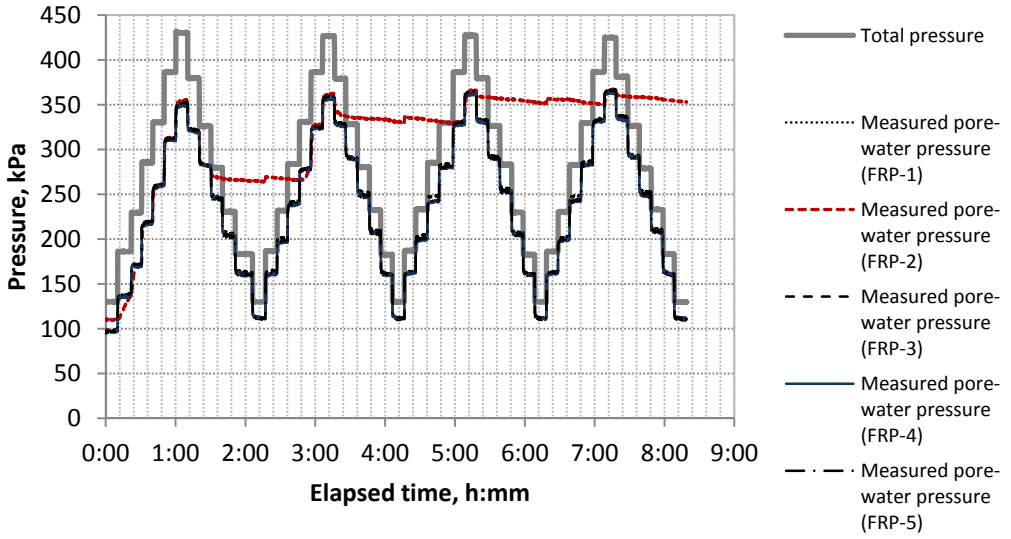

*(b) All FRPs except FRP-2 show a continuous hydraulic connection (σ_p= 239 kPa, **T**=-2.9±0.02°C)*

Figure 4-14. Examples of continuous and discontinuous hydraulic connection of the pore-water phase and FRPs. The deviation in FRP-2 response (case b) is due to Ice-blockage caused by collapse of fragile ice structure in saline sand

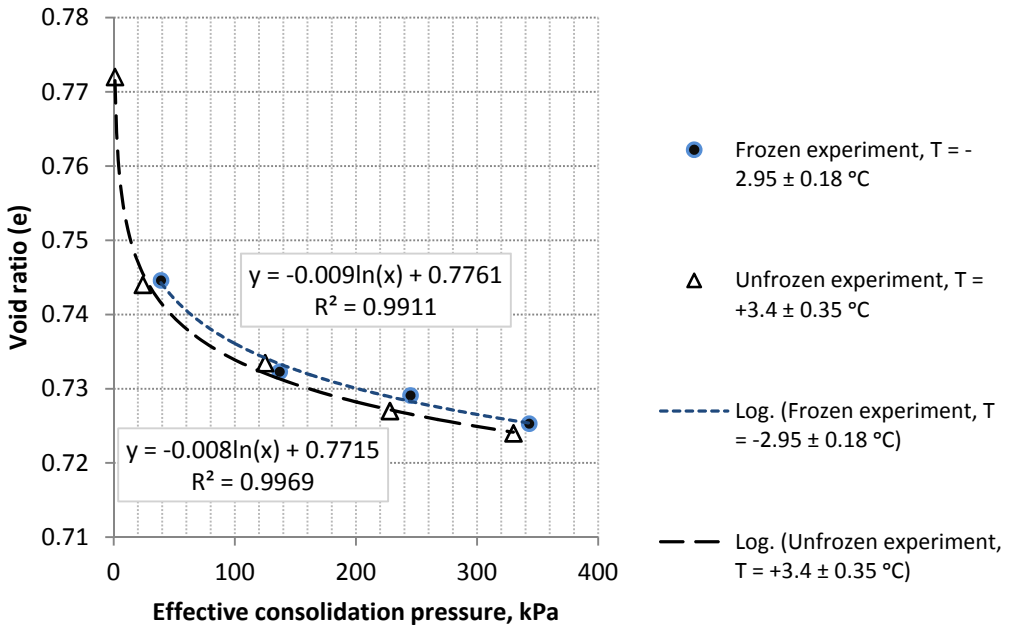

Figure 4-15. Decimated consolidation graphs for partially frozen and unfrozen saline sand specimens (only results from consolidation steps are shown with no details related to freezing-thawing, loading-unloading, and $\bar{B}$-tests)

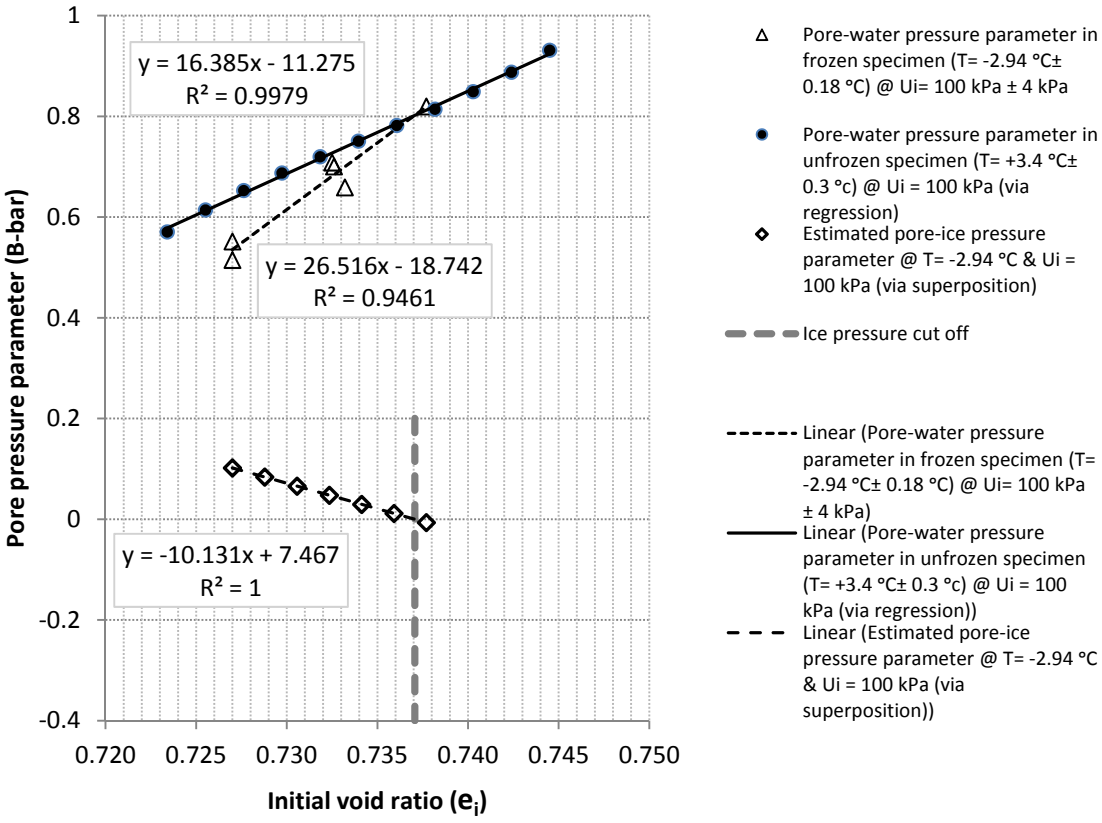

Figure 4-16. Estimation of average pore-ice pressure coefficient ($\bar{B}_{ice}$) based on algebraic superposition. When the specimen is undisturbed the fragile ice structure has very low stiffness and sustains negligible pressure ($\bar{B}_{ice} \approx 0$, ice pressure cut off)

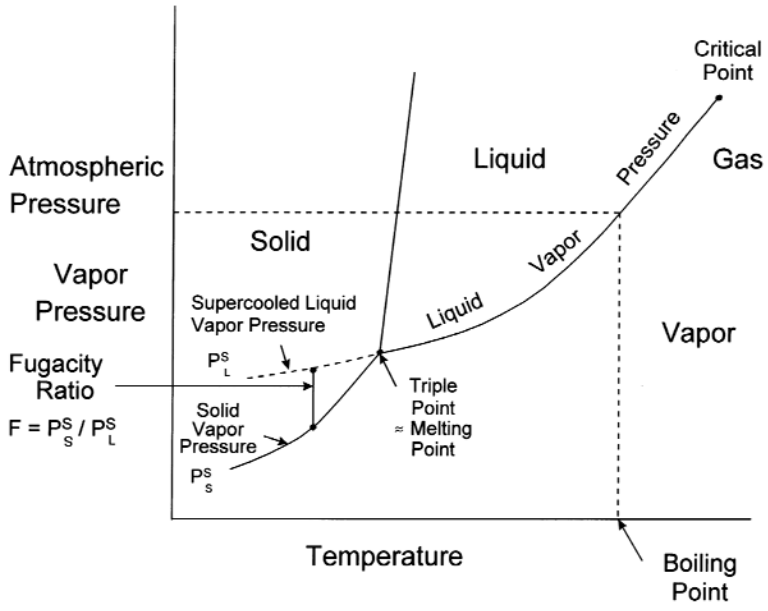

Figure 4-17. Pressure-temperature diagram of a pure substance (Sage and Sage 2000)

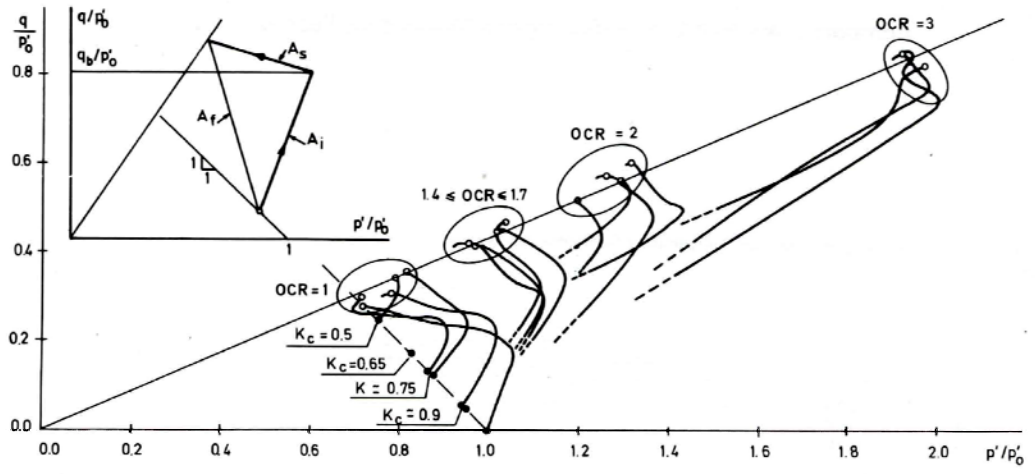

Coefficients of bilinear ESP: A_i, A_s, A_f, *and* $\frac{q_b}{P_0}$ $(K_c = \eta = \frac{q}{p})$

*Figure 4-18. Effects of stress history (**OCR** and K_c) on bilinear effective stress path (ESP)in soft clay specimens during undrained loading in triaxial cell (Sánchez and Sagaseta 1981)*

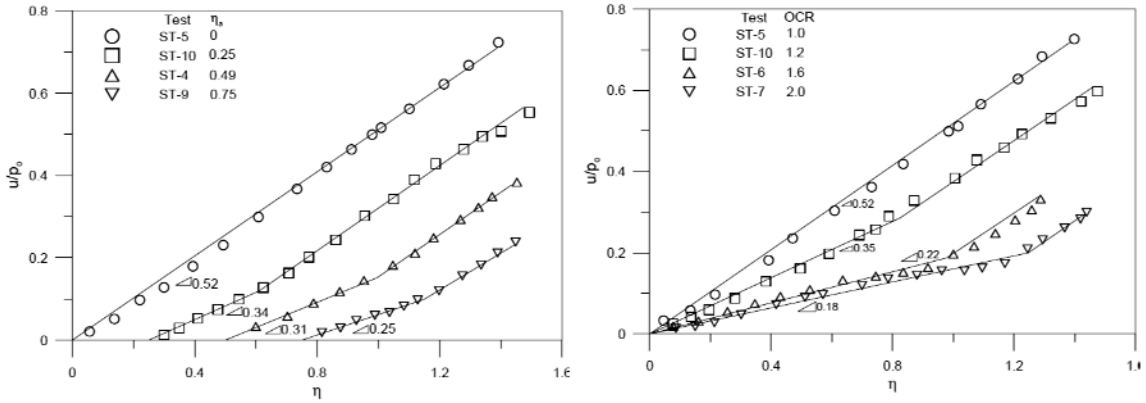

(a) *Anisotropically consolidated samples* (b) *Isotropically consolidated samples*

Figure 4-19. Linear and bilinear pore-water pressure response to monotonic undrained loading of soft clay samples in triaxial experiments (Balasubramaniam et al. 2007)

4.8 References

Agar, J.G., Morgenstern, N.R., and Scott, J.D. Geotechnical testing of Alberta oil sands at elevated temperatures and pressures. In Proceedings of the 24th US Symposium on Rock Mechanics, Rock Mechanics: Theory - Experiment - Practice., College Station, TX, USA1983. Assoc of Engineering Geologists, pp. 795-806.

Alavi, A.H., and Gandomi, A.H. 2011. A robust data mining approach for formulation of geotechnical engineering systems. Engineering Computations (Swansea, Wales), **28**(3): 242-274.

Alkire, B.D., and Andersland, O.B. 1973. The effect of confining pressure on the mechanical properties of sand-ice materials. Journal of Glacioloy, **12**(66): 469-481.

Andersland, B.D., and Alnouri, I. 1970. Time-dependent strength behavior of frozen soils. Journal of the Soil Mechanics and Foundations Division, ASCE, **96**(SM4): 1249-1265.

Arenson, L.U. 2002. Unstable alpine permafrost: a potentially important natural hazard. Ph.D. dissertation, Institute for Geotechnical Engineering Technische Wissenschaften ETH, Zurich, Switzerland.

Arenson, L.U., and Springman, S.M. 2005a. Mathematical descriptions for the behaviour of ice-rich frozen soils at temperatures close to 0 °C. Canadian Geotechnical Journal, **42**(2): 431-442.

Arenson, L.U., and Springman, S.M. 2005b. Triaxial constant stress and constant strain rate tests on ice-rich permafrost samples. Canadian Geotechnical Journal, **42**(2): 412-430.

Arenson, L.U., and Sego, D.C. 2006. The effect of salinity on the freezing of coarse-grained sands. Canadian Geotechnical Journal, **43**(3): 325-337.

Ashby, M.F., and Duval, P. 1985. The creep of polycrystalline ice. Cold Regions Science and Technology, **11**(3): 285-300.

Ashby, M.F., and Jones, D.R.H. 1998. Engineering materials 2: an introduction to microstructures, processing, and design. Butterworth-Heinemann, Oxford.

Balasubramaniam, A.S., Handali, S., Phienweja, N., and Kuwano, J. 1989. Pore-pressure stress ratio relationships for soft clay. *In* 12th International Conference on Soil Mechanics and Foundation Engineering. A.A. Balkema, Rio de Janeiro, Brazil, pp. 11-14.

Balasubramaniam, A.S., Oh, E.Y.N., Lee, C.J., Handali, S., and Seah, T.H. 2007. A more fundamental approach to predict pore-pressure for soft clay. Lowland Technology International, **9**(1): 11-17.

Barden, L. 1965. Consolidation of compacted and unsaturated clays. Géotechnique, **15**: 267-286.

Barnes, P., Tabor, D., and Walker, J.C.F. 1971. The friction and creep of polycrystalline ice. Proceedings of the Royal Society of London. Series A, Mathematical and Physical Sciences, **324**(1557): 127-155.

Baxter, C.D.P., Ravi Sharma, M.S., Moran, K., Vaziri, H., and Narayanasamy, R. 2010. Use of A=0 as a failure criterion for weakly cemented soils. Journal of Geotechnical and Geoenvironmental Engineering, **137**(2): 161-170.

Baykasoglu, A., Cevik, A., Ozbakir, L., and Kulluk, S. 2009. Generating prediction rules for liquefaction through data mining. Expert Systems with Applications, **36**(10): 12491-12499.

Bishop, A.W. 1954. Use of pore-pressure coefficients in practice. Géotechnique, **4**(4): 148-152.

Bishop, A.W., and Eldin, G. 1950. Undrained triaxial tests on saturated sands and their significance in the general theory of shear strength. Géotechnique, **2**(1): 13-32.

Bishop, A.W., and Henkel, D.J. 1962. The measurement of soil properties in the triaxial test. Edward Arnold Publishers Ltd., London.

Bishop, A.W., and Morgenstern, N. 1960. Stability coefficients for earth slopes. Geotechnique, 10(4): 129-153.

Black, D.K., and Lee, L.L. 1973. Saturating laboratory samples by back pressures. Journal of the Soil Mechanics and Foundations Divisions, **99**(SM1): 75-93.

Blume, K. 1976. Problems caused by air in hydraulic systems (in German). Industrie-Anzeiger, **98**(16): 275-276.

Bragg, R.A., and Andersland, O.B. 1981. Strain rate, temperature, and sample size effects on compression and tensile properties of frozen sand. Engineering Geology, **18**(1-4): 35-46.

Campanella, R.G., and Mitchell, J.K. 1968. Influence of temperature variations on soil behaviour. Journal of Soil Mechanics and Foundations Engineering Division, 94: 709-734.

Chamberlain, E.J., Groves, E., and Perham, R. 1972. The mechanical behavior of frozen earth materials under high pressure triaxial test conditions. Géotechnique, **22**(3): 469-483.

Chaney, R.C., Stevens, E., and Sheth, N. 1979. Suggested test method for determination of degree of saturation of soil samples by B value measurement. Geotechnical Testing Journal, **2**(3): 158-162.

Cole, D.M. 1995. A model for the anelastic straining of saline ice subjected to cyclic loading. Philosophical Magazine A, **72**(1): 231-248.

Corey, A.T. 1957. Measurement of water and air permeability in unsaturated soil. Proceedings of the Soil Science Society of America Journal, **21**(1): 7-10.

Dyminski, A.S., Steiner, M.T.A., and Villwock, R. Hierarchical ordering of extensometers readings from Itaipu dam. *In* 1st International Symposium on Life-Cycle Civil Engineering, IALCCE'08, June 11, 2008 - June 14, 2008, Varenna, Lake Como, Italy2008. CRC Press, pp. 929-934.

Eigenbrod, K.D., and Burak, J.P. 1990. Measurement of B-values less than unity for thinly interbedded varved clay. Geotechnical Testing Journal, **13**(4): 370-374.

Fish, A.M., and Zaretsky, Y.K. Strength and creep of ice in terms of Mohr-Coulomb fracture theory. *In* 8th International Offshore and Polar Engineering Conference, Montreal, Canada. 24-29 May 1998 1998. ISOPE, pp. 416-424.

Florin, G. 2011. Data mining: concepts, models and techniques. Springer, New York.

Fragaszy, R.J., and Voss, M., E. 1986. Undrained compression behavior of sand. Journal of Geotechnical Engineering, **112**(3): 334-347.

Fredlund, D.G., and Morgenstern, N.R. 1977. Stress state variables for unsaturated soils. Journal of the Geotechnical Engineering Division, ASCE, **103**(5): 447-466.

Fredlund, D.G., and Rahardjo, H. 1993. Soil mechanics for unsaturated soils. Wiley, New York.

Fung, Y.C. 1977. A first course in continuum mechanics. Prentice-Hall, Englewood Cliffs, N.J.

Gilbert, O.H. 1959. The influence of negative pore water pressures on the strength of compacted clays. MSc thesis, Massachusetts Institute of Technology.

Glen, J.W. 1955. The creep of polycrystalline ice. Proceedings of the Royal Society of London, **A228**: 519-538.

Golder, H.Q., and Skempton, A.W. The angle of shearing resistance in cohesive soils for tests at constant water content. *In* 2nd International Conference on Soil Mechanics and Foundation Engineering1948, pp. 185-192.

Gonzalez, O., and Stuart, A.M. 2008. A first course in continuum mechanics. Cambridge University Press, Cambridge.

Goughnour, R.R., and Andersland, O.B. 1968. Mechanical properties of a sand-ice system. Journal of the Soil Mechanics and Foundation Division, ASCE, **94**(SM4): 923-950.

Hivon, E.G. 1991. Behaviour of saline frozen soils. Ph.D. dissertation, University of Alberta, , Edmonton, Canada.

Hivon, E.G., and Sego, D.C. 1995. Strength of frozen saline soils. Canadian Geotechnical Journal, **32**(2): 336-354.

Ho, C.L., Vela, J.C., Clark, P.U., and Jenson, J.W. Evaluation of long-term time-rate parameters of subglacial till. *In* the 1996 ASCE National Convention. Geotechnical Special Publication, n 61, Washington, DC, USA. 10-14 November 1996 1996. ASCE, pp. 122-136.

Hooke, R.L., Mellor, M., Budd, W.F., Glen, J.W., Higashi, A., Jacka, T.H., Jones, S.J., Lile, R.C., Martin, R.T., Meier, M.F., Russell-Head, D.S., and Weertman, J. 1980. Mechanical properties of polycrystalline ice: An assessment of current knowledge and priorities for research : Report prepared for the International Commission on Snow and Ice, with support from the U.S. National Science Foundation. Cold Regions Science and Technology, **3**(4): 263-275.

Hvorslev, M.J. 1937. Uber die Festigkeitseigenschaften gestoerter bindiger Boeden (On the physical properties of disturbed cohesive soils). Ingeniorvidenskabelige Skrifter, **45**(A): 159 pp.

Jâky, J. 1944. A nyugalmi nyomâs tényezöje (The coefficient of earth pressure at rest). Magyar Mérnok és Epitész Egylet Közlönye (Journal for Society of Hungarian Architects and Engineers), **October**: 355-358.

Ladanyi, B. Bearing capacity of frozen soils. . *In* 27th Canadian Geotechnical Conference, Edmonton, Alberta 6-9 November 1974 1974. Canadian Geotechnical Society, pp. 97-107.

Ladanyi, B. 1981. Mechanical behaviour of frozen soils. *In* International Symposium on the Mechanical Behaviour of Structured Media, Ottawa, Canada. 18-21 May 1981 1981. Elsevier, Amsterdam, pp. 205-245.

Ladanyi, B. Stress transfer mechanism in frozen soils. *In* 10th Canadian Congress on Applied Mechanics, University of Western Ontario, London, Ontario, Canada. 2-7 June 1985 1985, pp. 11-23.

Ladanyi, B., and Morel, J.-F. 1990. Effect of internal confinement on compression strength of frozen sand. Canadian Geotechnical Journal, **27**(1): 8-18.

Lade, P.V., and Hernandez, S.B. 1977. Membrane penetration effects in undrained tests. American Society of Civil Engineers, Journal of the Geotechnical Engineering Division, **103**(2): 109-125.

Lade, P.V., Yamamuro, J.A., and Bopp, P.A. Drained and undrained strengths of sand in axisymmetric tests at high pressures, Kyoto2006, pp. 87-102.

Lai, Y., Jin, L., and Chang, X. 2009. Yield criterion and elasto-plastic damage constitutive model for frozen sandy soil. International Journal of Plasticity, **25**(6): 1177-1205.

Lambe, T.W., and Whitman, R.V. 1969. Soil mechanics. Wiley, New York.

Lee, K.L., Morrison, R.A., and Haley, S.C. A note on the pore-pressure parameter B. *In* 7th International Conference for Soil Mechanics and Foundation Engineering, ICSMFE, Mexico City, Mexico1969, pp. 231-238.

Ma, W., Wu, Z., Zhang, L., and Chang, X. 1999. Analyses of process on the strength decrease in frozen soils under high confining pressures. Cold Regions Science and Technology, 29(1): 1-7.

MacLennan, J., Crivat, B., and Tang, Z. 2009. Data mining with Microsoft SQL server 2008. Wiley Pub., Indianapolis, IN.

Mathworks 2011. Matlab ver. 2011. Company website: http://www.mathworks.com.

Matyas, E.L. 1967. Air and water permeability of compacted soils. *In* Symposium on Permeability and Capillarity of Soils, Atlantic City.1966. American Society for Testing and Materials, pp. 160-175.

Mesri, G., and Ali, S. 1999. Undrained shear strength of a glacial clay overconsolidated by desiccation. Géotechnique, **49**(2): 181-198.

Mesri, G., Adachi, K., and Ullrich, C.R. 1976. Pore-pressure response in rock to undrained change in all-round stress. Geotechnique, **26**(2): 317-330.

Mitchell, J.K. 1976. Fundamentals of soil behavior. Wiley, New York.

Morgenstern, N.R. 1981. Geotechnical engineering and frontier resource development. Twenty-first Rankine Lecture. Géotechnique, 31(3): 303-365.

Myatt, G.J., and Johnson, W.P. 2009. Making sense of data II: a practical guide to data visualization, advanced data mining methods, and applications. John Wiley & Sons, Hoboken, N.J.

Nater, P., Arenson, L.U., and Springman, S.M. 2008. Choosing geotechnical parameters for slope stability assessments in alpine permafrost soils. *In* 9th international conference on permafrost. University of Alaska, University of Alaska, Fairbanks, USA, pp. 1261-1266.

Neuber, H., and Wolters, R. 1977. Mechanical Behaviour of Frozen Soils under Triaxial Compression, Translation, Report NRC/CNR-TT-1902, National Research Council of Canada, Ottawa, Ontario, Canada.

Oakdale Engineering 2008. Oakdale Engineering Datafit, ver. 9.05.059. Company website: http://www.oakdaleengr.com/.

Odom, L.R., and Henson, R.K. 2002. Data screening: essential techniques for data review and preparation. *In* Meeting of Southwest Educational Association. U.S. Department of Education, Austing, Texas, USA, p. 37.

Parameswaran, V.R., and Jones, S.J. 1981. Triaxial testing of frozen sand. Journal of Glaciology, **27**(95): 147-155.

Qi, J., and Ma, W. 2007. A new criterion for strength of frozen sand under quick triaxial compression considering effect of confining pressure. Acta Geotechnica, **2**(3): 221-226.

Razbegin, V.N., Vyalov, S.S., Maksimyak, R.V., and Sadovskii, A.V. 1996. Mechanical properties of frozen soils. Soil Mechanics and Foundation Engineering, **33**(2): 35-45.

Repetto-Llamazares, A.H.V., Høyland, K.V., and Kim, E. 2011. Experimental studies on shear failure of freeze-bonds in saline ice. Part II: Ice-ice friction after failure and failure energy. Cold Regions Science and Technology, **65**(3): 298-307.

Roggensack, W.D., and Morgenstern, N.R. Direct shear tests on natural fine-grained permafrost soils. *In* 3rd International Conference on Permafrost, Edmonton, Alberta, Canada. 10-13 July 1978 1978. National Reseach Council of Canada, pp. 728-735.

Roman, L.T. 2003. Potential for use of time-analogy methods in mechanics of frozen soils. Soil Mechanics and Foundation Engineering, **40**(4): 146-151.

Roman, L.T., Zhu, Y., Zang, C., Ma, W., and Zhang, J. Using method of temperature-time analogy to determine long-term strength of frozen soil in triaxial compression. *In* 7th International Symposium on Ground Freezing, Nancy, France. 24-28 October 1994 1994. A.A. Balkema, pp. 417-418.

Sadovskii, A.V., Bondarenko, G.I., Tikhomirov, S.M., and Konstantinov, A.V. 1987. Freezing-together strength of sea ice and bottom soils in shelf zone. Soil Mechanics and Foundation Engineering, **24**(5): 189-193.

Sage, M., and Sage, G. 2000. Vapor Pressure. *In* Handbook of property estimation methods for chemicals, CRC Press.

Sanchez, J.M., and Sagaseta, C. 1981. Undrained behaviour of soft clays in triaxial tests. International Conference on Soil Mechanics and Foundation Engineering, **1**: 771-774.

Sánchez, J.M., and Sagaseta, C. Undrained behaviour of soft clays in triaxial tests. *In* International Conference on Soil Mechanics and Foundation Engineering, Stockholm, Sweden. 15-19 June 1981 1981. A. A. Balkema, pp. 771-774.

Sánchez, J.M., Sagaseta, C., and Ballester, F. Influence of stress history on undrained behaviour of soft clays. *In* 7th European Conference on Soil Mechanics and Foundation Engineering, Helsinki, Finland. 1 September 1979 1979. British Geotechnical Society, pp. 257-262.

Sayles, F.H. Triaxial and creep tests on frozen Ottawa sand. *In* North American Contribution to the 2nd International Permafrost Conference 1973. National Academy of Sciences, pp. 384-391.

Sayles, F.H. 1974. Triaxial constant strain rate tests and triaxial creep tests on frozen Ottawa sand. CRREL Technical Report 253, U.S. Army Cold Regions Research and Engineering Laboratory (CRREL), Hanover, N.H., USA.

Sego, D.C., and Morgenstern, N.R. 1983. Deformation of ice under low stresses. Canadian Geotechnical Journal, **20**(4): 587-602.

Sinha, N.K. 1978. Rheology of columnar-grained ice. Experimental Mechanics, **18**(12): 464-470.

Skempton, A.W. 1948a. A study of the geotechnical properties of some post-glacial clays. Geotechnique **1**(1): 7-22.

Skempton, A.W. A study of the immediate triaxial test on cohesive soils. *In* 2nd International Conference on Soil Mechanics and Foundation Engineering1948b, pp. 192-196.

Skempton, A.W. 1948c. The effective stresses in saturated clays strained at constant volume. *In* 7th International Congress for Applied Mechanics, pp. 378-392.

Skempton, A.W. 1954. Pore-pressure coefficients A and B. Geotechnique, **4**(4): 143-147.

Smith, I.R. Data mining seismic shothole drillers' log records: Regional baseline geoscience information in support of pipeline proposal design, assessment, and development. *In* ASME International Pipeline Conference, IPC 2008, Calgary, AB, Canada. 29 September- 3 October 2008 2009. American Society of Mechanical Engineers, pp. 299-303.

Song, L. 1984. Measurement of mechanical properties of frozen soil using the single specimen method (in Chineese). Meitan Xuebao/Journal of the China Coal Society, **1**: 21-30.

Sparkes, A.D.W. Theoretical considerations of stress equations for partially saturated soils. *In* 3rd African Conference on Soil Mechanics and Foundation Engineering, Salisbury1963, pp. 215-218.

Tinoco, J., Correia, A.G., and Cortez, P. A data mining approach for jet grouting uniaxial compressive strength prediction. *In* World Congress on Nature and Biologically Inspired Computing, NABIC 2009, Coimbatore, India. 9-11 December 2009 2009. IEEE Computer Society, pp. 553-558.

Tsytovich, N.A. 1975. The mechanics of frozen ground. Scripta Book, Washington, D.C.

Veyera, G.E., Charlie, W.A., Doehring, D.O., and Hubert, M.E. 1992. Measurement of the pore-pressure parameter C less than unity in saturated sands. Geotechnical Testing Journal, **15**(3): 223-230.

Villwock, R., Steiner, M.T.A., and Dyminski, A.S. Data mining applied to the instrumentation data analysis of a large dam. *In* 7th International Conference on Intelligent Systems Design and Applications, ISDA'07, October 22, 2007 - October 24, 2007, Rio de Janeiro, Brazil2007. Inst. of Elec. and Elec. Eng. Computer Society, pp. 949-954.

Vyalov, S., and Oun, Y. 1991. Testing and design of single piles with allowance for creep. Soil Mechanics and Foundation Engineering, **28**(3): 104-110.

Vyalov, S.S., and Shusherina, Y.P. 1964. Resistance of frozen soils to triaxial compression. Translation from Merzlotnye Issledovaniya, No.4, 340-375, Defence Documentation Centre, Cameron Station, Alexandria, Virginia, USA.

Vyalov, S.S., and Roman, L.T. Prediction of long-term creep of soils by methods of time analogies. *In* 10th European Conference on Soil Mechanics and Foundation Engineering, Florence, Italy. 26-30 May 1991 1991. A.A. Balkema, pp. 285-286.

Vyalov, S.S., Maksimyak, R.V., and Razbegin, V.N. Deformation and failure of ice as an anisotropic body (in Russian). *In* Problems of Soil Mechanics and Engineering Permafrostology, Stroiizdat, Moscow1990, pp. 16-24.

Vyalov, S.S., Gmoshinskii, V.G., Gorodetskii, S.E., Grigorieva, V.G., Zaretskii, K., Pekarskaia, N.K., and Shusherina, Y.P. 1965. The strength and creep of frozen soils and calculations for ice-soil retaining structures. CRREL Translation 76, U.S. Army Cold Regions Research and Engineering Laboratory (CRREL), Hanover, N.H., USA.

Wissa, A.E.Z. 1969. Pore-pressure measurement in saturated stiff soils. Journal of the Soil Mechanics and Foundations Division, ASCE, **95**(SM4): 1063-1073.

Witten, I.H., Frank, E., and Hall, M.A. 2011. Data mining : practical machine learning tools and techniques. Morgan Kaufmann, Burlington, MA.

Wroth, C.P., and Houlsby, G.T. Soil mechanics - property characterization and analysis procedures. *In* 11th International Conference on Soil Mechanics and Foundation Engineering, San Francisco. 12-16 August 1985 1985. A.A. Balkema, pp. 1-55.

Yang, Y., Lai, Y., and Chang, X. 2010. Laboratory and theoretical investigations on the deformation and strength behaviors of artificial frozen soil. Cold Regions Science and Technology, **64**(1): 39-45.

Zaretskii, Y., Vorontsov, É., and Baizakov, A. 1991. Static and dynamic pore-pressure in sandy soils. Soil Mechanics and Foundation Engineering, **28**(2): 69-73.

Zaretsky, Y.K., and Fish, A.M. Model of viscoplastic deformation of frozen and unfrozen soils and ice. *In* 6th International Offshore and Polar Engineering Conference, Los Angeles, CA, USA. 26-31 May 1996 1996. Int Soc of Offshore and Polar Engineerns (ISOPE), pp. 291-296.

5. Summary of the findings and their practical significance

5.1 Summary of the findings

5.1.1 Development of FRP for measuring pore-pressures in partially frozen soils

Theory and technical requirements to correctly measure pore-water pressures in partially frozen soils were discussed and used to guide the design of Filter-less Rigid Piezometer (FRP).

Further insights into the governing role of tertiary compressibility in total compressibility of pore-fluids were presented that were not considered in the previous soil mechanics literature related to pore-pressure measurements. These considerations aid interpretation of the measured pore-pressures and guide the selection of piezometer fluid. Moreover, piezometer fluid was regarded as a "hydraulic fluid" and lessons learned from machinery hydraulics were adapted and incorporated in the design of the FRPs.

The roles of filters in piezometers and conditions where filters are not required, or should not be used, are discussed. Use of a filter can delay and alter the pore-pressure response of the measuring device, reduce reliability, add to system flexibility, and risk loss of hydraulic connection between the piezometer fluid and the pore fluid, especially in partially frozen soils. In FRPs, the interface

of the piezometer fluid with pore-water is transferred into the soil, without having a filter in between, by using a droplet of oil injected into the soil from the tip of the FRP.

The continuity of pressures in unfrozen pore-water is required when considering pore-water as an independent phase according to the definition of continuum in mechanics, to evaluate fluid flow and constitutive equations. Further, hydraulic connection between the fluid phases in the soil and in the measuring system is required to properly measure pore-pressures. Moreover, the methods for confirming the continuity of unfrozen water phase were compared. Further, practical and experimental significance of conducting experiments at subfreezing temperatures close to $0^{o}C$ and at low confining and backpressures were outlined.

The shortcomings of the previously used methods for measuring pore-water pressure in soils at subfreezing temperatures were summarized and the critical needs for developing a miniature piezometer for measuring pore-water pressure distribution in freezing, thawing, and frozen soils were outlined. These measurements have application in better understanding the behavior of these soils as they freeze and thaw and when they are subjected to external loads. They also have application in measuring hydraulic conductivity and effective stress resistance and deformation material properties.

5.1.2 Interpretation of the response of FRPs and factors affecting the measurements

Testing of Filter-less Rigid Piezometer (FRP) and interpretation of the measured pore-pressures using FRPs for measuring pore-water pressures in partially frozen soils in the laboratory were discussed. Validity of the measurements was verified by observing that the measured pore-water pressures closely reflect the independent change of backpressures applied to the partially frozen saline sand specimens. Further, effects of air entrainment, de-saturation, pore-fluid temperature, ambient temperature fluctuations, and testing system compliance on the interpretation of the measured pore-water pressures were studied. The calibration method used in this research compensates for a majority of the testing equipment imperfections.

It was also demonstrated that the interface characteristics between the loading piston and the pore-liquid has an influence on the delayed response during the unloading scenarios, as well as on the effects of de-saturation, air-entrainment, and pore-fluid temperature on the measured pore-pressures, and is a function of the tensile strength and adhesion of the pore-fluid to the loading piston. Further study of this matter was not within the scope of the current research and remains for future research.

The fundamental concepts discussed in this thesis enhance understanding of methods used for measuring pore-pressures in multi-phase porous media. FRP may also have application in measuring pore-water pressures in stiff clays and in liquefaction assessment of sands and silts under dynamic loading, owing to its rigidity (only very small volume transfer of liquid is required to transfer the pressures) and high frequency data logging (time intervals as small as 0.01 sec).

5.1.3 Stress transmission in a partially frozen soil

First time measurements of Skempton's B-bar coefficient in a partially frozen soil under laterally confined conditions and at various initial void ratios were presented and compared with that in the unfrozen state. Thus, by assuming superposition, stress distribution between the soil matrix, pore-ice, and unfrozen pore-water were evaluated. The pore-ice pressure coefficient ($\overline{\boldsymbol{B}}_{\boldsymbol{ice}}$) was introduced and it was observed that its value increased at a rate more than 10 times faster than the rate of void ratio decrease in the saline sand specimen having initial salinity of 30±1 ppt NaCl and at -2.94 ± 0.18^{o}C,. Effects of pore-ice structure, pore-ice pressure cut off, stress relaxation in pore-ice, and ice-melt on pore-ice pressure were discussed.

First time measurements of pore-water pressure distribution within a partially frozen soil during undrained warming were presented. It was shown that the pore-water pressures dropped sharply (up to 283 kPa for 0.76^{o}C warming) within the first 4 hours of application of the warming temperatures. Correlation models were suggested to predict induced pore-pressures associated with undrained warming.

Further, the decrease rate of load bearing by the ice matrix with increasing temperature was evaluated for an overconsoliated partially frozen saline sand specimen at subfreezing temperatures close to 0°C. For this specimen, $\frac{\partial \bar{B}_{ice}}{\partial T} = -0.0349/\,^{o}\text{C}$ was estimated.

It was further observed that preconsolidation manifests itself in two ways in both partially frozen and unfrozen specimens:

(a)- Bilinear response of the measured pore-water pressures with an inflection point at a total stress that approximates the overconsolidation pressure plus pore-water pressure

(b)- Reduction of $\bar{\boldsymbol{B}}$

With increasing preconsolidation pressure, the primary pore-water pressure coefficient ($\bar{\boldsymbol{B}}_{\boldsymbol{i}}$) and the secondary pore-water pressure coefficient ($\bar{\boldsymbol{B}}_{\boldsymbol{s}}$) remained almost constant or slightly decreased. With increasing backpressure, $\bar{\boldsymbol{B}}_{\boldsymbol{i}}$ increased whereas $\bar{\boldsymbol{B}}_{\boldsymbol{s}}$ remained nearly constant or only slightly increased (i.e. $\bar{\boldsymbol{B}}_{\boldsymbol{i}}$ approached $\bar{\boldsymbol{B}}_{\boldsymbol{s}}$). It was also hypothesized that the inflection point might reflect a critical state and that $\bar{\boldsymbol{B}}_{\boldsymbol{i}}$ and $\bar{\boldsymbol{B}}_{\boldsymbol{s}}$ may reflect initial and incremental $\boldsymbol{A}$ pore-pressure coefficients, $\boldsymbol{A}_{\boldsymbol{i}}$ and $\boldsymbol{A}_{\boldsymbol{s}}$, observed by Sánchez and Sagaseta (1981) for unfrozen soft clay specimens. $\bar{\boldsymbol{B}}$ values in the partially frozen state were smaller than that in unfrozen state due to the contribution of the ice matrix in resisting loads.

Validity of the measured pore-water pressures within partially frozen saline sand specimens and their anomalies were discussed. Further, it was shown that the change in effective stress under undrained loading is not zero when the solid phase is of appreciable stiffness relative to the fluid phase; hence frictional resistance is not zero under undrained conditions in partially frozen sand.

5.1.4 New classification: unfrozen, frozen, and partially frozen soils

Based on the discussion related to the continuity of phases previously outlined in this research it is suggested to identify three classes of soils as follows:

1. **Frozen soils**: soils containing pore-ice, in which unfrozen pore-water is not continuous

2. **Partially frozen soils**: soils containing pore-ice, in which unfrozen pore-water is continuous

3. **Unfrozen soils**: soils with no pore-ice

It should be noted that the above classification is more useful in identification of mechanical behavior of soils than the previous classifications based solely on temperature (permafrost or non-permafrost soil) or solely based on the existence of ice (frozen and unfrozen).

5.2 Limitations of the findings

5.2.1 Validity of the measured pore-water pressures

Validity of the measured pore-water pressures within a partially frozen saline sand specimen was verified for temperatures warmer than -3.9^{o}C in this research. However, some random anomalies in the continuity of pore-water pressures were observed (due to local ice-blockage) at temperatures colder than -2.6^{o}C but was not observed at temperatures warmer than -1.8^{o}C for experiments with 30±1 ppt saline sand and consolidation pressure of 330 kPa. It is worth noting that the freezing point of seawater at 30±1 ppt salinity is approximately -1.6^{o}C (Fofonoff and Millard Jr 1983). Freezing point depression in saline sand at 30±1 ppt NaCl salinity is approximately -1.8^{o}C (Hivon and Sego 1990).

If we assume that at the same level of volumetric unfrozen water content two partially frozen sand specimens at different salinities have the same continuity condition in pore-water pressures, one can evaluate applicability of the findings of this research to a different soil. The unfrozen water in a soil at subzero temperatures is strongly related to the fines content of the soil and the geometry of the pore space (also to salinity), whereas the continuity of the water films mainly depends on the distribution of the fines (also unfrozen water) that fill the pore space between the coarser soil particles (Konrad 1999). The partially frozen saline sand at 30±1 ppt salinity and -3.9^{o}C has a volumetric unfrozen water content $\boldsymbol{\theta_u} = 13.9\%$. The interpolated temperature is about -1.1^{o}C to have the same amount of unfrozen water content in a specimen at 10±1 ppt salinity. In fine grained soils such as clays and silts, greater volume of unfrozen water content exists compared to sand at

the same temperatures (Figure 2-3.c) and therefore it is expected that findings of this research are applicable at colder temperatures in these finer grained soils.

It should be noted that the actual temperature at which the pore-water in the partially frozen saline sand specimen at 30±1 ppt is continuous could be colder than -3.9°C. The reason for this is that the top drain of the MQS cell clogs at colder temperatures and even though quick warming of top plate was used to ensure continuity in the top drain and the pore-water in the specimen, there might be a difference between the reported -3.9°C and the '*coldest*' temperatures for which unfrozen pore-water in that soil specimen had continuous pressures (despite local blockages at temperatures colder than -2.6°C). To overcome the problem of ice blockage of the top drain, it is suggested to modify the MQS cell so that flash warming of the drain line is possible without changing the temperature of the specimen. To minimize the overall effect of such warming procedures, it is suggested to use larger specimens and measure pore-water pressures within the specimen away from the boundaries.

5.2.2 Limitations in using pore-ice pressure coefficient

Pore-ice pressure coefficient ($\overline{\boldsymbol{B}}_{\boldsymbol{ice}}$) was evaluated assuming '*superposition principle*' and that the soil matrix carries the same amount of stress in both partially frozen and unfrozen states provided the soil has undergone the same strain history; for sand having the same initial void ratio (Ladanyi and Morel 1990).

The '*superposition principle'* implies that the system is linear and additive; if input x_1 generates response Y_1 and input x_2 generates response Y_2 then input $x_1 + x_2$ generates response $Y_1 + Y_2$. The superposition principle provides an approximation of the actual behavior as the real systems are only approximately linear within a specific range of inputs. For the case of partially frozen saline sand, even though it is assumed that the sand matrix is a linear elastic material, the ice matrix is not linear and also its response is time-dependent (creep or relaxation). Especially, the fragile needle-ice matrix (Arenson and Sego 2006) is collapsible. For the case of partially frozen clay or silt, both the ice matrix and the soil matrix are non-linear and their deformations depend on time.

Therefore, the time factor, and other parameters should be incorporated in the models that attempt to describe the behavior by assuming allocation of specific portion of stress to each phase. In this research, response after 10 minutes was uniformly used amongst all experiments to provide a consistent comparison.

In this research, variables that might affect the measurements such as soil history (preconsolidation stress and void ratio) and initial loading conditions (initial backpressure, void ratio, and total stress) were considered. A *Data mining technique* was used to screen the most important contributing parameters based on the small generated database of the responses. It was found that only initial condition variables (initial void ratio and initial backpressure) met significance level of 0.1 for entry into the model. Soil history variables met significance level of 0.2 for experiments on unfrozen saline sand specimens. As a general rule, the more influential variables are used in the modeling, the more accurate the predicted result. For the best use of data mining techniques to model complex systems, generating a large data base of inputs and responses is required which was not in the scope of this research.

5.3 Practical significance of the findings of this research

For the first time pore-water pressure distribution within a partially frozen soil subjected to undrained loading, independent backpressures, and undrained warming was accurately measured and continuity of the measured pore-water pressures was validated. Hence, it was shown that pore-water is an independent phase with pore-pressures responding to change in total stresses but independent of the applied total stress. Therefore effective stresses and effective stress material properties should be used for analysis and design in these soils. Furthermore, stress distribution between the soil matrix, pore-ice, and unfrozen pore-water were evaluated for a partially frozen soil. The significance of findings of this research in evaluating effective stress and effective friction angle in undrained loading were presented in Chapter 4. Significance associated with slope stability in warm and warming permafrost, analysis and design of foundation in permafrost, analysis of thaw subsidence, building constitutive models for partially frozen soils, and analysis of

water flow and contaminant transport within partially frozen soils are outlined in the following sections.

5.3.1 Significance in slope stability analysis in warm permafrost

Duncan and Wright (2005) summarized ten common factors that reduce soil strength and six common factors that increase shear stresses and hence reducing the factor of safety against sliding in temperate soils. It is of particular importance in permafrost slopes that strength of a soil is reduced by increase in pore-water pressure (reduced effective stress) and cracking (in tension). On the other hand, shear stress in soil is increased due to water pressure in cracks at the top of the slope (short term hydrostatic water pressure on soil) and increase in soil weight due to increase in water content. The confirmation and quantification of the above statements is challenging as several factors such as continuity of the water phase, temperature, temperature gradient and direction of heat flow, salinity, and time (creep, mass and heat transfer) control the mechanics of the instability of soil and rock masses in permafrost.

Considering various aspects of the stability of soil masses in permafrost is beyond the scope of the current research. The literature on stability of soil masses in permafrost has been reviewed by other authors (Mason 1995; McRoberts 1973; Stoker 1989; Tsui 1987). Huggel et al. (2010) provided a recent review on the literature on slope failure hazards due to global warming. McSaveney (2002) reported massive rock and ice falls (up to 11.8 million m^3), earthquakes (up to 3.9 Richter), floods (up to 7.8 million m^3 water), and rapid rock-ice flow to long distances (up to 7.5 km at 60m/s) caused by "instability of slopes" in high mountain permafrost.

The role of effective stress and liquefaction in the stability of freezing, thawing, and frozen slopes has been reviewed by several authors (Cleall et al. 2006; Finn et al. 1978; Harris and Lewkowicz 2000; Harris et al. 2003; Liu and Wang 2006; Yao and Broms 1965). Findings of the present research show that effective stress material properties and effective stress analysis should be used to evaluate resistance and deformation of the partially frozen soils. This will significantly enhance the analysis of slope stability in warm permafrost slopes. Further, the findings of this study

showed that in stiff, near saturated, or partially frozen soils $\bar{B}$ less than unity should be expected; hence, change in effective stress is not zero under undrained conditions. Therefore, the material develops frictional resistance against slope movement and instability. Further, rebound and warming of permafrost slopes creates negative pore-pressures in ice-poor partially frozen sand; this provides for added resistance.

Frozen permafrost slopes that have undergone warming may have already developed large negative pore-water pressures (similar to Figure 4-11.a) that may suddenly change to positive pore-pressures as:

- Additional water from melting ice increases the degree of saturation (especially in varved soils with non-homogenous ice distribution)
- Positive pore-water pressures are generated during a sudden drop in air temperature after a thaw period due to impeded drainage (freezing of an unfrozen layer between two frozen layers)
- Soil deforms under undrained conditions

An example of sudden change in pore-water pressures due to application of backpressure is presented in Figure 3-22. The initial and subsequent pore-water pressures must be measured to evaluate the stability of the slopes under different thawing, freezing, and saturation scenarios.

Factors of safety are allocated more efficiently in limit state analysis and design methods. However, these methods are based on 'effective stress analysis'. Validity of using effective stress for analysis of soils at subzero temperatures close to 0^{o}C was verified in this research. Therefore, it is desired to adapt limit state analysis and design for slope stability analysis for slopes at subfreezing temperatures close to 0^{o}C. Eurocode 7 uses critical state as the ultimate limit state in slope stability (Bond and Harris 2008; Orr and Farrell 1999). For this, it is perceived that pore-water pressures and strength parameters at critical states are desirable in evaluating the 'ultimate limit state', especially when large, rapid deformations are anticipated during slope failure, at which conditions all of the overconsolidation-like effects are eliminated (Mayne and Swanson

1980). The pore-pressures developed during undrained shearing of soils depend on four main elements: (1) the initial effective vertical stress ($\boldsymbol{\sigma'_{vo}}$), (2) the degree of overconsolidation ($\boldsymbol{OCR}$), (3) the initial stress state ($\boldsymbol{K_i}$), and (4) the magnitude of the applied shear stress or strain. The critical state pore-pressure parameter is independent of these factors and has been viewed as a soil property (Mayne and Swanson 1980).

To adapt limit state analysis and design for slope stability analysis for slopes at subfreezing temperatures close to 0^{o}C, appropriate load and resistance factors should be established by considering various parameters such as time, temperature, ice content characteristics, soil type, and scenario (mode) of slope instability triggers.

5.3.2 Significance in analysis and design of foundations in permafrost

With global warming, the thermal regime in the near surface layer of the ground will change which impacts the stability and serviceability of foundations in permafrost regions. When a saturated soil is frozen at temperatures well below 0^{o}C it has a high shear resistance due to ice bonding. An example of a heavy oil tank supported on a foundation that has a ventilated gravel fill to keep the ground frozen is shown in Figure 5-1. With warming, the ice bonds will gradually weaken and melt which also may generate higher pore-water pressures and result in instability. The risk assesment during transition between the frozen and thawed conditions determines the expenditure and when and how it is allocated to ensure the safety and serviceability of this type of infrastructure. This is of significant interest for both the government and private sectors, as well as insurance companies. A realistic method that can accurately predict the stability and serviceability of such structures is desired.

Current methods of analysis and design of foundations in permafrost are solely based on total stresses and do not consider effective frictional resistance and pore-water pressures. In these methods, the burial depth of the foundation has no effect on the bearing capacity of the foundation due to overburden pressure but colder temperatures at deeper elevations generally increase shearing resistance due to existance of colder ice (Andersland and Ladanyi 2004). One implication

of the findings of this research is that the burial depth influences the bearing capacity of foundations on partially frozen soils because increasing burial depth increases the effective stress and hence the frictional resistance of the soil. On the other hand, delayed drainage of water produced from melting ice and its effect on reducing effective stress and instability of foundations should be evaluated in ice-rich soils that have low hydraulic conductivity in partially frozen or thawed state. It should be also noted that in some thawed soils, cracks would increase the hydraulic conductivity of the soil mass.

5.3.3 Significance in evaluation of thaw subsidence and constitutive modeling of partially frozen soils

The findings of this research will significantly enhance the evaluation of thaw subsidence and modeling deformation of partially frozen soils under applied loads and warming due to the important role of pore-water pressure generation and dissipation in evaluation of effective stresses and stress-strain behavior of partially frozen soils (Arenson et al. 2007; Neaupane et al. 1999; Panday and Corapcioglu 1995; Williams 1995; Zhang 2011). Creep approaches used for modeling deformation of frozen soils do not consider pore-water pressures and their dissipation when evaluating deformations. Measuring pore-water pressure distribution in partially frozen soils provides understanding to evaluate:

- Distribution of hydraulic conductivity within these soils via direct measurements
- Effective consolidation and effective pre-consolidation pressures
- Effective deformation modulus used for constitutive modeling
- Degree of consolidation and time required for reaching a specific degree of consolidation

5.3.4 Significance in evaluation of water flow and contaminant transport within partially frozen soils

Evaluation of water flow and contaminant transport in partially frozen soils requires measurement or estimation of pore-pressure gradients and is of paramount practical significance, especially with increased industrial activities in cold regions. These applications may include:

- Control and assessment of water resources (Kane and Stein 1983; Woo and Winter 1993)
- Ground freeezing methods for ground water control (McKenzie et al. 2007)
- Contaminant confinement (Andersland et al. 1996; Iskandar and Jenkins 1985)
- Risk assessment associated with contaminant transport (McCauley et al. 2002; Meyer and Wania 2008; Wiggert et al. 1997)
- Risk assesment associated with instability of partially frozen soil masses due to water movement and associated saturation process (Mackay 1983a)

Further, to measure hydraulic conductivity distribution within freezing, thawing, and frozen soils, knowledge of pore-water pressures and continuity of unfrozen water phase are required. This would have applications in frost heave and thaw weakening prediction models. Continuity of unfrozen water phase, development of negative pore-water pressures under undrained warming, and feasibility of measuring pore-water pressure gradients within soils at subfreezing temperatures will enhance analysis related to water flow and contaminant transport within partially frozen soils.

5.4 Recommendations for future research

Further research on the following topics is recommended:

1) Formulating resistance and deformation of partially frozen soils in terms of effective stresses
2) Optimizing hydraulic fluids for use as ‘piezometer fluid’
3) Extending the use of FRPs to other soil types and saturation levels

4) Investigating pore-water pressure distribution in freezing and thawing soils
5) Investigating the effects of the system compliance on the measured pore-water pressures
6) Investigating the characteristics of the interface between the loading piston and the pore-liquid and its effects on the stress transmission in soil
7) Conducting experiments to estimate pore-ice pressure at various temperatures as a function of time in different soils
8) Further improving the MQS cell:
    a. Using hard steel parts and cell wall
    b. Using higher number of O-rings for the loading piston if pneumatic loading system is used (3 to 5 O-rings are suggested)
    c. Using mechanical loading (no air pressure on O-rings more than atmospheric pressure)
    d. Submerge the whole cell in a thermally controlled bath for better thermal control
    e. Conducting strain controlled loading to reach pre-defined strains

5.5 Figures

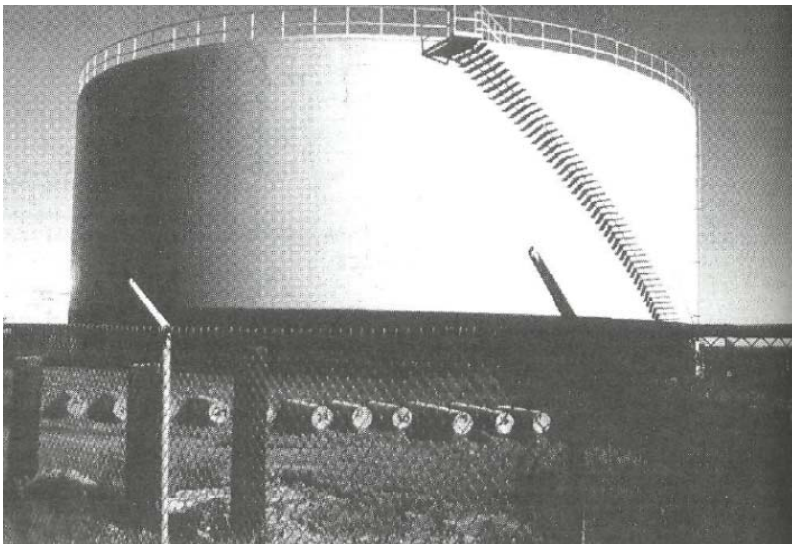

Figure 5-1. Heavy oil tank supported on a foundation that has a ventilated gravel fill to keep the ground frozen, Inuvik, Northwest Territory, Canada (Andersland and Ladanyi 2004)

5.6 References

Andersland, O.B., and Ladanyi, B. 2004. Frozen ground engineering. Wiley, Hoboken, NJ.

Andersland, O.B., Wiggert, D.C., and Davies, S.H. 1996. Frozen soil subsurface barriers: formation and ice erosion. Journal of Contaminant Hydrology, **23**(1-2): 133-147.

Arenson, L.U., and Sego, D.C. 2006. The effect of salinity on the freezing of coarse-grained sands. Canadian Geotechnical Journal, 43(3): 325-337.

Arenson, L.U., Springman, S.M., and Sego, D.C. 2007. The rheology of frozen soils. Applied Rheology, **17**(1): (12147)-12141 – (12147)-12114.

Berryman, J.G. 2002. Extension of poroelastic analysis to double-porosity materials: New technique in microgeomechanics. Journal of Engineering Mechanics, **128**(8): 840-847.

Bond, A., and Harris, A. 2008. Decoding Eurocode 7. Taylor & Francis, London ; New York.

Carroll, M.M. 1980. Mechanical response of fluid-saturated porous materials. *In* 15th International Congress of Theoretical and Applied Mechanics. North-Holland Publication Co., Toronto, Canada, pp. 251-262.

Cleall, P.J., Thomas, H.R., and Glendinning, M.C. Modelling the behaviour of freezing and thawing soil slopes. *In* 5th ICEG Environmental Geotechnics: Opportunities, Challenges and Responsibilities for Environmental Geotechnics - International Society of Soil Mechanics and Geotechnical Engineering's (ISSMGE) 5th International Congress, June 26, 2006 - June 30, 2006, Cardiff, Wales, United kingdom2006. Thomas Telford Services Ltd, pp. 1603-1610.

Duncan, J.M., and Wright, S.G. 2005. Soil strength and slope stability. John Wiley & Sons, Hoboken, N.J.

Finn, W.D.L., Yong, R.N., and Lee, K.W. 1978. Liquefaction of thawed layers in frozen soil. Journal of the Geotechnical Engineering Division, **104**(10): 1243-1255.

Fofonoff, P., and Millard Jr, R.C. 1983. Algorithms for computation of fundamental properties of seawater. Unesco Technical Papers in Marine Science **44**: 1-53.

Gassmann, F. 1951. Über die Elastizität poröser Medien (Elasticity of porous media). Vierteljahrsschrift der Naturforschenden Gesselschaft, **96**: 1-23. Translation available for download via "Stanford Exploration Project ". Accessed online on 28 Sep 2009 at http://sepwww.stanford.edu/sep/berryman/PS/gassmann.pdf.

Harris, C., and Lewkowicz, A.G. 2000. An analysis of the stability of thawing slopes, Ellesmere Island, Nunavut, Canada. Canadian Geotechnical Journal, **37**(2): 449-462.

Harris, C., Davies, M.C.R., and Rea, B.R. 2003. Gelifluction; viscous flow or plastic creep? Earth Surface Processes and Landforms, **28**(12): 1289-1301.

Henkel, D.J., and Wade, N.H. 1966. Plane Strain Tests on a Saturated Remolded Clay. Journal of the Soil Mechanics and Foundations Division, ASCE, **92**(SM6): 67-80.

Hivon, E., and Sego, D.C. 1990. Determination of the unfrozen water content in saline permafrost using Time-Domain Reflectometry (TDR). In 5th Canadian Permafrost Conference: Permafrost Canada. Accesed online at http://pubs.aina.ucalgary.ca/cpc/CPC5-257.pdf on October 7th 2009, Collection Nordicana, pp. 257-262.

Huggel, C., Salzmann, N., Allen, S., Caplan-Auerbach, J., Fischer, L., Haeberli, W., Larsen, C., Schneider, D., and Wessels, R. Recent and future warm extreme events and high-mountain slope stability, 6 Carlton House Terrace, London, SW1Y 5AG, United Kingdom2010. Royal Society of London, pp. 2435-2459.

Iskandar, I.K., and Jenkins, T.F. Potential use of artificial ground freezing for contaminant immobilization. *In* Proceedings of the International Conference on New Frontiers for Hazardous Waste Management, Pittsburgh, PA, USA1985. EPA, pp. 128-137.

Kane, D.L., and Stein, J. 1983. Water movement into seasonally frozen soils. Water Resources Research, **19**(6): 1547-1557.

Konrad, J.-M. 1999. Frost susceptibility related to soil index properties. Canadian Geotechnical Journal, **36**(3): 403-417.

Ladanyi, B., and Morel, J.-F. 1990. Effect of internal confinement on compression strength of frozen sand. Canadian Geotechnical Journal, **27**(1): 8-18.

Liu, H.-J., and Wang, P.-X. 2006. Stability analysis of loss of stability caused by freeze and melt of earthen side slopes of highways. Harbin Gongye Daxue Xuebao/Journal of Harbin Institute of Technology, **38**(5): 764-766.

Mackay, J.R. 1983. Downward water movement into frozen ground, western arctic coast, Canada. Canadian Journal of Earth Sciences, **20**(1): 120-134.

Mason, J.A. 1995. Effects of glacial-interglacial climate change on mass wasting, southeastern Minnesota. Ph.D. dissertation, The University of Wisconsin, Madison, United States.

Mayne, P.W., and Swanson, P.G. The critical-state pore-pressure parameter from consolidated-undrained shear tests. *In* Laboratory Shear Strength of Soil, Chicago, IL, USA. 25 June 1980 1980. ASTM, Special Technical Publication 740, pp. 410-443.

McCauley, C.A., White, D.M., Lilly, M.R., and Nyman, D.M. 2002. A comparison of hydraulic conductivities, permeabilities and infiltration rates in frozen and unfrozen soils. Cold Regions Science and Technology, **34**(2): 117-125.

McKenzie, J.M., Voss, C.I., and Siegel, D.I. 2007. Groundwater flow with energy transport and water–ice phase change: Numerical simulations, benchmarks, and application to freezing in peat bogs. Advances in Water Resources, **30**(4): 966-983.

McRoberts, E.C. 1973. Stability of slopes in permafrost. Ph.D. dissertation, University of Alberta, Canada.

McSaveney, M.J. 2002. Recent rockfalls and rock avalanches in Mount Cook national park, New Zealand. *In* Catastrophic landslides, effects, occurrence and mechanisms. Geological Society of America, Reviews in Engineering Geology, Volume XV, Boulder, pp. 35–70.

Meyer, T., and Wania, F. 2008. Organic contaminant amplification during snowmelt. Water Research, **42**(8-9): 1847-1865.

Neaupane, K.M., Yamabe, T., and Yoshinaka, R. 1999. Simulation of a fully coupled thermo–hydro–mechanical system in freezing and thawing rock. International Journal of Rock Mechanics and Mining Sciences, **36**(5): 563-580.

Orr, T.L.L., and Farrell, E.R. 1999. Geotechnical design to Eurocode 7. Springer, London ; New York.

Panday, S., and Corapcioglu, M.Y. 1995. Solution and evaluation of permafrost thaw-subsidence model. Journal of Engineering Mechanics, **121**(3): 460-469.

Sanchez, J.M., and Sagaseta, C. 1981. Undrained behaviour of soft clays in triaxial tests. International Conference on Soil Mechanics and Foundation Engineering, **1**: 771-774.

Skempton, A.W. 1954. Pore-pressure coefficients A and B. Geotechnique, **4**(4): 143-147.

Stoker, K.J.L. 1989. Active layer detachment slope failures on Fosheim Peninsula, Ellesmere Island, Northwest Territories. M.Sc. thesis, University of Toronto, Canada.

Tsui, P.C. 1987. Geotechnical investigations of glaciotectonic deformation in central and southern Alberta. Ph.D. dissertation, University of Alberta, Canada.

Wiggert, D.C., Andersland, O.B., and Davies, S.H. 1997. Movement of liquid contaminants in partially saturated frozen granular soils. Cold Regions Science and Technology, **25**(2): 111-117.

Williams, P.J. 1995. Permafrost and climate change: geotechnical implications. Philosophical Transactions - Royal Society of London, A, **352**(1699): 347-358.

Woo, M.-K., and Winter, T.C. 1993. The role of permafrost and seasonal frost in the hydrology of northern wetlands in North America. Journal of Hydrology, **141**(1-4): 5-31.

Yao, L.Y.C., and Broms, B.B. 1965. Excess pore-pressures which develop during thawing of frozen fine-grained subgrade soils. Highway Research Record(101): 39-57.

Zhang, T. 2011. Linear elastic constitutive relation for multiphase porous media using microstructure superposition: Freeze-thaw soils. Cold Regions Science and Technology, **65**(2): 251-257.